

**The influence of a green roof  
configuration's moisture balance on  
hydrological performance**

Simon Poë

A thesis submitted in part fulfilment of the  
requirements for the degree of Doctor of  
Philosophy in Civil Engineering

Department of Civil and Structural  
Engineering

December 2016



# Declaration

I declare that no portion of the work contained in this thesis has been submitted in support of an application for another degree or qualification of this or any other university or other institute of learning. The work has been my own except where indicated. All quotations have been distinguished by quotation marks and the sources acknowledged.

# Acknowledgements

I would not have written this thesis had it not been for the encouragement, assistance and patience of Dr Virginia Stovin. I am grateful for the support that was provided at every stage of the work.

This project would not have been possible without the support of my employer, Alumasc Exterior Building Products Ltd. The time and financial resources committed by the company to allow me to research the performance of green roofs is greatly appreciated.

I would like to acknowledge the valuable input from a number of people involved in this project over the years. Firstly, to Paul Osborne and his technical team, for their support and guidance during the establishment of the trials. Secondly, to the team of people involved in the Marie Curie Industry-Academia Partnerships and Pathways project, and in particular, Joerg Werdin (for all of his support in maintaining the green roof test beds and for his work in characterising the substrates) and Dr Zoe Dunsiger (for her help in establishing the vegetated microcosms prior to the ET trials). The organisation of the Hadfield data set into per-event data by Simon de-Ville, a fellow PhD candidate, was also particularly important.

Finally, I would like to thank my family for their sacrifices over the seven years of this work, especially Shona, Callum and Alex. This work took a little longer than expected. Sadly, not everybody that started this journey finished it with me. I dedicate this thesis to my brother, Mark.

# Abstract

Climate change and urbanization has increased the risk of pluvial flooding. Sustainable Drainage Systems (SuDS) aim to control a greater proportion of rainwater at source. Green roofs can partly offset the loss of urban terrestrial landscape and provide additional capacity for the retention and detention of rainwater. The objective of this research was to improve the understanding of the physical controls that affect a green roof's hydrological response. Experimental studies were undertaken to monitor the performance of nine different extensive (80 mm substrate) green roof configurations.

A four-year record of rainfall, runoff, climate and moisture content data has been analysed for a field research site in Sheffield. Nine test beds incorporated three substrates with different moisture retention characteristics and three different vegetation treatments (Sedum, Meadow Flower and non-vegetated). Consistent differences were observed. The effects of vegetation and substrate were most evident for rainfall events where the depth exceeded 10 mm: mean per-event retention varied between beds from 14% to 70%. Retention was highest from the configuration with the highest moisture storage capacity (Sedum-vegetated HLS) and lowest from the configuration with the lowest moisture storage capacity (non-vegetated LECA). The difference between rainfall depth and available moisture capacity provided a highly credible indication of runoff. Evapotranspiration (ET) regenerates the moisture retention capacity. Experimental studies in a climate-controlled chamber enabled the monitoring of ET from the nine configurations across continuous dry periods of up to 28 diurnal cycles in spring and summer. ET rates were variably influenced by climate, vegetation treatment, soil and residual moisture content.

A conceptual hydrological flux model was developed to allow both long term continuous simulation of runoff and drought risk and per-event responses to design storms. The model includes a function that links ET rates to residual moisture content, and is validated against observed runoff data. Detention was characterised via the calibration of a reservoir-routing model that linked net rainfall to the measured runoff response. The parameter values identified here – when combined with the retention model component – provide a generic mechanism for predicting the runoff response to a time-series or design rainfall for any unmonitored system with comparable components, permitting comparison against regulatory requirements.

# Table of Contents

1	Introduction.....	1
1.1	Background .....	1
1.2	Aims and objectives .....	2
1.3	Thesis structure and content.....	4
1.4	Publications .....	6
2	Literature review .....	8
2.1	Chapter overview .....	8
2.2	Sustainable drainage systems (SuDS).....	8
2.2.1	Introduction to SuDS .....	8
2.2.2	Drivers.....	10
2.2.3	SuDS regulations and performance standards .....	11
2.3	Green roofs.....	12
2.3.1	Green roof configuration.....	12
2.3.2	Green roof classifications.....	14
2.3.3	Conceptual benefits of green roofs .....	15
2.4	Physical influences upon hydrological response.....	18
2.4.1	Fundamental soil-water physics.....	19
2.4.2	The influence of substrate upon moisture balance.....	25
2.4.3	The hydrological importance of a configuration's vegetation treatment ..	28
2.4.4	Incremental moisture capacity of drainage layers.....	32
2.4.5	Incidence of precipitation.....	33
2.4.6	Evapotranspiration and the influence of climate.....	34
2.5	Reported quantitative hydrological performance of green roofs.....	36
2.5.1	Runoff reduction .....	36
2.5.2	Evapotranspiration (ET).....	38

2.5.3	Peak attenuation & delay .....	39
2.6	Modelling hydrological response .....	41
2.6.1	Rainfall simulation .....	42
2.6.2	Modelling runoff from green roofs .....	42
2.6.3	Evapotranspiration calculations .....	48
2.6.4	Derivation of actual evapotranspiration .....	52
2.6.5	Existing storm water models used with green roofs .....	53
2.6.6	Future modelling requirements .....	54
2.7	Summary of literature review .....	55
3	Characterisation of green roof materials .....	57
3.1	Chapter overview .....	57
3.2	Motivation .....	57
3.3	Materials and methods .....	58
3.3.1	Introduction to the configurations .....	58
3.3.2	Substrate characterisation tests .....	60
3.3.3	Vegetation treatments .....	62
3.3.4	Drainage layer characteristics .....	66
3.4	Results .....	67
3.4.1	Substrate characteristics .....	67
3.4.2	Vegetation .....	73
3.5	Discussion .....	74
3.6	Conclusions .....	77
4	Field evaluation of green roof hydrological performance .....	79
4.1	Chapter overview .....	79
4.2	Motivation .....	80
4.3	Materials and methods .....	80
4.3.1	Experimental setup .....	80

4.3.2	Test configurations.....	81
4.3.3	Data collection .....	83
4.3.4	Data analysis methods.....	91
4.4	Results .....	94
4.4.1	Rainfall event data .....	94
4.4.2	Rainfall and runoff during AE9 events.....	98
4.4.3	Rainfall-Runoff profiles for selected events .....	100
4.4.4	Per-event retention .....	103
4.4.5	Peak attenuation .....	105
4.4.6	Peak delay .....	109
4.4.7	Detention parameter ‘k’ .....	110
4.4.8	Summary of hydrological response to AE9 events.....	111
4.5	Discussion .....	112
4.5.1	Physical controls upon retention performance.....	112
4.5.2	Physical controls upon detention performance .....	126
4.5.3	Physical controls upon the initialisation of runoff.....	133
4.5.4	Physical controls upon the regeneration of the SMD via ET.....	141
4.6	Conclusions .....	145
5	Regeneration of retention capacity via Evapotranspiration .....	147
5.1	Chapter overview .....	147
5.2	Motivation .....	147
5.3	Materials and methods.....	148
5.3.1	Trial configurations.....	151
5.3.2	Data collection methods.....	152
5.3.3	Controlled condition settings .....	155
5.3.4	Data analysis and interpretation.....	158
5.4	Results .....	161



5.4.1	Configuration-mean ET .....	161
5.4.2	Specific ET responses of individual configurations.....	165
5.4.3	Diurnal ET patterns .....	169
5.5	Discussion .....	170
5.5.1	The influence of climate upon ET .....	170
5.5.2	The effect of moisture content upon ET .....	173
5.5.3	The effects of green roof configuration .....	174
5.5.4	Summary of key influences.....	179
5.6	Conclusions .....	179
6	Model development and refinement.....	181
6.1	Chapter overview .....	181
6.2	Motivation .....	182
6.3	Materials and methods.....	182
6.3.1	Conceptual hydrological model .....	182
6.3.2	Model implementation .....	183
6.3.3	Model validation methods.....	184
6.4	Model refinement .....	186
6.4.1	PET calculation .....	186
6.4.2	Soil moisture extraction functions (SMEFs).....	194
6.4.3	ET calculation .....	211
6.4.4	Detention modelling parameters .....	213
6.5	Model Validation.....	216
6.5.1	Validation of retention model using AE9 data.....	216
6.5.2	Validation of detention model.....	219
6.6	Discussion .....	230
6.7	Conclusions .....	231
7	Model application.....	232

7.1	Chapter overview .....	232
7.2	Motivation .....	232
7.3	Materials and methods.....	233
7.3.1	30 year simulation.....	233
7.3.2	Design storm events .....	235
7.4	Results .....	238
7.4.1	30 year simulation.....	238
7.4.2	Design storm events .....	242
7.5	Discussion .....	253
7.6	Conclusions .....	254
8	Conclusions.....	256
8.1	Chapter overview .....	256
8.2	Summary .....	256
8.3	Key findings .....	257
8.3.1	Influence of a configuration's physical characteristics.....	257
8.3.2	Hydrological responses of green roofs in field conditions .....	258
8.3.3	Regeneration of capacity via ET during controlled condition tests.....	262
8.3.4	Development of a hydrological model for extensive green roofs.....	264
8.3.5	Application of the developed hydrological model.....	266
8.3.6	Concluding remarks .....	268
8.4	Discussion .....	269
8.5	Further work .....	270

## List of Figures

Figure 2.1: Conceptual SuDS management train.....	8
Figure 2.2: Replication of the natural growing environment in a green roof .....	12
Figure 2.3: Typical green roof classifications (courtesy of Alumasc).....	14
Figure 2.4: Tortuosity of flow through variably saturated media .....	20
Figure 2.5: Balance of forces in pore-water.....	23
Figure 2.6: Capillary rise due to matric potential .....	23
Figure 2.7: The effect of moisture content upon meniscus radii, $r_m$ .....	24
Figure 2.8: The importance of pore sizes to capillary rise.....	26
Figure 2.9: Conventional detention metrics (adapted from Stovin et al., 2015b).....	40
Figure 3.1: Photograph of the three substrates (left: HLS; centre: SCS; right: LECA)..	58
Figure 3.2: Sedum (left) and Meadow Flower (right) vegetation treatments .....	59
Figure 3.3: Sample substrate blocks .....	61
Figure 3.4: ZinCo Floradrain® FD25 (left) and DBV12 (right) drainage layers .....	67
Figure 3.5: Granulometric distributions for HLS, SCS and LECA .....	68
Figure 3.6: Images of HLS (left), SCS (centre) & LECA (right) in hardened resin.....	70
Figure 3.7: LECA Substrate.....	71
Figure 3.8: Soil Water Characteristic Curve for HLS, SCS and LECA .....	72
Figure 3.9: Sedum vegetation appearance through an annual cycle .....	75
Figure 3.10: Meadow Flower appearance through an annual cycle.....	76
Figure 4.1: Field research site at Hadfield Building, University of Sheffield .....	81
Figure 4.2: Differences in Meadow Flower treatment over time.....	82
Figure 4.3: Field research weather station equipment .....	83
Figure 4.4: Runoff collection tank .....	86
Figure 4.5: Calibration results for PDCR1830 pressure transducers .....	87
Figure 4.6: Smoothing of runoff storage tank readings by PDCR1830 transducers.....	88
Figure 4.7: Section and plan of test configuration .....	89
Figure 4.8: Linear regression to convert CS616 $\mu$ to $\theta$ .....	90
Figure 4.9: Depth-Duration-Frequency classification of rainfall events .....	95
Figure 4.10: Mean monthly temperature and relative humidity .....	96
Figure 4.11: Mean monthly solar radiation and sunlight hours .....	97
Figure 4.12: Rainfall versus runoff for AE9 events.....	98
Figure 4.13: Cumulative runoff responses for nine test beds for two spring events.....	100

Figure 4.14: Cumulative runoff responses for nine test beds for two summer events..	101
Figure 4.15: Cumulative runoff responses for nine test beds for two autumn events...	101
Figure 4.16: Cumulative runoff responses for nine test beds for two winter events ....	102
Figure 4.17: Per-event retention for all AE9 events .....	103
Figure 4.18: Per-event retention for AE9 ( $P \geq 10\text{mm}$ ) events .....	104
Figure 4.19: Per-event retention for AE9 events, categorised by rainfall depth.....	105
Figure 4.20: Peak intensity of rainfall versus runoff during AE9 events .....	106
Figure 4.21: Peak attenuation for AE9 events .....	107
Figure 4.22: Peak attenuation for AE9 ( $P \geq 10 \text{ mm}$ ) dataset .....	107
Figure 4.23: Peak attenuation for AE9 events, categorised by rainfall depth.....	108
Figure 4.24: Peak delays for AE9 dataset .....	109
Figure 4.25: Rainfall-runoff profiles for two events to highlight peak delays .....	110
Figure 4.26: Calibrated values for the reservoir routing coefficient $k$ ( $\text{mm}^{1-n}/\text{min}$ ).....	110
Figure 4.27: Per-event retention for AE9, categorised by vegetation treatment.....	112
Figure 4.28: Interception losses from TB1, TB2, TB3 and TB7 .....	114
Figure 4.29: Relationship between interception losses and soil moisture content.....	115
Figure 4.30: Seasonal-mean interception losses .....	115
Figure 4.31: Per-event retention for AE9 dataset, categorised by substrate type .....	116
Figure 4.32: Seasonal mean per-event retention.....	118
Figure 4.33: Seasonal mean rainfall and runoff.....	119
Figure 4.34: Configuration mean soil moisture deficit after the ADWP .....	120
Figure 4.35: Rainfall minus SMD versus runoff (TB1).....	122
Figure 4.36: Rainfall minus SMD versus runoff (TB2).....	123
Figure 4.37: Rainfall minus SMD versus runoff (TB3).....	124
Figure 4.38: Rainfall minus SMD versus runoff (TB7).....	125
Figure 4.39: Peak attenuation for AE9 dataset, categorised by vegetation treatment ..	128
Figure 4.40: Peak delay for AE9 dataset, categorised by vegetation treatment.....	129
Figure 4.41: Peak attenuation for AE9 dataset, categorised by substrate type .....	130
Figure 4.42: Peak delay for AE9 dataset, categorised by substrate type .....	131
Figure 4.43: Seasonal-mean peak attenuation.....	132
Figure 4.44: Depth-averaged $\theta$ at first discharge .....	133
Figure 4.45: Peak rates of runoff as a function of rainfall intensity .....	135
Figure 4.46: Peak delays as a function of rainfall intensity .....	135

Figure 4.47: Rainfall and runoff during EV258.....	136
Figure 4.48: Rainfall and runoff intensities during EV258.....	137
Figure 4.49: Rainfall, runoff and moisture content during EV258 .....	138
Figure 4.50: Moisture profiles at first discharge.....	139
Figure 4.51: Moisture balance during a spring day – 22/05/2012 (EV172) .....	142
Figure 4.52: Moisture balance during a summer day – 25/06/2013 (EV269) .....	142
Figure 4.53: Moisture balance during an autumn day – 03/09/2012 (EV207) .....	143
Figure 4.54: Moisture balance during a winter day – 03/12/2013 (EV297) .....	144
Figure 5.1: Configuration of Test Set-up.....	148
Figure 5.2: Composition of Microcosms .....	149
Figure 5.3: Schedule of trials .....	150
Figure 5.4: AWEC Glasshouse Facility .....	151
Figure 5.5: Climate Control Unit .....	151
Figure 5.6: MF on HLS – early stage of growth.....	152
Figure 5.7: MF on HLS – after growth in glasshouse.....	152
Figure 5.8: Test configurations in the climate-controlled chamber .....	153
Figure 5.9: Load cell, platform & tray .....	154
Figure 5.10: Modular 600 Data logger.....	154
Figure 5.11: Calibration of load cell .....	154
Figure 5.12: Climatic Conditions in Chamber for (a) spring and (b) summer trials.....	156
Figure 5.13: $ET_{CUM}$ for Sedum on HLS (6 replications).....	159
Figure 5.14: Configuration-mean $ET_{CUM}$ for spring (left) and summer (right).....	162
Figure 5.15: Configuration-mean $ET_D$ for spring (left) and summer (right).....	163
Figure 5.16: ET losses from all three Sedum-vegetated beds.....	166
Figure 5.17: ET losses from all three Meadow Flower beds .....	167
Figure 5.18: ET losses from all three non-vegetated beds.....	168
Figure 5.19: Diurnal ET (Low SMD) .....	169
Figure 5.20: Diurnal ET (High SMD).....	169
Figure 5.21: Diurnal ET loss patterns .....	170
Figure 5.22: Seasonal-mean $ET_D$ .....	171
Figure 5.23: Configuration-mean daily ET as a function of moisture availability .....	172
Figure 5.24 : ET/PET versus $S_e$ .....	173
Figure 5.25: $ET_{CUM}$ from Configurations with Different Plant Options.....	175

Figure 5.26: Vegetation-mean $ET_D$ in spring & summer.....	176
Figure 5.27: Substrate-mean $ET_D$ in spring & summer.....	178
Figure 6.1: Conceptual green roof hydrological model .....	183
Figure 6.2: PET values for the Hadfield research site between 2011 and 2013 .....	186
Figure 6.3: Calculated PET versus maximum measured ET .....	189
Figure 6.4: Sensitivity of $PET_{FAO56}$ to albedo, $\alpha$ .....	192
Figure 6.5: Existing Soil Moisture Extraction Functions with seasonal mean data .....	195
Figure 6.6: Existing SMEFs with configuration mean data.....	195
Figure 6.7: ET vs $ET_{PRED}$ for Sedum-vegetated configurations using existing SMEFs.....	197
Figure 6.8: ET vs $ET_{PRED}$ for Meadow Flower configurations using existing SMEFs .....	198
Figure 6.9: ET vs $ET_{PRED}$ for non-vegetated configurations using existing SMEFs ...	199
Figure 6.10: ET/PET – Potential Relationship.....	201
Figure 6.11: SWCC reproduced using the van Genuchten-Mualem approach.....	202
Figure 6.12: Relative diffusivity using van Genuchten-Mualem approach .....	203
Figure 6.13: Correlation of Relative Diffusivity to ET/PET .....	203
Figure 6.14: ET/PET vs $S_e$ using the $S_e$ Power SMEF .....	206
Figure 6.15: ET vs $ET_{PRED}$ for Sedum-vegetated configurations using new SMEFs... ..	207
Figure 6.16: ET vs $ET_{PRED}$ for Meadow Flower configurations using new SMEFs.....	208
Figure 6.17: ET vs $ET_{PRED}$ for non-vegetated configurations using new SMEFs .....	209
Figure 6.18: Diurnal distribution of ET in spring (left) and summer (right) .....	212
Figure 6.19: Sensitivity of runoff predictions to changes in k.....	214
Figure 6.20: Measured vs Predicted SMD and runoff values .....	217
Figure 6.21: Predicted runoff response of TB1 to EV228 with and without routing ...	220
Figure 6.22: Runoff hydrographs for TB2 and TB4 during EV227 (01/12/2012) .....	222
Figure 6.23: Runoff hydrographs for TB2 and TB7 during EV258 (13/05/2013) .....	223
Figure 6.24: Runoff hydrographs for EV45 (30/08/2010).....	224
Figure 6.25: Runoff hydrographs for EV228 (05/12/2012).....	225
Figure 6.26: Runoff hydrographs for EV246 (09/02/2013).....	227
Figure 6.27: Runoff hydrographs for EV264 (28/05/2013).....	228
Figure 7.1: Monthly mean rainfall and PET during a 30 year simulation .....	234
Figure 7.2: Rainfall and runoff for year 1 of a 30-year time series ( $S_e$ Power SMEF). ..	239
Figure 7.3: Responses of TB2, TB4 & TB7 to 6 hour, 1 in 30 year event in summer .	245
Figure 7.4: Influence of season on response of TB2 to 1 in 30 year event.....	246

Figure 7.5: Influence of SMD on response of TB2 to 1 in 30 year event.....	247
Figure 7.6: Influence of ADWP on response of TB2 to 1 in 30-year event in summer	249
Figure 7.7: Influence of return period on response of TB2 to a summer event .....	250

## List of Tables

Table 2.1: Green roof categories.....	14
Table 2.2: Previously reported ET measurements from green roofs .....	39
Table 3.1: Physical characteristics of species in the Alumasc Blackdown Sedum mat..	63
Table 3.2: Physical characteristics of the species in the Meadow Flower mix.....	64
Table 3.3: Substrate characteristics according to FLL (2008) test methods .....	67
Table 4.1: Length of Antecedent Dry Weather Periods.....	95
Table 4.2: Seasonal climatic data for AE9 events.....	97
Table 4.3: Rainfall – Runoff statistics for AE9 events .....	99
Table 4.4: Configuration-specific k values and goodness of fit statistics.....	111
Table 4.5: Maximum measured values of $\theta$ during AE9 events .....	122
Table 5.1: Allocation of Trays to Load Cells.....	153
Table 5.2: Soil-water characteristics of the tested substrates.....	160
Table 5.3: Moisture Balance changes with ET from planted configurations.....	161
Table 5.4: Mean $ET_{CUM}$ by vegetation and substrate after a 14 day ADWP .....	164
Table 6.1: Crop factor ( $k_c$ ) values .....	190
Table 6.2: $PET_{FAO56}$ with calibrated plant- & season specific albedo coefficients.....	193
Table 6.3: van Genuchten-Mualem parameter values for HLS and SCS .....	202
Table 6.4: Modelling decay parameters .....	205
Table 6.5: Configuration- and vegetation-specific k values .....	213
Table 6.6: Event- and configuration- k values using least-squares fitting.....	221
Table 7.1: Mean values of $S_e$ at the beginning of the ADWP (AE9 events) .....	236
Table 7.2: Rainfall statistics from the 30 year simulation .....	238
Table 7.3: Summary of the hydrological responses to the 30 year simulation .....	240
Table 7.4: Drought stress indicators.....	241
Table 7.5: Responses to design rainfall events with 30 year return period.....	252

## List of Abbreviations

<i>ADWP</i>	Antecedent dry weather period
<i>AE</i>	All events in which a credible dataset existed for any TB
<i>AE9</i>	All events in which a credible dataset existed for all 9 TBs
<i>API</i>	Antecedent precipitation index
<i>AWEC</i>	Arthur Willis Environmental Centre
<i>CAM</i>	Crassulacean acid metabolism
<i>CIBSE</i>	Chartered Institution of Building Services Engineers
<i>CIRIA</i>	Construction Industry Research & Information Association
<i>CSO</i>	Combined sewer overflow
<i>CV</i>	Coefficient of variation
<i>DDF</i>	Depth Duration Frequency
<i>ET</i>	Evapotranspiration
<i>EV</i>	Event
<i>FEH</i>	Flood Estimation Handbook
<i>FLL</i>	Forschungsgesellschaft Landschaftsentwicklung Landschaftsbau
<i>GRO</i>	Green Roof Organisation
<i>HLS</i>	Heather and Lavender Substrate
<i>IAPP</i>	Industry-Academia Partnerships & Pathways
<i>IL</i>	Interception losses
<i>IPCC</i>	Inter-governmental Panel on Climate Change
<i>KG</i>	Koitzsch & Golf (SMEF)
<i>LECA</i>	Lightweight expanded clay aggregate
<i>MF</i>	Meadow Flower
<i>MWHC</i>	Maximum water-holding capacity
<i>NSME</i>	Nash-Sutcliffe Modelling Efficiency
<i>NV</i>	Non-vegetated
<i>OM</i>	Organic matter
<i>PBIAS</i>	Percent Bias
<i>PET</i>	Potential evapotranspiration
<i>PSD</i>	Particle-size distribution
<i>RH</i>	Relative humidity
<i>SCS</i>	Sedum Carpet Substrate
<i>SD</i>	Storm duration
<i>SMD</i>	Soil moisture deficit
<i>SMEF</i>	Soil moisture extraction function
<i>SP</i>	Spring
<i>St. Dev</i>	Standard deviation
<i>SU</i>	Summer
<i>SuDS</i>	Sustainable drainage systems
<i>SWCC</i>	Soil-water characteristic curve
<i>TB</i>	Test bed



<i>TS</i>	Transient storage
<i>UKCP09</i>	United Kingdom Climate Projections 2009
<i>USDA</i>	United States Department of Agriculture
<i>VPD</i>	Vapour pressure deficit
<i>VSD</i>	Void-size distribution

## List of Symbols

<i>D</i>	Diffusivity
<i>d<sub>50</sub></i>	Median particle diameter
<i>D<sub>r</sub></i>	Relative diffusivity
<i>e<sub>a</sub></i>	Actual vapour pressure
<i>e<sub>s</sub></i>	Saturated vapour pressure
<i>ET<sub>c</sub></i>	Crop-specific ET
<i>ET<sub>CUM</sub></i>	Cumulative evapotranspiration
<i>ET<sub>D</sub></i>	Daily evapotranspiration
<i>ET<sub>H</sub></i>	Hourly evapotranspiration
<i>g</i>	Acceleration due to gravity (9.81 m/s <sup>2</sup> )
<i>G</i>	Soil heat flux
<i>h</i>	Hydraulic head
<i>h<sub>c</sub></i>	Capillary rise
<i>h<sub>t</sub></i>	Cumulative depth of transient storage
<i>I</i>	Annual heat index
<i>I<sub>t</sub></i>	Irrigation at time <i>t</i>
<i>K</i>	Hydraulic conductivity
<i>k</i>	Detention parameter, <i>k</i>
<i>K(ψ)</i>	Unsaturated hydraulic conductivity
<i>k<sub>c</sub></i>	Crop factor
<i>K<sub>s</sub></i>	Saturated hydraulic conductivity
<i>K<sub>sf</sub></i>	Hydraulic conductivity at the surface
<i>ℓ</i>	Coefficient related to the pore-size distribution of the substrate
<i>m</i>	Empirical shape factor
<i>p</i>	Mean daily % of annual day time hours
<i>PET<sub>BC</sub></i>	PET using Blaney-Criddle method
<i>PET<sub>CUM</sub></i>	Cumulative potential evapotranspiration
<i>PET<sub>FAO56</sub></i>	PET using FAO-56 Modified Penman-Monteith method
<i>PET<sub>HG</sub></i>	PET using Hargreaves approach
<i>PET<sub>PT</sub></i>	PET using Priestley-Taylor method

$PET_{TH}$	PET using Thornthwaite approach
$P_{MAX}$	Maximum rainfall intensity
$P_t$	Precipitation or rainfall at time $t$
$q$	Flow
$Q_{in_t}$	Flow into transient storage at time $t$
$Q_{MAX}$	Maximum runoff rate
$Q_{out_t}$	Flow out of transient storage at time $t$
$Q_t$	Runoff at time $t$
$R_a$	Extra-terrestrial solar radiation
$r_m$	Radius of the meniscus
$R_n$	Net solar radiation
$R_{nl}$	Net long-wave solar radiation
$R_{ns}$	Net short-wave solar radiation
$R_u$	Ideal gas constant
$S_e$	Effective saturation, $S_t/S_{MAX}$
$S_{MAX}$	Maximum moisture storage capacity
$S_t$	Moisture stored at time $t$
$S_{VEG}$	Storage capacity in the vegetation layer
$T_{ABS}$	Absolute temperature
$T_{MAX}$	Maximum temperature
$T_{MEAN}$	Mean temperature
$T_{MIN}$	Minimum temperature
$t_n$	Mean monthly temperature
$t_{PMAX}$	Time of peak rainfall
$t_{QMAX}$	Time of peak runoff
$U$	Mann-Whitney U coefficient
$u_a$	Pore air pressure
$u_w$	Pore water pressure
$V$	Flow of transpiration towards the leaf
$VS_t$	Smoothed volume of water in the runoff collection tank
$V_t$	Volume of water in the runoff collection tank
$z$	Height or depth
$\alpha$	Albedo
$\beta$	Empirical shape factor
$\gamma$	Psychrometric constant
$\delta$	Change
$\Delta$	Slope of saturation vapour pressure curve
$\delta f / \delta t$	Infiltration rate
$\varepsilon$	Empirical seasonal and vegetation coefficient

$\eta$	Viscosity of water
$\theta$	Volumetric soil moisture content
$\theta_{<PWP}$	Hygroscopic volumetric soil moisture content
$\theta_{FC}$	Volumetric soil moisture content at field capacity
$\theta_{LOW}$	Volumetric soil moisture content in lower zone of substrate
$\theta_{MAX}$	Maximum measured volumetric soil moisture content
$\theta_{MID}$	Volumetric soil moisture content in middle zone of substrate
$\theta_{PWP}$	Volumetric soil moisture content at permanent wilting point
$\theta_r$	Residual volumetric soil moisture content
$\theta_s$	Volumetric soil moisture content at saturation
$\theta_{TOP}$	Volumetric soil moisture content in upper zone of substrate
$\lambda$	Latent heat of vaporisation
$\mu$	Period
$\rho_w$	Density of water
$\sigma$	Surface tension
$\tau$	Empirical shape factor
$\varphi$	Contact angle
$\psi$	Soil-water potential
$\psi_f$	Soil-water potential at the wetting front
$\psi_g$	Gravitational soil-water potential
$\psi_m$	Matric soil-water potential
$\psi_o$	Osmotic potential
$\psi_s$	Soil-water potential at the surface
$\omega$	Empirical shape factor
$\chi$	Constant energy term in the Priestley-Taylor PET method



# 1 Introduction

## 1.1 Background

The recent trends of urbanization and climate change pose important challenges in urban areas. The risk of urban pluvial flooding has increased due to the replacement of moisture permeable landscapes with impermeable surfaces that are designed to divert rainwater away from its source as quickly as possible. During extreme storm events, traditional below-ground drainage networks often fail to cope with runoff from the increased impervious surface areas in urban spaces. Many drainage systems convey both storm and foul water. Surcharges in such systems can lead to overflows that cause untreated sewage to enter urban watercourses and pose significant public health risks. More resilient storm water management infrastructures are required.

Complementary drainage capacity is increasingly being provided through Sustainable Drainage Systems (SuDS). SuDS aim to control a greater proportion of rainwater at source, mimicking the pre-development hydrology of the site as closely as possible. The SuDS design philosophy relies upon multiple components acting within an interconnected network of devices. SuDS components will typically facilitate the storage, infiltration, conveyance and/or treatment of rainwater. SuDS designs consider not only hydraulic performance, but also the benefits to amenity, ecology and water quality. Regulatory frameworks in many countries either have been or are in the process of being updated to reflect the need for SuDS in new developments and to remove barriers to their uptake. Quantitative performance requirements are increasingly being prescribed through the publication of design standards.

Green roofs are a viable SuDS component because they can partly offset the loss of urban terrestrial landscape and help to maintain the site's pre-development hydrology through the effects of retention and detention of rainwater. In this context, retention refers to the volume of rainfall that is retained within the green roof system and does not leave the roof as runoff. The retention response is affected by the configuration, antecedent conditions and rainfall characteristics. Detention refers to the temporal delay that occurs between rain (that is not retained) falling on to the roof and emerging as runoff. Detention combines the effects of delays in runoff due to plant cover, vertical movement through the substrate, interactions between the plant roots and the substrate, horizontal transfer

across the drainage layer and, on a full-scale roof, the subsequent route into the collection system that is downstream of the roof.

The extent of the hydrological benefit that green roofs provide within a SuDS network is not well-quantified. A number of green roof hydrological research programmes have reported highly variable retention levels. However, this is to be expected when research has been conducted using different configurations in cities across the world (e.g. Sheffield, Tokyo, Auckland and Toronto). Runoff responses depend on a complex set of processes and interactions involving roof configuration (slope, aspect, drainage layer, substrate type and depth, and vegetation), rainfall characteristics (duration, depth, intensity) and antecedent conditions (in particular the role of evapotranspiration [ET] in restoring the system's moisture holding capacity).

Without the ability to predict hydrological performance with sufficient accuracy, design engineers are less likely to include green roofs within sustainable drainage strategies. Any transferable green roof hydrological model will require a physically-based ET prediction methodology that accounts for the simultaneous impact of climate, the nonlinear relationship between the soil moisture deficit (SMD) and ET and the divergent responses attributable to the physical characteristics of different green roof configurations.

This thesis specifically addressed a current research gap by identifying the influences of configuration, climate and moisture balance on the SMD at the start of an event and demonstrating how these influences can be accounted for in the modelling of runoff. Long-term field studies were combined with controlled condition tests.

## **1.2 Aims and objectives**

The overall aim of this thesis is to improve the understanding of the physical controls that affect a green roof's hydrological response, leading to the development of a model that accounts for the relevant physical parameters and processes. This will help to reduce the uncertainty that surrounds the quantitative hydrological performance of green roofs. An important objective of this thesis is to identify and model the complex inter-event processes that control the antecedent moisture condition of different green roof configurations and, when considered alongside rainfall characteristics, govern the retention response. Once the retention response has been identified, any runoff due to

excess rainfall can be modelled temporally via a detention modelling component. The time-series runoff predictions generated by the combined model will be of use to drainage engineers who must model the per-event response of green roofs within a catchment scale drainage network.

The following objectives are important to the realisation of the overall aim of this research:

1. To undertake a review of existing literature and research with a view to identifying (a) the physical parameters that influence the hydrological performance of a green roof and any relevant theoretical frameworks, and (b) the modelling requirements of drainage engineers and potentially suitable methods.
2. To characterise the vegetation treatments and substrates to explain observed responses through references to measured physical characteristics. As such, the results of this research can be meaningful for, and transferable to, other green roof configurations.
3. To generate an empirical data set to underpin analyses of hydrological performance of different green roof configurations; identifying the specific influences of configuration, rainfall characteristics and antecedent moisture conditions on the observed response.
4. To devise and conduct an experimental programme to evaluate the drying cycle behaviour of different green roof configurations independently from the incidence of rainfall, controlling the length of and climatic conditions during the antecedent dry weather period (ADWP).
5. To parameterize the two-stage model based on analyses of the experimentally-derived results for the drying and wetting cycles.
6. To apply the developed model to demonstrate its practical value to designers and its capacity to account for the physical influences that have been identified as important during this research.

### **1.3 Thesis structure and content**

The work reported here was carried out on a part-time basis between 2009 and 2016. This thesis contains eight chapters. Chapter 1 justifies the need for the research by providing a brief overview of the problem and outlines how this work aimed to address the identified problem.

Chapter 2 contains a review of the current literature. Initially, the need for additional complementary drainage capacity is outlined. Sustainable Drainage Systems (SuDS), and the regulations that govern their performance are briefly described. Green roofs, and their design, are introduced with a particular emphasis on their potential to act as a storm water management component. A detailed review of physical parameters that can influence the hydrological response of green roofs precedes a review of previous research findings relating to their quantitative hydrological contribution. Finally, current modelling methodologies are described and future modelling requirements identified.

Chapter 3 describes the important physical characteristics of the configurations that were tested as described in Chapters 4 and 5 and modelled as presented in Chapters 6 and 7.

Chapters 4 and 5 follow a similar structure. The experimental set-up and test configurations are introduced before outlining data collection methods and any assumptions required to convert raw data into the appropriate units. Results are then presented and discussed. The same nine configurations were used in both trials.

Chapter 4 outlines the experimental programme related to the hydrological responses of different green roof configurations at a field research site in Sheffield, UK. The site consisted of a weather station, rain gauges and nine green roof test beds (each 3 m<sup>2</sup> and individually gauged for runoff). The responses of nine test beds to 48 rainfall events are presented. Subsequent analyses identified the physical influences that led to the observed hydrological outcomes.

Chapter 5 contains the results and discussions relating to a further experimental programme concerning the regeneration of available moisture capacity through evapotranspiration. Settings in a climate-controlled laboratory replicated typical UK spring and summer conditions. Microcosms were established for each of the nine test beds and subjected to continuous dry weather periods of up to 28 days without irrigation. Load



cells continuously monitored the weight of each microcosm, initially at field capacity, throughout the ADWP. The change in mass was inferred as moisture lost by ET. The decay in ET (as a proportion of potential ET) was quantified with respect to time and moisture availability. Comparisons were made between the nine configurations, including analyses by vegetation and substrate type.

Chapter 6 combines the findings of previous chapters to develop, refine and validate a two-stage modelling approach. The retention model estimated any runoff from a volumetric perspective by considering rainfall and the available capacity at the onset of the event. This runoff volume was distributed temporally via a detention model. Potential refinements to the developed model were presented. Additional empirical factors were shown to offer marginal improvements in the accuracy of the model in reproducing observed responses of seasonal vegetation.

Chapter 7 contains the results of the application of the developed model to both continuous long-term (30 year) simulations and synthetic design storm events. The continuous simulation provides insights into the long-term retention responses of different vegetation treatments, including any expected requirement for irrigation. The application of the model to design storm events provides greater transparency of a green roof's potential SuDS contribution. The sensitivity of model outputs to changes in important modelling assumptions was assessed; identifying the need for clear guidance regarding the scenarios to be modelled within SuDS calculations.

Chapter 8 summarises the main conclusions of the work and relates the important findings back to the initial aims and objectives of this research. Recommendations are made for further work in related areas.

## **1.4 Publications**

As of July 2016, a total of four published journal papers and three conference papers have resulted from work contained in or related to this thesis. References for all research papers are presented below.

### **Chapter 4**

Berretta, C., Poë, S., Stovin, V. (2014a). Moisture content behaviour in extensive green roofs during dry periods: The influence of vegetation and substrate characteristics, *Journal of Hydrology*, 511, 374-386.

Stovin, V., Poë, S., De-Ville, S. and Berretta, C. (2015a). The influence of substrate and vegetation configuration on green roof hydrological performance, *Ecological Engineering*, 85, 159–172.

Poë, S., Stovin, V., Dunsiger, Z. (2011). The Impact of Green Roof Configuration on Hydrological Performance. Proceedings of the 12th International Conference on Urban Drainage. Porto Allegre, Brazil, 11-16 September.

Berretta, C., Poë, S., Stovin, V. (2014b). The Influence of Substrate and Vegetation on Extensive Green Roof Hydrological Performance. Proceedings of the 13th International Conference on Urban Drainage. Sarawak, Malaysia, 7-12 September.

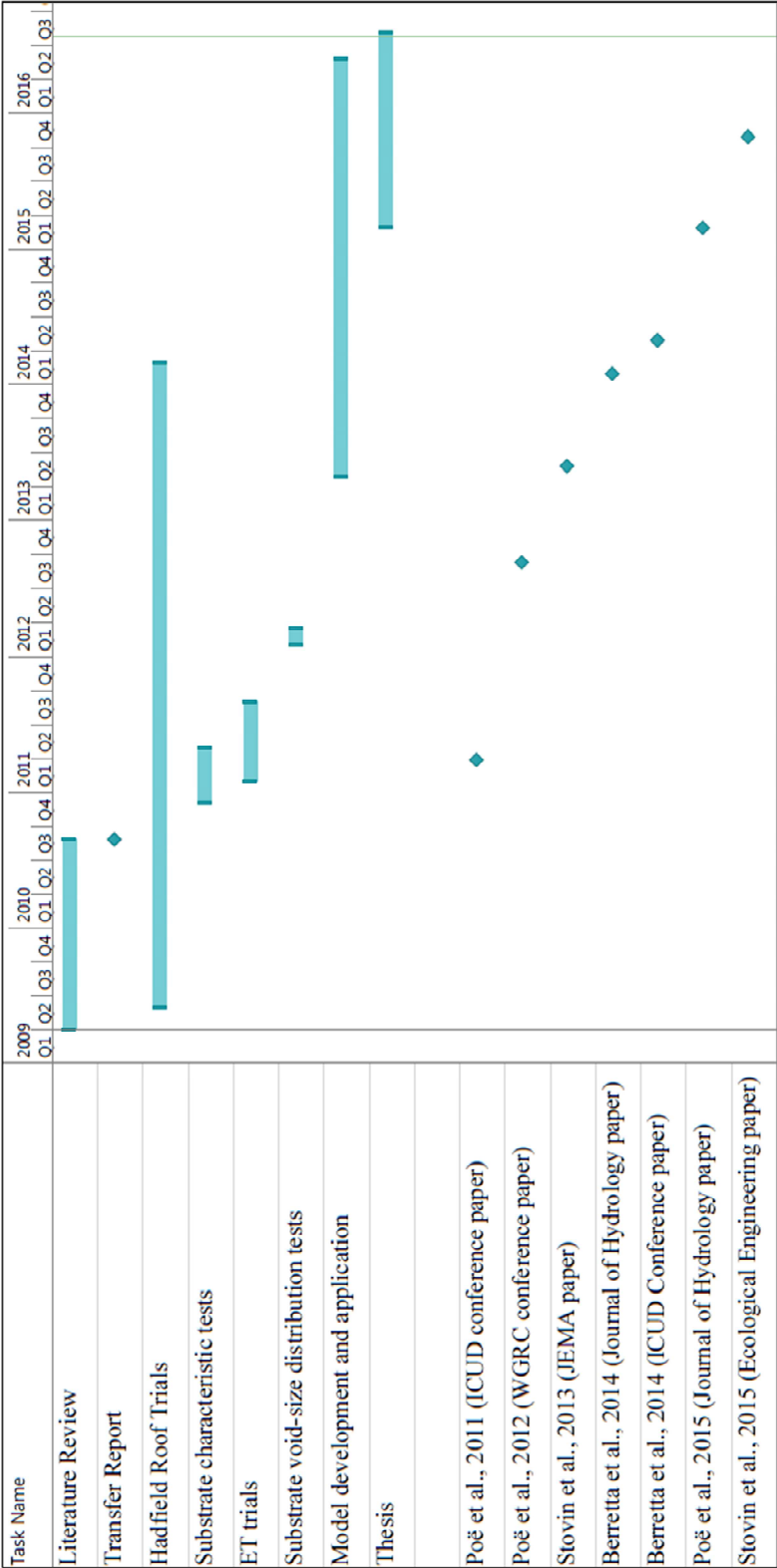
### **Chapter 5**

Poë, S., Stovin, V. and Berretta, C. (2015). Parameters influencing the regeneration of a green roof's retention capacity via evapotranspiration, *Journal of Hydrology*, 523, 356-367.

Poë, S., Stovin, V. (2012). Advocating a physically-based hydrological model for green roofs: Evapotranspiration during the drying cycle, Proceedings of the World Green Roof Congress, 18-21 September 2012, Copenhagen, Denmark.

### **Chapter 6 and 7**

Stovin, V., Poë, S. and Berretta, C. (2013). A modelling study of long term green roof retention performance, *Journal of Environmental Management*, 131, 206-215.



## 2 Literature review

### 2.1 Chapter overview

The practical and regulatory drivers for the expansion of the UK's storm water drainage capacity through the addition of complementary sustainable drainage measures will be reviewed prior to considering the conceptual contribution that green roofs can provide within a network of sustainable drainage systems (SuDS). The physical influences affecting the hydrological response of green roofs will be assessed through consideration of the previous research findings and explained with references back to the relevant theories. Finally, the methods employed to predict the hydrological response of green roofs, including the application of selected physical theories, will be evaluated.

### 2.2 Sustainable drainage systems (SuDS)

#### 2.2.1 Introduction to SuDS

SuDS are defined as “a sequence of management practices and control structures designed to drain surface water in a more sustainable fashion than some conventional techniques” (National SUDS Working Group, 2004). The key objectives of SuDS are to control surface water runoff volumes and flow rates so as to reduce the risk of flooding (DEFRA, 2011). Figure 2.1 highlights the conceptual sequence of control structures.

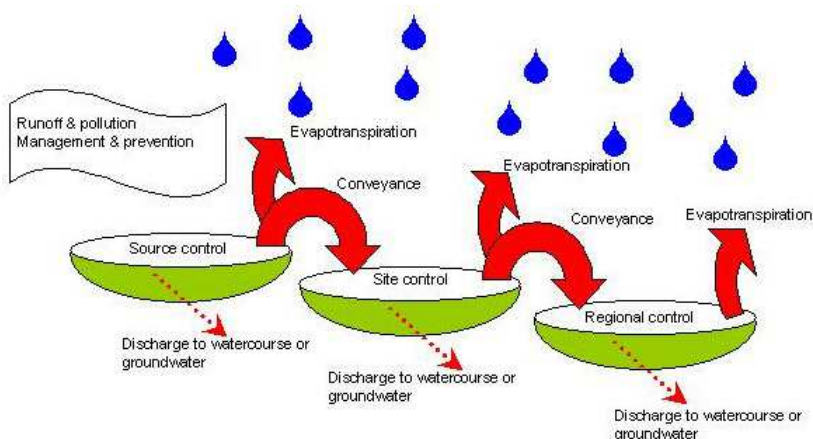


Figure 2.1: Conceptual SuDS management train

From <http://www.sudswales.com/education/background/the-suds-treatment-train/>  
(based on CIRIA, 2007b).

Ultimately, seeking to control a greater proportion of rainwater at source and replicating runoff from an equivalent greenfield site, SuDS will typically provide retention and detention benefits. Retention refers to withholding storm water for reduced discharge into watercourses (e.g. as a result of infiltration or evapotranspiration [ET]). Detention implies temporary storage, with an unchanged volume of storm water discharging at a later time and/or over an elongated period; thereby reducing peak runoff rates (Argue, 1986).

In this research project, the focus will be on the SuDS contribution of green roofs. However, green roofs will need to be combined with other SuDS devices if a more holistic drainage strategy is to be delivered to mitigate flood risk arising from more extreme rainfall events (Mentens *et al.*, 2006; Stovin *et al.*, 2013). Certain SuDS measures are applicable to individual buildings (i.e. rainwater harvesting, green roofs etc.), whereas others are more communal in nature (i.e. land drainage systems, swales etc.). Even for building-specific measures, there will be a downstream impact on the communal drainage system.

CIRIA (2015) provides detailed guidance on the range of potential components of a SuDS management train. The SuDS design philosophy relies upon multiple components acting within an interconnected network of devices. Each component will typically fulfil one or more of the six primary functions (CIRIA, 2015):

1. Rainwater harvesting: diverting rainwater from an impervious surface, through a filtration process, for storage within tanks (or polypropylene cellular products), from where it can be pumped back into the building or its surrounding vegetation for non-potable usage;
2. Pervious surfacing systems: pervious surfaces (i.e. permeable paving blocks, reinforced grass areas) that reduce the runoff that is conveyed to the drainage system by allowing water to seep through the surface into an underlying storage facility, from where it can either infiltrate the ground or be released to surface water;
3. Infiltration systems: allowing infiltration of water into the ground for slow release into the soil (e.g. infiltration trenches – shallow depressions in the surface where runoff can be stored until it infiltrates the soil – often used in conjunction with soakaways);

4. Conveyance systems: conveying flows to downstream storage systems and, where possible, providing flow and volume control and treatment. A common example is a swale – a broad, shallow, grassy channel that is designed to convey runoff to infiltration trenches;
5. Storage systems: controlling peak flows (and, where possible, reducing volumes of runoff) via storage and gradual release (attenuation), e.g. wetlands, detention basins, blue roofs etc.
6. Treatment systems: facilitating the removal or reduction of contaminant levels in runoff, typically involving a form of filtration or hydrodynamic separation.

Green roofs have a pervious surface and include a soil substitute that can provide storage and filtration benefits. Rainfall can be retained within the growing medium, from where it can either be returned to the atmosphere via ET or gradually released as runoff. The main quantitative metrics to evaluate the storm water management contribution by green roofs are runoff reduction, peak attenuation and peak delay (Versini *et al.*, 2015).

### **2.2.2 Drivers**

The UK's storm water drainage systems are antiquated and inadequate for the requirements of the expanding modern built environment. This was demonstrated during the pluvial flooding that was observed in 2007 (Ellis, 2010 in Nawaz *et al.*, 2015). In 2007, urban flooding was estimated to cost £270 million a year in England and Wales, with 80,000 homes at risk (POST, 2007). However, the floods that occurred later that year were estimated to have cost £4 billion (Environment Agency, 2010). Poor storm water management practices increase the risk of flooding, but other causes, such as fluvial flooding, must also be considered. UKCIP02 foresaw an increased frequency of localised flooding as a result of the greater summer rainfall intensity and higher winter rainfall volume (Greater London Authority, 2008). Without corrective action, by the 2080s the costs of urban flooding are projected to rise to as much as £10 billion a year (DEFRA, 2008). One in six properties in the UK (5.2 million) are classified as “at risk” of flooding and 3.8 million of these properties are at risk of surface water flooding (Environment Agency, 2009).

Approximately 40% of the UK's drainage infrastructure conveys both storm and foul water (POST, 2007). There are over 20,000 combined sewer overflow (CSO) discharges per annum in the UK (Nawaz *et al.*, 2015). CSOs can cause untreated sewage to enter urban watercourses, posing significant health risks (e.g. hepatitis A, E-Coli). However, upgrading the entire network is neither feasible nor practical. The Government's Water Strategy for England (published by DEFRA in 2008) acknowledged that "below-ground piped systems can never be built large enough to cope with the extreme rainfall events." Complementary measures that provide additional drainage capacity are therefore required.

### **2.2.3 SuDS regulations and performance standards**

Regulatory frameworks now reflect the need for Sustainable Drainage Systems (SuDS) in the UK's built environment. The Flood and Water Management Act (2010) placed responsibilities on the Environment Agency to develop and implement a national flood (and coastal erosion) risk management strategy. The Act (a) introduced requirements for new properties to include SuDS and for existing buildings to improve flood resistance and (b) removed key barriers to the uptake of SuDS (e.g. withdrawing the automatic right of connection to sewer, introducing a duty to adopt, and creating a legal framework for incentive schemes and enforcement powers).

National performance standards for SuDS (DEFRA, 2011) have been published to support building regulations and planning policies. A basic requirement is to avoid discharge to a surface water body or sewer during the first 5 mm of a rainfall event. Further quantitative limits – based upon equivalent greenfield runoff responses – are prescribed for the volume and peak rate of runoff that result from different design storm events (e.g. 1 in 1 year, 1 in 100 years). Designers can choose to restrict either (i) peak flow rates and the volume of runoff, such that greenfield responses are mimicked during 1 in 100 year events, or (ii) peak flow rates alone, limiting peak runoff to 2 litres per second per hectare (or the greenfield mean annual flood) for a 1 in 100 year event. Addressing the specific requirement for flood risk, clause D5 also stipulates that surcharges should not occur on the site during a 1 in 30 year rainfall event or in any part of a building (or neighbouring sites) during a 1 in 100 year event. These permitted runoff

rates are only expected to be achievable if attenuation measures, rainwater harvesting, infiltration systems and/or storage facilities are incorporated in the design (CIRIA, 2015).

## 2.3 Green roofs

### 2.3.1 Green roof configuration

The term “green roof” has many pseudonyms – living roof, brown roof, biodiverse roof, sedum roof, eco-roof, grass roof, turfed roof, vegetated roof etc. They are defined as roofs that have been “purposely fitted or cultivated with vegetation” (CIBSE, 2007). However, their scope has been further extended to encompass a range of landscaping options, including paved or bare soil surfaces.

Green roofs are constructed from a range of components that replicate the natural growing environment for plants, without requiring the same depth and weight of construction (see Figure 2.2).

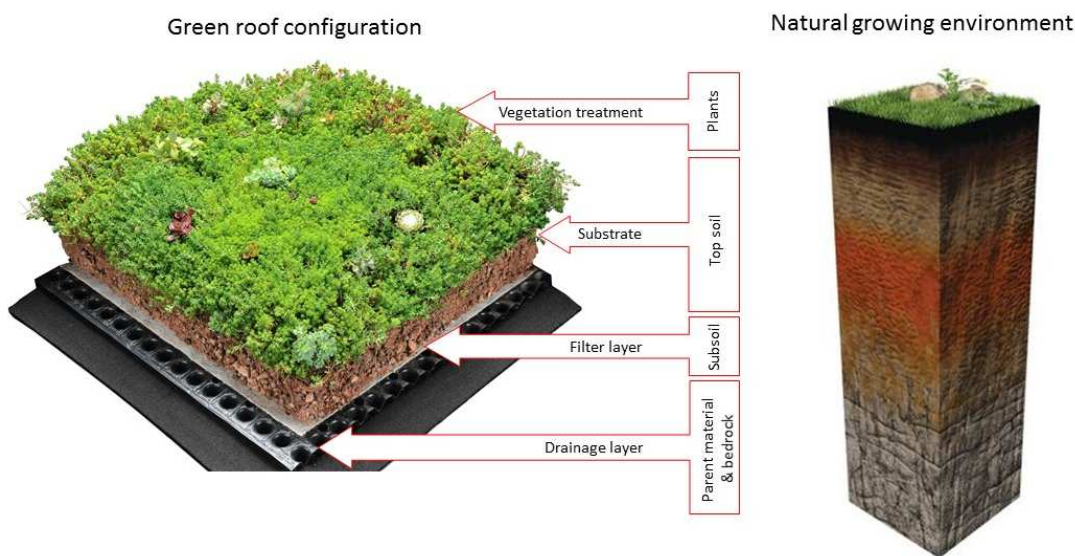


Figure 2.2: Replication of the natural growing environment in a green roof

(Adapted from <https://www.studyblue.com/notes/n/ap-environmental-science-study-guide-2013-14-hallman/deck/10441126>)

A green roof typically comprises, from the upper layer down:

- Vegetation: With an appropriate configuration (i.e. substrate composition and depth), a broad range of vegetation treatments can be accommodated within a green roof



system; ranging from hardy Sedum species and other succulents to more water-intensive herbaceous perennials, wildflowers, grasses, shrubs and lawns.



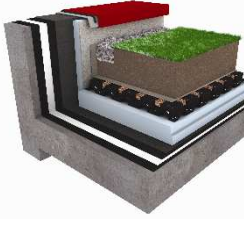
- **Substrates:** To replicate the function of a top soil in a natural landscape, a lightweight engineered substrate acts as a growing medium to plants, providing roots with the appropriate water, air and nutrient balance.
- **Filter Sheets:** Non-woven geotextiles that allow water to permeate through the system without the excessive downward loss of fines particles from within the overlying substrate.
- **Drainage layers:** The primary function of a drainage layer, much like bedrock in nature, is to convey excess gravitational water away from a green roof that is at field capacity (avoiding suffocation of the plants' roots) towards a receiving body. A green roof drainage layer is typically formed into a cusped profile using a synthetic material (e.g. HD-PE). Some cusped profiles facilitate a secondary function of storage; retaining moisture for diffusion back into the substrate during drought periods. Alternatively, mineral drainage layers can be used.

In addition to the four principal components of a green roof, the waterproofing integrity of the roof will be provided via a waterproofing layer, complete with an integral, or separate, root inhibitor. A range of commercial options are available, including bituminous or synthetic membranes and structural “hot melt” monolithic membranes, with life expectancies of up to 50 years.

### 2.3.2 Green roof classifications

There are three primary categories of green roofs; each varying according to its configuration and its intended purpose. These categories are summarised in Table 2.1.

Table 2.1: Green roof categories

Type	<i>Extensive/Biodiverse</i>	<i>Semi-intensive</i>	<i>Intensive</i>
			
<i>Figure 2.3: Typical green roof classifications (courtesy of Alumasc)</i>			
<b>Intended purposes:</b>			
	An ecological protection layer for: <ul style="list-style-type: none"> <li>▪ Wildlife habitat</li> <li>▪ Air &amp; Water quality</li> <li>▪ Lower carbon emissions</li> <li>▪ Storm water attenuation</li> </ul>	Increased diversity of plants affording increased colour all-year around	A roof affording benefits of a small urban park or domestic garden, offering recreational and amenity benefits
<b>Typical Configuration:</b>			
<i>Drainage Layer</i>	▪ 25 mm depth	▪ 40 mm depth	▪ 60 mm depth
<i>Substrate</i>	<ul style="list-style-type: none"> <li>▪ 50-80 mm depth</li> <li>▪ Low organic matter</li> <li>▪ Nutrient deficient</li> <li>▪ Highly permeable</li> </ul>	<ul style="list-style-type: none"> <li>▪ 80-150 mm depth</li> <li>▪ Higher organic matter</li> <li>▪ Medium permeability</li> </ul>	<ul style="list-style-type: none"> <li>▪ &gt;200 mm depth</li> <li>▪ Highest organic matter</li> <li>▪ Low permeability</li> </ul>
<i>Vegetation</i>	<ul style="list-style-type: none"> <li>▪ Sedum, herbs, grasses &amp; wildflowers</li> </ul>	<ul style="list-style-type: none"> <li>▪ Grasses, shrubs and woody plants</li> </ul>	<ul style="list-style-type: none"> <li>▪ Lawn, bushes, shrubs and small trees</li> <li>▪ Hard landscapes</li> <li>▪ Water features</li> </ul>
<b>Design Considerations:</b>			
<i>Weight</i>	60 – 155 kg / m <sup>2</sup>	190 – 225 kg / m <sup>2</sup>	200 kg / m <sup>2</sup> +
<i>Maintenance</i>	Minimal	Periodic	Regular
<i>Irrigation</i>	No	Periodic	Regular

The focus of this research project will be on the most widely implemented, extensive green roof type (Hakimdavar *et al.*, 2014). Extensive green roofs are suitable for a broad range of buildings due to their lightweight nature and low maintenance requirements.

### **2.3.3 Conceptual benefits of green roofs**

Conceptually, green roofs are suitable for inclusion in SuDS management trains. The four SuDS design criteria, developed by CIRIA (2007), indicate that consideration is not limited to hydraulic performance, but also extends to improvements in water quality, amenity benefits and ecological enhancements. Green roofs can provide some level of contribution against each of these criteria:

#### *2.3.3.1 Water quality improvement*

Precipitation generally has low pollution levels. Green roofs can filter pollutants (and nutrients) from water and act as “a source of phosphorous and potassium and a sink for nitrogen” (Berndtsson *et al.*, 2006). Previous research has highlighted the low quantities of heavy metals (excluding Zinc) in runoff from green roofs (Gobel *et al.*, 2007). However, the main improvement in the quality of runoff from green roofs is through the reduction of pollutant pick up by runoff on route to the receiving water body (Getter *et al.*, 2007). This reduction is associated with lower runoff volumes and velocities.

#### *2.3.3.2 Amenity benefits*

Amenity benefits are typically associated with intensive green roofs that provide green space (e.g. roof garden, communal parkland) for relaxation, recreation or entertainment. However, extensive green roofs still afford aesthetic and wellbeing benefits through increased access to green spaces (Banting *et al.*, 2004; Gedge & Frith, 2004; Wong *et al.*, 2003a). It has also been claimed that the cleaner and cooler air that green roofs can facilitate can bring about “reductions in a person’s heart rate and blood pressure, and can aid general well-being” (Gedge & Frith, 2004), whereas lack of greenery can increase stress levels (Zuberich, 2004 – in Banting *et al.*, 2004).

### 2.3.3.3 Ecological enhancements

Green roofs can provide a variety of ecological benefits:

#### a) Carbon Consumption

A green roof can help to both reduce carbon emissions from a building and capture carbon locally. A green roof cannot be specified in place of thermal insulation (Wong *et al.*, 2003). However, green roofs can (i) reduce heat conduction into buildings (Liu & Minor, 2005) and (ii) absorb solar radiation as a result of the processes of photosynthesis, respiration, transpiration and evaporation from green roof vegetation (Niachou *et al.*, 2001). The scale of the impact upon carbon reduction will depend upon individual building characteristics, such as the size and use (Sonne, 2006), the efficiency of the heating or cooling equipment (Liu & Minor, 2005), roof insulation levels (Niachou *et al.*, 2001) and also the green roof configuration (Del Barrio, 1998). There is uncertainty surrounding the level of reductions in energy use that can be achieved with a green roof. Estimated savings range from 4.15 kWh/m<sup>2</sup>/year in Toronto (Banting *et al.*, 2004) to 30 kWh/m<sup>2</sup>/year in Canary Wharf, London (Greater London Authority [GLA], 2008). Further work is required here. GLA (2008) equates 0.43 kg of carbon dioxide reduction to every kWh of energy. This would suggest that between 1.8 and 12.9 kg CO<sub>2</sub>/m<sup>2</sup>/year could be saved by green roofs.

#### b) Urban Heat Island Effect (UHIE) Reduction

Urban Heat Islands are created in urban areas as a result of (i) increased storage of sensible heat (due to the reduced area of evaporating surfaces), (ii) greater long-wave radiation (due to interchange between tall buildings), (iii) reduced turbulent heat transfer in urban streets and (iv) anthropogenic heat release caused by fuel combustion and the metabolism of people and animals (Santamouris *et al.*, 2007). It is believed that “the centre of London can experience temperatures up to 9 °C higher than the surrounding greenbelt” (GLA, 2008). Higher temperatures affect health and comfort, produce high air pollution levels and lead to increased energy demand and water consumption (Solecki *et al.*, 2005; Synnefa *et al.*, 2007). There are two recognised means of reducing UHIE (CIRIA, 2007) – increasing vegetation and increasing roof reflectivity (albedo). Green roofs fulfil both functions and are therefore “increasingly being proposed as mitigation for the UHIE” (CIRIA, 2007). However, “localised and

sporadic implementation of green roofs will not result in reduction” (Banting *et al.*, 2004). For every degree reduction in the UHIE, GLA (2008) estimates energy savings of approximately 495 kWh for the Greater London area. Banting *et al.* (2004) believe that realistic reductions of between 0.5 °C and 2.0 °C would yield energy savings of 2.37 kWh/m<sup>2</sup>/year, given sufficient green roofing in Toronto.

c) Air Quality Improvement

Green roofs have the potential to improve air quality in densely-populated urban areas (Carter & Keeler, 2008). Green roofs can trap particulates and capture gases, such as nitrogen oxide, ozone and carbon monoxide (Banting *et al.*, 2004). Localised reductions in air temperature, as a result of the cooling effect associated with plant transpiration, can also benefit air pollution levels during extreme summer conditions.

d) Biodiversity

Biodiversity is important to the quality of life (DEFRA, 2002b) and is fundamentally important to the field of medicine. Ecologists and economists conservatively estimated the value of nature to society to be \$33 trillion per annum (Costanza *et al.*, 1997). The loss of habitat is the greatest threat to biodiversity (Costanza *et al.*, 1997). The increased tendency towards urbanisation (DEFRA, 2002) typically leads to the replacement of soft, vegetated landscapes with hard surfaces (Lundholm, 2007). The restoration or creation of compensatory habitats is therefore necessary to minimise biodiversity loss. Green roofs cannot directly replace ground-based habitats. However, they can form green corridors that are designed to provide food and habitat for creatures displaced by urban development (Brenneisen, 2003; Gedge, 2003). The beneficiaries would include a number of species that are of conservation concern (Grant *et al.*, 2003) and/or listed in biodiversity action plans.

#### 2.3.3.4 *Hydraulic performance*

Whilst roof greening in isolation will never fully solve the urban runoff problem (Mentens *et al.*, 2006), green roofs can act as a viable SuDS device (Jennings *et al.*, 2003), controlling rainfall at source in urban areas. Here, high land prices make ground-level urban greenery expensive or impossible (Mentens *et al.*, 2006) and roofs contribute significant land area (Carter & Keeler, 2008). An estimated 200,000,000 m<sup>2</sup> of roof space

in UK city centres would be suitable for roof greening with little or no structural modification (The Green Roof Guide: <http://www.greenroofguide.co.uk/what-are-green-roofs>, accessed 21 January 2016).

Green roofs have the potential to reduce storm water problems in UK cities (CIBSE, 2007) in the following ways (Tarr, 2002 in GLA, 2008):

- Storage of rainwater in substrate, drainage layers and on plants;
- Photosynthesis – biochemical incorporation of water by plants;
- Evapotranspiration – uptake of water and release by plants as vapour and/or evaporation from the substrate and foliage.

Green roofs can therefore reduce rainfall runoff rates due to the plant cover (by interception), the substrate (by detention and retention for ET) and the additional storage capacity in the underlying drainage reservoir. However, the extent of the hydrological benefit that green roofs provide within the Sustainable Drainage Systems (SuDS) management train is not well-quantified. A number of green roof hydrological research programmes, typically from temperate mid-latitudes, have reported variable retention levels – with mean annual retention typically between 30 and 86% (Li & Babcock, 2014) and per-event retention between 0 and 100% (Berghage *et al.*, 2007; Stovin *et al.*, 2012). There are, however, physical influences that affect the hydrological response. These factors will now be reviewed.

## **2.4 Physical influences upon hydrological response**

The moisture balance of a green roof is an important control upon its hydrological performance. The storage capacity, and the extent to which it is available at the start of a rainfall event, is an important influence upon a green roof's hydrological response (Stovin *et al.*, 2012; Bengtsson *et al.*, 2005; DeNardo *et al.*, 2005; Stovin *et al.*, 2013).

The configuration of the green roof is important both to the maximum storage capacity and to the residual moisture content at the onset of a rainfall event (Bengtsson *et al.*, 2005; DeNardo *et al.*, 2005; Stovin *et al.*, 2013). The storage capacity of a green roof is typically the aggregate of the storage volume within three different elements: vegetation, substrate and the reservoir layer (also known as a drainage layer). However, the characteristics of

the substrate (Getter *et al.*, 2007; Miller, 2003; Graceson *et al.*, 2014; Madre *et al.*, 2014; Carbone *et al.*, 2015) and the vegetation treatment (Rowe *et al.*, 2012; Farrell *et al.*, 2012; Whitinghill *et al.*, 2014; Vanuytrecht *et al.*, 2014; MacIvor & Lundholm, 2011) are believed to be the more important factors affecting the moisture balance, as this is where capacity is typically regenerated via ET.

External influences also affect moisture balance:

- The incidence of precipitation, i.e. rainfall depth and intensity (Carter & Rasmussen, 2006; Palla *et al.*, 2009; Stovin *et al.*, 2012; Fassman-Beck *et al.*, 2013).
- Climatic factors affect the availability of latent heat energy to cause evaporation (Mentens *et al.*, 2006; Villareal, 2007; Berghage *et al.*, 2009).

First, the forces that drive or resist soil-water movement (i.e. the retention and release tendencies of the vegetation and growing media) will be considered. Their relevance to a green roof's hydrological response (Koehler & Schmidt, 2008) will then be demonstrated.

#### **2.4.1 Fundamental soil-water physics**

Manning (1987) summarised the soil-water flows through porous media as:

- 1) Moisture is drawn into the soil matrix due to molecular forces.
- 2) Strong hydrogen bonds form to create strong adhesive matric forces that lead to adsorption of water to the particle.
- 3) Surface tension creates cohesive matric forces that cause water to fill the small pores (capillary water).
- 4) As further water enters the soil matrix, larger pores fill with water until such time as gravity dominates, creating saturated flow conditions and destroying menisci at the air-water interfaces to force water downwards and out of the soil.
- 5) Gravitational water leaves the soil matrix until equilibrium is reached between the gravitational potential,  $\psi_g$ , and matric potential,  $\psi_m$  (at between -5 kPa and -30 kPa). Here, the soil is at field capacity ( $\theta_{FC}$ , where unsaturated flow conditions prevail). As water continues to leave the soil, through capillary action causing drying,  $\psi_m$  becomes

increasingly negative, retaining water with ever greater tenacity until permanent wilting point,  $\theta_{PWP}$ , is reached (at approximately -1500 kPa).

These processes will now be considered in further detail.

Darcy's law (1856) states that the rate of soil-water flow through a porous medium will be proportionate to the pressure gradient in the soil (i.e. the difference in hydraulic head, which is the sum of the pressure and elevation heads) and dependent upon the permeability of the soil:

$$q = -\left(\frac{\delta h}{\delta z}\right) \cdot K \quad \text{Equation 2.1}$$

Where:

- $q$  = flow rate (L/T)
- $\delta h$  = Difference in hydraulic head
- $\delta z$  = Distance between two points (L)
- $K$  = hydraulic conductivity (L/T)

Darcy's law is relatively simple to apply to saturated media. However, Buckingham (1907) identified that hydraulic conductivity varied as a function of moisture content in partially saturated soils (see Figure 2.4).

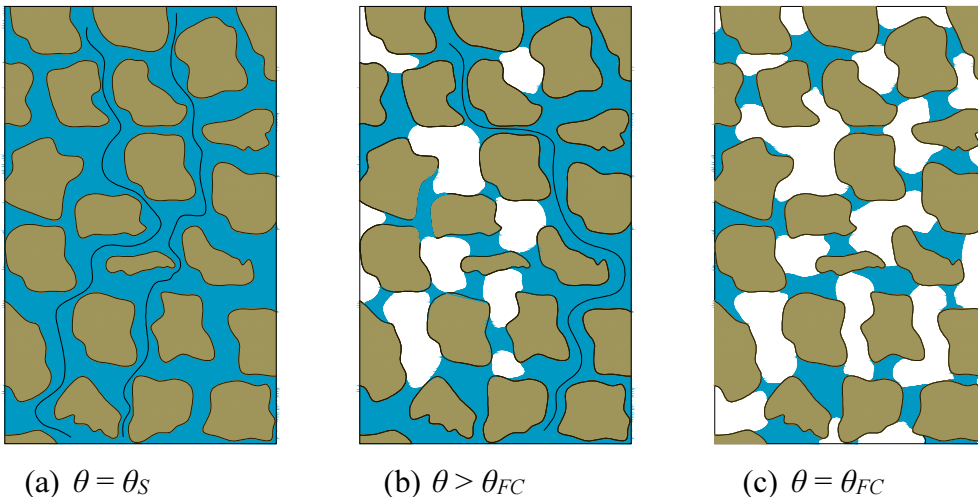


Figure 2.4: Tortuosity of flow through variably saturated media

At saturation ( $\theta_s$ ), tortuosity (i.e. the length of the flow paths) is expected to be negligible. However, once air starts to fill the pores, replacing water, tortuosity will increase until no continuous water pathways exist and greater drag forces occur between the water and the



soil matrix. Buckingham (1907) published an equation that is typically referred to as the Darcy-Buckingham equation:

$$q = -K(\psi) \frac{\delta h}{\delta z} \quad \text{Equation 2.2}$$

Where  $k(\psi)$  is the unsaturated hydraulic conductivity and  $\delta h$  divided by  $\delta z$  is the hydraulic gradient in the direction of flow.

Buckingham introduced the concept that soil-water flow is driven by potential energy and that the two key soil-water relationships are moisture content-potential,  $\theta(\psi)$ , and hydraulic conductivity-moisture content,  $K(\theta)$ . With soil-water movement tending to be slow, kinetic energy can be discounted as a driver of soil-water flux (White, 1997). Potential energy is the most important factor in determining the status and movement of soil-water (Brady & Weil, 2008). The gradient of potential energy with distance between points is the force that causes flux (Hillel, 1998). Flow is (i) directly proportional to this driving force, and (ii) inversely related to the resistance to flow (i.e. the hydraulic conductivity) (White, 1997). Thermodynamic laws dictate that soil moisture will move out of areas with high (less negative) water potential towards low (more highly negative) potential.

There are four types of potential energy – osmotic, gravitational, matric and pressure potential. However, due to the highly permeable nature of green roofs, the pressure potential (that would result from surface ponding) can be neglected.

#### 1. Osmotic Potential ( $\psi_o$ )

An osmotic pressure difference between fluid in plant roots and pore-water is the driving force for the extraction of water from soil by the plants (Manning, 1987). Transpiration occurs when vapour pressure in the air is less than in the leaf cells. A plant's root system absorbs soil-water, trans-locating it through the xylem to stomatal cavities in the leaf, where it is vaporised by radiant and sensible heat energy from the sun. This water loss produces a deficit in the leaf cells that translates into a suction (osmotic) force being transmitted back to the root. The driving forces for and resistances against transpiration are summarized by van den Honert (1948) in Equation 2.3:

$$V = \frac{\psi_{soil} - \psi_{root}}{R_{cortex}} = \frac{\psi_{root} - \psi_{leaf}}{R_{xylem}} = \frac{\psi_{leaf} - \psi_{air}}{R_{stoma}} \quad \text{Equation 2.3}$$

Where  $V$  is the flow of transpiration towards the leaf.

$$\psi_o = -\frac{R_u T_{ABS}}{V} \ln\left(\frac{P_1}{P_0}\right) \quad \text{Equation 2.4}$$

Where  $R_u$  is the ideal gas constant,  $T_{ABS}$  is the absolute temperature,  $P_1$  and  $P_0$  are the partial pressures of water vapour in equilibrium with free water at the two points being considered.

As water is absorbed by the roots, so  $\theta$  reduces, increasing  $\psi_m$  in the surrounding soil and attracting water towards the higher  $\psi_m$  in the root zone (at a rate dependent upon the potential gradient and hydraulic conductivity of the soil). The uptake of water by plant roots therefore cannot be ignored (Raats, 2001) However, soil-water movement can be predominantly attributed to  $\psi_g$  and  $\psi_m$  (Manning, 1987) as they will typically dominate in saturated and variably-saturated conditions respectively.

## 2. Gravitational Potential ( $\psi_g$ )

Gravitational potential ( $\psi_g$ ) will be dictated by the volume and elevation of soil-water:

$$\psi_g = \rho_w \cdot g \cdot \delta z \quad \text{Equation 2.5}$$

Where  $g$  is the acceleration due to gravity ( $9.81 \text{ m/s}^2$ ) and  $\rho_w$  is the density of water.

## 3. Matric Potential ( $\psi_m$ )

In variably saturated soils, the largest pores (macro pores) will typically be air-filled. Water movement will be confined to micro pores and the matric potential ( $\psi_m$ ) gradient between two points will be the driving force for any moisture flux. There are no simple methods of deriving absolute values, but generally  $\psi_m$  reflects the difference in pore air pressure ( $u_a$ ) and pore water pressure ( $u_w$ ):

$$\psi_m = u_a - u_w \quad \text{Equation 2.6}$$

The differential in pressure at the air-water interface occurs due to the hydrogen bonding that results from the polarity of water molecules. Adhesion is the attraction of water

molecules to solid surfaces. These forces are very strong but are only effective close to the soil surfaces; such that only a very thin film of moisture can form. Cohesion is the force of attraction of water molecules to each other. As Figure 2.5 demonstrates, cohesive forces allow the soil to indirectly restrict the freedom of water beyond the soil-liquid interface (Brady & Weil, 2008).

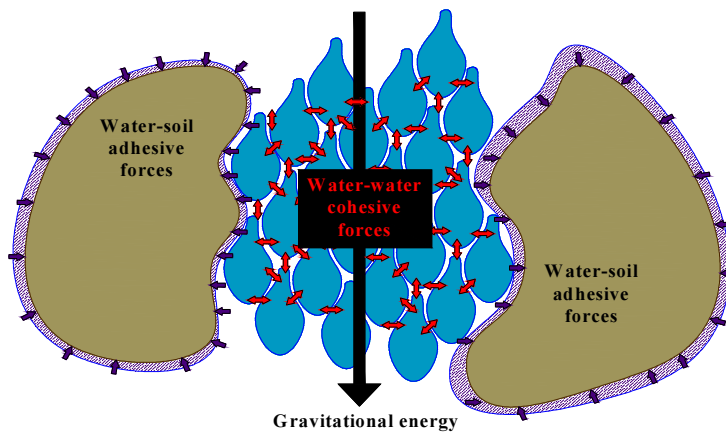


Figure 2.5: Balance of forces in pore-water

Adhesive-cohesive forces give rise to surface tension and capillarity. Air in soil is typically at atmospheric pressure (i.e. nominally zero), but the pressure of matric water is negative, creating a pressure differential that creates surface tension ( $\sigma$ ) and leads to the formation of menisci at the air-water interface (see Figure 2.6).

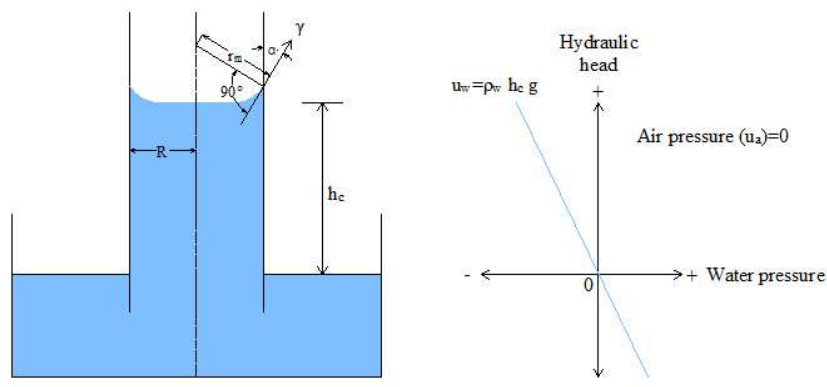


Figure 2.6: Capillary rise due to matric potential

Capillary rise originates due to the surface tension at the air-water interface. Capillary rise ( $h_c$ ) can be determined mathematically by using the capillary function (see Equation 2.7).

$$h_c = \frac{2 \cdot \sigma \cdot \cos\varphi}{\rho_w \cdot g \cdot r_m} \quad \text{Equation 2.7}$$

Where:

- $\sigma$  = surface tension (F/L)  
 $\rho_w$  = density of water (M/L<sup>3</sup>)  
 $\varphi$  = contact angle  
 $r_m$  = radius of the meniscus at the air-water interface (L)

As soil-water water is withdrawn from the soil, moisture is increasingly retained within the smallest pores, and so the meniscus radii,  $r_m$ , will reduce. Consequently, the pressure differential (and  $\psi_m$ ) increases exponentially (see Figure 2.7).

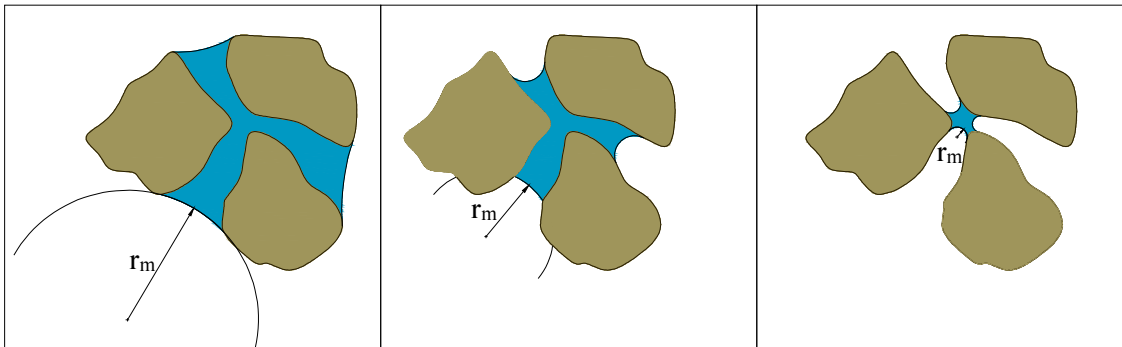


Figure 2.7: The effect of moisture content upon meniscus radii,  $r_m$

The soil-water characteristic curve (SWCC) represents the relationship between  $\theta$  and  $\psi_m$  for a soil. The SWCC is related to the size and interconnectivity of a soil's pores, and therefore, to its structure and texture. The relationship between  $\theta$  and  $\psi$  is not unique, but is influenced by historical wetting and drying. This phenomenon is known as hysteresis. Hysteresis has a number of potential causes (Tuller *et al.*, 1999):

1. Different soil-water contact angles for advancing and receding menisci;
2. Non-uniform shapes and arrangements of interconnected pores – pores dry via the smaller radius whereas they are wetted through the largest. This is often referred to as the 'ink bottle' effect;
3. Entrapment of air in pores; and
4. Shrinkage and swelling of the soil particles.

### 2.4.2 The influence of substrate upon moisture balance

An important proportion of a green roof's moisture storage capacity is provided within the substrate. The hydrological response to a storm event will therefore be strongly influenced by the physical characteristics of the growing medium (Carbone *et al.*, 2015). Green roof growing media differ from ground soils in that they are highly engineered, lightweight growing media, typically of higher mineral content, highly aerated and with few fine particles (Friedrich, 2005). Their primary functions are to provide the appropriate balance of air, water and nutrients to support vegetation. However, from a hydrological perspective, the important characteristics of growing media include porosity, permeability, field capacity and permanent wilting point (Beattie & Berghage, 2004).

#### 2.4.2.1 Substrate structure

Porosity largely dictates a soil's capacity for water and air. A balance of approximately 40% water holding capacity and 20% aerated pore space at saturation is ideal for a plant's needs on green roofs (Beattie & Berghage, 2004). To obtain this water-air balance, the substrate will need to be configured with particles that facilitate the appropriate proportions of different pore sizes to serve specific functions (Rowell, 1994):

- Transmission pores ( $>50 \mu\text{m}$ ) – macro pores that ensure drainage following saturation, aeration of the growing media at  $\theta_{FC}$  and facilitate root penetration should constitute a minimum 10% of the growing media's volume.
- Storage pores ( $0.2\text{-}50 \mu\text{m}$ ) – micro pores that store water for plant consumption should represent a minimum of 15% of the volume.
- Residual pores ( $<0.2 \mu\text{m}$ ) – micro pores where water is held so tightly that it is not available to plants, but largely dictates the mechanical strength of the soil should comprise a maximum 20% of the volume.

The relative proportion of transmission, storage and residual pores will dictate the two key hydrological states that govern available water limits:

1. Field capacity ( $\theta_{FC}$ ) – the maximum volume of soil-water that can resist gravity to remain in the substrate following a storm event. Here, matric potential is broadly in equilibrium with gravitational potential. At this stage, water will have

vacated macro pores, yet remains in micro pores, from where capillary forces can subsequently induce slow water movement.

2. Permanent wilting point ( $\theta_{PWP}$ ) – the volume of soil-water that is retained in the soil with such high matric pressure that the plants' suction forces are insufficient to extract any further moisture. As a result, plants will permanently wilt (but not necessarily die). Transmission and storage pores are empty.

The difference between these two boundary states reflects the maximum storage capacity of the green roof ( $S_{MAX}$ ). However,  $S_{MAX}$  will seldom be fully available (Berghage *et al.*, 2007; Stovin *et al.*, 2012) due to the presence of residual stored moisture,  $S_t$  (Koehler & Schmidt, 2008). During dry periods between rainfall events,  $S_t$  is depleted via ET at rates that are, in part, dependent upon the substrate's inter-particle pore-space distribution (Graceson *et al.*, 2013). ET rates are expected to decay exponentially with respect to time (Fassman & Simcock, 2011; Kasmin *et al.*, 2010) as available moisture reduces. Substrates therefore need to have a well-graded distribution of particle (and void) sizes to ensure adequate retention, sufficient drainage and increasing resistance to soil-water movement as soil-water content falls (Miller, 2003). As *Equation 2.7* demonstrated, capillary pressures are partially dependent upon pore sizes. Capillary pressures are inversely related to pore size (see Figure 2.8).

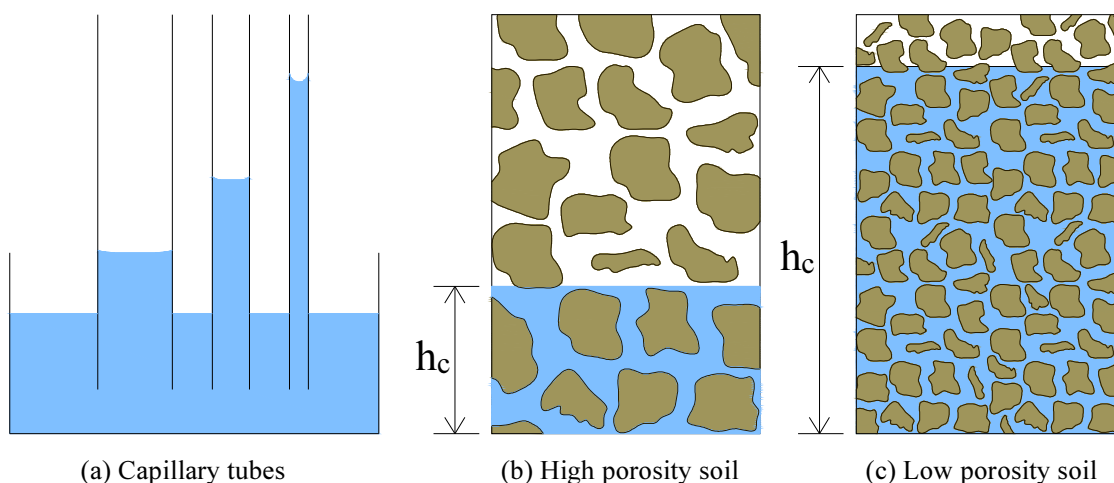


Figure 2.8: The importance of pore sizes to capillary rise

The capillary tubes analogy demonstrates that a cylinder with a smaller radius will typically facilitate greater capillary rise than cylinders with larger radii. The same will apply to pores in soil matrices; such that more highly negative pressures exist in the small

pores. Capillary rise will therefore be lowest in the most permeable substrates and highest in substrates with low hydraulic conductivity. Whilst the potential height of capillary rise does not provide any indication of the temporal rate of rise, the Lucas-Washburn-Rideal equation (Lucas, 1918; Washburn, 1921; Rideal, 1922) highlighted that pore radii and surface tension are also important controls on the rates of capillary rise. Furthermore, Poiseuille's law demonstrates that the rate of water movement through a soil during wetting will also be dependent upon the pore-size; with the flow rate being proportionate to the fourth power of the radius of the pore:

$$q = \frac{\pi r^4}{8\eta} \left( \frac{-\delta h}{\delta z} \right) \quad \text{Equation 2.8}$$

Where  $r$  is the radius of the pore and  $\eta$  is the viscosity of water.

The hydrological performance of any substrate will therefore be governed by the size, shape and arrangement of growing media particles and associated voids (Miller, 2003) in conjunction with the soil's chemical composition and texture.

#### 2.4.2.2 Substrate texture

Variable hydrogen bonding between the water and soils of different composition affects the absorptive, adsorptive and desorption behaviour of the green roof. Adhesion of water to minerals is typically less than that of water to organic matter (OM). The texture of the soil is a particular influence at high matric pressures, where moisture is primarily retained by adsorption. However, soil structure (and void-size distribution [VSD] in particular), are important at low matric suctions (i.e. 0 to -100 kPa), where  $\theta$  is retained as capillary water (Hillel, 1998). A higher proportion of inorganic material (e.g. crushed brick) will limit biomass growth (Graceson *et al.*, 2014) and constrain plant growth (Vijayaraghavan & Raja, 2014). Yet, a higher OM content can facilitate a greater shoot biomass of the vegetation (Graceson *et al.*, 2014). The maximum retention capacity of the green roof can therefore be increased (Graceson *et al.*, 2014; Carbone *et al.*, 2015), but the permeability reduced (Carbone *et al.*, 2015), by increasing OM content within a substrate, as a result of (i) greater adhesive forces in the substrate, and (ii) higher biomass.

The fact that a substrate's OM content is expected to increase over time (Getter *et al.*, 2007; Berndtsson *et al.*, 2010) could potentially explain why retention is often reported

to be higher from older green roofs (i.e. due to the associated greater moisture capacity) (Getter *et al.*, 2007).

#### 2.4.2.3 Substrate depth

The depth of a substrate affects (a) the substrate's maximum storage capacity (Nagase & Dunnett, 2011), and (b) the diversity of colonizing plants that can survive in the green roof (Madre *et al.*, 2014). A broader range of species and taller plants are feasible with deeper substrates (Fassman & Simcock, 2012) due to the greater plant-available moisture and reduced drought stress risk (Fassman *et al.*, 2010).

However, from a storm water management perspective, the extent to which this additional capacity mitigates runoff will vary (Clark *et al.*, 2008) depending upon:

1. The incidence of rainfall (Fassman-Beck *et al.*, 2013). The incremental capacity of the deeper substrate will only retain additional rainfall when the rainfall depth is sufficient to exceed the available storage capacity of the shallower construction. Often, a deeper substrate will retain moisture for a longer period of time, limiting the effectiveness of a deeper substrate to regenerate its available retention capacity (Clark *et al.*, 2008); and
2. The physiological behaviour of the vegetation (Lu *et al.*, 2015). Increasing the depth of substrate for shallow-rooted plants will be of limited benefit (Lu *et al.*, 2015). Indeed, moisture retention may be higher in the shallower substrate, due to the higher root mortality and associated accumulation of biomass (Lu *et al.*, 2015).

#### 2.4.3 The hydrological importance of a configuration's vegetation treatment

Vegetation directly contributes to the hydrological performance of a green roof via (i) the interception of rainfall by its foliage, (ii) evaporation and (iii) transpiration. The extent of this contribution will be influenced by the specific physical and physiological characteristics of the vegetation type (Berghage *et al.*, 2007; Whittinghill *et al.*, 2014). The physical properties, or 'architecture' of a plant will largely govern the extent to which it can intercept rainfall for subsequent evaporation. A plant's physiology will affect the rate at which transpiration of moisture occurs from within the soil matrix. These two characteristics will now be considered in further detail.



#### 2.4.3.1 *Plant architecture*

Initial interception and evaporation losses are affected by the effective leaf surface area, which is dependent upon the leaf exposure and shape. A greater total leaf area will typically result in higher interception by and evaporation from the canopy (Koshimizu, 2008; MacIvor & Lundholm, 2011). The total surface area of a vegetated canopy will therefore typically exceed that of the soil beneath, providing a greater bearing surface for water to be intercepted and evaporated. Mat-forming low-lying vegetation treatments will typically intercept more rainfall than a coverage comprising of tall, thin vegetation, but less than a canopy of broadleaf plants (Dunnett *et al.*, 2008; Lundholm *et al.*, 2010; Nagase & Dunnett, 2012).

Yet, in contrasting the performance of vegetated and non-vegetated roofs, findings have been inconclusive. Whilst a fully established vegetation treatment would typically have a coverage in excess of 80% (Fassman-Beck *et al.*, 2013), Morgan *et al.* (2013) observed that the incorporation of vegetation benefitted a green roof's hydrological performance provided that the coverage exceeded 20%. This improved response observed from vegetated configurations would be consistent with (a) the findings of Ouldboukhidine *et al.* (2012) and Berghage *et al.* (2007), who observed higher ET from vegetated configurations (until plant-available water restricted further ET), and (b) the greater overall capacity of a vegetated configuration (Wadzuk *et al.*, 2013).

Conversely, MacIvor & Lundholm (2011) concluded that non-vegetated roofs retained more rainfall than most green roofs with vegetation. One potential explanation for this would be the different responses to solar radiation (Rowe *et al.*, 2012). In a vegetated configuration, less than 20% of solar radiation would be expected to be transmitted to the growing medium, with up to 30% reflected and 60% absorbed through photosynthesis (Weng *et al.*, 2004 in Berardi *et al.*, 2014). However, the lower albedo of dark bare substrate surfaces would typically be associated with (i) lower reflectivity, (ii) lower absorption due to the absence of plant photosynthesis, and therefore (iii) higher transmission of solar radiation to the substrate; increasing evaporation potential. A further potential contributing factor influencing this conclusion could be that non-vegetated configurations would typically have a higher surface roughness compared with vegetated surfaces (Chorley, 1969). The resulting effect of reducing turbulent air flow

and increasing aerodynamic resistance would also encourage greater evaporation. It would therefore appear that a trade-off is to be expected between the increased interception storage and transpiration associated with a vegetated configuration and the faster evaporation from non-vegetated configurations.

#### 2.4.3.2 *Plant physiology*

A plant's physiology affects the storage of water in its plant tissues and the subsequent transpiration of vapour through its stomata. Transpiration levels are largely governed by the root structure (MacIvor & Lundholm, 2011), leaf succulence (Farrell *et al.*, 2012) and type of photosynthesis (Berardi *et al.*, 2014). The availability of moisture within the substrate (Nyambayo & Potts, 2010) will also be an important control.

#### **Root structure**

Sedum vegetation is generally considered to have high drought tolerance (Berardi *et al.*, 2014; Wadzuk *et al.*, 2013). Many Sedum species have shallow root systems (Farrell *et al.*, 2012) that result from their slow growth tendency (Nagase & Dunnett, 2011). The associated low biomass is related to the high survival rate of Sedum in drought conditions (Farrell *et al.*, 2012). Conversely, grasses and forbs will tend to have larger roots and increased biomass. These roots fill large voids in the substrate, increasing moisture capacity (Nagase & Dunnett, 2011). However, large roots will typically result in poor drought tolerance (Lu *et al.*, 2014). During prolonged drought periods, herbs and grasses will typically require additional irrigation (Rowe *et al.*, 2012). Subject to the incidence of rainfall, such additional irrigation could reduce the available moisture capacity, to the potential detriment of storm water retention (Fassman-Beck *et al.*, 2013).

#### **Leaf succulence**

Wadzuk *et al.* (2013) highlighted that succulents can store between 1 and 10 mm of moisture within the leaf structure (although it was not clear whether this was per plant or per square metre of vegetation). Leaf succulence provides an additional sink (absorbing significant water volumes by swelling in size [Berghage *et al.*, 2007]) and source of moisture. This additional moisture source can encourage plant survival during prolonged drought periods, when the soil moisture content is restrictive to plant water uptake via the roots (van Willert, 1992 in Farrell *et al.*, 2012).

### **CAM photosynthesis**

Plants that have crassulacean acid metabolism (CAM) are typically more drought tolerant than 95% of plant species (Voyde *et al.*, 2010b). Plants consume water by opening stomata. CAM plants open their stomata to metabolise at night when temperatures are cooler. Evaporative loss is therefore expected to be lower compared to C3 or C4 plants that transpire soil-water during warm daylight conditions. As a consequence, ET from CAM plants tends to be controlled to a greater extent than would be the case with C3 or C4 species, (e.g. Meadow Flowers and grasses) (Nagase & Dunnett, 2012).

Sedums are typically assumed to be CAM plants. However, the universal CAM classification of the Sedum genus is subject to question. Rezaei (2005) did not observe ET under night time conditions – an important characteristic of CAM vegetation. Starry *et al.* (2014) hypothesised that a disruption to the CAM process could be caused by the thermal properties of green roof substrates; retaining heat and creating buffered temperature cycles. However, there is increasing evidence to suggest that many Sedum species typically used on extensive green roofs may be “CAM cycling” species, i.e. plants that switch between CAM and C3 photosynthesis (Voyde, 2011; Sayed, 2001). CAM cycling species will rapidly consume moisture when it is abundantly available, but will regulate consumption when availability is constrained (Starry *et al.*, 2014). CAM triggers are believed to be species dependent (Pilon-Smits *et al.*, 1991 in Starry *et al.*, 2014) but can include temperature, moisture availability, light and nutrient availability (Starry *et al.*, 2014). Voyde (2011) concluded that the trigger for Sedum to switch from C3 to CAM was moisture-related (i.e. when availability is constrained).

#### *2.4.3.3 Implications of different vegetation treatments*

A range of vegetation treatments can be accommodated within extensive green roof configurations. However, treatments generally fall into one of two broad categories. Succulents, including species belonging to the Sedum genus, are considered to represent the ideal vegetation for the harsh rooftop microclimates (Monterusso *et al.*, 2005; Cook-Patton & Bauerle, 2012). The use of herbaceous perennials is intended to increase biodiversity and aesthetic appeal (Benvenuti, 2014). Caution is urged regarding the use of grasses with high transpiration rates (Snodgrass & Snodgrass, 2006). There is a need to consider the “trade-off” between drought tolerance and runoff reduction capacity.

Grasses and herbs are expected to have higher ET whereas succulents will increase drought tolerance (Vanuytrecht *et al.*, 2014). Plants with high transpiration rates, such as herbaceous perennials and grasses, will deplete the available soil moisture more rapidly – increasing available moisture capacity for retention of subsequent events but equally exacerbating drought conditions (MacIvor & Lundholm, 2011).

The incidence of rainfall will also be a factor here. Equally, seasonal (and geographical) climate changes must be expected to influence the contribution of vegetation to the hydrological response. A plant's architecture and physiology will typically vary seasonally. The greatest contribution by vegetation is expected in summer conditions (Schroll *et al.*, 2011). Plant growth tends to be less vigorous during winter months (Gedge & Frith, 2004), contributing to the lower ET rates observed in winter. Predictably, therefore, no significant differences were observed between vegetated and non-vegetated configurations in winter (Dunnett *et al.*, 2008b).

#### **2.4.4 Incremental moisture capacity of drainage layers**

The primary function of a green roof drainage layer is to facilitate the drainage of excess, gravitational water (Miller, 2003); avoiding suffocation of plant roots. Highly permeable mineral aggregates can be used for this purpose. However, a secondary storm water management function (of reservoir storage and detention) is possible with many commercially-available, cusped synthetic drainage layers (typically manufactured from high density polyethylene [HD-PE] or high impact polystyrene [HIPS]). Some reservoir layers have water storage capacities greater than 10 l/m<sup>2</sup>. However, the contribution of the reservoir layer to retention is expected to be relatively low due to its position beneath the substrate. Vesuviano (2014) identified that water in the reservoir recharges the overlying soil at a rate of 0.0675 mm/day.

Further capacity (of between 2 and 12 l/m<sup>2</sup>) can be added with geotextile (polyester) fleeces that are positioned beneath the drainage layer. However, it is anticipated that the regeneration of its capacity in between events will be insignificant in terms of a regular contribution to retention.

The drainage layer and any underlying geotextile can contribute to the detention performance, delaying peak runoff (Miller, 2003). Excess gravitational water will first fill the water-holding capacity of the profile. Once full, further runoff will track horizontally

across the drainage layer to the roof perimeters before being directed underneath the drainage layer towards the outlet. The time taken for this excess moisture to travel through the underside of the drainage layer profile would typically be expected to be shorter if it travels in direct contact with the relatively hard and smooth waterproofing layer, rather than a porous fleece.

#### **2.4.5 Incidence of precipitation**

Storm water management generally considers responses to extreme rainfall events (i.e. low frequency, high volume) rather than routine rainfall. Concepts relating to rainfall intensity, duration and return period are discussed further in 2.6.1. The hydrological response of any drainage system will be significantly influenced by the incidence of rainfall (i.e. depth, duration, frequency and intensity). Whilst the duration of the event (in conjunction with the intensity) will typically influence the overall rainfall depth, it is suggested that the hydrological response of the green roof is not well correlated to the duration of the event in isolation (Versini *et al.*, 2015). Rainfall depth is an important influence upon retention response (Fassman-Beck *et al.*, 2013). The retention percentage will typically decrease as rainfall depth increases (Voyde *et al.*, 2010a; Stovin *et al.*, 2012). Green roofs will be expected to retain small events (Hilten *et al.*, 2008). Absorption of initial rainfall is typical (Carter & Rasmussen, 2006; Liu & Minor, 2005) with the first 5 mm of rainfall often believed to be retained (Greater London Authority, 2008). In the UK, 30-40% of rainfall events are sufficiently small for no measurable runoff to occur (CIRIA, 2007). Events with rainfall depths of less than 2 mm will rarely generate any significant runoff (Fassman-Beck *et al.*, 2013). However, for larger events, the contribution of the green roof will gradually decline as the ratio of rainfall to available moisture capacity increases, converging towards the response of a standard roof (Liu & Minor, 2005). Retention performance will be heavily skewed depending upon the number of small events that are included in the data being analysed. The seasonal distribution of rainfall events can also be considered to influence the response (Carson *et al.*, 2013 in Nawaz *et al.*, 2014; Stovin *et al.*, 2012). The impact of rainfall depth on peak flows was also identified by MacMillan (2004): a peak reduction of 85% was measured for events with less than 10 mm of rainfall, yet peak attenuation fell to 46% when 40 mm of rain fell.

The frequency of precipitation will influence the soil moisture conditions at the outset of, during and following a storm event (van Seters *et al.*, 2007; Koshimizu, 2008; Getter *et al.*, 2007; Liu & Minor, 2005). Retention will decrease when there is an insufficient dry weather period between rainfall events (Jennings *et al.*, 2003). The length of the antecedent dry weather period (ADWP) is therefore recognised as an important influence upon the hydrological response of the green roof (Stovin, 2009).

Conceptually, the intensity of rain falling on to a green roof can be considered to influence its hydrological response (Getter *et al.*, 2007; Koshimizu, 2008). Intense storms can encourage saturated flow conditions to develop near the surface, inducing gravitational fluxes. At the wetting front (below), water flows into the drier underlying soil in response to both  $\psi_m$  and  $\psi_g$ . A gradual wetting process results in the pores in the upper zones of the soil becoming saturated, increasing  $\psi_g$ . Percolation rates then depend on the extent of the matric resistance. Conversely, during light events, unsaturated flow occurs, with water drawn into smaller pores by  $\psi_m$  (Brady & Weil, 2008). However, the high permeability of most green roof substrates means that the saturated hydraulic conductivity will typically exceed the maximum probable rainfall intensity. Rainfall intensity is therefore unlikely to profoundly affect retention performance.

#### **2.4.6 Evapotranspiration and the influence of climate**

In isolation, the length of the drying cycle – or Antecedent Dry Weather Period (ADWP) – “fails to characterise the complex processes that account for the roof’s residual moisture content” (Stovin *et al.*, 2012). The hydrological cycle is driven by gravitational forces and solar energy; inducing moisture vapour transfer from the earth’s surface to the atmosphere via ET. The rate at which this transfer takes place is important to a green roof’s response to a subsequent storm event. ET is an important control upon the hydrological performance of green roofs as it “delimits the storage available within the soil for retention of additional precipitation” (Wadzuk *et al.*, 2013).

There are three key, but interdependent, processes involved during ET; firstly, an upward capillary flux through the soil profile towards the soil’s upper horizons; secondly, evaporative losses from the surface to atmosphere; and thirdly, transpiration of soil-water by plants. Forces inducing evaporation and transpiration losses are a function of the microclimate (i.e. solar radiation, air temperature, wind, relative humidity) and of the

plant's physiology. However, the rate at which these forces induce ET also depends upon the soil-water characteristics of the substrate (i.e. field capacity [ $\theta_{FC}$ ], permanent wilting point [ $\theta_{PWP}$ ], permeability), any additional moisture storage capacity within the vegetation layer and the plant's physiological response at the prevailing moisture content (Koehler & Schmidt, 2008).

ET has two constituent parts, representing both a mass and energy flux. Evaporation is the physical process of water transfer to the atmosphere, whilst transpiration is the evaporation of water from the leaf stomata via the vascular system of the plant (Verstraeten *et al.*, 2008). A net transfer of water molecules into the surrounding air will occur if there is a vapour pressure gradient between the evaporating surface and air (Cain, 1998). Any such change of state from liquid to vapour will require the application of latent heat to break the bonds between water molecules. This heat energy is typically provided by solar radiation and air temperature, whilst the moisture-holding capacity of the overlying air is also affected by wind speed and relative humidity (Voyde *et al.*, 2010b; Berndtsson, 2010).

#### 2.4.6.1 Air Temperature

Temperature and relative humidity largely govern the moisture-holding capacity of the atmosphere. Conceptually, warmer temperatures produce greater heat energy that should, all things being equal, result in greater potential evaporation. Equally, the capacity of the air to hold evaporated vapour will be greater – translating into higher actual evaporation levels. Retention will typically be greatest in warm seasons (Villareal *et al.*, 2004). Liesecke (1993, in Mentens *et al.*, 2006) observed that in warm weather, growing media can retain between 11-20% more storm water than during cold weather. It has been reported (Kasmin *et al.*, 2010) that, in the temperate climate of the UK, ET may be less than 1 mm/day for much of the year and, as such, long ADWPs will be required for the green roof to regenerate its full available moisture capacity. The reduced ability of the green roof to dry out during winter inter-event periods (due to low ET) contributes to seasonal differences (Voyde *et al.*, 2010b; Berghage *et al.*, 2009; Mentens *et al.*, 2006; Graceson *et al.*, 2013; Schroll *et al.*, 2011).

#### 2.4.6.2 *Relative Humidity*

The driving force for matric (and osmotic) movement is differential vapour pressures in soil-water and water-saturated plant tissue compared to the relatively drier external air (Berghage *et al.*, 2007). Therefore in dry conditions, where the saturation vapour pressure of water is high and actual vapour pressure of water in the air is low, a large saturation deficit will result in greater PET.

#### 2.4.6.3 *Solar and Terrestrial Radiation*

Terrestrial (or long-wave) radiation generally leads to higher temperatures in the atmosphere, increasing the air's ability to hold vapour. However, it is solar (or short-wave) radiation that provides the main source of energy required for ET, providing latent heat for vaporisation. The greater intensity and duration of sunlight further explains the better hydrological performance of green roofs in summer months, when more intense radiative heat leads to greater ET losses and increased soil moisture deficit (SMD).

#### 2.4.6.4 *Wind*

Wind enhances the turbulent transfer of vapour away from the moist vegetation treatment towards the dry atmosphere. High wind speeds will therefore replace saturated air above the vegetation with drier overlying air at a faster rate; increasing the vapour pressure deficit (VPD). Formulae such as the FAO-modified Penman-Monteith equation will be discussed in Section 2.6.3.

## **2.5 Reported quantitative hydrological performance of green roofs**

One of the major barriers to more widespread uptake of green roofs in the UK is the lack of quantified scientific evidence to substantiate their hydrological performance (Berndtsson, 2010; Fioretti *et al.*, 2010 in Nawaz *et al.*, 2015). Understanding of the hydrological performance of green roofs has been complicated by (a) the number of different design configurations (Fassman-Beck *et al.*, 2013), (b) the climate in which the research has been conducted and (c) the methodology adopted to report results. Here, the findings of previous research will be considered.

### **2.5.1 Runoff reduction**

Mean annual retention is a relevant metric, as retention of even small rainfall events can lower the risk of CSO discharges and resultant water pollution levels (Getter *et al.*, 2007;



Nawaz *et al.*, 2015). Li & Babcock (2014) highlighted that mean annual retention by green roofs ranged between 30 and 86%. This wide range reflects differences in climate and configuration. Predictably, mean annual retention was highest in the most arid environments. In Australia, Razzaghmanesh & Beecham (2014) measured a mean annual retention of 74%. Lower retention was recorded in the more temperate climates of the UK (Stovin *et al.* (2012): 50%) and Denmark (Locatelli *et al.* (2014): 32-57%). Fassman-Beck *et al.* (2013) highlighted the influence of seasonal climate on retention in Auckland (New Zealand). Here, mean annual retention was 56%. However, median retention in summer was 92%. The importance of the incidence of rainfall to retention was also apparent when contrasting the findings of Fassman-Beck *et al.* (2013) with the earlier conclusions of Voyde *et al.* (2010a) at the same site. In an earlier study, an increased mean annual retention of 66% was reported. Van Woert *et al.* (2005) demonstrated the effect that the incorporation of vegetation can have upon the hydrological response. Mean annual retention from vegetated configurations was 60.6%. However, without vegetation, this fell to 50.4%.

It is therefore apparent that major differences in retention can result from differences in (i) configuration, (ii) climate, and (iii) incidence of rainfall.

An even greater range of values was observed when considering per-event retention. Stovin *et al.* (2012) observed that per-event retention in the UK ranged between 20 and 100%, with a median of 59%. Palla *et al.* (2011) measured a similar range of retention in Italy (10 to 100%), with a mean value (85%). Two important controls on per-event retention have been identified. Firstly, the incidence of rainfall; and secondly, the climatic conditions. Fassman-Beck *et al.* (2013) concluded that per-event retention in summer ranged between 83 and 92%. Yet, in winter this fell to 66%.

Meanwhile, the importance of rainfall depth to per-event retention has been reported by numerous researchers who have identified the inverse relationship between rainfall depth and retention:

- Rowe *et al.* (2003) found that retention was 98% for light rain showers ( $P < 2$  mm/day), but fell to 50% when rainfall exceeded 6 mm/day.

- In Toronto (Canada), Banting *et al.* (2004) measured retention of 85.1% when rainfall depths were between 20 and 29 mm; falling to 68.2% for depths between 30 and 39 mm and to 50.3% when rainfall exceeded 40 mm.
- Carter & Rasmussen (2006) noted that for events with rainfall less than 25.4 mm, retention was 88%. However, when larger events occurred, retention reduced to 54% (rainfall between 25.4 and 76.2 mm) and 48% (when rainfall was in excess of 76.2 mm).
- Hakimdavar *et al.* (2014) found that, in New York (USA), retention was 85% when rainfall was less than 20 mm, but only 32% for events with more than 40 mm of rainfall.

### **2.5.2 Evapotranspiration (ET)**

One of the primary reasons for seasonal differences in retention is the different rates of ET that occur seasonally (and geographically). ET measured from green roofs has ranged from 0.0 mm/day (Koehler & Schmidt, 2008) to 6.2 mm/day (Hickman *et al.*, 2010). Differences in climate and configuration (and specifically, its available moisture capacity) can be seen to largely explain the variation in reported ET values. The previously-reported ET values are highlighted in Table 2.2.

Here, clear seasonal trends can be determined. In winter, ET rates have generally been less than 1 mm/day and represent only a fraction of the daily ET rates observed in other seasons. Moisture availability has also been identified as an important control upon ET. When moisture availability was constrained, ET has generally been observed to fall towards zero (van Woert *et al.*, 2005; Koehler & Schmidt, 2008). Berghage *et al.* (2007), DiGiovanni *et al.* (2010) and Lazzarin *et al.* (2005) all measured ET of less than 1.0 mm/day in such conditions.

Table 2.2: Previously reported ET measurements from green roofs

Author	Location	Vegetation	ET <sub>D</sub> (mm/day)			
			Spring	Summer	Autumn	Winter
Rezaei (2005)	Pennsylvania (USA)	Sedum (80%)	-	1.8-2.7	0.8	0.8
		None	-	0.8-1.5	0.5	0.8
Koehler & Schmidt (2008)	Germany	Sedum	0.6-1.5	1.5-4.5	0.6-1.5	0.1-0.5
DiGiovanni <i>et al.</i> (2010)	New York (USA)	Sedum	-	5.0-6.0	-	-
Hickman <i>et al.</i> (2010)	Pennsylvania (USA)	Sedum	-	3.0-6.2	-	-
Lazzarin <i>et al.</i> (2005)	Italy	Sedum	-	1.9	-	1.3
Berghage <i>et al.</i> (2007)	Pennsylvania (USA)	Sedum	-	1.4-3.0	-	-
Voyde <i>et al.</i> (2010)	Auckland (N. Zealand)	Sedum & NZ Ice Plants	-	0.2-3.2	-	-
Marasco <i>et al.</i> (2014)	New York (USA)	Sedum Xeroflor	-	5.1	-	0.1

### 2.5.3 Peak attenuation & delay

Detention processes are difficult to characterise because many of the conventional detention parameters such as peak attenuation and delay are distorted by the effects of retention. Only when a system is at field capacity at the onset of an event will detention metrics reflect the pure detention performance. There is no single universally-applied metric that allows detention performance to be described (Stovin *et al.*, 2015b). However, here the detention response, using conventional metrics (see Figure 2.9) will be explored.

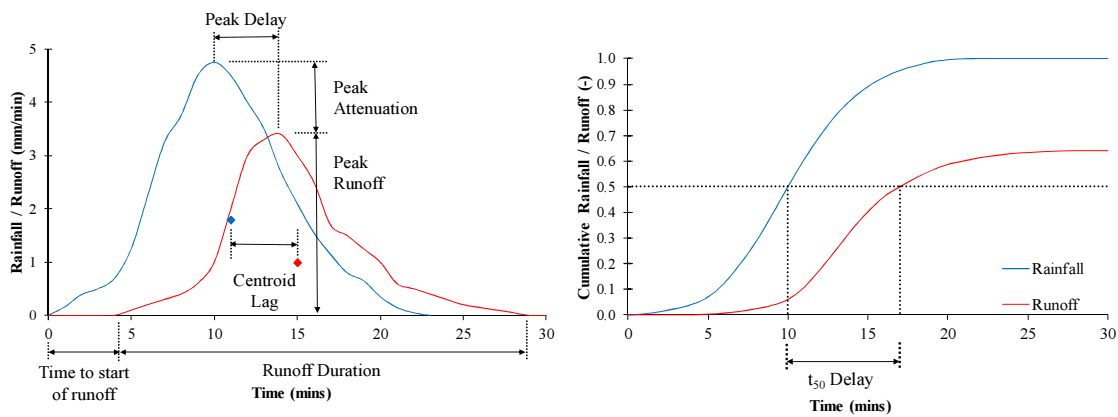


Figure 2.9: Conventional detention metrics (adapted from Stovin *et al.*, 2015b)

As with retention, it is expected that green roof configuration will impact upon peak attenuation and delay. Detention can be improved by increasing the depth of soil, reducing the roof pitch or introducing components such as drainage layers to increase the time of concentration (Palla *et al.*, 2009). However, peak attenuation will depend on the volume and frequency of rainfall and the residual soil moisture content (Palla *et al.*, 2009).

### 2.5.3.1 Peak attenuation

The importance of rainfall depth and available capacity to peak attenuation has been demonstrated by Liu & Minor (2005). They identified peak flow reductions of just 10-30% when the green roof was already at field capacity. Hakimdavar *et al.* (2014) identified an inverse relationship between peak attenuation and rainfall depth. For events with rainfall greater than 40 mm, peak attenuation was 51%. Yet, when rainfall was less than 20 mm, this increased to 89%. It is therefore expected that the broad range of peak attenuation values reported previously largely reflect differences in the incidence of rainfall. In Italy, Palla *et al.* (2011) identified a range of between 80 and 100%, whereas in Auckland, Fassman-Beck *et al.* (2013) reported lower values of 62-90%. In Denmark, Locatelli *et al.* (2014) recorded a broader range of lower peak attenuation rates (i.e. 10-78%). This was generally consistent with the findings of Li & Babcock (2014), who reported peak attenuation of between 22 and 93%. Carter & Rasmussen (2006) also reported a mean peak attenuation (of 57%) that would be consistent with the range of values reported in northern Europe. However, in the warmer climate of Italy and 400 mm deep substrate, Palla *et al.* (2011) reported mean peak attenuation of 97%.

In most cases, reported detention performance was not qualified with the time interval against which values were derived. Yet, as Stovin *et al.* (2015b) pointed out, detention metrics such as peak attenuation are sensitive to the time step used for the data analysis. For example, peak rainfall intensity will generally be lower when assessed at 5-minute intervals rather than at 1-minute steps. As such, peak attenuation values will need to state the time interval used in the calculation.

### 2.5.3.2 Peak delay

Peak delays are generally relatively short for green roofs. Previous research has shown that delays can range from zero (Locatelli *et al.*, 2014; Hakimdavar *et al.*, 2014) to 4.2 hours (Hakimdavar *et al.*, 2014). DeNardo *et al.* (2005) reported delays of 2 hours, whilst Carter & Rasmussen (2006) found delays to be shorter - up to 10 minutes. Locatelli *et al.* (2014) identified a range of between 0 and 40 minutes. Hakimdavar *et al.* (2014) demonstrated that peak delays can be affected by rainfall depths. Delays of between 0.2 and 1.6 hours were identified for 114 small events (i.e. less than 20 mm). Longer delays (of between 1.4 and 4.2 hours) were recorded across 20 medium-sized events (i.e. between 20 and 40 mm). However, for 14 large events (i.e. greater than 40 mm), peak delays were negligible, reaching a maximum of 0.1 hours.

## 2.6 Modelling hydrological response

One of the limiting factors that hinders more widespread green roof installations is the lack of adequate modelling tools (Elliott & Trowsdale, 2007). There are hundreds of urban storm water models in existence and it is not the intention to conduct a comprehensive review of each technique here. More detailed reviews of storm water models have been written by Zoppou (2001) and Elliott & Trowsdale (2007) *inter alia*. Here, a broader introduction to different modelling methods will be provided.

Simple models, comprising only a rainfall-runoff model, can be used to estimate long-term average data. However, generally, storm water models typically comprise two elements: a volumetric rainfall-runoff model and a transport model (Zoppou, 2001). The latter will typically take the form of a routing approach; with a number of approaches available depending upon the required complexity.

The simulation of rainfall will be an important input to all models. This will be considered here first. The methods of modelling runoff (and transport, where applicable) will then be reviewed according to whether they are categorised as statistical or deterministic models.

### **2.6.1 Rainfall simulation**

The choice of rainfall simulation techniques is typically limited to one of two approaches: (i) design rainfall events, or (ii) longer time series based upon observed or synthetic rainfall data. Design rainfall events can be derived through selection of an event with a specific return period (or probability) and duration. The most commonly adopted approach is the Depth-Duration-Frequency (DDF) method that was originally prescribed in the Flood Studies Report (NERC, 1975) and further updated in the Flood Estimation Handbook (CEH, 1999). The calculated design rainfall depth can be distributed according to one of several rainfall profiles, depending upon the season and percentage of storms that were less peaked than the design event. A summer profile (based upon rainfall between May and October) typically has shorter periods of higher intensity rainfall, producing the worst-case scenario when sizing components to manage runoff from impervious surfaces. A winter profile (based on rainfall between November and April) typically has more evenly distributed rainfall throughout the event's duration. Winter profiles are expected to produce the worst case scenario for storage and downstream attenuation components (CIRIA, 2015). At present, this approach is the most commonly-used. Time-series rainfall is not yet routinely adopted due to cost and availability concerns; particularly in view of the recommended minimum length of time series being two or three times the length of the return period (CIRIA, 2015).

### **2.6.2 Modelling runoff from green roofs**

Currently, there is no consensus as to the most accurate approach to quantifying soil-water fluxes (Wang *et al.*, 2008), leading to the development of a variety of models, often adopting different approaches and principles.

#### *2.6.2.1 Statistical models*

Statistical models rely upon the identification of equations (often derived via regression analyses) that mathematically relate influential variables to observed outcomes. Where the statistical relationship includes references to the laws of physics, statistical models

can be considered to be conceptual, or physically-based. However, the majority of statistical models are empirical in nature.

The latest UK SuDS design guidance (CIRIA, 2015) recognises that calculating the runoff rate for a specific site will not be precise; particularly when small catchments of less than 25 square kilometres in area are considered. However, reasonable estimates from consistently-applied calculation methods are sufficient (CIRIA, 2015). Regression-based runoff estimation models are almost universally applied by UK urban drainage engineers in the calculation of the volume and peak rates of runoff from pre- and post-developed sites and catchment areas (or regions).

The calculation of the peak rate and volume of runoff will typically employ one of two methods:

1. Modified Rational Method:

The HR Wallingford Modified Rational Method (HR Wallingford, 1981) – see Equation 2.9 – is an approach that calculates runoff ( $Q$  in l/s) as a function of rainfall intensity ( $i$  in mm/hour), catchment area ( $A$  in hectares) and a dimensionless coefficient,  $C$ , that is dependent upon the characteristics of the catchment.

$$Q = 2.78 \cdot C \cdot i \cdot A \qquad \text{Equation 2.9}$$

$C$  can comprise two elements: (i) a volumetric coefficient ( $C_v$ ) which reflects the storm pattern and the properties of the porous media (e.g. porosity), and (ii) a routing coefficient ( $C_r$ ) that allows for the catchment's infiltration properties. This approach is not unique and has parallels with the US Soil Conservation Service (now the Natural Resource Conservation Service [NRCS]) Curve Number (CN) coefficient that has been applied to green roofs by Carter & Jackson (2007). The HR Wallingford Modified Rational Method adopts a regression analysis to predict these coefficient values. In considering the response of a green roof to 10 events, Moran *et al.* (2005) determined a coefficient value of 0.5. This falls within the expected range of 0.1 to 0.7 that is published by the FLL (FLL, 2008). However, clearly, such a difference in the coefficient value (of up to 60% of runoff) will

have a major impact on runoff estimates. The accurate prediction of runoff using a modified rational approach will be entirely dependent upon deriving a meaningful value of  $C$ : this coefficient would need to have the capability to reflect the specific behaviour of the catchment and have the capacity to respond dynamically to changes induced in the catchment during the rainfall event.

2. A UK runoff model:

Two models are currently recommended (CIRIA, 2015) for the estimation of runoff: a variable UK runoff model (Packman, 1990) or the UKWIR UK runoff model (UKWIR, 2014). Both approaches calculate the percentage of runoff, by taking into account pervious and impervious areas and factoring it by a 30-day antecedent precipitation index (API) divided by the soil moisture depth. The UKWIR model enhanced the flexibility in the use of the API and soil classification inputs. Theoretically, both methods facilitate consideration of antecedent conditions and dynamic changes to the catchment as wetting takes place (such that the percentage runoff will increase). However, in practice, the 30-day API depends on the soil classification of the catchment area and is unlikely to be representative of a highly porous green roof substrate. Further consideration would therefore need to be given to the method of translating the catchment's characteristics to suit the plot's specific behaviour.

Stovin *et al.* (2012) reviewed regression-based models, concluding that they did not work well even when accounting for ADWP and various other inputs. The most important limitation upon the use of statistical models is that the derived equation will typically reflect a specific spatial arrangement and any change to one or more variables can change the mathematical relationship (Zoppou, 2001). Many drainage software packages that are used to model green roofs were developed for conventional drainage systems (Barbu & Ballesterro, 2015) and often cannot simulate the complex flow routing associated with highly porous substrates (Elliott & Trowsdale, 2007). Physically-based models are considered to be more accurate than empirical models (Palla *et al.*, 2012). As such, there is a need to develop accurate models that are physically-based but simple to use (Carbone *et al.*, 2015). CIRIA (2015) postulates that any green roof hydrological model should (i) reflect the specific characteristics of a green roof (preferably following calibration against



observed data), (ii) include a plant-specific and moisture-adjusted ET rate, and (iii) incorporate an extended time-series analysis that permits antecedent conditions and dynamic changes in moisture content to be accounted for. In the absence of such an approach, CIRIA (2015) currently recommends the use of the modified rational method that is outlined within BS EN 12056:3-2000.

#### 2.6.2.2 *Deterministic models*

Deterministic storm water models are based on the conservation laws that dictate soil-water flux. Hydrological models consider only equations for continuity. Hydraulic models combine the continuity approach with equations for the conservation of momentum and energy (Zoppou, 2001).

Hydrological storage (also known as mass balance) approaches continuously adjust storage as a function of inputs and outputs. This approach reflects the physical importance of residual moisture and maximum moisture capacity to the hydrological response. These approaches can have varying degrees of complexity. Storage functions can be linear or nonlinear and include one or more reservoirs from which transfers apply. However, a typical storage approach, similar to that used by Voyde *et al.* (2010a), would be the water balance as Equation 2.10:

$$\delta S_t = P_t + I_t - ET_t - Q_t \quad \text{Equation 2.10}$$

Where  $\delta S$  is the change in stored moisture,  $P$  is precipitation,  $I$  is irrigation,  $ET$  is evapotranspiration and  $Q$  is runoff (all in mm) at time  $t$ . Rearranging the equation allows runoff to be calculated via Equation 2.11:

$$Q_t = P_t + I_t - ET_t - \delta S_t \quad \text{Equation 2.11}$$

Most models function on the basis that  $Q_t$  only exceeds zero once residual storage ( $S_t$ ) reaches its maximum capacity ( $S_{MAX}$ ). Once  $S_t$  is equal to  $S_{MAX}$ , the transport (or routing) procedure can be applied to this volumetric surplus (or transient storage) to distribute predicted runoff temporally. To date, routing coefficients have typically been calibrated against observed performance of a gauged catchment with set characteristics. However, it is expected that the routing parameters can account for a soil's physical characteristics (e.g. hydraulic conductivity). Contrary to the scope of the coefficient employed in the

modified rational method, the physical basis of these routing coefficients will only need to reflect the detention parameters (and therefore saturated flow conditions). This type of model has been applied in previous green roof research efforts and has produced reasonable results (Kasmin *et al.*, 2010), particularly in small events (Berghage *et al.*, 2007).

However, more complex models can be used. The determination of a soil's  $\psi$ - $\theta$  relationship (in the form of the soil water characteristic curve, SWCC) can be used to inform soil-water movements. The nonlinear relationship between (and coupling effect of)  $\psi_m$  and  $\theta$  adds complexity to the modelling (Di Rado *et al.*, 2009) of soil-water movements. However, the link between moisture content, void-size distribution and the SWCC provides confidence that residual moisture balance can be used both to model resistance to moisture loss and to govern the point at which runoff would be expected to occur.

Conductivity approaches generally simulate flows in variably saturated soils, using the Richards (1931) equation. Richards combined Darcy's Law with the law of continuity, to account for inputs and outputs to establish the soil-water content at different potentials:

$$\delta\theta = \frac{\delta \left[ K_\psi \left( \frac{\delta\psi}{\delta z} + 1 \right) \right]}{\delta z} \quad \text{Equation 2.12}$$

The major constraint to wider use of this approach is the fact that the Richards' nonlinear partial differential equation offers no closed-form analytical solution. This was addressed by van Genuchten (1980), who developed hydraulic functions for soil-water retention ( $\theta$ ), hydraulic conductivity ( $K$ ) and diffusivity ( $D$ ):

$$\theta(\psi) = \theta_r + \left[ \frac{\theta_s - \theta_r}{(1 + |\tau\psi|^\beta)^m} \right] \quad \text{Equation 2.13}$$

$$K(\psi) = K_s \cdot S_e^\omega \left[ 1 - (1 - S_e^{1/m})^m \right]^2 \quad \text{Equation 2.14}$$

$$D(\theta) = \frac{(1 - m)K_s}{\tau m(\theta_s - \theta_r)} S_e^{\ell-1/m} \left[ (1 - S_e^{1/m})^{-m} + (1 - S_e^{1/m})^m - 2 \right] \quad \text{Equation 2.15}$$

Where  $\theta_r$  is the residual soil-water content and  $S_e$  is the effective saturation.  $\tau$ ,  $\beta$ ,  $m$  and  $\omega$  are all empirical shape factors that are related to soil texture and derivable from the SWCC.  $\ell$  is a coefficient related to the pore-size distribution of the substrate. The van Genuchten function is the most extensively used water retention equation. It accounts for important substrate characteristics and the main driving force for soil-water movement in unsaturated soils (i.e.  $\psi_m$ ). However, the approach has been criticised due to the interdependency and lack of physical meaning of the parameter values (Dexter *et al.*, 2008) and its failure to account for osmotic potential or hysteresis (Berghage *et al.*, 2007). Mualem (1976) established a statistical pore-size distribution model to derive more robust values for the parameter  $m$ , concluding that it is equal to  $1 - (1/\beta)$ . Pedotransfer functions (PTFs) are often used (Mermoud & Xu, 2006) to estimate the parameter values required for closed-form analytical expressions of  $\theta(\psi)$  and  $K(\psi)$ . However, PTFs can be perceived to be highly specific to a site's conditions (Jhorar *et al.*, 2004).

Other methods can be used to model infiltration. The Horton Infiltration Equation (Horton, 1940) is an empirical method that is also reliant upon a specific calibration (of a decay constant). The Green-Ampt approach (Green & Ampt, 1911) is one of the more commonly used infiltration models due to its physical basis combined with the fact that it can be solved iteratively without the computational complexity of the Richards approach:

$$q = \frac{\delta f}{\delta t} = -K_{sf} \left( \frac{\psi_f - (\psi_s + Z)}{Z} \right) \quad \text{Equation 2.16}$$

Where  $\delta f$  divided by  $\delta t$  is the infiltration rate,  $K_{sf}$  is the hydraulic conductivity corresponding to the surface water content,  $\psi_f$  and  $\psi_s$  are the soil-water potential at the wetting front and surface respectively and  $Z$  is the depth of the wetting front. This approach is, however, criticised for its limitations to saturated flow conditions (Barbu & Ballesterro, 2015) and the associated neglect of the influence of capillary drive (Chahinian *et al.*, 2005). This has led some to believe that the Richards equation, despite the intensive data input requirements, may be more suitable for green roofs due to the greater regularity of unsaturated flow conditions within green roofs (Barbu & Ballesterro, 2015). An integral part of a hydrological storage approach is the estimation of ET; the calculation of which will now be considered.

### 2.6.3 Evapotranspiration calculations

The success of any green roof hydrological model will depend upon the accuracy of its ET predictions. Voyde *et al.* (2010b) highlighted that “green roof ET has not been well quantified or thoroughly modelled” due to the absence of experimental data to underpin the modelling of ET losses for different vegetation treatments and climatic conditions. ET models are typically applied during ADWP; but not during rainfall events. It is assumed that ET during a rainfall event will be insignificant in view of the limited energy source (i.e. low solar radiation) and the reduced vapour pressure deficit, or VPD (Yang *et al.*, 2015). ET rates also tend to be minimal when compared with rainfall rates.

There are numerous theoretical approaches currently adopted to estimate potential evapotranspiration (PET); each with varying degrees of complexity. Commonly used approaches can be classified according to 2 categories:

1. Energy budget methods: the estimation of PET through consideration of thermal sources and sinks – net radiation, sensible and latent heat transfer to the atmosphere and sensible heat flux into the soil. Wilson (1990) criticises this approach for the requirement to conduct significant and specific experimentation to obtain the necessary data.
2. Combination methods: provide a more holistic estimate of PET by accounting for the combined influences of heat energy (using an energy budget approach) and vapour transfer (using aerodynamic methods). Aerodynamic methods typically model the removal of vapour from a surface (i.e. humidity gradient in a vertical direction and air flow turbulence) through consideration of the VPD at the surface-atmosphere interface and wind speeds.

Five PET modelling approaches are introduced below. However, for further detailed reviews of PET methods, see MacMahon *et al.* (2013), Weiss & Menzell (2008) and Nikam *et al.* (2014). The methods considered here include different degrees of complexity, in terms of computation and the number and availability of inputs, ranging from a simple temperature-based model (e.g. Blaney-Criddle method as per Blaney & Criddle, 1962) to more complex combination approach (FAO-modified Penman-Monteith as per Allen *et al.*, 1998).

### 2.6.3.1 Blaney-Criddle method

The Blaney-Criddle method estimates ET on the basis of temperature and daylight hours alone:

$$PET_{BC} = p(0.46 \cdot T_{mean} + 8) \quad \text{Equation 2.17}$$

Where  $p$  is the mean daily percentage of annual daytime hours, based on the latitude and month. This method is criticised for the oversimplified approach that reduces accuracy (Brouwer & Heibloem, 1986 in Wadzuk *et al.*, 2013). It is also acknowledged that the model was established to estimate PET in the USA and its use outside of this region was not initially intended. Consequently, the use of the Blaney-Criddle method in UK hydrological models is expected to be limited.

### 2.6.3.2 Hargreaves

Hargreaves & Samani (1985) developed a simplistic, energy based approach that requires only temperature as a meteorological input. Extra-terrestrial radiation is calculated without any radiation measurements being required. An empirical constant (0.0023) is also included:

$$PET_{HG} = 0.0023 \cdot \left(\frac{R_a}{\lambda}\right) \cdot (T_{MEAN} + 17.8) \cdot (T_{MAX} - T_{MIN})^{0.5} \quad \text{Equation 2.18}$$

Where  $R_a$  is the extra-terrestrial radiation,  $\lambda$  is the latent heat of vaporisation and  $T_{MEAN}$ ,  $T_{MAX}$  and  $T_{MIN}$  are the mean, maximum and minimum daily temperatures respectively.

### 2.6.3.3 Priestley-Taylor

The Priestley-Taylor (1972) approach is also an energy-based equation that requires temperature and radiation data as inputs:

$$PET_{PT} = \chi \left[ \frac{\Delta}{(\Delta + \gamma)} (R_n - G) \right] \quad \text{Equation 2.19}$$

Where  $\chi$  is a constant energy term,  $\Delta$  is the slope of the saturation vapour pressure (SVP) curve,  $\gamma$  is the psychrometric constant,  $R_n$  is net radiation and  $G$  is soil heat flux.

As a simplified version of the Penman-Monteith calculation method, the absence of any aerodynamic term would be expected to predict lower ET in cooler conditions (e.g. night

time, winter), when the influence of aerodynamic factors would be expected to be high relative to radiative forces.

#### 2.6.3.4 Thornthwaite equation

The Thornthwaite approach is an empirical estimation of PET from close-set vegetation that is based on temperature and sunshine hours (Wilson, 1990). The approach benefits from the need for relatively few inputs that are generally available:

$$PET_{TH} = PE_x \left( \frac{DT}{360} \right) \quad \text{Equation 2.20}$$

Where  $D$  is the number of days in the month,  $T$  is average number of daylight hours in a month and  $PE_x$  is the monthly PET (in mm), given by:

$$PE_x = 16 \left( \frac{10t}{I} \right)^a \quad \text{Equation 2.21}$$

Where  $I$  is the annual heat index (the sum of twelve monthly indices,  $i$ ):

$$I = \sum_1^{12} i \quad \text{Equation 2.22}$$

And

$$i = \left( \frac{t_n}{5} \right)^a \quad \text{Equation 2.23}$$

Where  $t_n$  is the mean monthly temperature (in °C) and  $a$  is an empirical factor, calculated as:

$$a = (675 \cdot 10^{-9})I^3 - (771 \cdot 10^{-7})I^2 + (179 \cdot 10^{-4})I + 0.492 \quad \text{Equation 2.24}$$

The Thornthwaite approach can produce a reasonable approximation of PET (Kasmin *et al.*, 2010). However, caution is urged in its application (Wilson, 1990). Firstly, the equation is temperature-based and does not specifically account for one of the key driving forces for ET (i.e. solar radiation). Secondly, this approach does not consider the role of the vegetation; leading Kasmin *et al.* (2010) to apply a further empirical calibration factor.

### 2.6.3.5 *FAO-modified Penman-Monteith Approach*

The FAO-modified Penman-Monteith Method (FAO56) adapted the original Penman-Monteith method, following a collaboration led by the Food and Agriculture Organisation (FAO) of the United Nations (Allen *et al.*, 1998). Briefly, FAO56 estimates ET for a reference crop of green grass with uniform height (0.12 m), surface resistance (70 s/m) and albedo (0.23) in response to climatological factors, i.e. radiation, air temperature, relative humidity and wind speed. The reference ET value,  $PET_{FAO56}$ , is calculated as a daily ET rate, as follows:

$$PET_{FAO56} = \frac{0.408 \Delta (R_n - G) + \gamma \frac{900}{T + 273} U_2 (e_s - e_a)}{\Delta + \gamma (1 + 0.34 U_2)} \quad \text{Equation 2.25}$$

Where  $e_a$  and  $e_s$  are the actual and saturated vapour pressures and  $U_2$  is the wind speed.

Consensus is that the Penman-Monteith combination approach is the most physically justifiable (Beven, 2001; Liu & Todini, 2002) and avoids unnecessary empiricism (Cain, 1998). This combination approach reflects many of the physical influences that affect ET. Radiative forcing dominates the energy balance of a green roof. Here, net radiation ( $R_n$ ) is calculated the difference between net short-wave (incoming) radiation ( $R_{ns}$ ) and net long-wave (outgoing) radiation ( $R_{nl}$ ).  $R_{ns}$  reflects the reduction in incoming solar radiation ( $R_s$ ) as a consequence of the reflectivity, or albedo ( $\alpha$ ), of the plant surface. Radiative forcing is balanced by convective and evaporative heat flux from the plant and soils, together with conduction into the substrate and long-wave radiation (Luo *et al.*, 2011). Soil heat flux is, however, typically neglected as it represents a relatively small component of the overall energy balance (Allen *et al.*, 1998).

The modified version also has the capacity to mimic a canopy's resistance to PET as a function of the physiological properties of the vegetation, the transfer of heat and the way in which turbulence in the lower atmosphere controls the movement of water vapour from the surface to the atmosphere (Feller, 2011). The aerodynamic part of the model functions on the premise that the lower the VPD (i.e. the difference between  $e_a$  and  $e_s$ ), the lower the PET. However, as the air dries, the VPD increases, leading to higher PET. The slope of the saturation vapour pressure curve ( $\Delta$ ) reflects the ratio of a change in the vapour

pressure versus a change in air temperature whilst the wind speed ( $U_2$ ) influences the rate at which saturated air is replaced with drier air.

Equation 2.25 does not specifically account for crop characteristics and soil properties (Allen *et al.*, 1998). However, an additional crop factor ( $k_c$ ) can account for any differences in transpiration rates between (and indeed within) species, as a function of the growth stage, microclimate and level of maintenance (Perlmann, 2008 in Feller, 2011). This coefficient is calculated relatively to the reference crop value as follows:

$$k_c = ET \div PET_{FAO56} \quad \text{Equation 2.26}$$

Where ET is the observed, crop-specific ET rate.

#### 2.6.4 Derivation of actual evapotranspiration

It is known that ET does not always equal PET. PET assumes that the availability of moisture is sufficient so as not to restrict ET. However, in practice, configurations will not always be fully wetted. Typically, therefore, some form of function is required to reduce PET in line with moisture availability when calculating actual ET. Zhao *et al.* (2013) presented numerous soil moisture extraction functions (SMEFs) that factored PET to obtain a more realistic forecast of ET as moisture availability changes. The SMEFs considered by Zhao *et al.* (2013) all factored PET by  $\theta_t$  as a proportion of  $\theta_{FC}$ . However, here,  $S_{MAX}$  is considered instead of  $\theta_{FC}$ . It is expected that this is a more relevant parameter, as  $\theta_{<PWP}$  will not typically be released through ET. Consistent with the approach adopted by Stovin *et al.* (2013), the moisture balancing factor is taken as the ratio of available,  $S_t$ , to maximum storage,  $S_{MAX}$ . This ratio represents the effective saturation,  $S_e$ , of the system:

$$S_e = \frac{S_{MAX} - SMD_t}{S_{MAX}} \text{ or } \frac{S_t}{S_{MAX}} \quad \text{Equation 2.27}$$

Five of the SMEFs presented by Zhao *et al.* (2013) will be considered here; each reflecting different relationships between ET and moisture availability:



$$\text{Koitzsch \& Golf (1) [KG1]:} \quad ET_{PRED} = PET \cdot \left[ \frac{S_e^2}{S_e^2 + (1 - S_e)^2} \right] \quad \text{Equation 2.28}$$

$$\text{Koitzsch \& Golf (2) [KG2]:} \quad ET_{PRED} = PET \cdot 2 S_e^2 \cdot \left[ \frac{1}{(1 + S_e)^2} \right] \quad \text{Equation 2.29}$$

$$\text{Roberts (1):} \quad ET_{PRED} = PET \cdot 2 S_e \cdot \left[ \frac{1}{(1 + S_e)^{S_e}} \right] \quad \text{Equation 2.30}$$

$$\text{Roberts (2):} \quad ET_{PRED} = PET \cdot S_e^{0.5} + (S_e^{0.5} - S_e) \quad \text{Equation 2.31}$$

$$\text{S}_e \text{ Linear:} \quad ET_{PRED} = PET \cdot S_e \quad \text{Equation 2.32}$$

The use of functions to predict actual ET using PET estimates will be considered in Chapter 6.

### 2.6.5 Existing storm water models used with green roofs

Here, five hydrological models that are often employed for the prediction of a green roof's response will be briefly introduced.

#### 2.6.5.1 Hydrus-1D

The Hydrus-1D approach (Simunek *et al.*, 2008a; Simunek *et al.*, 2008b) is based upon the Richards' equation with soil-water retention accounted for in either single porosity models (van Genuchten-Mualem, modified van Genuchten, Brooks-Corey or Kosugi) or dual porosity/dual permeability models. A range of soil categories are pre-loaded, but further options are available for non-conventional substrate types. The software includes a range of options for the two boundary conditions associated with a one dimensional approach complete with root water uptake models. PET can be modelled via the Penman-Monteith or Hargreaves approach. The Hydrus-1D model was used by Hilten *et al.* (2008) to predict the hydrological response of a green roof. However, they found that runoff was over-predicted for larger events (i.e. rain depth in excess of 20 mm).

#### 2.6.5.2 SWMM

The SWMM (version 5.0) model (Rossman, 2010) is a commonly-used water balance approach. This software models flows between the atmosphere, the landscape and the conveyance system. Once inputs exceed the reservoir's available storage capacity, runoff

occurs. A range of routing equations, based on the conservation of mass and continuity, can be employed, depending upon the required complexity. Versini *et al.* (2015) used the SWMM version 5.0 (Rossman, 2004) with a modification that facilitated characterisation of the vegetation, substrate and drainage layer within a linear reservoir approach. However, the approach of Versini *et al.* (2015) was calibrated against a single year of data; a year in which no significant rainfall events were recorded.

#### 2.6.5.3 *SWMS\_2D*

The SWMS\_2D model (Simunek *et al.*, 1994) simulates two dimensional flow in variably saturated soils, accounting for prescribed head and flux boundaries, by solving the Richards equation via finite element analyses. Palla *et al.* (2009) applied the SWMS\_2D model for the modelling of a green roof's hydrological response.

#### 2.6.5.4 *Soil Water Atmosphere & Plant Model (SWAP)*

The Soil Water Atmosphere & Plant Model (SWAP) (van Dam, 2000; van Dam *et al.*, 2008) is a water balance model with water movement modelled by combining Darcy's Law with the law of continuity (Ines & Droogers, 2002). Spatial and temporal differences in soil-water are accounted for by the van Genuchten (1980) and Mualem (1976) functions. ET is modelled using the Penman-Monteith approach. A generic crop growth model simulates leaf photosynthesis and crop growth.

#### 2.6.5.5 *Earth Pledge Green Roof Storm Water Modelling System*

The Earth Pledge Green Roof Storm Water Modelling System is a mass balance approach, incorporating data on storms, soil, plant, precipitation, wind, solar radiation and relative humidity (Hoffman, 2006). This model includes a function for hysteresis, and enables prediction of ET. However, it contains over-simplistic assumptions in respect of initial water content (with options to select 'dry', 'moderately saturated' or 'fully saturated') and allows  $\theta$  to be reduced to zero during the drying cycle.

### 2.6.6 **Future modelling requirements**

The fundamental processes in the physically-based model are ET and flow under both saturated and unsaturated conditions (Li & Babcock, 2014). Hydrological processes are known to be highly variable. Yet, the objective is to capture these processes without introducing unnecessary complexity (Elliott & Trowsdale, 2007). It is important to quantify each element of the hydrological budget, taking into account the technical

performance of the configuration and the influence of the climate (Lamera *et al.*, 2014). Conceptually, a moisture balance approach can capture the complex inter-event processes that affect retention that cannot reasonably be modelled through regression analyses (Stovin *et al.*, 2012; Simmons *et al.*, 2008).  $\theta_t$  at the onset of rainfall appears to be a good indicator of antecedent conditions; more so than antecedent rainfall patterns (Versini *et al.*, 2015). Systematic experimentation at variable levels of moisture availability would therefore help to characterise roof substrates (Metselaar, 2012). Future research therefore needs to better identify the influence of different physical processes within the hydrological cycle (Soutis *et al.*, 2005 in Jayasooriya & Ng, 2014), and in particular, the prediction of  $\theta_t$  as a result of the regeneration of available capacity via ET during the ADWP.

## **2.7 Summary of literature review**

The need for complementary sustainable drainage components has been highlighted by the recent increase in the frequency of pluvial flooding. Green roofs have been shown to provide benefits in attenuating runoff. Physical theories indicate that substrate composition will have an important influence upon the hydrological properties of the system. Seasonal climate will also influence the drying cycle. There is an acknowledged need for greater availability of empirical data that can be used to validate predictive hydrological models for green roofs (Elliott & Trowsdale, 2007; Jayasooriya & Ng, 2014).

The volume of water that is retained, evaporated, transpired or discharged will vary depending on (i) the green roof configuration (i.e. drainage layer, growing media type and depth, plant layer) and (ii) climatic variables (e.g. incidence of rainfall, solar radiation, relative humidity, air temperature and wind speed) that affect available moisture capacity. However, these two variables cannot be considered independently of each other.

Research to date has reported highly variable hydrological performance by green roofs. It is hypothesised that these variations can be attributed to differences in the physical system or conditions of the test regime. There is therefore a need for more comprehensive design tools that can take into account all relevant variables to accurately depict the SuDS performance of green roofs (Sailor, 2008; Mentens *et al.*, 2006).

Whilst average annual retention measures are relevant, the primary concern of engineers is the attenuation of peak runoff rates during potentially flood-inducing, large storm events (Berghage *et al.*, 2007). As such, a predictive model must have the dynamic capacity to analyse per-event responses at high temporal resolutions (i.e. < 10 minutes). In particular, consideration must be afforded to the method of calculating antecedent moisture conditions (Beven, 2001) and therefore runoff by accounting for the influence that numerous hydrological processes, heterogeneous climatic factors and soil characteristics have upon nonlinear soil-water movements. Conceptually, a deterministic water balance model, including the calculation of ET as a function of PET and moisture availability, would appear to be consistent with the identified need for a physically-based model with an appropriate level of complexity.

### **3 Characterisation of green roof materials**

#### **3.1 Chapter overview**

The green roof test configurations are introduced and important physical characteristics of the main elements (i.e. vegetation, substrate and drainage layer) are identified. Substrate characteristics, such as density, porosity and permeability are quantified via laboratory tests and converted into meaningful indicators of hydrological performance, such as moisture-holding capacities. Further tests explore each substrate's specific relationship between moisture content and soil-water potential as well as the size and distribution of particles. Vegetation treatments are characterised via references to databases that describe important plant traits. Photographs are used as part of a qualitative review of the vegetation treatments throughout an annual cycle. Finally, the potential implications of identified systematic differences upon a green roof's hydrological performance are discussed.

This research was linked to an EU-funded Marie Curie Industry-Academic Partnerships and Pathways (IAPP) collaboration on "Green Roof Systems" between the University of Sheffield and ZinCo. Tests that were carried out by others as part of this collaboration are acknowledged where applicable.

#### **3.2 Motivation**

The characterisation of the vegetation treatments and substrates considered here will underpin:

- New insights into the effects of configuration on retention and detention performance;
- The development of hypotheses that can potentially explain empirical observations;
- Greater awareness of the potential implications for storm water management of systematic differences in green roof configurations; and
- Transparency required to ensure that the results of this research are meaningful for, and transferable to, other green roof configurations.

### 3.3 Materials and methods

A green roof typically consists of three key elements – a drainage/reservoir layer (often including a protection fleece [below] and filtration sheet [above]), growing medium (or substrate) and vegetation. The growing medium provides the vegetation with nutrients, air and water, discharging any excess water into the drainage layer, from where a proportion of the excess water can be stored for evaporation back into the substrate during periods of drought. However, the primary hydrological benefit of the drainage layer is in delaying peak flows (Miller, 2003) as storm water must travel horizontally over the drainage layer to its perimeter, before tracking back underneath to the nearest drainage outlet. Here each of these three elements will be characterised using quantitative and qualitative data.

#### 3.3.1 Introduction to the configurations

Nine extensive green roof configurations were trialled; each varying systematically in their substrate composition and vegetation treatment. Each configuration comprised a combination of three substrates and three vegetation treatments. With the intention of providing universally-applicable findings, two commercially-available substrates supplied by Alumasc – Heather & Lavender Substrate (HLS) and Sedum Carpet Substrate (SCS) – were considered, alongside a bespoke substrate based on the widely used Lightweight Expanded Clay Aggregate (LECA). The LECA-based substrate contains 80% LECA, 10% loam (John Innes No. 1) and 10% compost by volume. Differences in the particle sizes of the three substrates are evident in Figure 3.1. The settled substrate depth was 80 mm in all instances.



*Figure 3.1: Photograph of the three substrates (left: HLS; centre: SCS; right: LECA)*

Three configurations were vegetated with Alumasc Blackdown Sedum Mat, three with Meadow Flower and three had no vegetation. The two vegetated treatments are shown in Figure 3.2.



*Figure 3.2: Sedum (left) and Meadow Flower (right) vegetation treatments*

Sedum species were chosen because they are the most commonly adopted plant species in UK green roof applications. Their tolerance of extreme temperatures and high wind speeds plus their limited water consumption requirements (van Woert *et al.*, 2005) are often cited as the important reasons for their use with green roofs. The Meadow Flower treatment comprised a mix of flowers and grasses that increase biodiversity potential (Benvenuti, 2014) but are less tolerant to drought than Sedum (Lu *et al.*, 2014). The Meadow Flower mix did, however, include three succulent Sedum species. Non-vegetated configurations provided a basis against which the contribution of vegetation could be evaluated, whilst equally indicating the hydrological performance of a ‘brown’ or biodiverse roof.

These configurations were trialled with a ZinCo Floradrain FD25 drainage layer in a long-term field research programme (as detailed in Chapter 4) and with the ZinCo DBV12 drainage layer in ET trials under controlled-conditions (see Chapter 5).

### 3.3.2 Substrate characterisation tests

#### 3.3.2.1 FLL tests to determine substrates' physical characteristics

Laboratory tests of the substrates were carried out according to the Guidelines for the Planning, Construction and Maintenance of Green Roofing of the German Landscape Development and Landscaping Research Society (FLL, 2008). A UK code of best practice for green roofs was developed in 2011 (GRO, 2011) and updated in 2014 (GRO, 2014). However, GRO simply refers to FLL characterisation tests. These tests were performed by Joerg Werdin and Ruzica Mohorko as part of the Marie Curie Industry-Academia Partnerships & Pathways (IAPP) research programme. The tests identified basic physical properties of the substrates, including apparent density (dry condition and at maximum water capacity), porosity, maximum water holding capacity (MWHC), particle-size distribution (PSD), permeability and OM. To address the uncertainty associated with subsampling heterogeneous mixtures, a sample splitter was used and 3-6 replicate samples were tested, depending on the analysis.

Soil texture and structure (i.e. particle size distribution [PSD] and void size distribution [VSD]) are important controls on the filling and emptying of voids (Manning, 1987); affecting the tenacity with which water is held in pores (Miller, 2003) and capillarity. Whilst matric pressures are directly affected by VSD, PSD was measured due to the simplicity of experimental determination and the significant correlations between PSD and VSD, and between VSD and the water retention curve (Hwang & Choi, 2006). The PSD of the substrates was measured via sieve analysis; recording the proportion ( $w/w$ ) of the substrate that passed through mesh sizes (0.063, 0.212, 0.355, 0.425, 0.5, 0.71, 1.0, 2.0, 4.0, 6.3, 10.0 and 20.0 mm) as prescribed by FLL Guidelines (2008). In some soil science disciplines, a greater number of sieves are used. However, whilst natural soils will contain a broad range of particle sizes, green roof substrates are produced with a graded distribution, comprising a limited number of components and a small proportion of silt particles. The smaller number of sieves is therefore appropriate.

#### 3.3.2.2 Quantitative assessment of void-size distribution

VSD is an important influence on a substrate's  $\theta(\psi)$  relationship. Void (or pore) sizes affect (i) the mechanical strength of the soil, (ii) plant root penetration, (iii) drainage and aeration during the wetting cycle and (iv) the extent to which retained soil-water is



available to plants (Rowell, 1994). PSD is intrinsically linked to VSD, but is a more readily-measurable parameter. There are empirical methods that attempt to equate PSD to VSD (e.g. Arya & Paris, 1981). However, here, an attempt was made to analyse the arrangement of particles and voids, using a method broadly as described in Marcelino *et al.* (2007) and as applied to green roof substrates by Graceson *et al.* (2013). Dr. Graceson assisted the author with these trials (conducted at Harper Adams University College).

The substrates were dried in the oven at 105 °C before each filling three square plant containers (70 x 70 mm) to a depth of 80 mm (see Figure 3.3).



*Figure 3.3: Sample substrate blocks*

*Top – left: substrate-filled pots; right: resin added; bottom – left: solid block; right: cut blocks ready for polishing)*

A solution of xylene and Uvitex fluorescent dye (1 g of dye to 10 ml of xylene) was mixed with a resin hardening mix (8 g of resin hardener and a small amount of styrene) and applied to fully submerge the substrate. Once the resin had fully saturated the substrate, such that no further infiltration was witnessed, the samples were left to harden over

several days in a well-ventilated area. Each sample was then cut into two blocks and polished. Finally, samples were photographed under ultra-violet light. It was intended that image analysis could be conducted using ImageJ software (Ferreira & Rasband, 2011), leading to a quantitative estimate of the size and number of voids in each substrate.

### *3.3.2.3 Soil Water Characteristic Curve (SWCC)*

A Soil Water Characteristic Curve (SWCC) expresses the relationship between moisture content ( $\theta$ ) and soil moisture potential ( $\psi$ ). The SWCC was determined by Joerg Werdin for the three substrates using the pressure plate extraction method (Carter, 1993). The principle of this test is to gradually extract water from initially-saturated samples by applying increasing pressures; providing information regarding the plant available water. Field capacity corresponds to a suction of approximately 35 kPa (0.35 bar). Permanent wilting point corresponds to a suction of 1500 kPa (15 bar) (Fassman and Simcock, 2012; Hillel, 1971). Here, tests were run with three samples per substrate at pressures of 35, 100, 200, 300, 400, 500, 1,000 and 1,500 kPa. Two pressure plate extractors were used, both manufactured by Soil Moisture Equipment Corporation. A 1600 Pressure Plate Extractor was used for tests up to 500 kPa. A 1500F1 Pressure Plate Extractor was used for the tests at 1,000 and 1,500 kPa. Due to the specific characteristics of the green roof substrates the standard test procedure proposed by the manufacturer was slightly modified. A wet strengthened filter paper (Whatman No. 113) was attached to the bottom of the sample rings to avoid collection of sample residues on the ceramic plate at the end of the test. A mixture of kaolin and water was spread on the ceramic plate to ensure contact between the sample and the ceramic plate.

### **3.3.3 Vegetation treatments**

The characterisation of vegetation typically refers to either some physical measurement (e.g. height, spread, leaf area index) or to a categorisation (e.g. genus, species, hardiness, photosynthetic pathway).

#### *3.3.3.1 Physical characteristics of the vegetation treatments*

Here, the physical and physiological characteristics of the species within the two vegetation treatments were researched, using various databases and resources. However, no physical measurements of plant traits or dimensions were attempted. The relevant

physical characteristics of six species in the Alumasc Blackdown Sedum mat are shown in Table 3.1.

Table 3.1: Physical characteristics of species in the Alumasc Blackdown Sedum mat

Species Name	Leaf Area (mm <sup>2</sup> ) <sup>a</sup>	Spread (cm) <sup>c</sup>	Height (cm) <sup>c</sup>	Leaf Shape <sup>d</sup>	Rooting Depth (cm) <sup>d</sup>	Photosynthetic pathway <sup>f</sup>	Hardiness <sup>c</sup>
<i>Sedum acre</i>	6 <sup>b</sup>	20	5	Acicular <sup>e</sup> (L=1-3xW)	Shallow	C3	USDA 4
<i>Sedum album</i>	17-32	20	15	Acicular <sup>e</sup> (L=1-3xW)		C3	USDA 4
<i>Sedum hispanicum</i>		20	7	Acicular <sup>e</sup>		C3/ CAM	USDA 6
<i>Sedum reflexum</i>		20	20			CAM	USDA 4
<i>Sedum sexangulare</i>	6-9	20	10	Acicular <sup>e</sup>		C3	USDA 4
<i>Sedum spurium</i>	111-229	20	15	Cuneate (L=1-3xW)		C3	USDA 5

<sup>a</sup> Kleyer *et al.* (2008) unless otherwise stated.

<sup>b</sup> Wright *et al.* (2004).

<sup>c</sup> Snodgrass & Snodgrass (2006).

<sup>d</sup> Fitter & Peat (1994).

<sup>e</sup> Kühn *et al.* (2004).

<sup>f</sup> TRY Database (Kattge *et al.*, 2012): <http://www.try-db.org>, accessed 18<sup>th</sup> July 2016.

The Meadow Flower contained 24 species of ‘wild’ and ‘cultivated’ plants as part of a formulation designed by Dr. Nigel Dunnett at the University of Sheffield. The physical and physiological characteristics of each species are shown in Table 3.2.

The Meadow Flower mix therefore comprises species that are expected to have greater height, larger leaf sizes and greater variation in root depth and leaf shape than with Sedum. All of these characteristics indicate that Meadow Flower will be at greater risk of drought stress than Sedum due to higher ET:

*Plant height:* Tall plants can be exposed to greater aerodynamic drag and have more difficulty in supplying their leaves with water (Ennos, 1999).

Table 3.2: Physical characteristics of the species in the Meadow Flower mix

Species Name	Leaf Area (mm <sup>2</sup> ) <sup>a</sup>	Spread (cm) <sup>c</sup>	Height (cm) <sup>c</sup>	Leaf Shape <sup>d</sup>	Rooting Depth (cm) <sup>f</sup>	Photosynthetic pathway <sup>f</sup>	Hardiness <sup>j</sup>
<i>Achillea millefolium</i>	411	15	40	Pointed (L>3W)	10-50	C3	H7
<i>Allium schoenoprasum</i>	297-725	15	25	Pointed (L>3W)		C3	H6
<i>Anthemis tinctoria</i>	121-1363	25	48			C3	H4
<i>Armeria maritima</i>	26-157	15	15	Pointed (L>3W)	10-50	C3	H5
<i>Calamintha nepeta</i>	108 <sup>b</sup>	60 <sup>g</sup>	80 <sup>g</sup>	Simple <sup>h</sup>		C3	H6 <sup>g</sup>
<i>Centaurea scabiosa</i>	4352	30 <sup>j</sup>	55 <sup>j</sup>	Cuneate (L>3W)	Deep	C3	H7
<i>Dianthus carthusianorum</i>		30 <sup>j</sup>	30 <sup>j</sup>	Grass-like <sup>h</sup>		C3	H7
<i>Dianthus deltoids</i>	21-27	30	20	Pointed (L>3W)		C3	H6
<i>Hieracium aurantiacum</i>	753-2160	20	20	Long leaf <sup>h</sup> (L>3W)		C3	USDA 5 <sup>h</sup>
<i>Hieracium pilosella</i>	86	20	30	Simple <sup>g</sup>		C3	USDA 6 <sup>h</sup>
<i>Jasione montana</i>	19-59	50 <sup>h</sup>	50 <sup>h</sup>	Long leaf <sup>h</sup> (L>3W)	0-10	C3	USDA 6 <sup>h</sup>
<i>Leontodon autumnalis</i>	40-3592	50 <sup>h</sup>	50 <sup>h</sup>	Cuneate (L>3W)		C3	USDA 5-10 <sup>h</sup>
<i>Limonium latifolium</i>		30 <sup>j</sup>	75 <sup>j</sup>			C3	H7
<i>Linum perenna</i>	19-60	30 <sup>g</sup>	20 <sup>g</sup>	Cuneate (L>3W)	10-50	C3	H7 <sup>g</sup>
<i>Melica ciliata</i>	106-240	30 <sup>j</sup>	55 <sup>j</sup>	Grass-like <sup>h</sup>		C3	H6
<i>Origanum vulgare</i>	511	20	35	Cuneate (L=1-3xW)		C3	H6
<i>Petrorhagia saxifraga</i>		30 <sup>g</sup>	20 <sup>g</sup>	Acicular <sup>h</sup>		C3	USDA 2-9 <sup>g</sup>
<i>Salvia pratensis</i>	6576	30	58	Cordate (L=1-3xW)	Deep	C3	H7
<i>Silene uniflora (maritime)</i>	273	25	10		Deep	C3	USDA 3 <sup>c</sup>
<i>Teucrium chamaedrys</i>	115-177	30 <sup>g</sup>	30 <sup>g</sup>	Broad <sup>i</sup>	37 <sup>i</sup>	C3	USDA 5-9 <sup>g</sup>
<i>Thymus vulgaris</i>	6 <sup>b</sup>	30 <sup>j</sup>	20 <sup>j</sup>	Broad <sup>i</sup>	59 <sup>i</sup>	C3	H6
<i>Sedum acre</i>	6 <sup>b</sup>	20	5	Acicular <sup>h</sup> (L=1-3xW)	Shallow	C3	USDA 4 <sup>c</sup>
<i>Sedum album</i>	17-32	20	15	Acicular <sup>h</sup> (L=1-3xW)		C3	USDA 4 <sup>c</sup>
<i>Sedum reflexum</i>		20	20			CAM	USDA 4 <sup>c</sup>

<sup>g</sup> Plants for a Future: [www.pfaf.org](http://www.pfaf.org), accessed on 29 June, 2016.

<sup>h</sup> BBC: [www.bbc.co.uk/gardening/plants](http://www.bbc.co.uk/gardening/plants), accessed on 29 June 2016.

<sup>i</sup> Paula *et al.* (2009).

<sup>j</sup> Royal Horticultural Society: [www.rhs.org.uk](http://www.rhs.org.uk), accessed 29 June 2016.

*Leaf size:* A small leaf size is conducive to the formation of a thin boundary of still air above the leaf which helps to improve water use efficiency when moisture availability is low (Garnier *et al.*, 2016). However, larger leaves have a greater mass to maintain, increasing drought risk (Butler & Orians, 2011).

*Root depth:* Vegetation with deep roots can often lower the risk of drought stress by accessing moisture that would be below the root zone of many shallow-rooted plants. However, in green roof constructions with shallow (80 mm) depths of substrate, this is not expected to be the case (Butler & Orians, 2011).

*Leaf shape:* All of the Sedum species in the Sedum mat (and the Meadow Flower mix) are classed as succulents (Kattge *et al.*, 2012). As a result, it is expected that moisture will be retained in the leaves of Sedum species, increasing storage capacity relative to Meadow Flower. Many of the Sedum species have acicular (pointed shaped) leaves. However, their length to width ratio is typically lower than with many of the species in the Meadow Flower mix, which contains a large number of species that have long blade-shaped leaves (i.e. grass-like). As a result, this vegetation would typically have a lower coverage than Sedum (MacIvor & Lundholm, 2011) which could lead to higher evaporation from the exposed underlying wet substrate.

*Photosynthetic Pathway:* According to the TRY database (Kattge *et al.*, 2012), one of the Sedum species (*Sedum reflexum*) in the Meadow Flower mix is classified as having a CAM photosynthetic pathway. All other species in the mix are classified as C3. The Sedum mat also contains *Sedum reflexum* plus one additional species (*Sedum hispanicum*) that is classified in the database as CAM cycling (i.e. generally acting as a C3 plant, but where a CAM response can be triggered). It is not known what triggers the change (Voyde, 2011; Sayed, 2001). Moisture restrictions are believed to be one possible trigger (Starry *et al.*, 2014). It is therefore possible that when moisture availability is limited, ET from Sedum vegetation will be reduced to a greater degree than it will be from Meadow Flower.

*Hardiness*: In the UK, the Royal Horticultural Society (RHS) uses hardiness categories that are broadly based on UK-specific growing conditions ([www.rhs.org.uk](http://www.rhs.org.uk), accessed 29 June 2016), including:

- H4: Tolerate temperatures of -10 to -5 °C. Hardy in most UK areas.
- H5: Tolerate temperatures of -15 to -10 °C. Hardy even in severe UK winters.
- H6: Tolerate temperatures of -20 to -15 °C. Hardy in the UK and northern Europe.
- H7: Tolerate temperatures below -20 °C. Hardy in the severest European climates.

Categorisation under the United States Department of Agriculture (USDA) approach is based on the average annual extreme minimum winter temperature (over a 30 year period) in increments of 5 °F. For example, Zone 1a is for a minimum temperature of between -60 and -55 °F, Zone 1b for between -55 and -50 °F, Zone 2a for between -50 and -45 °F and so on for up to Zone 13b, for temperatures of between 65 and 70 °F (see <http://planthardiness.ars.usda.gov>, accessed on 29 June 2016). As such, the UK and USDA numbers broadly equate to each other (i.e. H4 is approximately USDA 4). The Meadow Flower mix comprises two species with low hardiness (i.e. *Petrorhagia saxifrage* and *Silene uniflora*). However, equally, there are some species (e.g. *Salvia pratensis* and *Teucrium chamaedrys*) with greater hardiness than the species in the Sedum mat. Due to the number of species in the Meadow Flower mix, each with different tolerance levels, it is possible that the dynamics of the plant species composition will change over time (Dunnett *et al.*, 2008b; Rowe *et al.*, 2012).

### 3.3.4 Drainage layer characteristics

Two drainage layers were employed during the research. ZinCo FD25 was used in field trials and ZinCo DBV12 was used in ET trials. The characteristics of both drainage layers are as published by Alumasc in the relevant product data sheets (Alumasc 2006a & 2006b). The ZinCo Floradrain® FD25 drainage layer is a 25 mm high element that is thermoformed from HD-PE into a double cusplate (see Figure 3.4). As such, this ‘egg box’ profiled drainage layer has a water reservoir capacity of up to 3 l/m<sup>2</sup>. At a 2% hydraulic gradient, the maximum in-plane flow rate is 0.85 l/(s·m). For the ET laboratory trials, an alternative drainage layer – ZinCo DBV12 – was used. The DBV12 drainage layer is a single cusplate (i.e. a studded sheet). This product is sometimes used for drainage near to

foundation walls (having an in-plane flow rate of 3.2 l/(s·m) at 100% hydraulic gradient). At a 2% hydraulic gradient, the maximum in-plane flow rate is 0.4 l/(s·m). However, importantly, the product has zero water storage capacity, even in horizontal applications.



Figure 3.4: ZinCo Floradrain® FD25 (left) and DBV12 (right) drainage layers

By using the DBV12 drainage layer in ET trials, the differences in retention for each plant-soil combination could be considered independently of any contribution from the underlying drainage layer. In each case, an additional geo-textile (ZinCo SF filter sheet) was installed between the drainage layer and the substrate to allow the filtration of water without the passage of soil solids.

### 3.4 Results

#### 3.4.1 Substrate characteristics

##### 3.4.1.1 Physical characteristics

Table 3.3 summarises the results of the FLL characteristic tests on the three substrates.

Table 3.3: Substrate characteristics according to FLL (2008) test methods

Characteristic	Units	HLS		SCS		LECA	
		Mean	St. Dev	Mean	St. Dev	Mean	St. Dev
Dry Density	g/cm <sup>3</sup>	0.95	0.04	1.06	0.05	0.41	0.00
Wet Density	g/cm <sup>3</sup>	1.36	0.02	1.45	0.07	0.76	0.02
Total Pore Volume	%	63.8	1.6	59.8	2.0	84.8	0.0
MWHC (field capacity)	%	41.2	2.3	39.1	2.1	35.0	1.6
Air content at MWHC	%	22.6	0.8	20.7	4.1	49.8	1.5
Organic Content	%	3.8	0.1	2.3	0.5	6.0	0.3
Permeability	mm/min	1 - 15		10 - 35		>30	
Particle Size < 0.063mm	%	2.3	1.3	1.9	0.3	1.5	1.1
d <sub>50</sub>	mm	4.2	0.5	5.2	0.5	4.9	0.2

The dry density of the LECA substrate was less than half that of the HLS and SCS substrates. This is consistent with the very high porosity of LECA (84.8%). A large proportion of the pores in LECA do not appear to retain matric moisture. Even when the substrate has a moisture content equal to its MWHC of 35%, 49.8% of the substrate was filled with air. The physical composition of the two brick-based substrates (i.e. HLS and SCS) was broadly similar. Differences are marginal, but HLS has a lower density, higher porosity and greater MWHC than SCS. OM was lowest in SCS and highest in LECA.

Considerable uncertainty surrounds the permeability data, due to (a) the small size of test samples that comprise relatively heterogeneous green roof substrates, and (b) the FLL test procedure that requires only a 10 mm drop in head above highly permeable substrates. Further work to refine these test procedures has been called for (Fassman & Simcock, 2012) to derive a more meaningful permeability measurement for green roof substrates. The three substrates generally complied with FLL requirements for permeability (i.e. 0.6-70 mm/min). However, a range of measured values is presented here to reflect this uncertainty. This data serves as a guide only but allows comparative assessment of the substrates. The lowest permeability was observed with HLS and the highest with LECA.

Considering the granulometric distributions of HLS, SCS and LECA, all three substrates were almost wholly comprised of sand and gravel sized particles (see Figure 3.5).

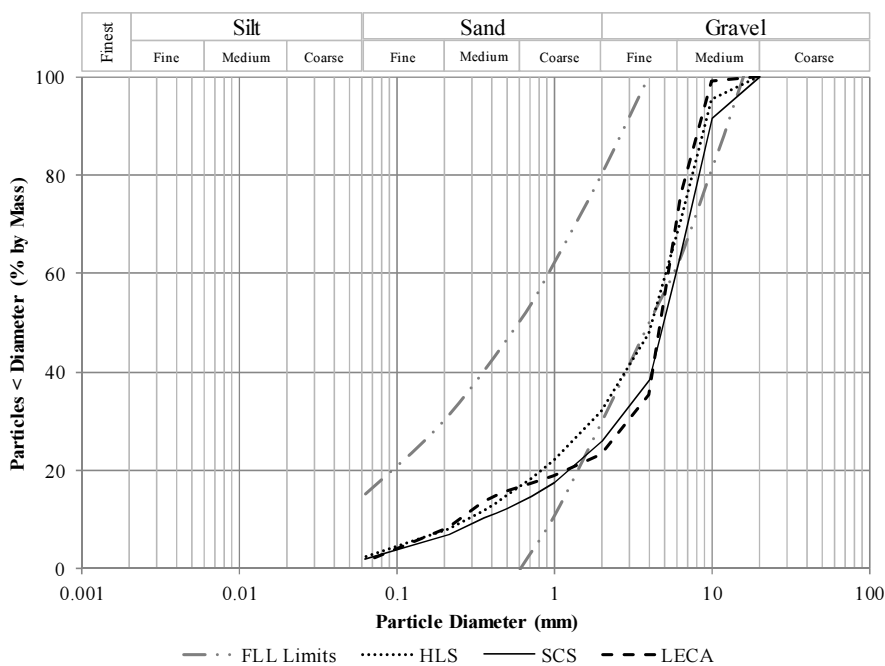


Figure 3.5: Granulometric distributions for HLS, SCS and LECA

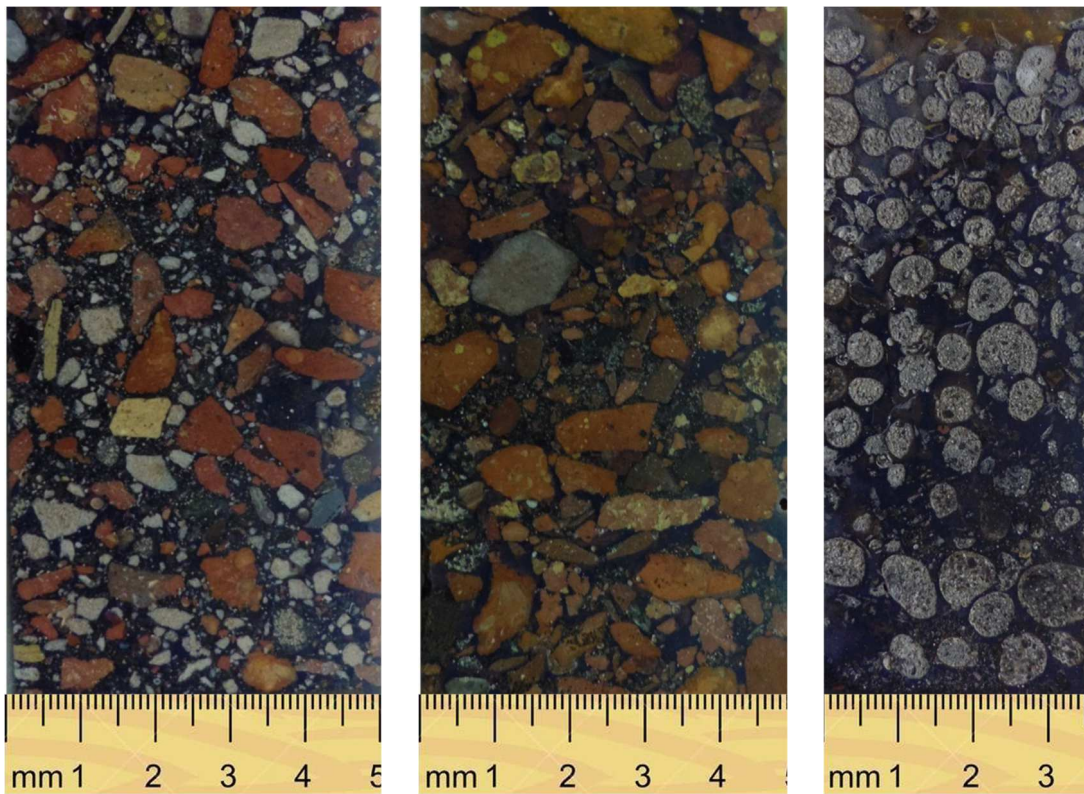


The silt content (i.e. particles less than 0.063 mm in diameter) of all three substrates was minimal; with mean values ranging between 1.5% (*w/w*, with LECA) and 2.3% (HLS). Standard deviations were shown in Table 3.3. None of the substrates contained ‘coarse gravel’ (i.e. particles greater than 20 mm in diameter). Both SCS and LECA fell marginally outside of the FLL Guidelines (FLL, 2008) for acceptable substrate compositions on extensive green roofs due to the small proportion of particles between 1.0 and 4.0 mm in diameter. 53% of LECA’s composition would be classed as ‘fine gravel’ (2.0 to 6.3 mm). However, 41% of the substrate was composed of particles between 4.0 and 6.3 mm in diameter. This is indicative of a substrate that is not well-graded. The ‘fine gravel’ content of HLS and SCS was lower than LECA (39% and 37% respectively). In HLS, the proportion of ‘sand’ (0.063 to 2.0 mm) and ‘medium gravel’ (6.3 to 20 mm) was similar (approximately 29%). However, the ‘medium gravel’ content was highest in SCS (37%). Consequently, the ‘sand’ content of SCS was lower (24%) than in HLS.

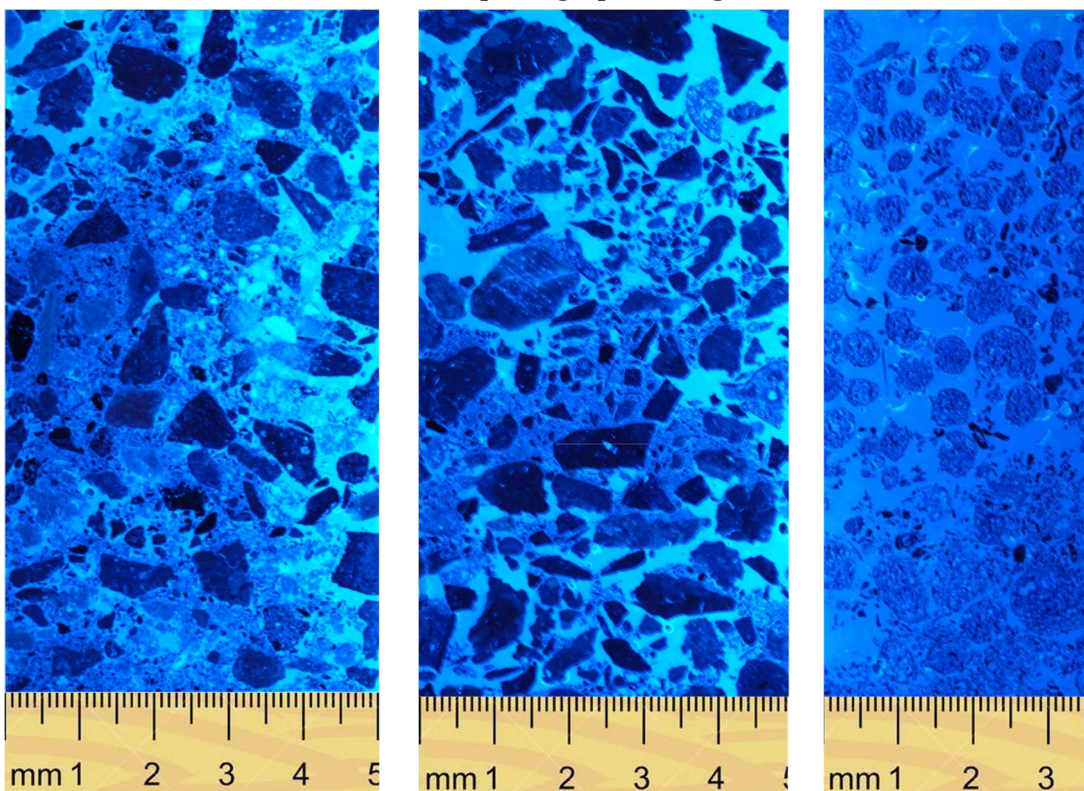
#### 3.4.1.2 *Void-size distribution*

The photographic images of the polished blocks under ultra-violet light were not of a sufficient quality to quantitatively assess the VSD of the three substrates. This problem has previously been noted by Graceson *et al.* (2013) – internal-to-aggregate pores can be very difficult to impregnate with resin whilst inter-aggregate voids can be interconnected to such an extent that it is impossible to separate them. However, the images were suitable for some qualitative assessments of the packing and distribution of particles in the soil matrices (see Figure 3.6).

The images appear to confirm many of the findings of the FLL characteristic tests. The better grading of the particle sizes in the HLS and SCS substrates, compared to LECA, was evident here. The high proportion of fine particles (both organic and inorganic matter) in HLS and the greater number of large particles in SCS were identified in the images. As a consequence of these properties, typically, voids in SCS appeared to be larger than in HLS, where voids were generally smaller.



*Standard photographic images*



*Images under ultra-violet light*

*Figure 3.6: Images of HLS (left), SCS (centre) & LECA (right) in hardened resin*

The spherical shape of the LECA particles appeared to result in OM being washed out of the upper and middle zones of the substrate, settling towards the lower zone of the sample. Large voids were therefore observed in higher zones. In certain LECA samples, flotation of particles was observed when the resin mixture was added. This was particularly apparent in Figure 3.7. This trend would be consistent with the fact that this substrate has a density at MWHC of  $0.76 \text{ g/cm}^3$  (i.e. less than water). It was not possible to draw definitive conclusions from the images. However, there was evidence to suggest that the porous nature of the expanded clay aggregate contributed to additional moisture storage potential that would be internal to the aggregate.

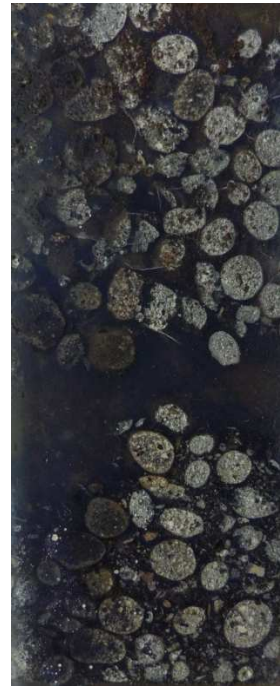


*Figure 3.7: LECA Substrate*

#### 3.4.1.3 Soil-water characteristic curve

Figure 3.8 demonstrates the results of the SWCC tests and, for HLS and SCS plots a logarithmic fit that best describes the  $\theta$ - $\psi$  relationship.

A log linear correlation was observed between  $\theta$  and  $\psi$  for both HLS and SCS. Only minor differences were observed in the SWCC for HLS and SCS substrates. A marginally steeper gradient was observed in the  $\theta$ - $\psi$  relationship for HLS than for SCS; indicating a slightly greater change in the residual moisture content within HLS for the same change in potential energy. A slight deviation in moisture release was observed once  $\theta$  fell to 0.18, with a slower moisture release from SCS. However, once  $\theta$  was less than 0.11, the same moisture release behaviour was observed for the two substrates. No clear  $\theta$ - $\psi$  relationship could be established for LECA. Indeed, in some instances, water content apparently increased with rising  $\psi_m$ . It is expected that the difficulty in deriving a SWCC for LECA can be explained by the previously-identified issues (i.e. large voids due to a high proportion of similarly-sized particles and associated settlement of the organic content combining with internal to the aggregate moisture storage that is released at higher matric pressures).

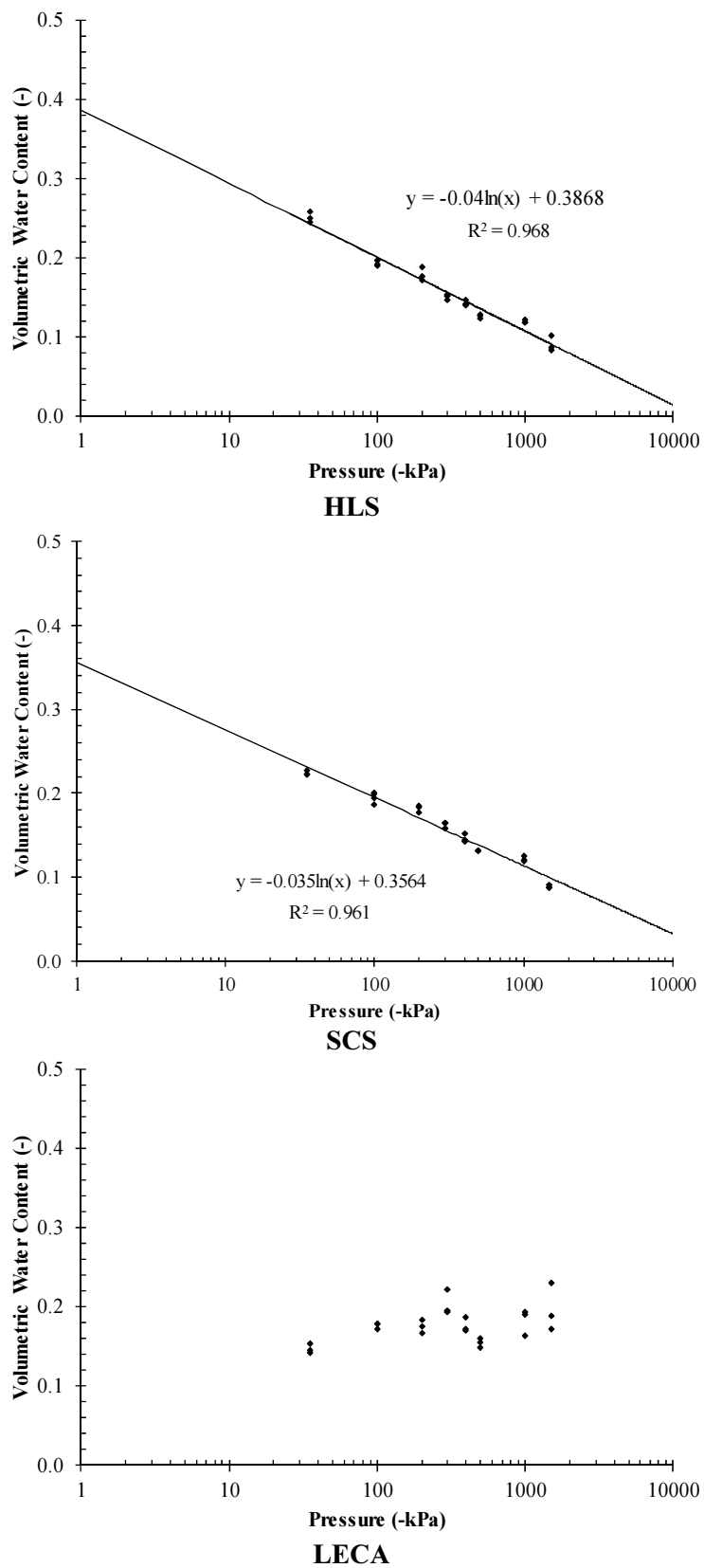


Figure 3.8: Soil Water Characteristic Curve for HLS, SCS and LECA

At a pressure of 35 kPa (i.e. nominal field capacity),  $\theta$  was 0.25 and 0.22 for HLS and SCS respectively. The values derived from the SWCC were therefore much lower than the respective values of MWHC that were derived during the FLL characterisation tests. The  $x$  axes of the SWCC plots were set to allow the extrapolation of the SWCC line to matric pressures as low as 1 kPa. At this threshold, the values of  $\theta$  approached the MWHC values. Doubts must therefore be expressed as to the validity of the conventional definition of field capacity when considering highly-porous green roof substrates. Further work has already been called for in this area (Fassman & Simcock, 2012).

Equation 3.1 (HLS) and Equation 3.2 (SCS) demonstrate the similarity with which changes in soil moisture content affect potential energy within the two substrates:

$$\psi = \text{Exp} \left( \frac{\theta - 0.03868}{-0.04} \right) \quad \text{Equation 3.1}$$

$$\psi = \text{Exp} \left( \frac{\theta - 0.03564}{-0.0351} \right) \quad \text{Equation 3.2}$$

These two equations will be employed in later chapters.

### 3.4.2 Vegetation

The appearance of the two vegetation treatments across a full annual cycle (starting approximately 18 months after initial planting) is shown in Figure 3.9 (Sedum mat) and Figure 3.10 (Meadow Flower mix). In each case, there was evidence of the traits referenced in Table 3.1 and Table 3.2.

Consistent with a succulent species' tendency to retain moisture in its leaf structure, the leaves of certain Sedum species in the mat were seen to swell from spring onwards. Flowering was at its most abundant in late spring and early summer. However, generally, the treatment formed a mat of low-growing vegetation with any flowers being low in height and short-lived. As expected, in late summer and early autumn, red and brown colours dominated the Sedum vegetation. Lower moisture availability would partially explain this. With both vegetation treatments, plant growth appeared to be either stunted or dormant from mid-autumn throughout the winter. At this time, as would be expected, the vegetation was a low-growing ground cover of plants without flowers. In the case of Sedum, the coverage of green plants appeared to reduce, leaving scope for weed seeds to

germinate and form part of the Sedum vegetation. This would be consistent with Sedum's expected response to wet conditions. However, earlier in the year (i.e. in spring and summer), the foliage of both vegetation treatments was more varied and interesting.

With Meadow Flower, a greater variation in the traits of the plants was observed. Some tall thin grasses formed alongside lower-growing species. In late spring and early summer, a range of leaf sizes and shapes were observed, including long and thin grass-like leaves to broader cordate-shaped leaves. During spring and summer months, the leaf area of Meadow Flower appeared to be greater than that of Sedum. However, at no point did any plants reach the heights shown in Table 3.2. By late summer, the foliage of the Meadow Flower treatment was dominated by red and brown colours, increasingly sparse and almost wholly comprised of low-growing mat-forming grasses and plants. This is consistent with expectations of an increased risk of drought stress with Meadow Flower.

### **3.5 Discussion**

A substrate's particle-size and void-size distribution governs its maximum storage (or field) capacity (Beattie & Berghage, 2004) and the extent of matric potential – the driving force for soil-water movements in unsaturated conditions (Manning, 1987). Substrates with a higher proportion of small voids will be expected to have a greater retention capacity and lower permeability. This was observed here with HLS: MWHC was highest (41.2%) and permeability was lowest (between 1 and 15 mm/min). Despite its greater overall porosity, LECA had a lower MWHC (35.0%) due at least in part to the size and connectivity of voids in the LECA substrate. LECA contained the lowest proportion of small particles ( $1.5\% < 0.063$  mm) and a high proportion of similarly-sized particles.

The three substrates have different material compositions but similar PSD curves. The similarities are not surprising considering that two of the substrates were developed according to the FLL guidelines which restrict the range of permissible granulometric distributions. However, whilst PSD is often used as a readily-measurable alternative to more complex methods of determining VSD, a substrate's PSD does not take into account differences in shape or arrangement of particles. As such, caution is required when using the PSD to infer moisture retention and release characteristics of substrates; particularly where they are dominated by large spherically-shaped particles (e.g. LECA). The void shapes and sizes of LECA were seen to be different to the two brick-based substrates.

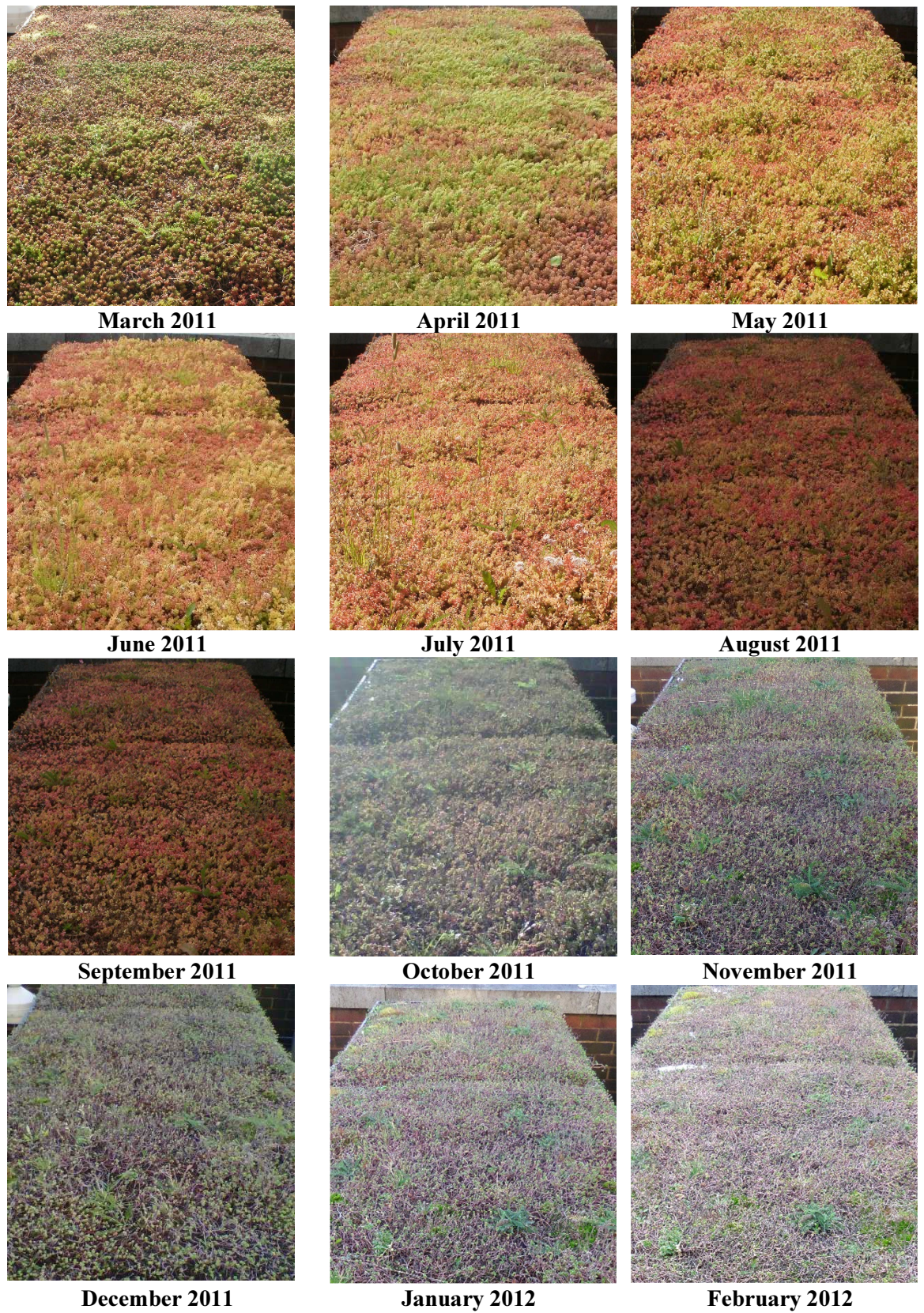


*Figure 3.9: Sedum vegetation appearance through an annual cycle*

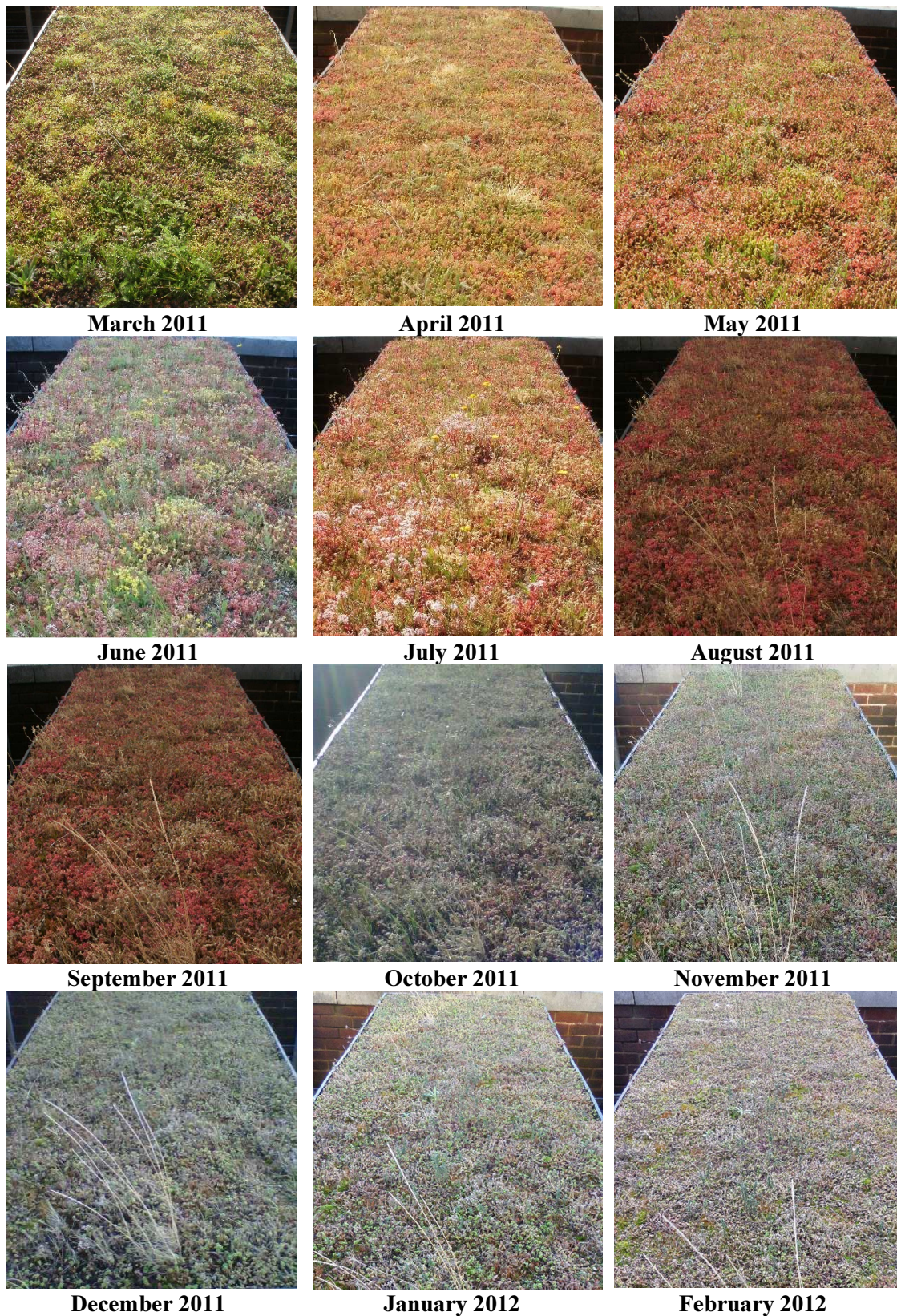


*Figure 3.10: Meadow Flower appearance through an annual cycle*



The development of a SWCC can provide accurate insights into the retention and release characteristics of a substrate. However, the derivation of a SWCC can be time-consuming; particularly when characterising the response at highly negative pressures (e.g. -1500 kPa). Indeed, as was observed here when testing the LECA substrate, obtaining a SWCC may not always be possible. Similarly, the applicability of conventionally quoted thresholds for permanent wilting point (-1500 kPa) and field capacity (-35 kPa) to green roof substrates requires further consideration. For HLS and SCS respectively,  $\theta$  was 0.09 and 0.089 when  $\psi$  was equal to -1500 kPa and 0.25 and 0.224 when  $\psi$  was -35 kPa. These values indicate that the moisture capacities of these substrates are substantially lower than the MWHC values obtained via the FLL tests. It is possible that these differences were due to either the procedure of sieving the substrate samples ahead of the low pressure (i.e. field capacity) tests or the subsampling and/or boundary effects associated with small sample sizes. However, the differences are sufficiently large to echo previous calls (Fassman & Simcock, 2012) for further research into the definitions of wilting point and field capacity when applied to green roofs.

### **3.6 Conclusions**

It was expected that Sedum vegetation would provide a more consistent, dense coverage of low-growing hardy plants relative to Meadow Flower. This was not the case. In spring and summer, the Meadow Flower treatment had a greater density of foliage. However, as expected, the lower tolerance of Meadow Flower to drought stress was witnessed in late summer.

- Differences in the responses of brick-based substrates are expected to be minor, but systematic. Greater differences exist when contrasting HLS and SCS with LECA.
- The HLS substrate contained the highest proportion of particles less than 0.063 mm (2.3%) and the lowest  $d_{50}$  (4.2 mm), resulting in the highest maximum water-holding capacity, MWHC (41.2%) and the lowest permeability (1-15 mm/min). This substrate is marketed as suitable for biodiverse and semi-intensive green roofs.

- SCS had the lowest porosity (59.8%) but the highest  $d_{50}$  (5.2 mm) of any trialled substrate. SCS had a marginally lower MWHC (39.1%) than HLS. The composition of SCS was optimised for use with Sedum vegetation, with a high proportion of crushed brick and the lowest OM content (2.3%) creating the nutrient poor growing conditions that Sedum prefer.
- The LECA substrate was very lightweight ( $0.41 \text{ g/cm}^3$  dry density), comprising a high proportion of large and similarly-sized spherical particles. LECA has a very high porosity (84.8%). 49.8% of the LECA substrate is air-filled at field capacity, such that MWHC is 35.0%. LECA had the highest OM content (6.0%). However, the poor grading of particle sizes contributed to the settlement of the OM towards the lower echelons of the substrate matrix.
- Sedum vegetation comprises hardy, succulent plants that have the greatest moisture storage potential. Three Sedum species have a C3 photosynthetic pathway, one has CAM and one is CAM cycling. Subject to the dominant species in the mat, some CAM behaviours may be expected. ET may be slower with Sedum than with Meadow Flower. However, greater tolerance is expected to drought and extreme temperatures.
- Meadow Flower contains some succulent species, but is mainly comprised of wild flowers and thirsty grasses. A greater density and variety of foliage was observed in summer but greater variability in coverage was witnessed during other seasons. ET rates are expected to be higher in spring and summer with Meadow Flower. However, this is expected to exacerbate drought conditions.

## 4 Field evaluation of green roof hydrological performance

### 4.1 Chapter overview

This chapter presents analyses of data derived from a field research study conducted at the Sir Robert Hadfield building at the University of Sheffield. Retention and detention performance are evaluated to identify the important controls upon the hydrological response of extensive green roofs. Per-event retention, peak attenuation and peak delay responses are presented for nine test beds during 48 individual storm events. The influences of rainfall depth, moisture balance and climatic conditions are analysed whilst also identifying variations that result from differences in green roof configuration.

Earlier analyses and discussions of the data presented here formed the basis of two journal papers and two conference papers.

Berretta, C., Poë, S., Stovin, V. (2014a). Moisture content behaviour in extensive green roofs during dry periods: The influence of vegetation and substrate characteristics, *Journal of Hydrology*, 511, 374-386.

Stovin, V., Poë, S., De-Ville, S. and Berretta, C. (2015a). The influence of substrate and vegetation configuration on green roof hydrological performance, *Ecological Engineering*, 85, 159–172.

Poë, S., Stovin, V., Dunsiger, Z. (2011). The Impact of Green Roof Configuration on Hydrological Performance. Proceedings of the 12th International Conference on Urban Drainage. Porto Allegre, Brazil, 11-16 September.

Berretta, C., Poë, S., Stovin, V. (2014b). The Influence of Substrate and Vegetation on Extensive Green Roof Hydrological Performance. Proceedings of the 13th International Conference on Urban Drainage. Sarawak, Malaysia, 7-12 September.

The test setup described here was financed by the EU's European Regional Development Fund and designed by Kasmin *et al.* (2010).

## 4.2 Motivation

In storm water management terms, the use of average annual green roof retention efficiencies to predict responses to a specific event fails to adequately characterise a number of important physical controls upon the hydrological response. The retention response is contingent upon antecedent conditions (Bengtsson *et al.*, 2005; DeNardo *et al.*, 2005) resulting from complex inter-event processes (Stovin *et al.*, 2012) that vary as a function of seasonal climate (Mentens *et al.*, 2006; Stovin *et al.*, 2012) and configuration characteristics (Villareal & Bengtsson, 2005; Graceson *et al.*, 2013). At present, evidence to demonstrate the hydrological performance of green roofs is insufficient (Berndtsson, 2010). A lack of quantitative data to describe the hydrological benefits of green roofs is a major barrier to wider uptake in the UK (Fioretti *et al.*, 2010 in Nawaz *et al.*, 2015). Empirical monitoring data is therefore required (Elliott & Trowsdale, 2007) to reduce the number of uncertainties associated with the large number of parameters that influence the response (Jayasooriya & Ng, 2014). Detention is expected to vary with a configuration's vegetation and substrate.

Here, field research data will be collected to facilitate the evaluation of per-event statistics for retention, peak attenuation and peak delay. Consideration will be afforded to the influence of rainfall depth and intensity, seasonal climate and configuration differences upon the hydrological response. The importance of moisture balance to the response will also be evaluated; identifying the extent to which runoff can occur prior to field capacity, the contribution of vegetation to interception losses and any errors that may be introduced by treating an extensive green roof as a single moisture store. Systematic differences in detention responses will also be identified and evaluated. In subsequent chapters, the empirical data set will serve to develop and test the validity of a predictive model.

## 4.3 Materials and methods

This research was conducted in parallel with the wider Marie Curie IAPP research programme on green roof hydrology at the University of Sheffield. Where applicable, resources made available as a result of this programme will be acknowledged.

### 4.3.1 Experimental setup

The research was conducted at a test site on a fifth-floor terrace of the Sir Robert Hadfield building (Grid Reference 53.3816, -1.4773) at the University of Sheffield. Established in

the summer of 2009, following the experimental design of Kasmin (2010), data have been collected since April 2010. Figure 4.1 provides a photographic overview of the site.

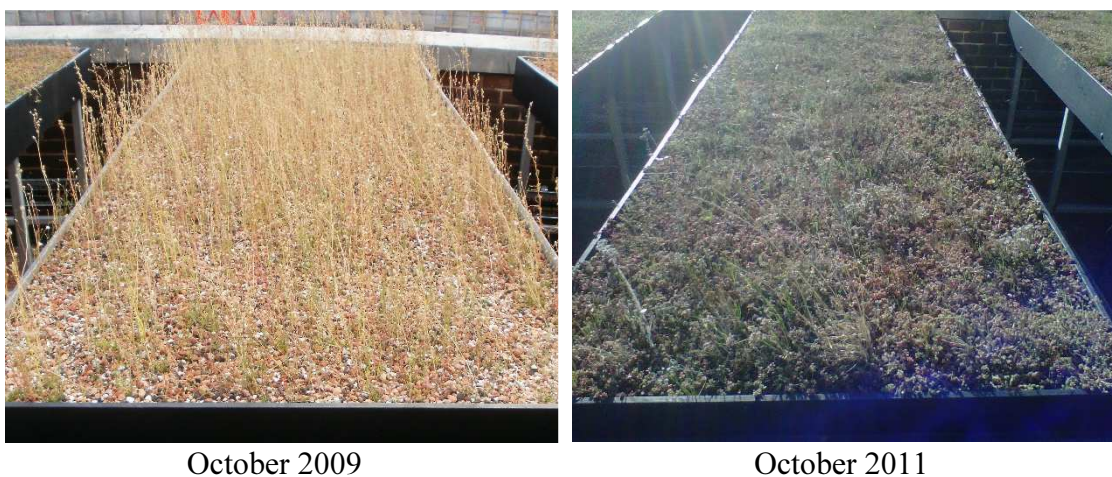


Figure 4.1: Field research site at Hadfield Building, University of Sheffield

### 4.3.2 Test configurations

10 green roof test beds (TB) – 3 metres in length and 1 metre wide – were installed to a 1.5° slope (i.e. the minimum typical gradient for a flat roof). A shallow gradient would be expected to improve the hydrological performance relative to a roof with a steeper slope (Getter *et al.*, 2007). All TBs consisted of an impervious hard plastic base, a drainage layer (ZinCo Floradrain FD 25-E), a filter sheet (ZinCo System filter SF), and one of three substrates (80 mm deep). The tenth test bed – initially containing a hybrid mix of recyclable brownfield site waste and subsequently replaced with a non-vegetated Marie Curie substrate – was monitored but does not form part of this research. The nine monitored TBs allowed the comparative evaluation of the responses of configurations that combined 3 substrates and 3 vegetation treatments. Researching a higher number of configuration variables was at the expense of greater replication. However, this was considered necessary to identify the physical influences of different substrates and vegetation treatments upon the hydrological response.

A detailed description of the substrates and vegetation treatments was provided in Chapter 3. Heather & Lavender Substrate (HLS) was installed on TB1, TB4 and TB7. Sedum Carpet Substrate (SCS) was adopted in TB2, TB5 and TB8. The substrate comprising 80% Lightweight Expanded Clay Aggregate, 10% loam (John Innes No. 1) and 10% compost (LECA) was installed on TB3, TB6 and TB9. Sedum vegetation was established on TB1, TB2 and TB3. Meadow Flower mix was grown on TB4, TB5 and TB6. TB7, TB8 and TB9 were maintained without vegetation. The two vegetation treatments were established in 2009 - ahead of data collection from 2010. Test beds were maintained more regularly than a typical extensive green roof (i.e. more than twice a year). Weeding was typically carried out at monthly intervals, coinciding with data collection, to avoid the growth of vegetation in the non-vegetated beds. Irrigation was only necessary once, during the summer of 2012. Predictably, the physical characteristics and appearance of the vegetation treatments changed seasonally and over time. In particular, the surface coverage of the Meadow Flower varied; becoming relatively sparse during winter months and, over time, becoming increasingly dominated by the hardy Sedum species within the species mix. Figure 4.2 provides a comparative snapshot of the Meadow Flower treatment in October 2009 and 2011.



*Figure 4.2: Differences in Meadow Flower treatment over time*

In October 2011, after two full growing cycles, the majority of taller grass species had been replaced by a combination of low-growing grasses and Sedum species. Over time, and particularly if subjected to prolonged periods of drought, it is expected that the hardy Sedum species would become increasingly dominant.

### 4.3.3 Data collection

Rainfall, runoff and weather station data were logged directly to a Campbell Scientific CR3000 data logger. An AM16/32 multiplexer extended the number of ports to allow collection of moisture content data from CS616 water content reflectometers. A program written in CR basic programming language was used to log and convert the collected data. The research data was collected from a Campbell Scientific weather station (as Figure 4.3a) to record hourly temperature, solar radiation, relative humidity, wind speed and barometric pressure, three rain gauges (as Figure 4.3b), runoff tanks (as Figure 4.3c) and moisture content reflectometers.



*a) Tripod for weather station*



*b) Rain gauge*



*c) Runoff collection tank*

*Figure 4.3: Field research weather station equipment*

#### 4.3.3.1 Climatic data

With the exception of rainfall, all climatic data was collected at hourly intervals. This was consistent with the minimum typical interval at which ET is estimated. Furthermore,

greater frequencies of data collection were not deemed to be necessary due to the relatively small changes in solar radiation, temperature, relative humidity and atmospheric pressure that would be expected to occur within time intervals of less than one hour.

### Solar Radiation

Net radiation acts to heat the air and ground or to evaporate water. Net short-wave radiation acts to vaporize water and is the difference between incoming short-wave radiation from the sun and outgoing short-wave radiation that is reflected by the surface. Incoming short-wave radiation was measured (in  $W/m^2$ ) via a pyranometer (SP LITE) in an unshaded location on the tripod. The photodiode detector created a voltage output that was proportionate to incoming solar radiation. The maximum published error across the spectrum of the SP-LITE is approximately  $\pm 5\%$ . The reading was converted to  $MJ/m^2/day$  by multiplying the value in  $W/m^2$  by 0.0864.

Long-wave radiation was not measured. Net long-wave radiation is the difference between incoming long-wave radiation – governed by the temperature and emissivity of the atmosphere – and outgoing long-wave radiation (dependent on the temperature and emissivity of the green roof surface). However, air temperature and relative humidity were measured.

### Temperature & Relative Humidity

A CS215 probe recorded air temperature and relative humidity; key indicators of the boundary air's capacity to 'absorb' vapour leaving the green roof. The sensor was protected from dust by a filter and from radiation by a shield. Relative humidity (RH) readings were referenced against a saturated water vapour pressure above liquid water (as defined by the World Meteorological Organisation). For RH, the manufacturer cites an accuracy of  $\pm 2\%$  (for 10 to 90%) or  $\pm 4\%$  (for 0 to 100%). RH exceeded 90% at times during the research programme. Temperature readings are stated as accurate to  $\pm 0.9\text{ }^\circ\text{C}$  (across the large temperature range of  $-40\text{ }^\circ\text{C}$  to  $+70\text{ }^\circ\text{C}$ ) or to  $\pm 0.4\text{ }^\circ\text{C}$  (if temperatures are measured across a shorter range of between 5 and  $40\text{ }^\circ\text{C}$ ). Here, air temperatures of less than  $5\text{ }^\circ\text{C}$  were recorded.



### Atmospheric Pressure

Atmospheric pressure readings were recorded by a CS100 barometric pressure sensor on an hourly basis. Accuracy for the temperature range of -20 °C to + 50 °C is quoted as  $\pm 1.5$  mb, whilst repeatability is  $\pm 0.03$  mb. The reading in millibars was multiplied by 0.1 to convert to kPa and was entered as an offset in the data logger program. Ultimately, this parameter was not utilised in the research, but was originally incorporated in the event that measurements would inform hydraulic head calculations.

### Wind

Wind speed data was captured primarily to inform the rate at which saturated air above the green roofs was replaced with drier air. A 05103 wind monitor (from Campbell Scientific) recorded horizontal wind speeds by producing an AC sine wave signal with a frequency that was proportional to the wind speed. Wind speed readings are stated by the manufacturer as being accurate to  $\pm 0.3$  m/s. Wind direction – not analysed in this research – was measured using a 10 K $\Omega$  potentiometer, with an accuracy of  $\pm 3^\circ$ .

#### *4.3.3.2 Rainfall data*

Three ARG-100 tipping bucket rain gauges (0.2 mm resolution) – manufactured by Environmental Measures Ltd – were used to measure rainfall depth at one minute intervals. Gauges were located at the same height as the TBs; between TB1 and TB2, TB5 and TB6, and TB9 and TB10 (TB10 was not part of the comparative experiment reported here). The rain gauges are clearly visible in Figure 4.1 and Figure 4.3. Rainfall and runoff data was collected at 1 minute intervals. Such high temporal resolution was chosen to analyse the sensitivity of runoff responses to even the most intense rainfall with a high degree of accuracy. The time interval adopted here also ensured that the data set was consistent with typical approaches to hydrological analyses (e.g. 1-minute, 5-minutes, 60-minutes etc.).

#### *4.3.3.3 Runoff data*

Ten runoff collection tanks, each fitted with a PDCR 1830 pressure transducer (manufactured by Druck Inc.), measured runoff volumetrically from each bed at one minute intervals. The collection tanks, located under each bed, incorporated a platform

200 mm above the base to increase measurement sensitivity at the beginning of each rainfall event and to avoid direct discharge onto the sensor (see Figure 4.4).

Electronic solenoid valves in each tank emptied either at maximum capacity (1.75 mV) or at daily intervals (initially at 9:00, and latterly at 14:00, when problems were experienced with the opening of valves at low temperatures during winter mornings).

PDCR1830 transducers have a published accuracy of 0.1% (nonlinearity and repeatability) and long-term stability of  $\pm 0.1$  mV per annum. However, specific calibrations were carried out on site.

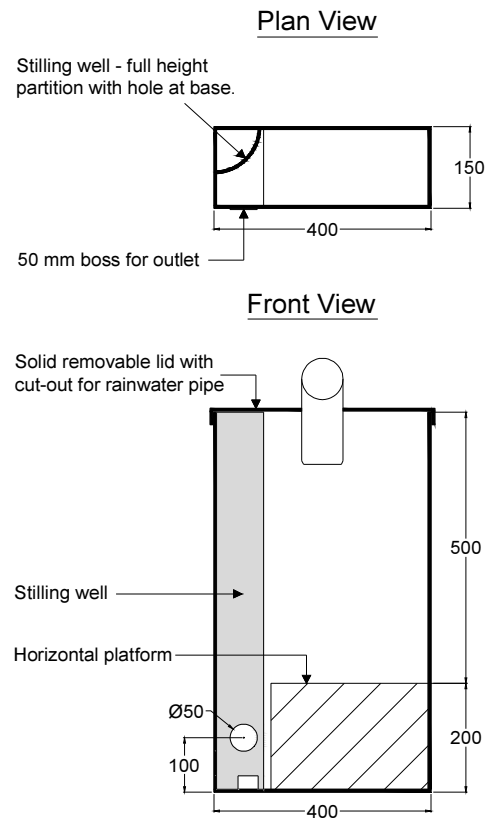


Figure 4.4: Runoff collection tank  
(all dimensions in mm)

Transducer readings of pressure were recorded at water volume increments of 0.2 litres (up to a cumulative volume of 2 litres, such that the water depth was above the platform in the tank) and thereafter in 2 litre increments. Generally, two linear trends were observed for the relationship between water volume and pressure (as Figure 4.5). This is consistent with the tank's configuration (i.e. the inclusion of the platform). Regression analyses were conducted for each tank, identifying the relevant linear trends and transition points ( $\delta xy$ ).

Runoff was calculated using Equation 4.1 through to Equation 4.3:

$$\begin{aligned}
 \text{If } Pressure \leq \delta xy: & \quad V_t = Pressure \times X_1 + Y_1 \\
 \text{Else:} & \quad V_t = Pressure \times X_2 + Y_2
 \end{aligned}
 \tag{Equation 4.1}$$

Where  $V_t$  was the volume of water stored in the tank at time  $t$ . Calibration checks were carried out periodically to determine any changes required to the  $X$  multipliers and  $Y$  intercepts so that the program could be updated accordingly.

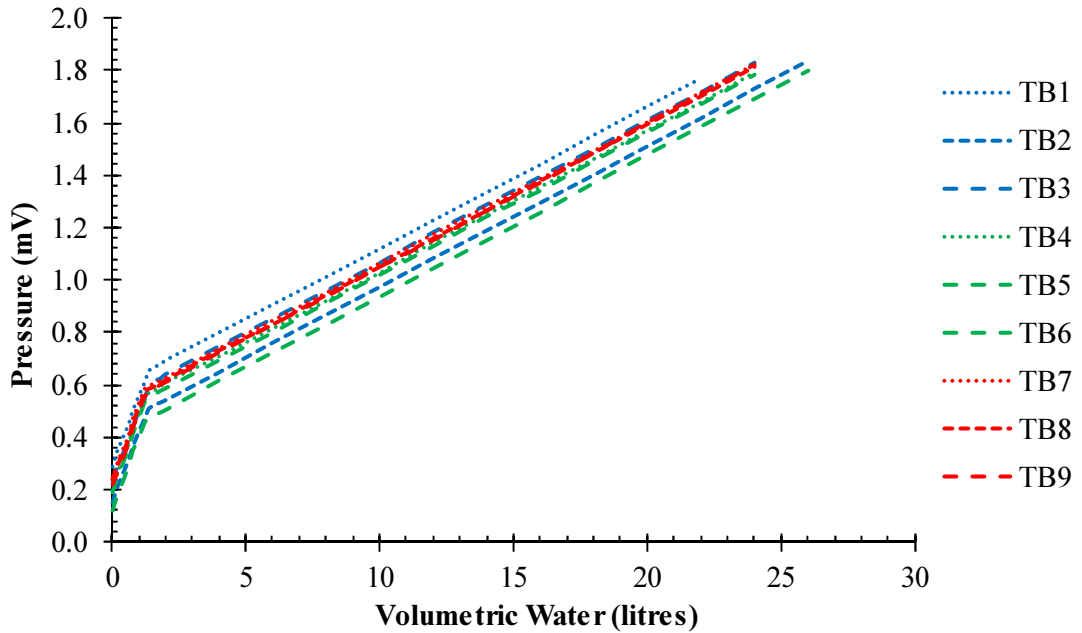


Figure 4.5: Calibration results for PDCR1830 pressure transducers

A data smoothing exercise was then performed on the changes to  $V_t$  during a runoff-generating event. The only physical justification for reduction in tank volumes would be during the opening of the solenoid valves for emptying. Therefore, to avoid overstating runoff as a result of minor transducer fluctuations, volume reductions of less than 0.1 litre were ignored; such that subsequent increases (back to equilibrium) were not falsely recorded as runoff:

$$\begin{aligned} \text{If } V_t \geq VS_{t-1} \text{ or } V_t < (VS_{t-1} - 0.1): & \quad VS_t = V_t \\ \text{Else:} & \quad VS_t = VS_{t-1} \end{aligned} \quad \text{Equation 4.2}$$

Where  $VS$  is the smoothed tank volume. Finally, runoff (in mm/m<sup>2</sup>) was calculated for each 3 m<sup>2</sup> bed as follows:

$$\begin{aligned} \text{If } VS_t < VS_{t-1}: & \quad Q_t = 0 \\ \text{Else:} & \quad Q_t = \frac{(VS_t - VS_{t-1})}{3} \end{aligned} \quad \text{Equation 4.3}$$

An example of the effect of smoothing is shown in Figure 4.6.

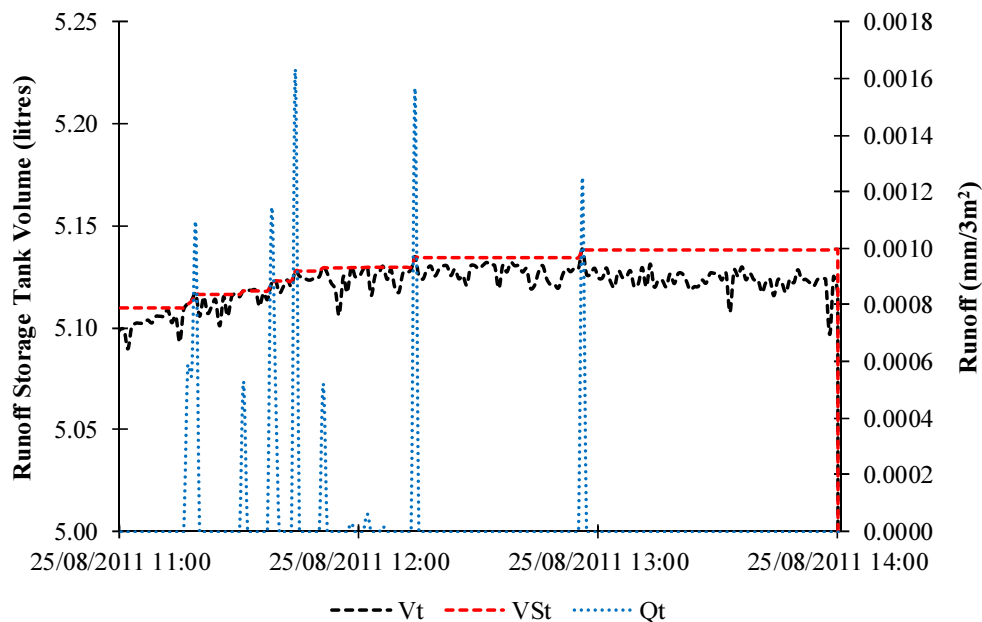


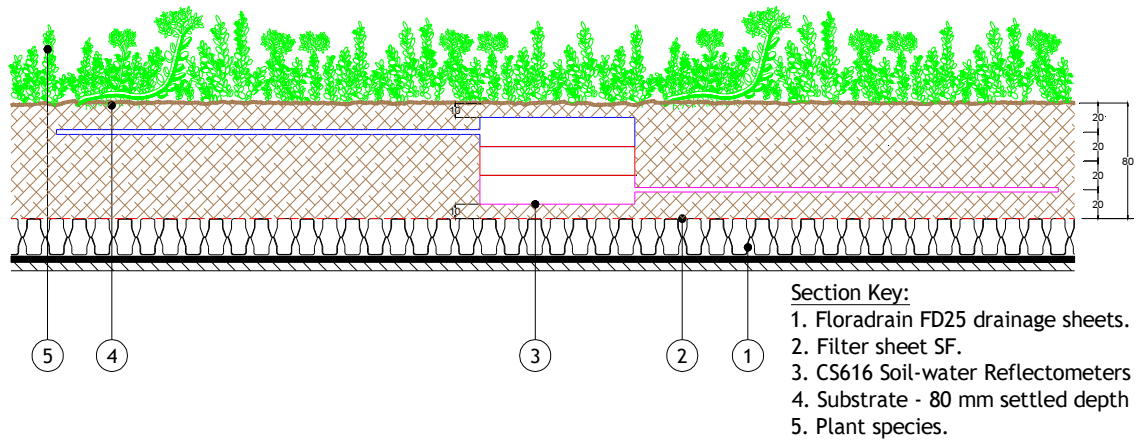
Figure 4.6: Smoothing of runoff storage tank readings by PDCR1830 transducers

#### 4.3.3.4 Moisture Content

The volumetric water content ( $\theta$ ) of the soil was measured using 12 number CS616 water content reflectometers installed into 4 beds (TB1, TB2, TB3 and TB7). Each bed contained a column of three CS616 water reflectometers to measure  $\theta$  at depths of 20 mm (upper zone,  $\theta_{TOP}$ ), 40 mm (middle zone,  $\theta_{MID}$ ) and 60 mm (lower zone,  $\theta_{LOW}$ ) relative to the surface (see Figure 4.7).

The CS616 probes were installed mid-length within each TB. Positioned in columns, the lower CS616 was placed onto 10 mm of levelled substrate. Substrate was manipulated by hand to minimise air voids surrounding the probes that can adversely affect accuracy. The printed circuit boards of the middle and upper CS616 probes were positioned onto the printed circuit boards of the probe below, rotated through 90 and 180 degrees respectively. The CS616 probes were differentially enabled to avoid inaccuracies attributable to noise, as simultaneously-enabled probes could not be located within 225 mm of each other. At 5 minute intervals, the data logger control port enabled the CS616 so that measurements could be taken. Sub-scan patterns were controlled by the CR basic data logger program.

Section:



Plan:

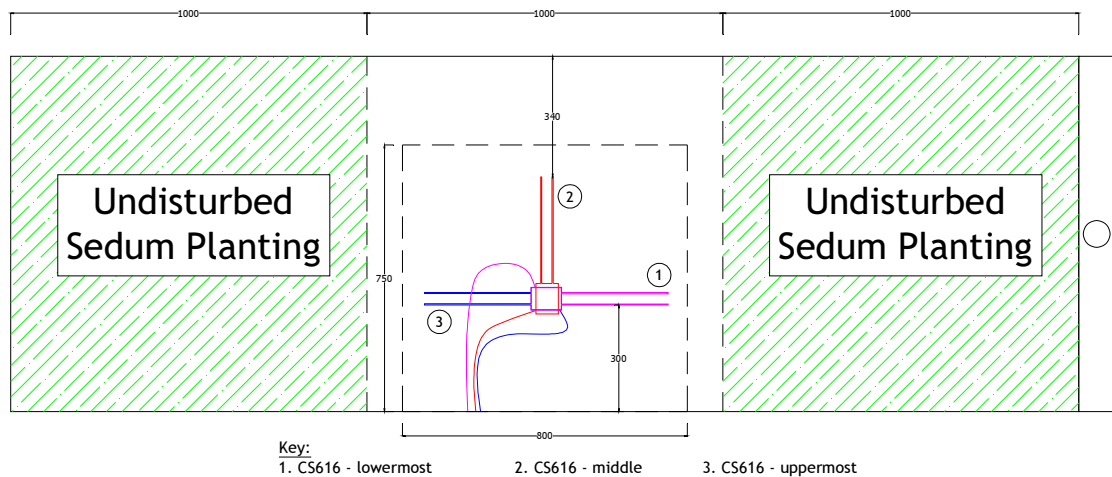


*Figure 4.7: Section and plan of test configuration*

The CS616 water content reflectometers operated in a similar manner to time domain reflectometry, except that the waveform and soil electrical conductivity were not measured by CS616. The CS616 is a transmission line oscillator that records the time for an electromagnetic pulse to reflect from the end of the probes. The period ( $\mu$ ) is derived from the travel time of the signal (Campbell Scientific Inc., 2006). The velocity of the pulse decreases (and so  $\mu$  increases) when moisture content increases. CS616 probes are sensitive to temperature. Campbell Scientific therefore publishes a standard temperature correction equation (Campbell Scientific Inc., 2006), which can be applied to the uncorrected  $\mu$  reading as follows:

$$\mu_{corr} = (\mu + (20 - T) \times (0.526 - 0.052\mu + 0.00136\mu^2)) \quad \text{Equation 4.4}$$

The manufacturer's published accuracy for CS616 readings is  $\pm 2.5\%$  for  $\theta$  between 0 and 50%. Published repeatability is 0.05% of  $\theta$ . Standard calibration equations are published by the manufacturer to convert  $\mu$  to  $\theta$ . However, due to the high porosity of green roof substrates, additional trials were carried out by Schwarz (2010) as part of a Knowledge Transfer Account research project at the University of Sheffield (funded by the Engineering and Physical Sciences Research Council). Schwarz (2010) compared known  $\theta$  with  $\mu$ ; concluding that a single calibration equation could be adopted to measure  $\theta$  in the range of 7 to 30% from all three substrates. As field capacities of the trialed substrates exceeded this upper limit, a regression analysis was conducted on the data collected by Schwarz (2010); identifying two lines of best fit with a transition point at  $\mu = 20.29$  (see Figure 4.8).

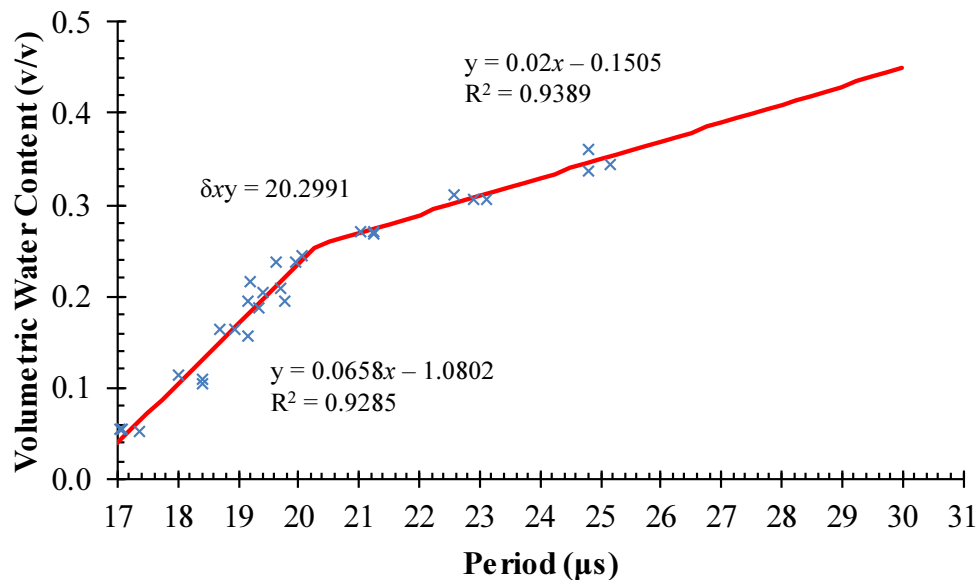


Figure 4.8: Linear regression to convert CS616  $\mu$  to  $\theta$

The following equations were therefore used to convert  $\mu$  to  $\theta$  for the three substrates:

$$\begin{array}{ll} \text{If } \mu > 20.29913: & \theta = 0.02\mu - 0.1505 \\ \text{Else:} & \theta = 0.0658\mu - 1.0802 \end{array} \quad \text{Equation 4.5}$$

#### 4.3.4 Data analysis methods

The data collection period spanned between February 2010 and February 2014. The rainfall record was divided into individual storm events assuming a minimum inter-event dry weather period of 6 hours (Stovin *et al.*, 2012) by Simon de-Ville (PhD candidate at the University of Sheffield). Rainfall depth was calculated as an average of the measurements from the 3 rain gauges. Only rainfall events with  $P \geq 2$  mm were analysed as it is typically assumed that impervious roof surfaces will have initial losses of up to 2 mm (Voyde *et al.*, 2010; Fassman-Beck *et al.*, 2013). Of the 323 individual storm events with  $P \geq 2$  mm, a full record is only available for all nine TBs for a subset of 48 events, approximately 15% of the broader dataset. This was due to measurement issues; predominantly associated with blockages in the valves of one or more bed. This data subset is referred to as AE9. The AE dataset includes all events for which a credible data record existed for each specific bed. The lowest number of valid runoff responses was 164 (TB9) and the highest was 257 (TB6). Any comparisons between TBs will be strongly influenced by the event rainfall characteristics, so all retention analyses are performed using the AE9 dataset to avoid skew in the results. Detention analyses will use the broader AE dataset.

##### 4.3.4.1 Rainfall and conventional runoff parameters

Rainfall,  $P$ , was calculated as the mean of the 3 gauges. Runoff,  $Q$ , was the depth of runoff occurring during rainfall and for a period of 6 hours after the last rainfall (i.e. consistent with the definition of the start of a new event). In some winter events, runoff from some beds was still observed after this 6 hour period. However, this was not common.

Important retention and detention metrics were calculated using Equation 4.6 through to Equation 4.8.

##### Per-event retention:

$$Retention = \frac{P - Q}{P} \times 100 \quad \text{Equation 4.6}$$

##### Per-event peak attenuation:

$$Peak\ Attenuation = \frac{P_{MAX} - Q_{MAX}}{P_{MAX}} \times 100 \quad \text{Equation 4.7}$$

Where  $P_{MAX}$  is maximum rainfall intensity and  $Q_{MAX}$  is peak runoff (in mm/5min).

**Peak delay:**

$$\text{Peak Delay} = t_{Q_{MAX}} - t_{P_{MAX}} \quad \text{Equation 4.8}$$

Where  $t_{P_{MAX}}$  and  $t_{Q_{MAX}}$  are the times at which peak rainfall and runoff were measured.

4.3.4.2 Detention parameter 'k'

Green roof detention combines the effects of delays in runoff due to plant cover, vertical movement through the substrate, interactions between the plant roots and the substrate, horizontal transfer across the drainage layer and, on a full-scale roof, the subsequent route into the collection system that is downstream of the roof. Stovin *et al.* (2015b) highlighted that many parameters typically used to describe detention performance (e.g. peak attenuation, centroid-to-centroid delay) fail to isolate actual detention from retention effects. Only when a system is at field capacity at the onset of an event will detention metrics reflect the pure detention performance. There is no single universally-applied metric that allows detention performance to be described (Stovin *et al.*, 2015b). Here, the 'conventional' detention metrics have been evaluated. However, the approach proposed by Stovin *et al.* (2015b), which assumes that the roof's detention characteristics are properties of the physical system, was also considered.

Kasmin *et al.* (2010) modelled detention performance using reservoir routing concepts:

$$h_t = h_{t-1} + Qin_t \delta t - Qout_t \delta t \quad \text{Equation 4.9}$$

in which  $Qin$  and  $Qout$  represent the flow rates into and out of the green roof respectively, in mm/min.  $h$  represents the depth of water temporarily stored within the substrate, in mm.  $\delta t$  represents the discretisation time step.  $Qout$  is given by:

$$Qout_t = kh_{t-1}^n \quad \text{Equation 4.10}$$

in which  $k$  and  $n$  are the reservoir routing parameters (scale and exponent respectively). Here,  $k$  has the units  $\text{mm}^{(1-n)}/\text{min}$ , whilst  $n$  is dimensionless. Based on a typical extensive green roof test bed, Kasmin *et al.* (2010) identified a  $k$  value of 0.15 (or 0.03 for a 5-minute time step) and an  $n$  value of 2.0. These initial estimates of  $k$  and  $n$  represent the



combined detention effects due to the roof's vegetation, substrate and drainage layer. When considering only the influence of the substrate layer, Yio *et al.* (2013) demonstrated that a model based on a fixed value of  $n$  was capable of predicting observed runoff profiles with almost no loss of accuracy when compared with a model for which both parameters had been optimised.

Here, model parameter  $n$  was fixed at 2.0 and the collected rainfall-runoff data was used to identify the model parameter ( $k$ ) that uniquely defines each individual system's detention characteristics. The *lsqcurvefit* function in MATLAB (2007) was utilized to identify the best-fit value of  $k$  for each individual event based on maximising the value of  $R^2$  (Young *et al.*, 1980) between the routed and monitored runoff profiles. The effects of retention (defined simply as Rainfall [ $P$ ] minus Runoff [ $Q$ ] in mm) were removed by setting initial SMD equal to retention. Event- and configuration-specific  $k$  values were identified for runoff at 1-minute intervals.

As the value of  $k$  is considered to be a system property, and therefore should not be affected by rainfall characteristics, the full AE dataset was used for this analysis. However, as it is not meaningful to assess detention for rainfall events that do not generate runoff, a minimum runoff threshold of 2 mm was applied. This resulted in between 71 and 136 events being used to identify the best-fit  $k$  value for each test bed. The individual event-based calibrated  $k$  values for each test bed were combined to determine the test bed's median  $k$  value.

#### 4.3.4.3 Moisture content measurements

Depth-averaged  $\theta$  was calculated for each of the four TBs as the mean value of the three probes in the column. The soil moisture deficit (SMD) prevailing at the start of the rainfall event was calculated using Equation 4.11:

$$SMD_t = (\theta_{FC} - \theta_t) \times 80 \quad \text{Equation 4.11}$$

Where  $\theta_t$  was the residual  $\theta$  at the start of rainfall.  $\theta_{FC}$  is unique for each substrate and was identified by the FLL tests (see Section 3.4.1). All analyses of moisture balance are conducted on 46 AE9 events (CS616 probes were not fitted for EV45 and EV65).

For seasonal mean data, summer comprised the months of June, July and August; autumn included September, October and November; winter months were December, January and February; and spring occurred in March, April and May.

## **4.4 Results**

The hydrological responses of the nine green roof configurations are presented here; identifying the extent to which green roofs fulfil important SuDS criteria, i.e. per-event retention, peak attenuation and peak delay. Detailed discussion of the physical controls upon the identified outcomes follows in Section 4.5.

### **4.4.1 Rainfall event data**

The hydrological response of green roofs is significantly influenced by the incidence of rainfall (Carter & Rasmussen, 2006) and by the antecedent conditions, such as the length of, and climatic conditions prevailing during the ADWP, that impact on moisture content (Bengtsson *et al.*, 2005). Here, first, each rainfall event will be compared against the Depth-Duration-Frequency (DDF) approach that is prescribed in the Flood Estimation Handbook (CEH, 1999). Subsequent consideration will be afforded to the climatic conditions during the ADWP ahead of evaluating the influence upon antecedent moisture content in the green roof.

#### *4.4.1.1 Rainfall events in AE9 dataset*

Rainfall measured during each AE9 event was plotted against the relevant DDF data for Sheffield (NERC, 1999) (see Figure 4.9).

The data set is characterised by a large number of high probability, small events. Just 2 of the 48 AE9 events had a return period in excess of 1 year. The majority of events (33) had  $P \leq 5$  mm, 9 events had  $P \geq 10$  mm; of which 4 events had  $P \geq 20$  mm.

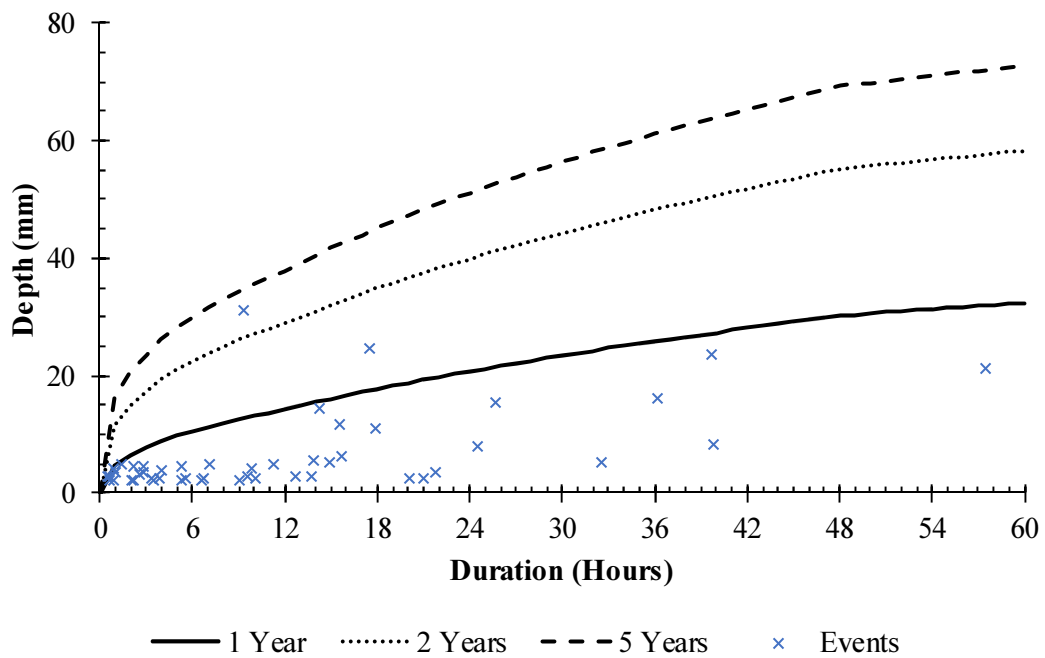


Figure 4.9: Depth-Duration-Frequency classification of rainfall events

#### 4.4.1.2 Antecedent Dry Weather Periods

The ADWPs preceding AE9 events were, typically for the UK, short. The longest ADWP was 10 days (ahead of EV207 in August 2012). However, the mean length of ADWP was 1.8 days. Table 4.1 categorises these ADWPs by length and season.

Table 4.1: Length of Antecedent Dry Weather Periods

	ADWP < 1 day	ADWP 1-3 days	ADWP of 3- 5 days	ADWP > 5 days	Total
<b>Spring</b>	6	4	2	0	<b>12</b>
<b>Summer</b>	7	5	2	2	<b>16</b>
<b>Autumn</b>	7	5	2	1	<b>15</b>
<b>Winter</b>	3	2	0	0	<b>5</b>
<b>Total</b>	<b>23</b>	<b>16</b>	<b>6</b>	<b>3</b>	<b>48</b>

Nearly half of all AE9 events had an ADWP of less than 1 day and just 3 events had an ADWP greater than 5 days. In winter, ADWP was always less than 3 days. ADWPs were typically longest in summer and shortest in winter. Mean ADWP was 1.5 days (in spring), 2.1 days (in summer), 1.6 days (in autumn) and 0.9 days (in winter).

When considering the regeneration of moisture capacity between events, it is not sufficient to consider the length of ADWP in isolation (Stovin *et al.*, 2012). Climatic variables, such as air temperature, relative humidity and solar and terrestrial radiation are

important influences on the drying behaviour of green roofs (Voyde *et al.*, 2010b). Figure 4.10 demonstrates the mean monthly data for temperature and relative humidity collected from the weather station during the three full calendar years of the research, i.e. 2011, 2012 and 2013.

Data collection issues were observed from the CS215 probe in February 2012. This data is therefore not presented. Predictably, temperatures were lowest in winter and highest in summer. Temperatures in spring were generally similar to autumn temperatures. The coldest winter and warmest summer were experienced in 2013, when mean daily temperatures were 3.0 °C in February (and 2.2 °C in March) and 19.4 °C in July. Year-on-year comparisons of relative humidity showed a high degree of consistency. Relative humidity was typically highest in the cold, wet months of winter and lowest in the warm, dry months of summer.

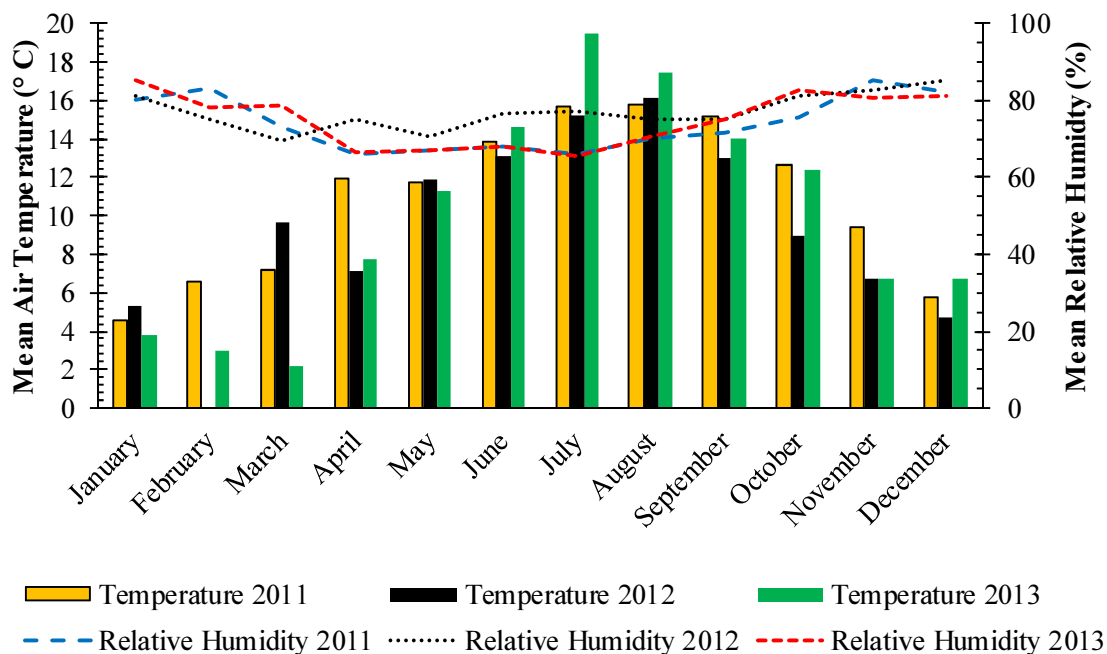


Figure 4.10: Mean monthly temperature and relative humidity

Similar seasonal trends were also observed in the solar radiation data (see Figure 4.11). Again, year-on-year comparisons of monthly average solar radiation showed little difference across the three years. Solar radiation ranged from a low of 1.3 MJ/m<sup>2</sup>/day (in December 2011, 2012 and 2013) to a high of 17.6 MJ/m<sup>2</sup>/day (in June 2011). Sunlight hours – calculated on the basis of the number of hours over which solar radiation was not equal to zero – ranged from 8.2 hours (in December 2012) to 17.2 hours (in June 2011).

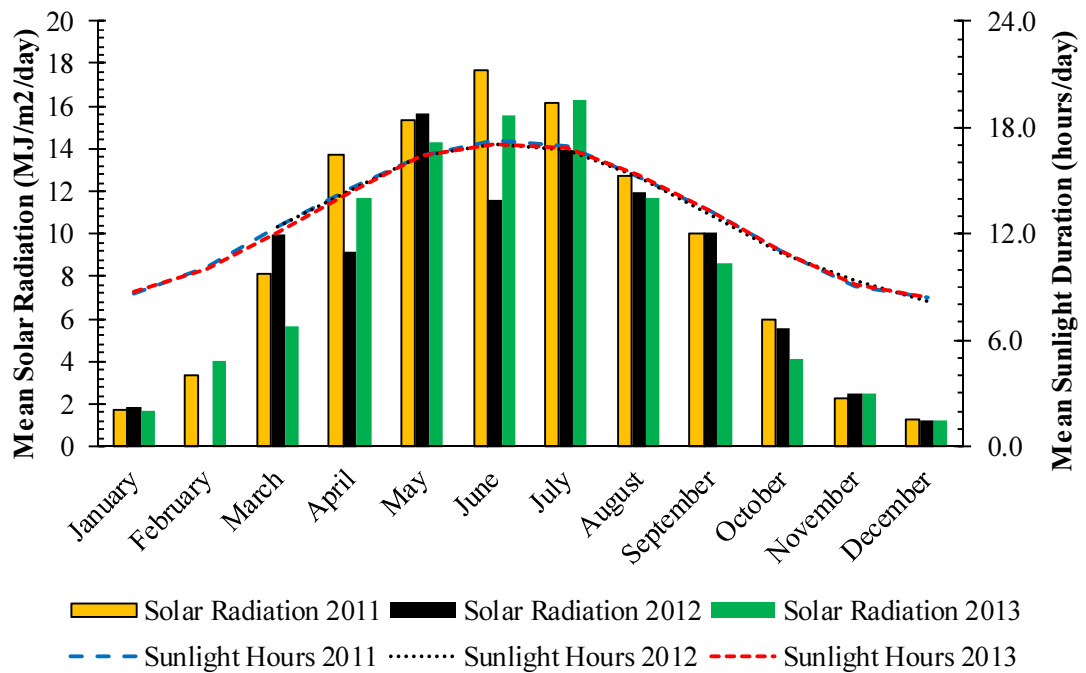


Figure 4.11: Mean monthly solar radiation and sunlight hours

Table 4.2 summarises the seasonal mean climatic data for the period in which the AE9 events occurred. The influence of these conditions upon potential evapotranspiration (PET) is also highlighted here.

Table 4.2: Seasonal climatic data for AE9 events

Climatic Variable	Units	Spring	Summer	Autumn	Winter
Mean rainfall	mm	8.1	6.0	3.8	12.4
Mean ADWP	Days	1.5	2.4	1.6	0.9
Mean temperature	°C	9.4	14.7	11.5	2.7
Mean relative humidity	%	78.0	72.8	76.9	78.4
Mean solar radiation	MJ/m <sup>2</sup> /d	11.4	12.4	4.8	3.5
Mean wind speed	m/s	2.3	1.8	2.9	2.0
Mean PET (FAO56)	mm/d	2.0	2.5	2.1	1.2
Mean PET (HG)	mm/d	2.1	2.4	0.8	0.3
Mean PET (PT)	mm/d	1.0	1.1	0.9	0.7

Predictably, PET was highest in summer (between 1.1 and 2.5 mm/day) and lowest in winter (between 0.3 and 1.2 mm/day). However, actual ET will have also been influenced by the greater per-event rainfall in spring (8.1 mm) compared to summer (6.0 mm). This is expected to have resulted in greater moisture availability in spring. A more in-depth review of PET methodologies is provided in Chapter 5.

#### 4.4.2 Rainfall and runoff during AE9 events

A level of retention was calculated from every TB in response to each AE9 event. Generally, runoff increased with rainfall depth. Rainfall and runoff are plotted for all AE9 events in Figure 4.12. Here, a solid line highlights the equilibrium between rainfall and runoff (i.e. zero retention). A further dashed line indicates expected runoff if retention of just the initial 5 mm of rainfall occurred.

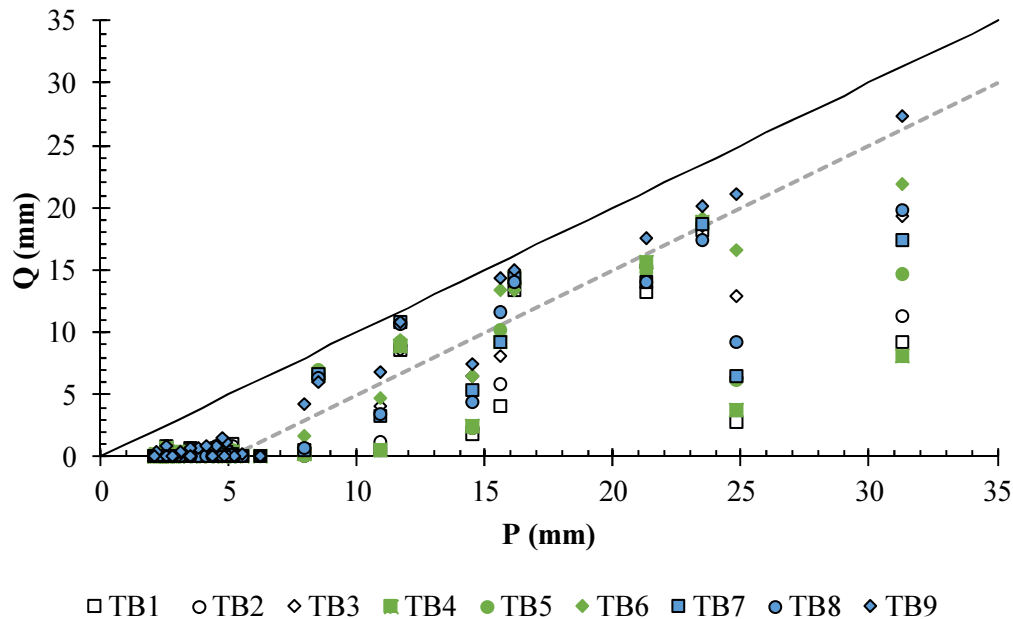


Figure 4.12: Rainfall versus runoff for AE9 events

There were 22 events where zero runoff was recorded from at least one TB. Of these, only one event had  $P \geq 5$  mm (EV174, when  $P = 5.0$  mm). However, in many more instances, runoff was less than 0.2 mm. The TBs with the highest number of events without runoff greater than 0.2 mm were TB7 and TB8 (35 number) and the lowest were TB6 and TB9 (27 number). In most instances, one or more TB retained the initial 5 mm of rainfall. However, runoff was measured from all TBs for at least one event when  $P \leq 5$  mm. The maximum runoff for such events ranged between 0.2 mm (TB8 during EV102 [ $P = 4.9$  mm]) and 1.5 mm (TB9 during EV259 [ $P = 4.7$  mm]). All events with  $P \geq 10$  mm led to runoff from every TB.

The hydrological responses of the TBs varied according to configuration. Table 4.3 summarises the rainfall and runoff values for each of the AE9 events.

Table 4.3: Rainfall – Runoff statistics for AE9 events

EV	Date	Season	ADWP (Days)	Rain Depth (mm)	Runoff (mm)								
					TB1	TB2	TB3	TB4	TB5	TB6	TB7	TB8	TB9
45	30/08/10	Summer	7.42	31.3	9.3	11.4	19.3	8.1	14.6	21.9	17.5	19.8	27.3
65	30/11/10	Autumn	3.75	5.1	1.0	0.8	0.5	0.4	0.5	0.3	0.3	0.3	0.2
102	06/07/11	Summer	0.33	4.9	0.0	0.0	0.1	0.2	0.4	0.0	0.3	0.2	1.2
105	20/07/11	Summer	0.26	2.1	0.0	0.0	0.0	0.0	0.0	0.0	0.0	0.0	0.0
107	18/08/11	Summer	2.18	2.2	0.0	0.0	0.0	0.0	0.0	0.0	0.0	0.0	0.0
108	21/08/11	Summer	3.79	14.5	1.8	2.4	6.5	2.4	2.4	6.5	5.4	4.4	7.5
109	25/08/11	Summer	0.80	10.9	0.6	1.2	4.1	0.6	0.6	4.8	3.3	3.5	6.8
110	04/09/11	Autumn	1.08	3.5	0.0	0.0	0.0	0.0	0.0	0.0	0.0	0.0	0.0
111	06/09/11	Autumn	0.27	2.7	0.0	0.0	0.0	0.0	0.0	0.0	0.0	0.0	0.0
112	06/09/11	Autumn	0.29	7.9	0.2	0.1	0.4	0.2	0.1	1.7	0.6	0.8	4.3
114	16/09/11	Autumn	0.42	3.0	0.0	0.0	0.0	0.0	0.0	0.0	0.0	0.0	0.0
115	18/09/11	Autumn	0.53	3.8	0.0	0.0	0.0	0.0	0.0	0.2	0.1	0.1	0.7
117	06/10/11	Autumn	1.16	2.5	0.0	0.0	0.1	0.0	0.0	0.2	0.0	0.0	0.0
123	21/10/11	Autumn	3.56	2.3	0.0	0.0	0.0	0.0	0.0	0.0	0.0	0.0	0.0
125	31/10/11	Autumn	0.54	3.1	0.4	0.0	0.1	0.4	0.2	0.4	0.0	0.0	0.3
131	22/11/11	Autumn	2.89	2.2	0.0	0.0	0.0	0.0	0.0	0.0	0.0	0.0	0.0
132	26/11/11	Autumn	0.27	4.5	0.7	0.8	0.4	0.5	0.3	0.4	0.0	0.1	0.9
133	27/11/11	Autumn	2.17	3.5	0.7	0.7	0.4	0.4	0.4	0.4	0.0	0.1	0.7
134	29/11/11	Autumn	1.27	2.6	0.9	0.9	0.9	0.7	0.6	0.5	0.0	0.1	0.8
156	06/03/12	Spring	0.29	2.5	0.0	0.1	0.1	0.0	0.0	0.2	0.0	0.1	0.0
172	19/05/12	Spring	4.29	4.7	0.0	0.0	0.0	0.0	0.0	0.0	0.0	0.0	0.0
174	24/05/12	Spring	3.94	5.0	0.0	0.0	0.0	0.0	0.0	0.0	0.0	0.0	0.0
176	03/06/12	Summer	1.82	2.5	0.0	0.0	0.0	0.0	0.0	0.0	0.0	0.1	0.0
178	09/06/12	Summer	1.26	4.1	0.0	0.0	0.4	0.0	0.0	0.4	0.0	0.1	0.9
194	14/07/12	Summer	1.78	2.1	0.0	0.0	0.0	0.0	0.0	0.0	0.0	0.0	0.0
198	01/08/12	Summer	0.64	2.8	0.0	0.0	0.0	0.0	0.0	0.0	0.0	0.0	0.0
199	06/08/12	Summer	0.94	3.5	0.0	0.0	0.0	0.0	0.0	0.0	0.0	0.0	0.0
201	17/08/12	Summer	0.35	2.9	0.0	0.0	0.0	0.0	0.0	0.0	0.0	0.0	0.0
207	31/08/12	Summer	10.0	2.7	0.0	0.0	0.0	0.0	0.0	0.0	0.0	0.0	0.0
208	20/09/12	Autumn	0.65	5.5	0.1	0.0	0.0	0.0	0.0	0.0	0.0	0.0	0.3
227	01/12/12	Winter	1.66	8.5	6.5	6.6	6.2	6.7	7.0	6.1	6.7	6.4	6.1
228	05/12/12	Winter	1.43	11.7	8.7	8.9	8.6	8.9	9.2	9.3	10.8	10.6	10.8
245	04/02/13	Winter	0.45	23.5	18.2	18.7	18.6	18.9	18.9	19.2	18.7	17.4	20.1
246	09/02/13	Winter	0.82	16.1	13.3	13.9	13.4	14.3	14.2	13.5	14.3	14.1	15.0
248	24/02/13	Winter	0.31	2.4	0.0	0.0	0.0	0.0	0.0	0.0	0.0	0.0	0.0
249	06/03/13	Spring	0.65	2.3	0.0	0.0	0.0	0.0	0.0	0.0	0.0	0.0	0.0
250	07/03/13	Spring	0.47	21.3	13.3	15.3	15.1	15.6	14.8	15.4	14.0	14.1	17.6
257	08/05/13	Spring	0.85	5.2	0.0	0.0	0.0	0.0	0.1	0.0	0.1	0.1	0.0
258	13/05/13	Spring	1.02	24.8	2.8	6.4	12.8	3.7	6.2	16.6	6.5	9.2	21.0
259	15/05/13	Spring	1.48	4.7	0.1	0.0	0.1	0.2	0.3	0.3	0.1	0.2	1.5
260	16/05/13	Spring	0.84	2.2	0.0	0.0	0.1	0.2	0.1	0.2	0.1	0.0	0.4
261	17/05/13	Spring	2.06	2.1	0.0	0.0	0.0	0.0	0.0	0.0	0.0	0.0	0.0
262	21/05/13	Spring	1.53	6.2	0.0	0.1	0.0	0.1	0.1	0.0	0.0	0.1	0.1
264	28/05/13	Spring	0.61	15.6	4.1	5.9	8.1	9.3	10.2	13.4	9.2	11.6	14.4
269	23/06/13	Summer	4.15	2.5	0.0	0.0	0.0	0.0	0.0	0.0	0.0	0.0	0.0
270	27/06/13	Summer	0.48	2.8	0.0	0.0	0.1	0.0	0.0	0.0	0.0	0.0	0.0
271	30/06/13	Summer	1.68	4.3	0.1	0.0	0.0	0.0	0.1	0.0	0.0	0.1	0.0
297	29/11/13	Autumn	5.90	4.8	0.0	0.0	0.0	0.1	0.0	0.0	0.1	0.1	0.0

#### 4.4.3 Rainfall-Runoff profiles for selected events

Before considering mean and median trends, the hydrological performance of the nine TBs during eight selected AE9 events (two of the largest events occurring in each of the four seasons) will be explored, with a view to highlighting some of the practical differences in the responses of each configuration. The influence of seasonal climate upon runoff will also start to become apparent here.

Two events – EV258 and EV264 – were chosen to represent rainfall events during spring. The rainfall and runoff profiles are illustrated in Figure 4.13.

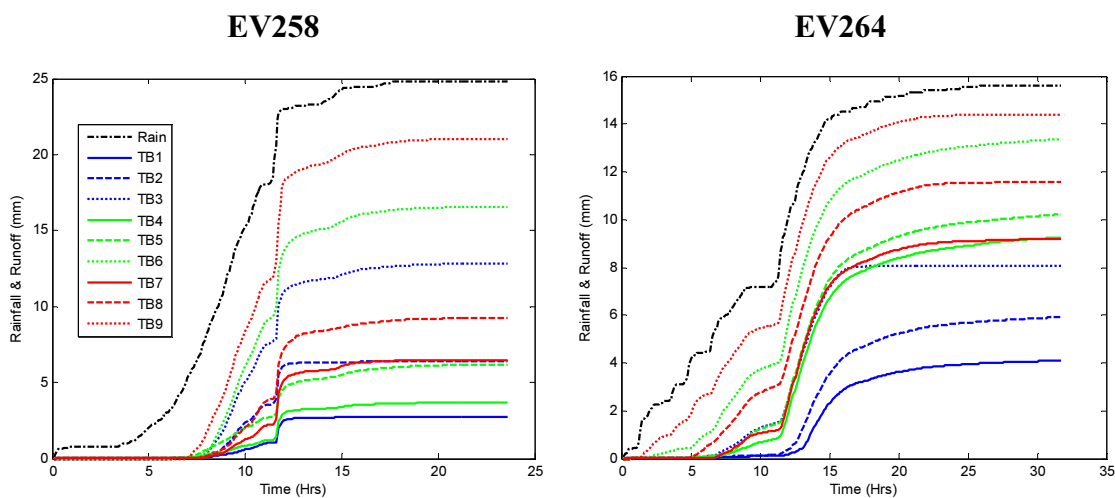


Figure 4.13: Cumulative runoff responses for nine test beds for two spring events

Here, a wide range of responses can be seen across the nine TBs. Generally, the lowest runoff was seen from TB1 and the highest from TB9. For example, during EV258, when 24.8 mm of rain fell, runoff ranged between 2.8 mm (TB1) and 21.1 mm (TB9). Similar patterns were observed during EV264. Runoff was lowest from Sedum-vegetated configurations and highest from LECA-based configurations. Runoff was initiated from all TBs at broadly similar times during EV258. Yet, during EV264, runoff was initiated from TB1 and TB2 at a noticeably later time than most other TBs. In both events, rates of runoff varied after the initialisation of runoff; indicating that detention performance varied as a result of differences in the configurations.



The two events selected for the summer season were EV45 and EV108 (see Figure 4.14).

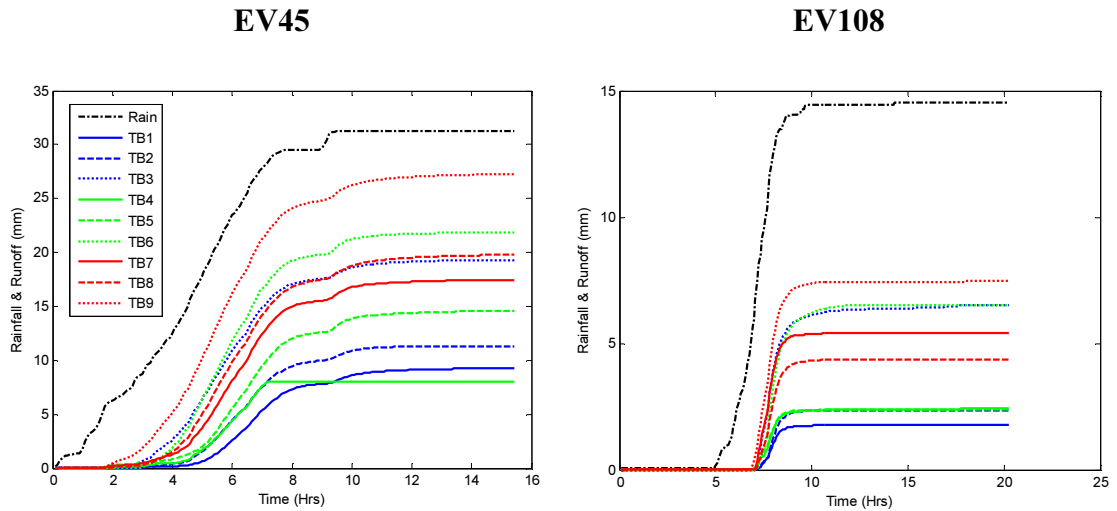


Figure 4.14: Cumulative runoff responses for nine test beds for two summer events

Here, the range of runoff values was greatest when rainfall depth was high. During EV45, when 31.3 mm of rain fell, following an ADWP of 7 days, runoff ranged between 8.1 mm (TB4) and 27.3 mm (TB9). This range reduced when considering responses to the 14.5 mm of rain that fell during EV108. Lowest runoff was 1.8 mm (from TB1). Highest runoff was 7.5 mm (from TB9). The contrast between the high moisture storage capacity of the HLS substrate and the lower capacity of LECA is evident in these summer events. Predictably, in view of the relatively low rainfall in autumn months, the range of runoff depths was lower in autumn events than in other seasons (see Figure 4.15).

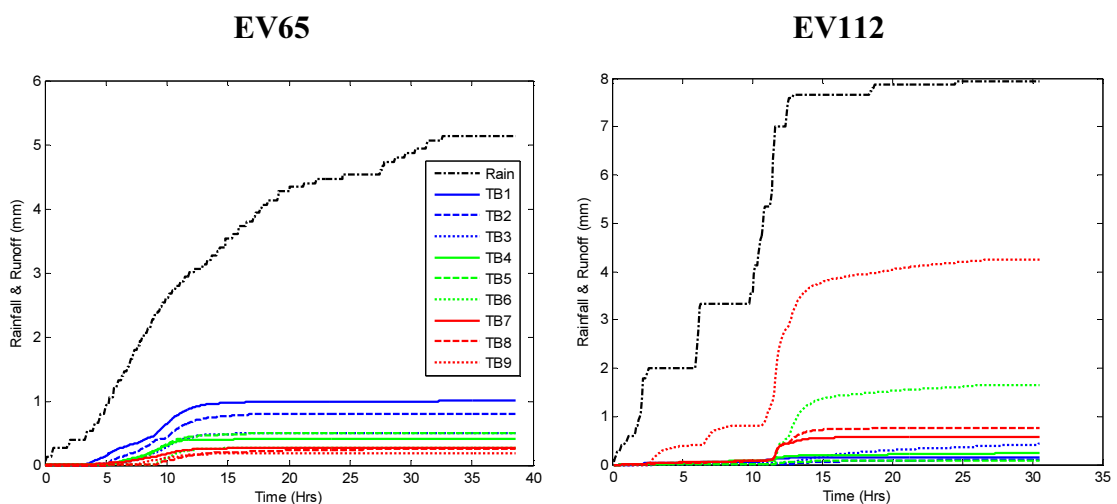


Figure 4.15: Cumulative runoff responses for nine test beds for two autumn events

In the response to EV65 runoff was very low from all TBs. Untypically, runoff was highest from the Sedum vegetated configurations and lowest from the non-vegetated configurations. However, differences were minor. Highest runoff was recorded from the HLS-based TB1 (1.0 mm). The more common trend of highest runoff from non-vegetated and LECA-based configurations was, however, observed for EV112. In both events, additional retention was observed after first runoff.

The range of hydrological responses was narrower with winter events, relative to the other seasons (see Figure 4.16).

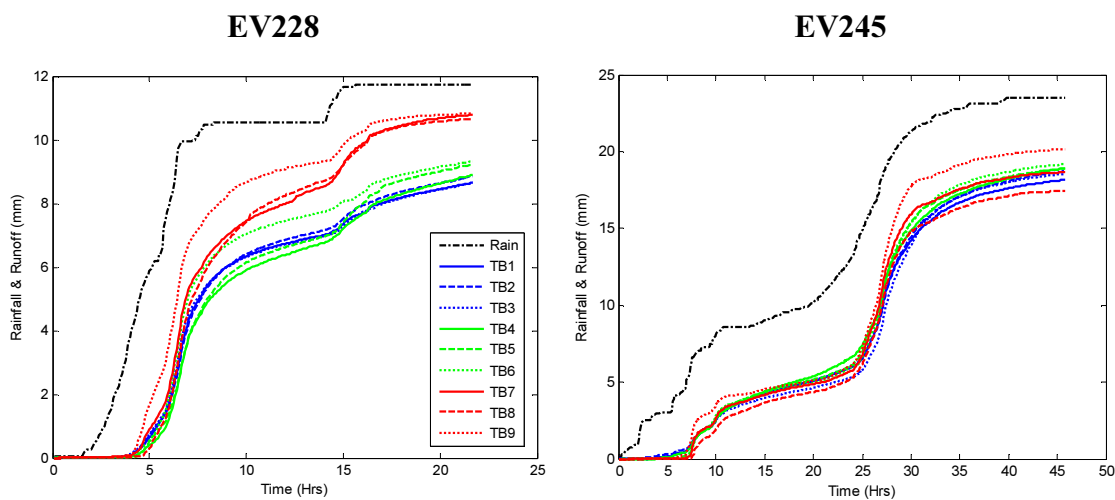


Figure 4.16: Cumulative runoff responses for nine test beds for two winter events

After retention of the initial rainfall, runoff during the two winter events typically replicated rainfall. This was particularly evident during EV245, when the range of runoff responses was very small (less than 2 mm) despite a relatively high rainfall depth of 23.5 mm. These small differences were consistent with configurations having virtually zero pre-event SMD as a result of the short (< 0.5 days) ADWP and the low energy available for ET in winter. A similar range of runoff differences was observed with EV228. Here, the lower rainfall contributed to less runoff. Runoff was ultimately highest from non-vegetated configurations. However, the responses of all TBs were broadly similar. The lower storage capacity of the non-vegetated TBs appeared to constrain retention to a marginally greater degree than the vegetated TBs.

The different responses of the TBs to the 8 events considered here highlights several important influences upon the hydrological performance of green roofs, including the

available moisture capacity, initialisation of runoff within different configurations and the importance of seasonal climate. All of these influences will be considered in greater detail in Section 4.5.

#### 4.4.4 Per-event retention

Median per-event retention has been chosen, rather than mean values, due to the large variation in the responses of the different TBs. Mean values will therefore only be referred to when considering smaller sub-sections of the data, such as categorisation by rainfall depth. Median per-event retention ranged between 98% (TB8) and 100% (TB2) (see Figure 4.17).

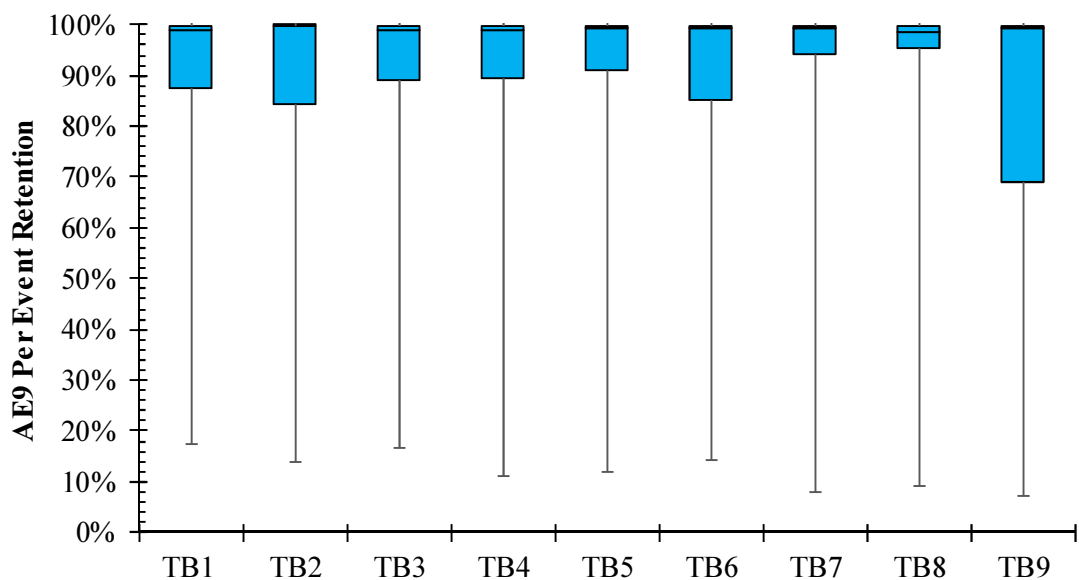


Figure 4.17: Per-event retention for all AE9 events

This very high retention can be largely attributed to the high frequency of events with small rainfall (and little or no runoff). Differences attributable to configuration were generally negligible when considering the full AE9 dataset. The lowest per-event retention by any singular TB was 7.1% (observed from TB9 during EV246). As such, the range of retention identified here (i.e. between 7.1 and 100.0%) was consistent with the findings of Palla *et al.* (2011), who identified a range of 10 to 100%. Minimum per-event retention for a Sedum-vegetated configuration was 13.9% (TB2) and for a Meadow Flower treatment was 11.1% (TB4) – both also measured during EV246.

Retention is heavily influenced by rainfall depth (Nawaz *et al.*, 2015). By considering  $P \geq 10$  mm, a greater range of configuration median per-event retention was identified (see Figure 4.18).

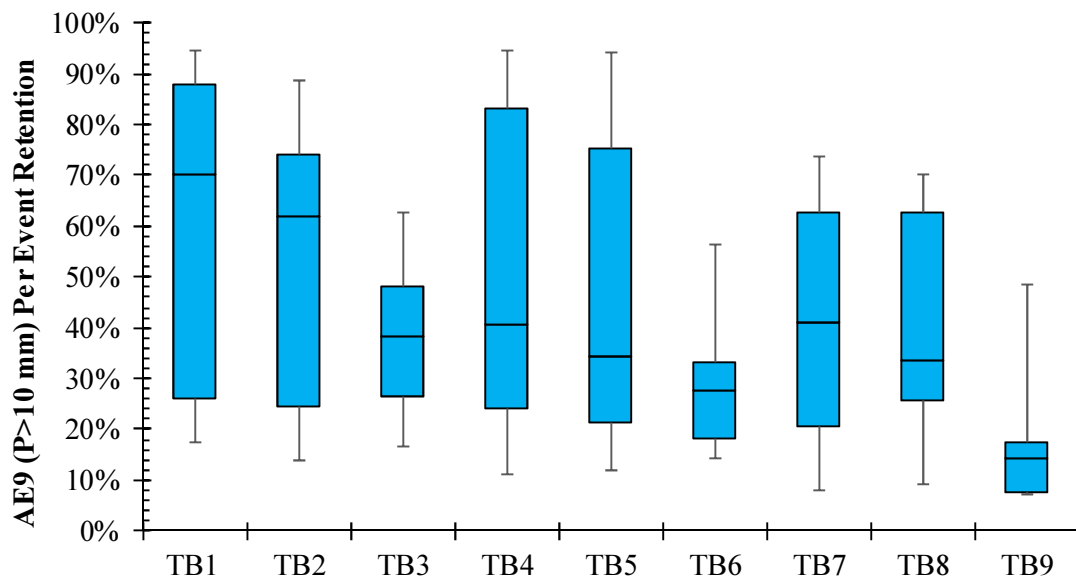


Figure 4.18: Per-event retention for AE9 ( $P \geq 10$ mm) events

When  $P \geq 10$  mm, median per-event retention was lowest from TB9 (14%) and highest from TB1 (70%). Retention efficiency was lowest from LECA and non-vegetated configurations and highest from HLS and Sedum configurations. The total and interquartile ranges of retention measured from LECA configurations were smaller than with other substrate types. It is expected that this reflects the greater storage capacity constraints of LECA, reducing the range of potential retention. As observed in Figure 4.12, runoff was typically highest when rainfall was high. Figure 4.19 highlights the different mean retention efficiencies of each TB for different rainfall depths.

When  $P < 5$  mm, retention ranged between 93.7% (TB9) and 99.1% (TB7). This high retention was expected as such rainfall depths would be lower than the maximum storage capacity of all TBs. As rainfall increased, configuration mean per-event retention levels had a greater range (e.g. when  $P \geq 20$  mm, retention ranged between 14.9% [TB9] and 54.8% [TB1]). The influence of vegetation treatment and substrate upon the hydrological response will be examined further in Section 4.5. However, the influence of rainfall depth upon retention is clearly demonstrated here.

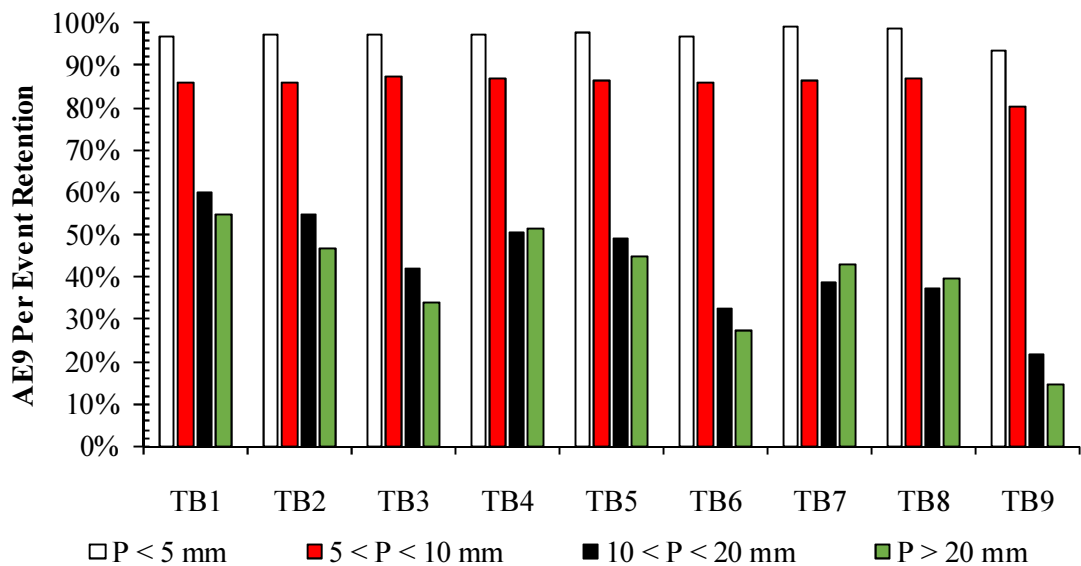


Figure 4.19: Per-event retention for AE9 events, categorised by rainfall depth

#### 4.4.5 Peak attenuation

Whilst runoff was clearly correlated with rainfall depth, the relationship between peak rainfall intensity ( $P_{MAX}$ ) and peak rates of runoff ( $Q_{MAX}$ ) was less obvious (see Figure 4.20).

Generally, some level of attenuation was apparent for all AE9 events. Peak rates of runoff were always less than peak rainfall intensity. With very low runoff being measured in response to a number of events, peak attenuation was predictably high. However, the event with the highest peak rainfall intensity (EV102,  $P_{MAX} = 2.27$  mm/5min) resulted in relatively low peak runoff ( $Q_{MAX} < 0.3$  mm/5min) from all TBs.  $Q_{MAX}$  ranged from zero (TB2 and TB6) to 0.26 mm/5min (TB9). Clearly, these very high levels of peak attenuation were significantly influenced by strong retention efficiencies; underpinned by the number of events with low rainfall depth.

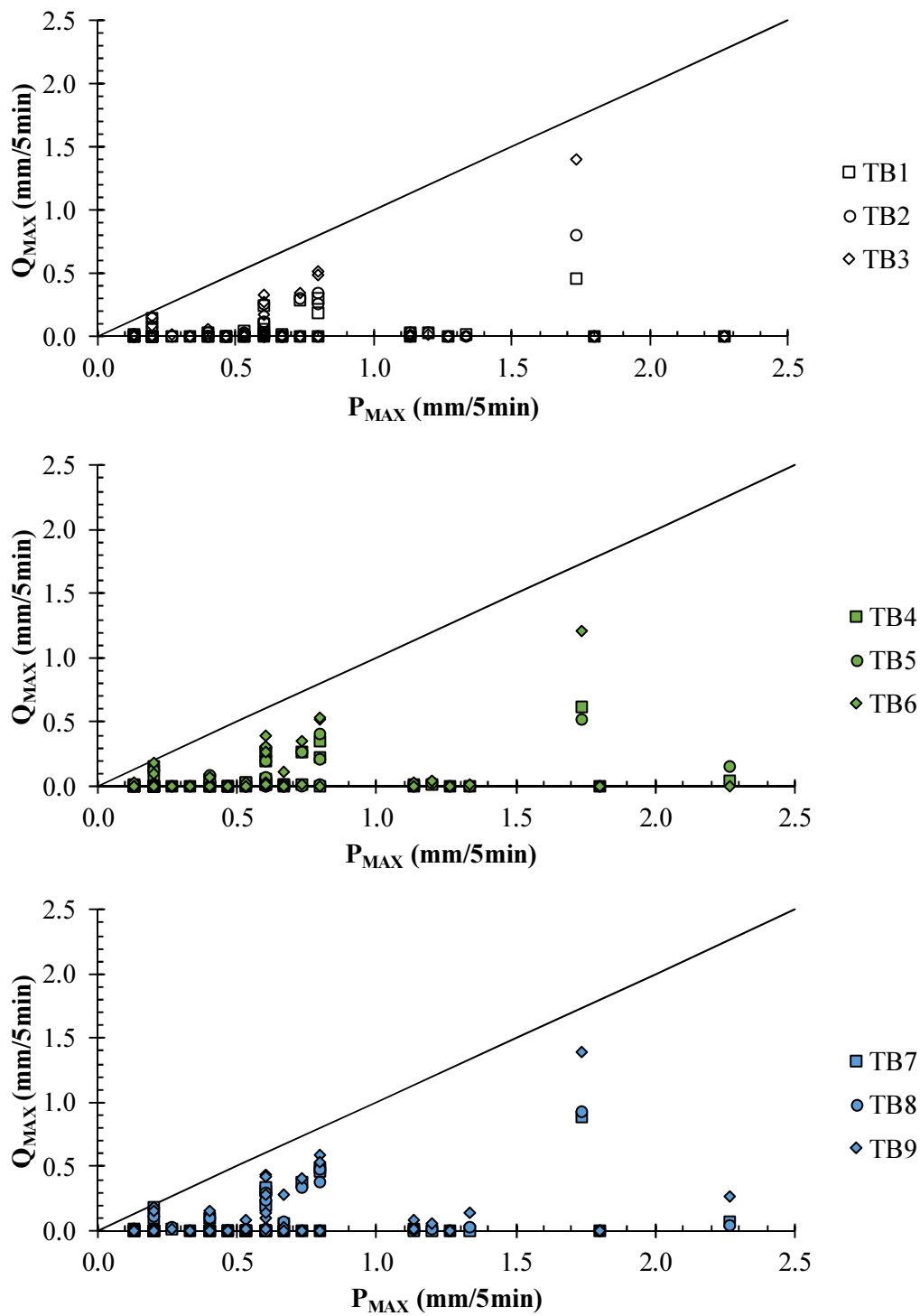


Figure 4.20: Peak intensity of rainfall versus runoff during AE9 events

Median peak attenuation for AE9 events ranged between 98% and 99% for all configurations (see Figure 4.21).

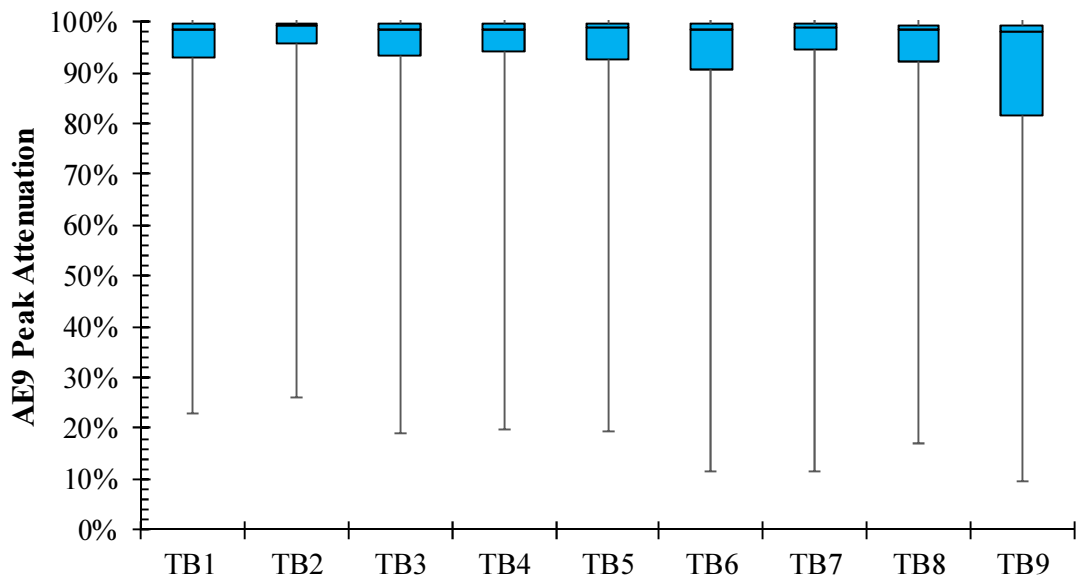


Figure 4.21: Peak attenuation for AE9 events

Minimum peak attenuation ranged between 9% (TB9) and 26% (TB2). However, the extent to which these minima are outliers is demonstrated by the range of Quartile 1 values (82% for TB9 up to 96% for TB2). As was the case with retention, peak attenuation was strongly influenced by rainfall depth. Figure 4.22 highlights peak attenuation trends when  $P \geq 10$  mm.

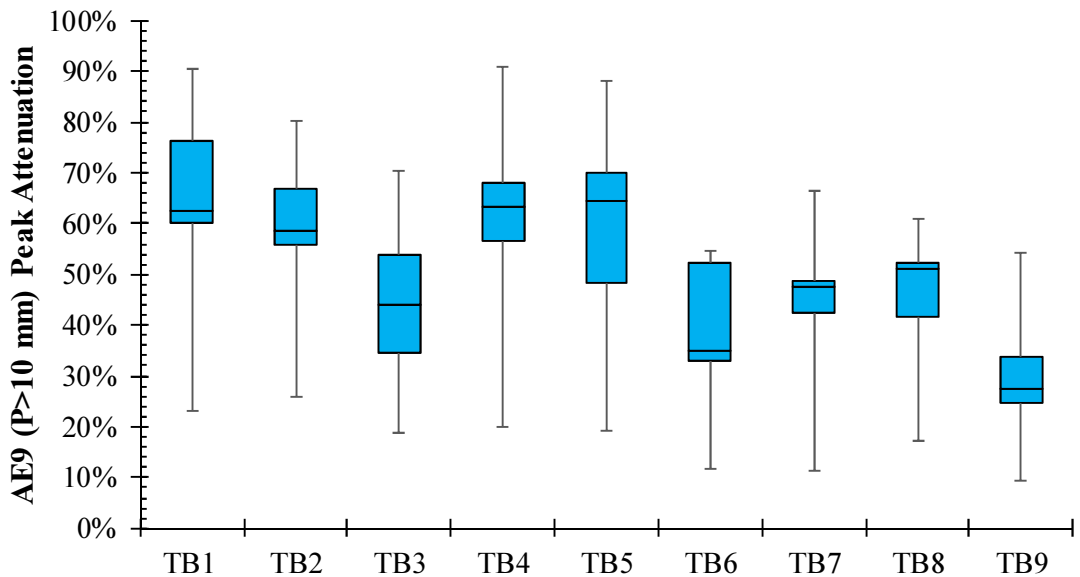


Figure 4.22: Peak attenuation for AE9 ( $P \geq 10$  mm) dataset

A wider range of median peak attenuation was observed; with the lowest median attenuation of 28% (TB9) and highest of 64% (TB5). Peak attenuation was lowest for

LECA-based and non-vegetated configurations. For Meadow Flower and non-vegetated configurations, peak attenuation was highest with SCS substrate. Yet, peak attenuation for Sedum vegetation was highest when HLS was the substrate. Predictably, peak attenuation was influenced by rainfall depth. Small differences attributable to configuration were observed when rainfall was less than 10 mm but larger ranges were measured when rainfall exceeded 10 mm (see Figure 4.23).

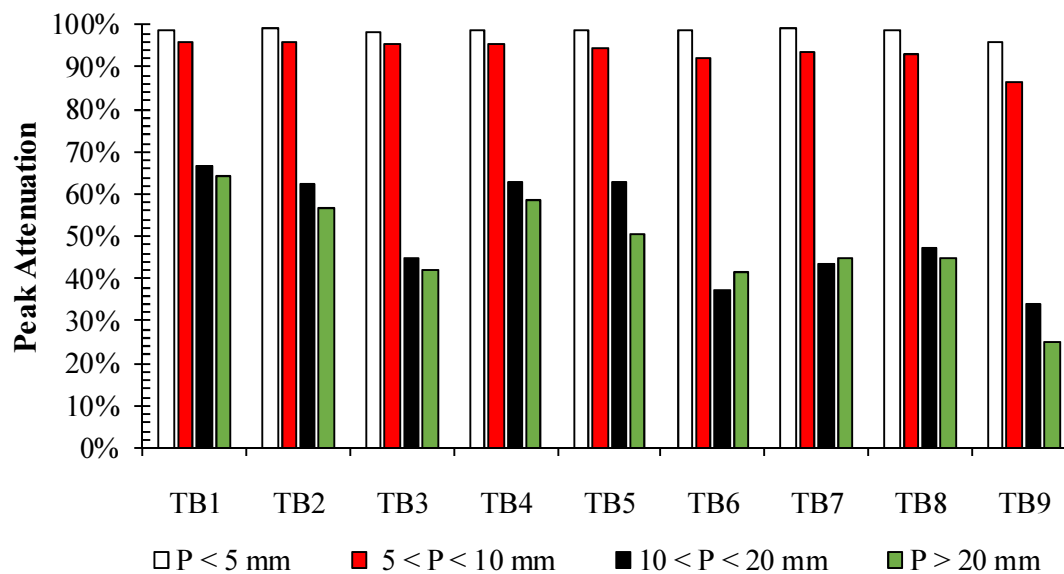


Figure 4.23: Peak attenuation for AE9 events, categorised by rainfall depth

The observations here broadly mirror the trends previously identified for retention. The highest configuration mean peak attenuation was recorded during events with the lowest rainfall depth. When rainfall was less than 5 mm, configuration mean peak attenuation ranged between 96.1% (TB9) and 99.0% (TB7). However, when rainfall was in excess of 20 mm, a wider range of attenuation was observed, with a low of 25.2% (TB9) and a high of 64.4% (TB1). These observations were broadly consistent with the findings of Hakimdavar *et al.* (2014). They identified peak attenuation of 89% when  $P < 20$  mm; falling to 62% when  $P > 20$  mm. As larger events were considered, the differences in the responses of the 3 substrates increased. It is expected that this was due to the greater storage capacity and lower permeability of HLS, contrasting against the lower capacity and higher permeability of LECA.



#### 4.4.6 Peak delay

Peak delays caused by green roofs are typically expected to be short. Locatelli *et al.* (2014) identified peak delays of up to 40 minutes, whilst DeNardo *et al.* (2005) recorded mean delays of 2 hours. The peak delays considered here are expected to be conservative when compared to delays from a full scale roof, where the path to the drainage outlet will typically be greater. However, runoff from a full-scale roof can be modelled by calculating the time of concentration as an additional modelling parameter. Figure 4.24 highlights the median peak delays for each TB during the AE9 events.

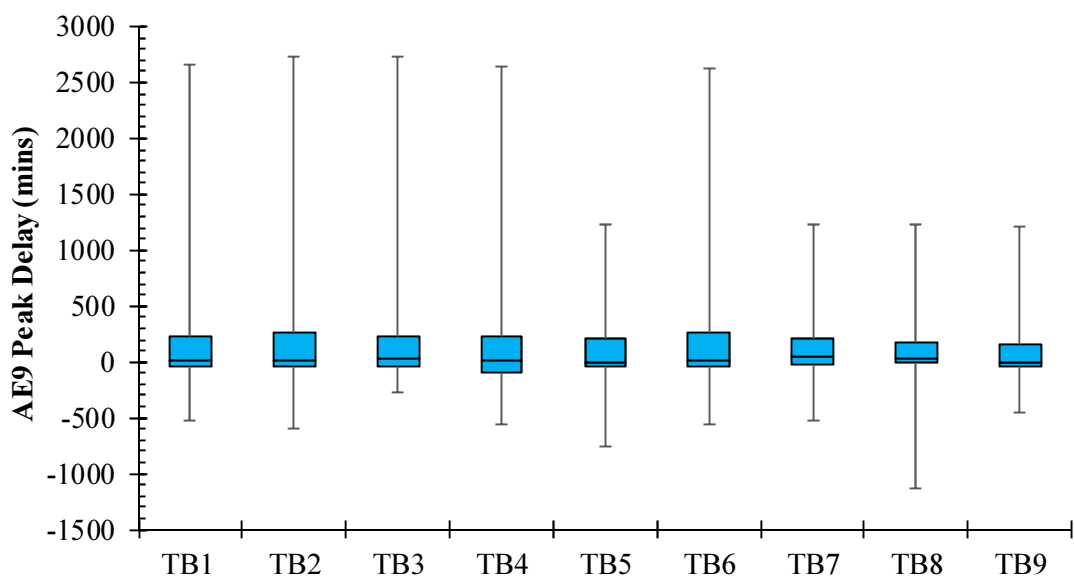


Figure 4.24: Peak delays for AE9 dataset

Peak delays were typically short. For AE9 events, median peak delays ranged between 28 minutes (TB9) and 75 minutes (TB7). However, the range of delays across the different events was broad. Configuration mean peak delays (ranging from 91 minutes [TB5] to 201 minutes [TB6]) had large standard deviations (301 minutes [TB5] and 499 minutes [TB6]). In many instances, ‘negative’ peak delays were calculated (i.e. peak runoff occurred prior to peak rainfall). The longest delays were typically associated with long rainfall durations with low rainfall intensities (see Figure 4.25).

During EV250, 21.3 mm of rain fell over 57.5 hours with a peak intensity of 0.2 mm/5min. Runoff from TB2 was 15.3 mm, with a peak rate of 0.08 mm/5min (TB2) being measured 2820 minutes (47 hours) after peak rainfall. During EV117, rainfall of 2.53 mm resulted in runoff that was nominally zero (0.003 mm) from TB8. This runoff

occurred 1130 minutes prior to peak rainfall and therefore calculated peak delay would be negative. Clearly, this parameter is not meaningful in this context. The value of reporting this metric to infer detention performance must be questioned.

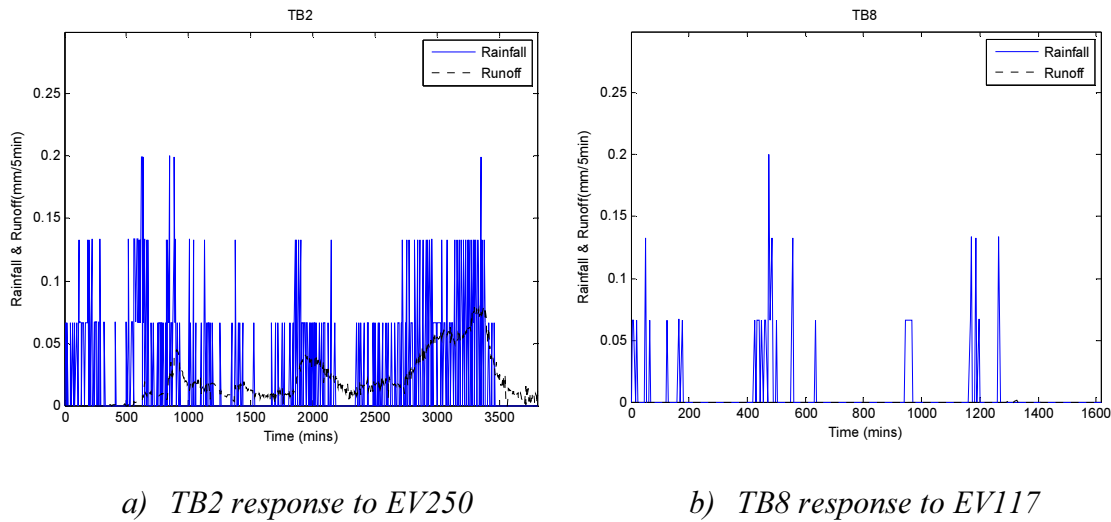


Figure 4.25: Rainfall-runoff profiles for two events to highlight peak delays

#### 4.4.7 Detention parameter ‘k’

The optimised values for the reservoir routing coefficient  $k$  (with units of  $\text{mm}^{1-n}/\text{min}$ ) are presented for each of the nine configurations in Figure 4.26.

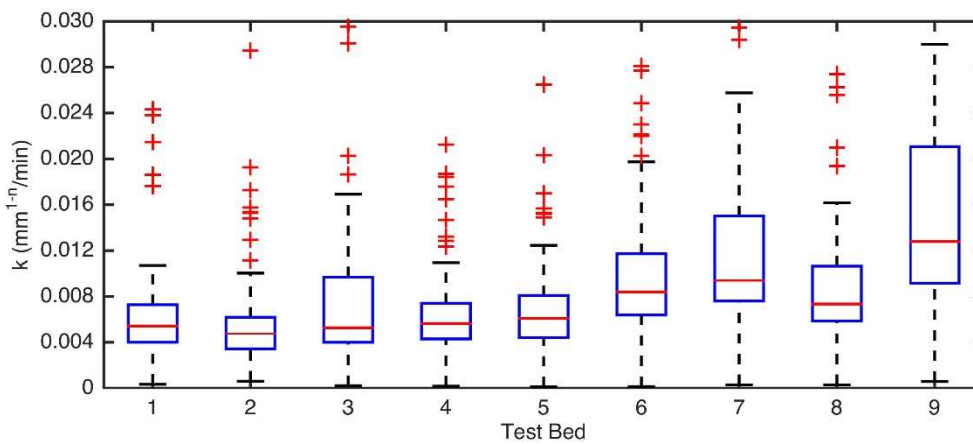


Figure 4.26: Calibrated values for the reservoir routing coefficient  $k$  ( $\text{mm}^{1-n}/\text{min}$ )

Systematic variations in detention performance were observed across the configurations. The configuration-median value of  $k$  and the mean  $R^2$  value are presented in Table 4.4.

Table 4.4: Configuration-specific  $k$  values and goodness of fit statistics

Test Bed	TB1	TB2	TB3	TB4	TB5	TB6	TB7	TB8	TB9
$k$ (mm <sup>1-n</sup> /min)	0.0054	0.0048	0.0052	0.0056	0.0060	0.0084	0.0094	0.0074	0.0128
Mean R <sup>2</sup>	0.855	0.875	0.836	0.868	0.862	0.844	0.860	0.842	0.863
$k$ (mm <sup>1-n</sup> /5min)	0.027	0.024	0.026	0.028	0.03	0.042	0.047	0.037	0.064

An independent-samples Kruskal-Wallis test showed that differences in the derived values of  $k$  due to substrate were not statistically significant ( $p$ -value = 0.67,  $p$ -value < 0.05 significance level). Predictably, the  $k$  value of LECA was higher than with HLS and SCS. However, no other systematic differences due to substrate could be identified. Differences in  $k$  due to vegetation were both systematic and statistically significant ( $p$ -value = 0.039,  $p$ -value < 0.05 significance level). Detention was highest (and  $k$  lowest) with Sedum and lowest with non-vegetated beds. A Mann-Whitney U test confirmed that the difference between the Sedum and non-vegetated configurations was significant ( $U$  = 5.67 versus a critical value of 3.91). However, the differences between Sedum and Meadow Flower ( $U$  = 3.33) and between Meadow Flower and non-vegetated beds ( $U$  = 2.33) were not statistically significant.

#### 4.4.8 Summary of hydrological response to AE9 events

For AE9 events, per-event retention ranged between 7% and 100%. Peak attenuation ranged between 9% and 100%. Retention and attenuation responses were heavily influenced by rainfall depth. When rainfall was low (i.e.  $P \leq 5$  mm), per-event retention and attenuation were both high (ranging from 93.7 to 99.1% and 96.1 to 99.0% respectively). However, for larger rainfall events (e.g.  $P \geq 20$  mm), response levels fell; retention falling to 14.9-54.8% and attenuation reducing to 25.2-64.4%. As expected, median peak delays were typically short (between 28 and 75 minutes). Differences due to configuration were apparent. These differences were greatest when rainfall was high. Configuration-median  $k$  (in mm<sup>1-n</sup>/min) ranged between 0.0048 (TB2) and 0.0128 (TB9) with statistically significant differences due to vegetation treatment. The influences upon these trends will be discussed in further detail in Section 4.5.

## 4.5 Discussion

In this section, detailed analysis of the AE9 data set will help to identify the physical controls upon retention, detention, initialisation of runoff and the regeneration of the SMD via ET.

### 4.5.1 Physical controls upon retention performance

#### 4.5.1.1 Vegetation treatment

The retention responses of different vegetation treatments were considered for Sedum (TB1 to TB3), Meadow Flower (TB4 to TB6) and non-vegetated beds (TB7 to TB9). Figure 4.27 contrasts vegetation mean per-event retention for each treatment.

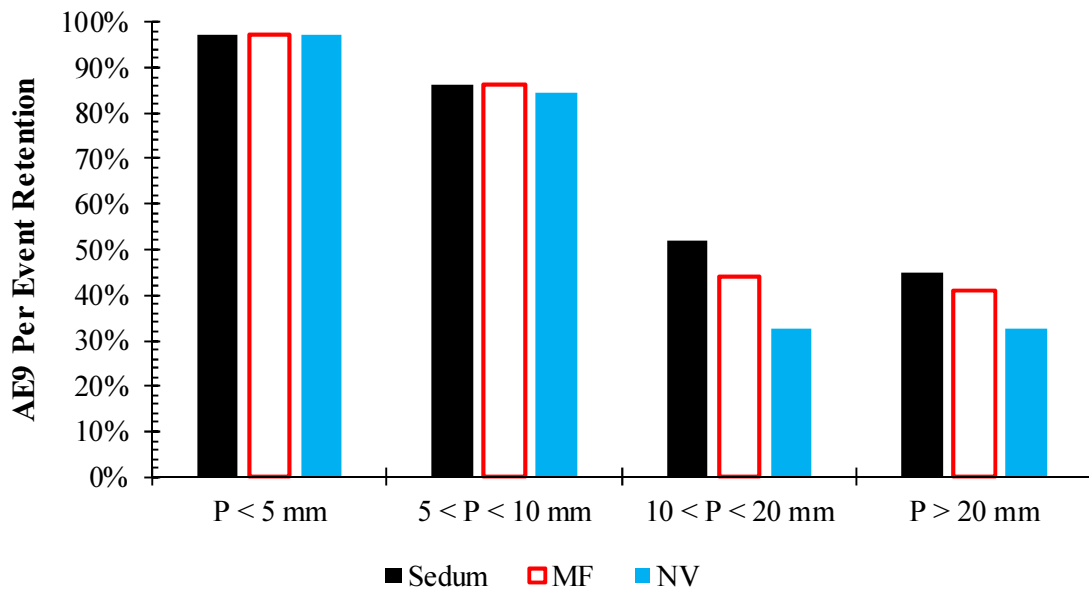


Figure 4.27: Per-event retention for AE9, categorised by vegetation treatment

The influence of vegetation treatment on per-event retention was minimal at low rainfall depths (i.e.  $P < 10$  mm) but became more important at higher rainfall depths. Retention ranged between 97.1% and 97.2% ( $P < 5$  mm) and between 84.6% and 86.4% ( $5 < P < 10$  mm). Predictably, as rainfall depth increased, retention from all vegetation treatments fell. When  $P \geq 10$  mm, retention was highest from Sedum (49.0%) and lowest from non-vegetated configurations (32.6%). The greater retention efficiency of Sedum measured here conflicts with the findings of many researchers who have identified lower retention by Sedum as a result of the more conservative transpiration loss (Nagase & Dunnett, 2010; Farrell *et al.*, 2012; Snodgrass & Snodgrass, 2006) compared with

vegetation treatments comprising grasses and herbs (e.g. Vanuytrecht *et al.*, 2014). Three phenomena could potentially explain the response observed here:

- (i) Sedum vegetation typically regulates its moisture consumption when plant-available moisture is constrained. In the UK's temperate climate, the frequency of rainfall is high and ADWPs are typically short. Moisture availability will not therefore have been as restrictive to plant water uptake as would be expected in warmer more arid climates. Furthermore only two species have CAM or CAM cycling behaviour;
- (ii) Sedum exhibited a dense, year-round vegetative coverage (including succulent leaves) that provided additional retention capacity; and
- (iii) A shallow, fibrous root structure (such as that believed to exist with Sedum) can increase biomass concentration (Lu *et al.*, 2015), reducing porosity and increasing moisture storage capacity by filling the larger pores. This may have been particularly important with the most porous substrate, LECA.

Further insight into the differences between Sedum and non-vegetated configurations can be provided through consideration of moisture balance changes. Moisture content, rainfall and runoff data was analysed to identify interception losses (IL) due to vegetation, i.e. the difference between rainfall and the sum of runoff and change in moisture content ( $IL = P - \delta\theta - Q$ ). Here,  $\delta\theta$  was measured from the CS616 probes, allowing evaluation on TB1, TB2, TB3 and TB7 only. ET during the event was considered negligible, due to the limited energy and the reduced vapour pressure deficit (Yang *et al.*, 2015). IL therefore equates to the interception of rainfall by vegetation (together with any depression storage). Figure 4.28 presents the interception losses for each bed.

Maximum interception losses ranged between 5.8 mm (TB7) and 8.0 mm (TB3). However, median values were lower: 2.4 mm (TB1 and TB2), 1.4 mm (TB3) and 1.7 mm (TB7). Differences in interception losses due to configuration were statistically significant (p-value = 0.002, p-value < 0.05 significance level). Predictably, median interception losses were typically greater with vegetated configurations. A Mann-Whitney U test confirmed that the difference between the Sedum-vegetated TB1 and non-vegetated TB7 bed was significant ( $U = 31.35$  versus a critical value of 21.95). It is

generally acknowledged (Voyde *et al.*, 2010a; Fassman-Beck *et al.*, 2013) that interception losses can reach 2 mm on impervious roofs. Interception losses were therefore expected even from the non-vegetated TB7.

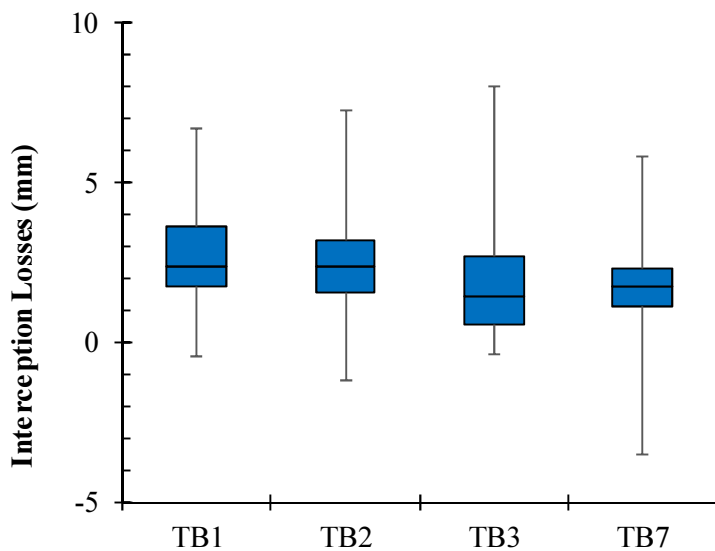


Figure 4.28: Interception losses from TB1, TB2, TB3 and TB7

Maximum interception losses indicate potentially important vegetative storage capacity (of up to 8 mm). This is consistent with the observations of Jarrett *et al.* (2006) in that Sedum can store up to 10 mm of moisture in its leaves. However, as median values demonstrate, this potential capacity will often not be fully realised. The extent to which interception losses benefitted retention was dependent on the availability of this capacity at the start of an event. The greatest interception losses from vegetated configurations would be expected when soil moisture availability is sufficiently low to restrict plant water uptake (Wolf & Lundholm, 2008). Maximum interception losses were observed during EV108; a summer event, when soil moisture content at the onset of rainfall was less than one third of field capacity. However, as Figure 4.29 demonstrates, no strong statistical correlation could be established between interception losses and the soil moisture content ( $R^2$  ranged from 0.30 [TB1] to 0.43 [TB2]).

With some exceptions, the general trend was for interception losses to be higher when soil moisture content was low; particularly for TB1 and TB2. For example, ahead of EV108, when interception losses were 5.6 mm (TB1), 7.3 mm (TB2) and 8.0 mm (TB3), at the onset of rainfall,  $\theta$  was 0.1 (TB1), 0.23 mm (TB2) and sufficiently low to induce a

negative reading of -0.13 for TB3. Similarly, initial gains (i.e. negative interception losses) were greatest during autumn and winter events, when soil moisture content was high (e.g. EV227 and EV228). It is possible that gains occurred due to snow melt and/or the presence of heavy dew.

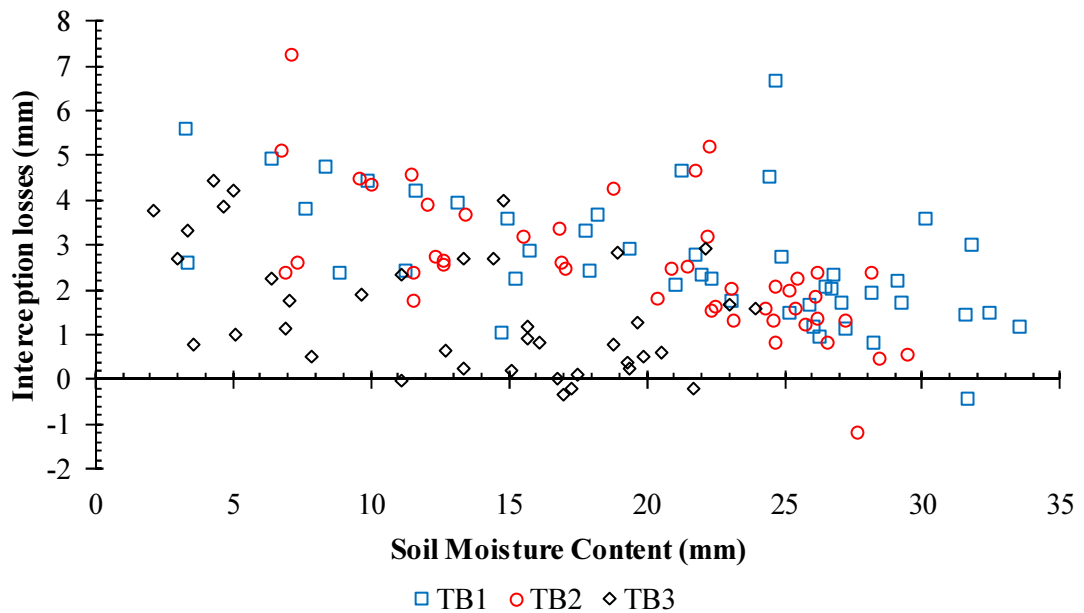


Figure 4.29: Relationship between interception losses and soil moisture content

Seasonal variations in the climate were also an important influence, with greater interception losses expected in warmer seasons. Figure 4.30 presents the seasonal mean per-event interception losses for each of the four test beds.

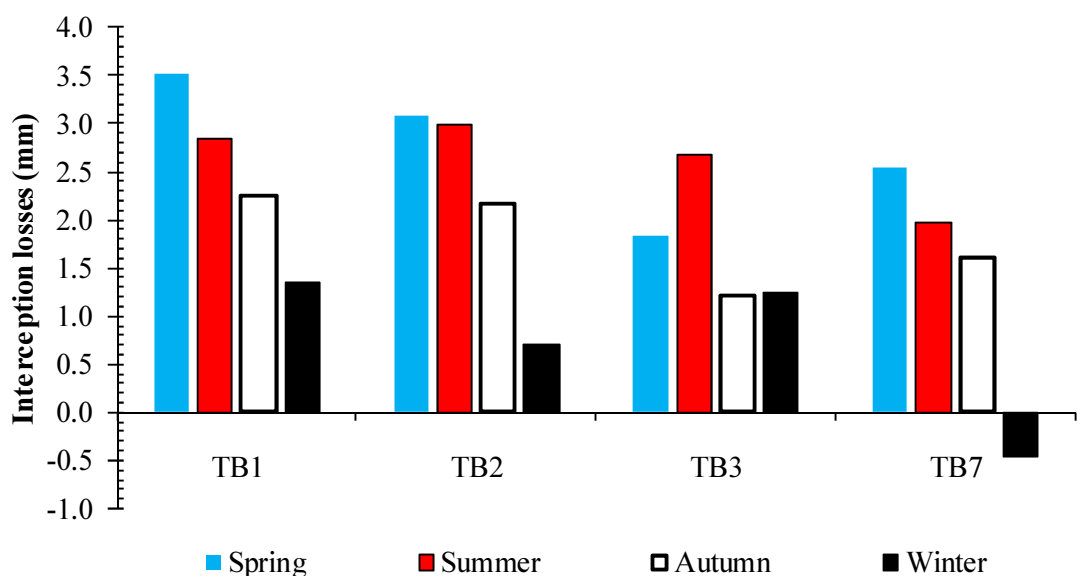


Figure 4.30: Seasonal-mean interception losses

Clear differences were observed between the interception losses during seasons when plants were active (i.e. spring and summer) and the cooler, wetter seasons when plants are typically approaching or in dormancy (i.e. autumn and winter). With the exception of the LECA-based TB3, interception losses in spring exceeded those in summer. However, these higher spring losses were facilitated by higher rainfall. Seasonal differences were also observed with the non-vegetated TB7. This is consistent with greater PET in the spring and summer seasons (due to warmer air and higher solar radiation) drying the exposed soil surface; leading to increased absorption and adsorption.

Here, it has been demonstrated that the Sedum vegetation can provide up to 8 mm of additional retention capacity. The extent to which this capacity is available will vary as a function of the ADWP, with higher interception losses typically following longer, drier and warmer ADWPs. In temperate climates, where soil moisture content is expected to be high throughout much of the year, the contribution of vegetation to interception losses will typically be limited.

#### 4.5.1.2 Substrate type

Consistent with the approach adopted in Section 4.5.1.1, the influence of substrate type upon retention is demonstrated in Figure 4.31.

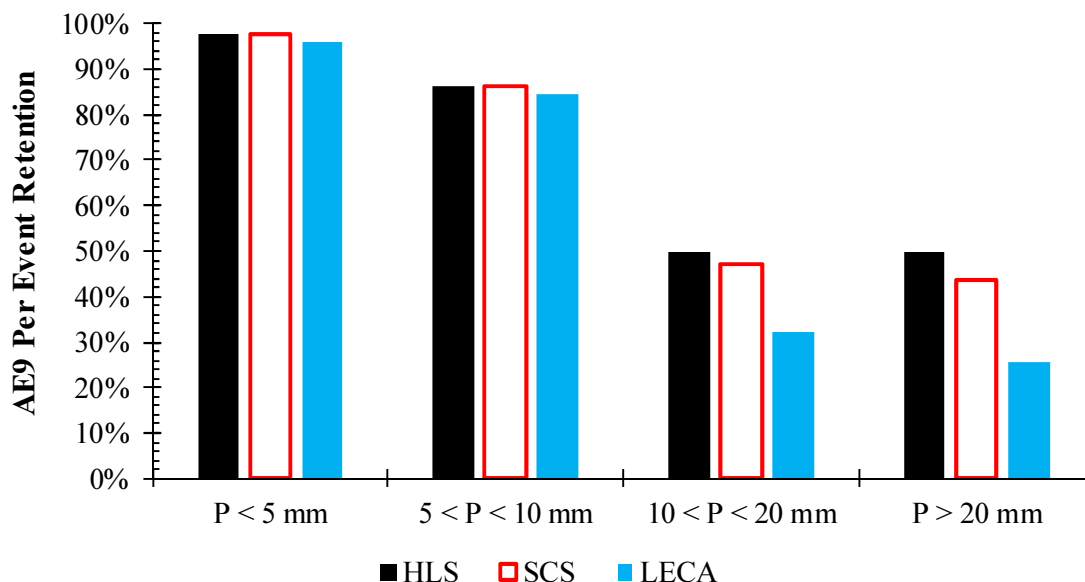


Figure 4.31: Per-event retention for AE9 dataset, categorised by substrate type



Differences in retention due to substrate were mostly observed when  $P \geq 10$  mm. Even when  $P \geq 10$  mm, there was little difference between the configuration mean retention response of HLS (49.8%) and SCS (45.5%). The lower retention by SCS is assumed to be associated with its smaller storage capacity relative to HLS. Marginally greater differences were observed when  $P \geq 20$  mm. Mean per-event retention from LECA-based configurations was 29.1% ( $P \geq 10$  mm), falling to 25.4% ( $P \geq 20$  mm).

The available moisture capacity in the substrate and the rainfall depth are two important controls upon retention (Stovin *et al.*, 2013; Palla *et al.*, 2009). Moisture balances within the substrate will be considered in detail in Section 4.5.1.4. However, retention response is known to be affected by the inter-particle storage space (Graceson *et al.*, 2013) and OM content (Graceson *et al.*, 2014; Carbone *et al.*, 2015) of a substrate. The lower retention efficiency of the LECA substrate is assumed to be associated with the high number of large particles (and voids) and the moisture storage space that is internal to the LECA aggregate that is not readily filled and regenerated. Conversely, HLS has a well-graded distribution of particle sizes and a greater number of small voids – characteristics that increase maximum retention capacity and reduce permeability (Carbone *et al.*, 2015). Greater differences attributable to substrate were observed when contrasting LECA with HLS and SCS.

The lumped effect of the plant-soil combination was also visible. The extent of plant growth was seen to vary as a result of the substrate mix. Whilst not directly measured here, the vegetation coverage was often visibly lower with LECA than with the HLS and SCS substrates. This was consistent with the findings of Vijayaraghavan & Raja (2014). The greater OM content of HLS would be expected to increase biomass, provide a greater nutrient supply and increase moisture-holding capacity (Graceson *et al.*, 2014).

The influence of substrate depth was not evaluated here. Instead, a depth of 80 mm was universally adopted. This reflects the current UK best practice for extensive green roofs (GRO, 2014). A greater depth of substrate may increase the storage potential. However, the extent to which this potential provides hydrological mitigation will depend upon the incidence of rainfall (Fassman-Beck *et al.*, 2013) and the drying rate (Voyde *et al.*, 2010b). It is acknowledged by many researchers (Fassman & Simcock, 2012; van Woert *et al.*, 2005; Madre *et al.*, 2014) that deeper substrates can facilitate a greater diversity of

plant species. However, deep substrates would be expected to provide minimal incremental retention benefits when used in conjunction with shallow-rooted vegetation. Indeed, shallower substrates may increase biomass concentration (Lu *et al.*, 2015) and moisture holding capacity.

#### 4.5.1.3 Seasonal climate

It is already evident that interception losses were seasonally influenced. However, the broader influence of seasonal climate on per-event retention is highlighted in Figure 4.32.

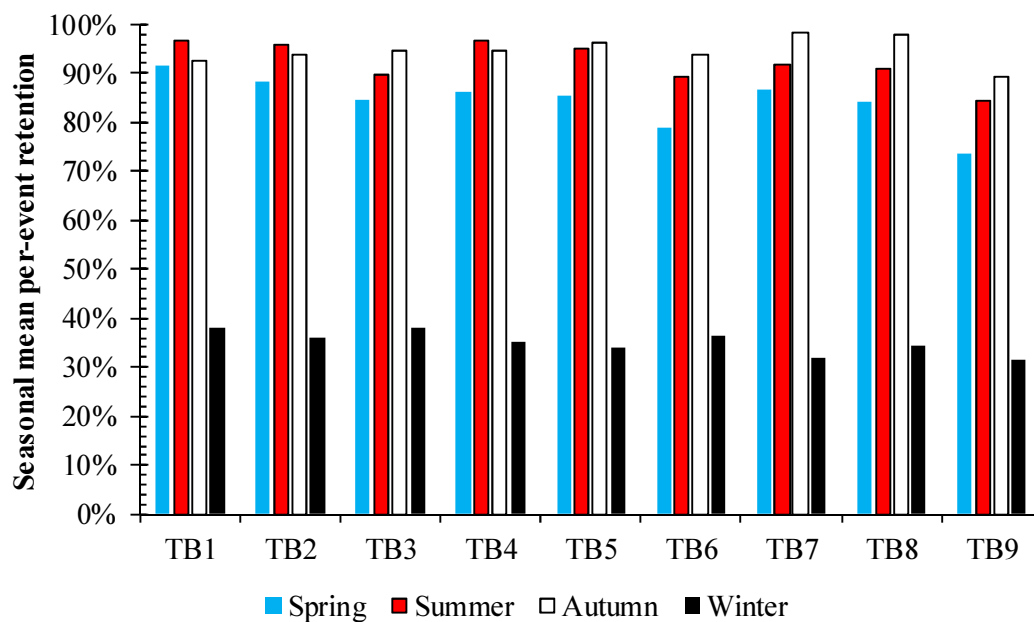


Figure 4.32: Seasonal mean per-event retention

Configuration-mean per-event retention was significantly lower in winter (31-38%) than in any other season. In all other seasons, seasonal mean per-event retention percentages were broadly similar across the configurations. In summer and autumn, when seasonal-mean retention ranged between 84-97% and 89-98% respectively, variations in each configuration's performance across the two seasons were always less than 4%. In spring, differences in seasonal-mean retention were greater, as retention fell as low as 74%. The retention responses in summer were similar to those observed by Fassman-Beck *et al.* (2013) in Auckland (83-92%) but different to winter retention levels (66%). It is expected that the lower retention efficiencies observed here reflect the wetter winter conditions experienced in the UK.

Seasonal differences in hydrological performance are often attributed to differences in ET (Berghage *et al.*, 2007; van Seters *et al.*, 2009; Mentens *et al.*, 2006). However, the seasonal distribution of rainfall can also be an important control (Stovin *et al.*, 2012; Carson *et al.*, 2013). The retention percentages alone do not portray the differences in mean per-event rainfall depths. In spring, mean per-event rainfall was greater (8.1 mm) than in both summer (6.0 mm) and autumn (3.8 mm), but lower than in winter (12.4 mm). Figure 4.33 presents the mean absolute values of seasonal rainfall and runoff.

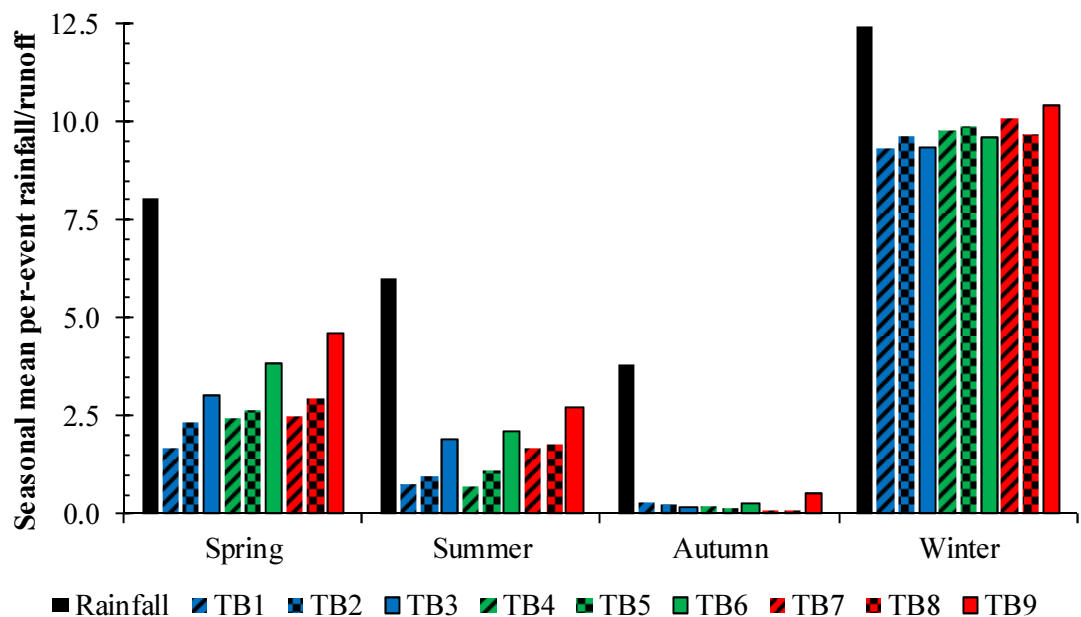


Figure 4.33: Seasonal mean rainfall and runoff

Here, the relatively low per-event rainfall in summer and autumn underpinned the low rates of runoff (and high retention percentages). In spring, the greater per-event rainfall resulted in more runoff and greater variation in retention performance across the configurations. As previously observed by Schroll *et al.* (2011), seasonal-mean per-event retention was heavily skewed by rainfall depth. In spring and summer, there were clear (but not statistically significant) trends for runoff to be least from Sedum and HLS configurations and greatest from non-vegetated and LECA-based configurations. In autumn, no discernible trends could be identified due to the very low runoff from all beds. However, in winter, consistent with the conclusions of Dunnnett *et al.* (2008b), the differences between vegetated and non-vegetated configurations were negligible. Runoff was high from all beds.

The influence of seasonal climate upon retention potential (rather than actual retention) was considered through analysis of the seasonal mean SMD prevailing at the start of a rainfall event. The SMD is an accurate representation of the substrate's retention capacity (Versini *et al.*, 2015). This analysis relies upon the CS616 moisture content data and therefore considers the regeneration of available capacity (or SMD) within TB1, TB2, TB3 and TB7 (see Figure 4.34).

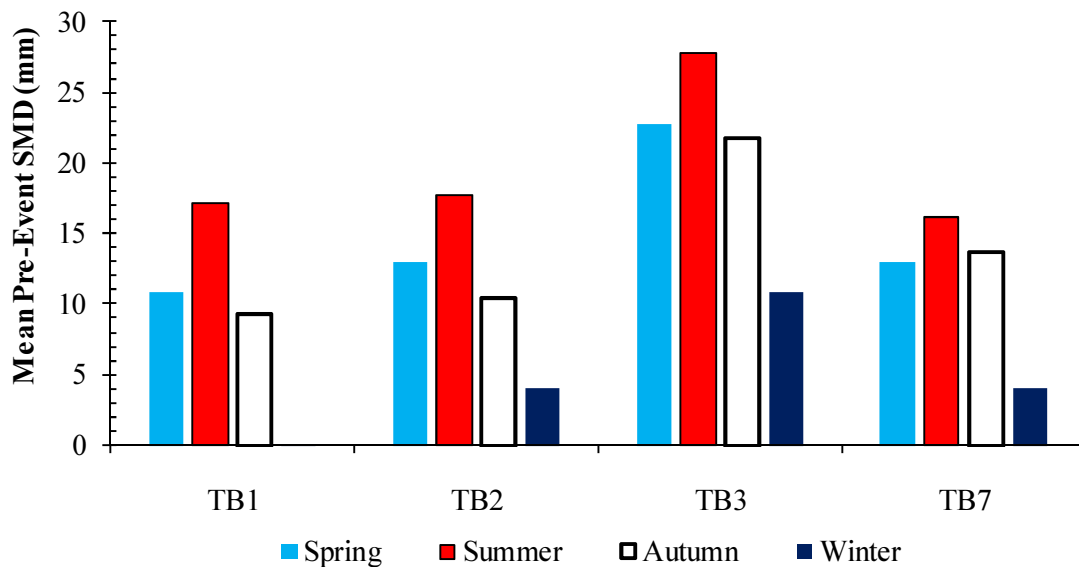


Figure 4.34: Configuration mean soil moisture deficit after the ADWP

Predictably, the greatest pre-event SMD was measured in summer conditions, followed by spring (vegetated configurations only), autumn and winter. The LECA-based TB3 had the greatest theoretical mean pre-event SMD. However, with LECA-based beds, runoff was frequently observed before  $\theta_{FC}$  (see Section 4.5.3.1). For this reason, the following analysis will focus solely on the SMD statistics for TB1 and TB2 (for vegetated configurations) and TB7 (for non-vegetated configurations).

Based on configuration-mean pre-event SMD, in summer, maximum potential retention would have been between 16.2 mm (TB7) and 17.7 mm (TB2). This would have reduced to between 10.9 mm and 13.0 mm in spring (for TB1 and TB7 respectively), 9.3 mm to 13.6 mm in autumn (for TB1 and TB7 respectively) and 0.1 mm to 4.1 mm in winter (for TB1 and TB2 respectively). This broadly reflects expectations regarding seasonal variations in retention (Schroll *et al.*, 2011) with lower retention efficiency in winter and autumn (Fassman-Beck *et al.*, 2013). However, Figure 4.34 also serves to highlight some influences of configuration on SMD. The lowest pre-event SMD was typically associated

with the substrate with the highest proportion of small particles. This would indicate that the time required to regenerate SMD was longest with HLS. Similarly, except during summer, SMD was higher with non-vegetated beds than with Sedum vegetation. This is consistent with the fast drying of a bare non-vegetated surface of a dark, porous substrate contrasting with the reduced evaporation from a configuration that was covered by a moist carpet of Sedum vegetation (Nagase & Dunnett, 2010). Clearly, the higher interception losses with vegetated configurations at least partially offset this difference. In view of the important influence that rainfall depth and available moisture capacity has upon retention efficiency, these parameters will now be considered in greater detail.

#### 4.5.1.4 Moisture balance

It is widely acknowledged that the SMD is an important influence upon a green roof's hydrological response (Stovin *et al.*, 2012; Bengtsson *et al.*, 2005; DeNardo *et al.*, 2005; Stovin *et al.*, 2013). In this section, the correlation between SMD, rainfall and runoff will be evaluated. Carter & Rasmussen (2006) and Teemusk & Mander (2007) concluded that rainfall discharged from the green roof only once  $\theta_{FC}$  was reached. Many hydrological models function on this basis. Here, the validity of this assumption will be tested by comparing actual runoff ( $Q$ ) with runoff predicted using Equation 4.12 ( $Q_{PRED}$ ).

$$\begin{array}{ll} \text{If } P - SMD \leq 0 & Q_{PRED} = 0 \\ \text{Else} & Q_{PRED} = P - SMD \end{array} \quad \text{Equation 4.12}$$

SMD (in mm) was calculated by deducting residual soil moisture, using CS616 data, from  $\theta_{FC}$  (in mm) of each substrate. Plant moisture storage was not included. First,  $\theta_{FC}$  was compared against the maximum moisture content ( $\theta_{MAX}$ ) measured during the eight AE9 events when CS616 probes were installed and runoff exceeded 2 mm.  $\theta_{MAX}$  was calculated as the maximum depth-averaged  $\theta$  in each test bed during the event (see Table 4.5).

Here,  $\theta_{MAX}$  in TB7 (0.409) was similar to the laboratory-derived  $\theta_{FC}$  for HLS (0.412). However, in the vegetated HLS-based configuration, TB1,  $\theta_{MAX}$  was higher (0.443). It is assumed that the plant biomass in the vegetated HLS configuration will have increased the moisture storage capacity of the system relative to non-vegetated HLS (Vijayaragahvan & Raja, 2014; Graceson *et al.*, 2014).  $\theta_{MAX}$  in TB2 (0.396) was also similar to  $\theta_{FC}$  for SCS (0.391).

Table 4.5: Maximum measured values of  $\theta$  during AE9 events

	<b>TB1</b>	<b>TB2</b>	<b>TB3</b>	<b>TB7</b>
EV108	0.138	0.151	-0.026	0.163
EV109	0.240	0.248	0.033	0.264
EV228	0.435	0.396	0.304	0.409
EV245	0.437	0.391	0.300	0.403
EV246	0.443	0.394	0.301	0.407
EV250	0.432	0.387	0.293	0.393
EV258	0.333	0.292	0.142	0.324
EV264	0.371	0.338	0.231	0.344
<b>Maximum</b>	<b>0.443</b>	<b>0.396</b>	<b>0.304</b>	<b>0.409</b>

However,  $\theta_{MAX}$  in TB3 (0.304) was lower than  $\theta_{FC}$  for LECA (0.350). Whilst runoff occurred from all TBs prior to  $\theta_{FC}$  during certain events, this was the case with LECA for all events. It is therefore hypothesised that the laboratory-derived  $\theta_{FC}$  for LECA was greater than the practical maximum (i.e.  $\theta_{MAX}$ ). In Section 4.5.3,  $\theta$  at the time of first runoff will be reviewed, considering also the distribution of moisture across the depth of the substrate.

Considering retention responses of each TB to all 48 AE9 events,  $Q_{PRED}$  was strongly correlated with actual runoff measured from TB1 (see Figure 4.35).

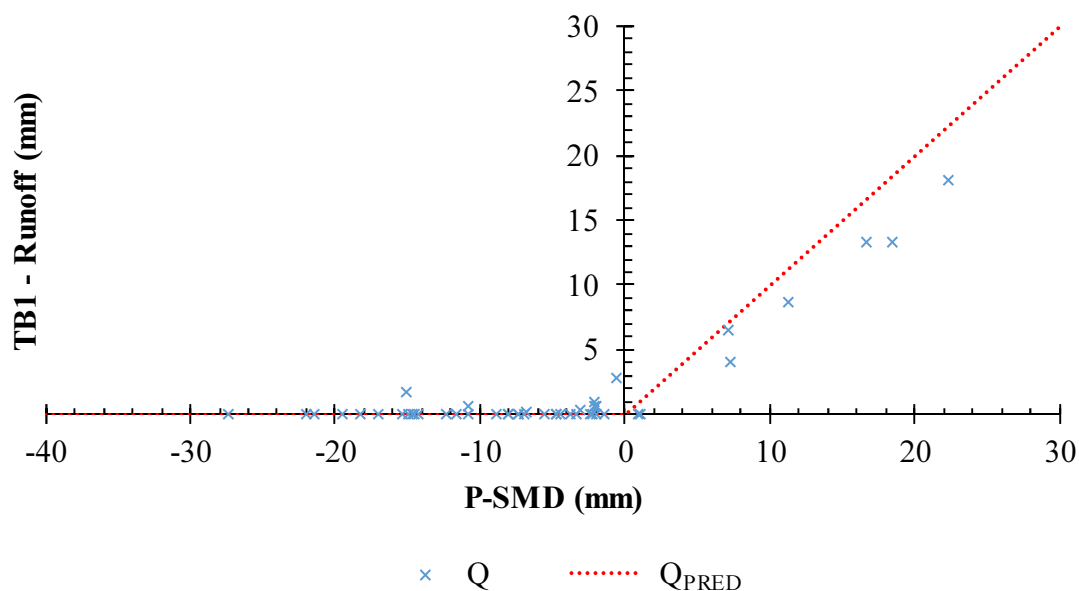


Figure 4.35: Rainfall minus SMD versus runoff (TB1)

Generally, runoff did not occur from TB1 when  $P-SMD < 0$ . However, there was a small number of exceptions. The largest discrepancy occurred during EV258 ( $P=24.8$  mm). Here, 2.8 mm of runoff was measured, despite capacity apparently being available to wholly retain this event. When  $P-SMD > 0$ , runoff was typically lower than  $Q_{PRED}$ . This is expected to be attributable to one or a combination of two factors: (a) interception losses by the *Sedum* vegetation, and (b) the low permeability of HLS led to detention of runoff by more than 6 hours after rainfall (i.e. the period during which runoff was measured). The latter hypothesis is supported by observations of small amounts of runoff still taking place at this time during some events (e.g. EV245).

$Q_{PRED}$  was also closely aligned to actual runoff from TB2 (see Figure 4.36).

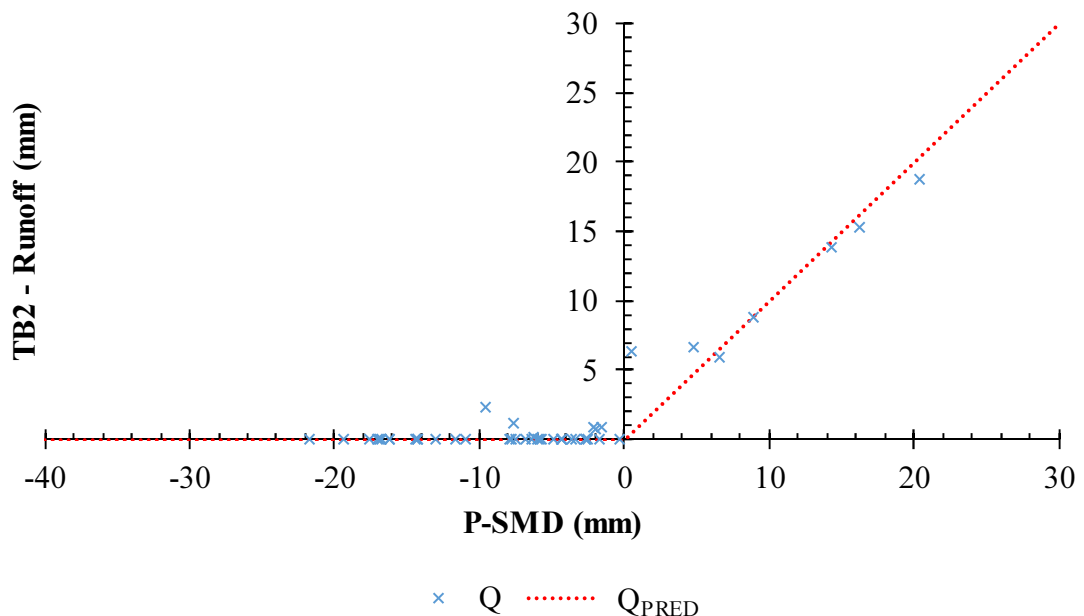


Figure 4.36: Rainfall minus SMD versus runoff (TB2)

The greatest under-prediction of runoff would have occurred during EV258, when  $Q_{PRED}$  was 0.4 mm but actual runoff was 6.4 mm. The interception losses and detention effects that were observed with TB1 were not evident to the same extent with TB2, as the maximum over-prediction of runoff was 1.7 mm (EV245). There are two possible explanations for the different responses of TB1 and TB2: (i) the lower effects of detention by SCS, associated with its higher permeability (relative to HLS); or (ii) lower interception losses due to the lower plant biomass (Vijayaraghavan & Raja, 2014; Graceson *et al.*, 2014) expected to be in the root zone of the SCS-based TB2 (compared

to HLS which has higher OM). Higher interception losses have been observed with Sedum vegetation when used with substrates with higher moisture capacity (Berghage *et al.*, 2007).

The LECA-based TB3 had the highest number of events (9) when runoff was greater than  $Q_{PRED}$  (see Figure 4.37).

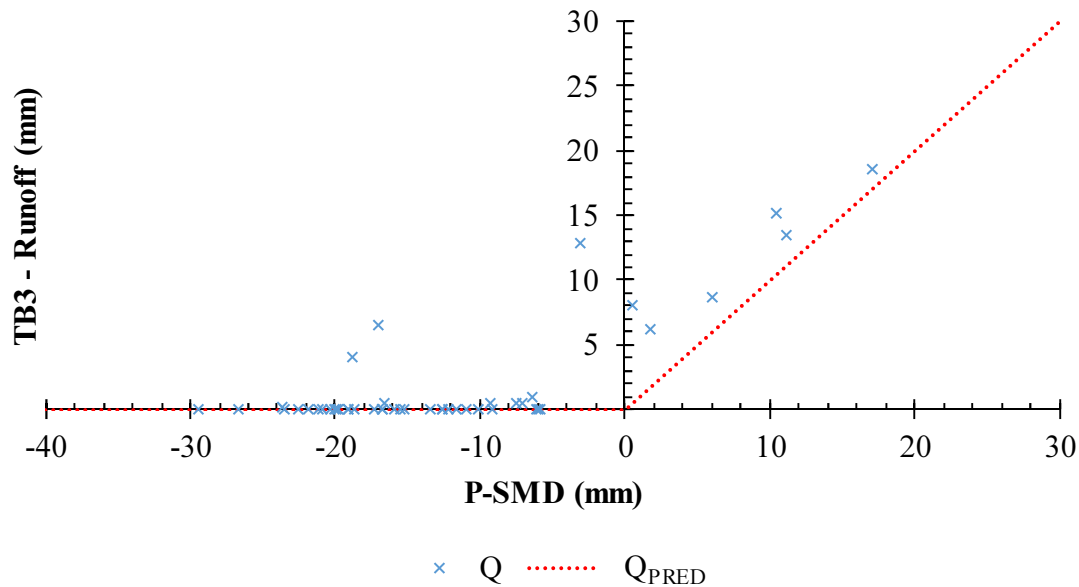


Figure 4.37: Rainfall minus SMD versus runoff (TB3)

In all 6 cases when rainfall exceeded SMD,  $Q_{PRED}$  would have under-predicted runoff by between 1.6 mm and 7.6 mm. It is expected that the previously presented hypothesis regarding the differences between the practical  $\theta_{FC}$  of LECA and the laboratory-derived values will have contributed to these errors. Other potential causes include (i) a differential distribution of moisture within the soil column and/or (ii) accuracy issues associated with the probes being inserted in the highly porous LECA medium. For those events where zero runoff was expected (i.e. when  $P-SMD < 0$ ), the greatest runoff measured was 12.8 mm (EV258). However, there were also two events when runoff occurred, despite apparently having capacity to fully retain the event and a further 17.0 mm (EV108) and 18.8 mm (EV109). These observations of earlier-than-anticipated runoff would be consistent with rainfall passing through a very dry substrate (a) before hydrophobicity had been overcome, or (b) due to preferential flow. Unlike with TB1 and TB2, there was no evidence of interception losses resulting from the addition of Sedum



vegetation. However, it is possible that these interception losses were effectively concealed by the differences in the practical and theoretical  $\theta_{FC}$  of LECA.

With the non-vegetated TB7, there were a greater number of events when  $Q_{PRED}$  under-predicted actual runoff, compared to TB1. However,  $Q_{PRED}$  was still predicted with a high degree of accuracy (see Figure 4.38).

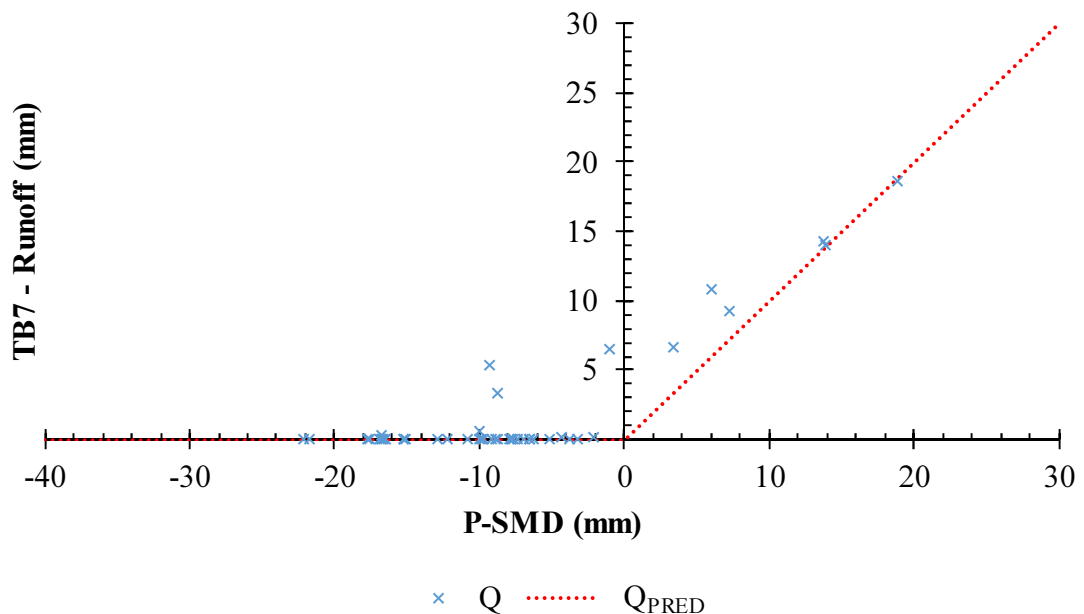


Figure 4.38: Rainfall minus SMD versus runoff (TB7)

For the 3 events with the highest runoff,  $Q_{PRED}$  accurately predicted runoff. However, for the other 3 events where  $P > SMD$ , runoff was as much as 4.8 mm higher than predicted (recorded during EV228, when 11.7 mm of rain fell). Of the events when available capacity was expected to be sufficient to wholly retain the rainfall, maximum runoff was 6.5 mm (during EV258). In contrast to the response of TB1, in no case here was runoff ever lower than  $Q_{PRED}$ . This was entirely consistent with the lower interception losses exhibited by a non-vegetated configuration.

Generally, runoff occurred when  $P > SMD$ . In some instances, runoff occurred despite capacity apparently being available. This was particularly evident when rainfall depth was high and/or when soil moisture content was very low. However, overall, the difference between rainfall and SMD provided a highly credible indication of runoff depths.

$R^2$  values ranged between 0.93 (TB7) and 0.99 (TB2). With the exception of TB3 (0.64), the NSME coefficients showed a very good fit between predicted and actual runoff (NSME ranged between 0.87 [TB7] and 0.94 [TB2]). These findings are consistent with previous conclusions that rainfall depth (Fassman-Beck *et al.*, 2013; Carson *et al.*, 2013) and initial moisture content (Voyde *et al.*, 2010a; Stovin *et al.*, 2013) are important influences upon retention efficiency. In section 4.5.3, the physical controls influencing runoff prior to field capacity will be analysed with a view to identifying the potential causes of the small predictive errors observed here.

#### 4.5.1.5 Summary of physical controls upon retention

Retention generally reflected the differential between rainfall depth and the available moisture capacity, or SMD. Seasonal rainfall differences were observed. SMD was affected both by the seasonal climate and the configuration. Retention potential was highest in summer and lowest in winter. Except during summer, the non-vegetated HLS-based bed (TB7) regenerated a marginally greater pre-event SMD than the Sedum-vegetated TB1. However, the greater interception losses associated with Sedum vegetation will have contributed to the higher per-event retention performance of TB1 versus TB7. Comparing the pre-event SMD across the two-brick based substrates, only minor differences were observed. SMD was marginally greater with TB2 (SCS) than with TB1 (HLS) in all seasons.

### 4.5.2 Physical controls upon detention performance

#### 4.5.2.1 Vegetation treatment

Differences in  $k$  values due to vegetation were shown to be systematic and statistically significant in Section 4.4.7. The highest  $k$  values were associated with non-vegetated configurations and the lowest with Sedum-vegetated configurations. Vegetation-median  $k$  (in  $\text{mm}^{\text{n-1}}/\text{min}$ ) was 0.0051 for Sedum, 0.0070 for Meadow Flower and 0.0092 for non-vegetated beds. Here, some hypotheses will be presented to explain these differences, whilst equally highlighting the importance of vegetation choice upon conventional detention parameters (i.e. peak attenuation and peak delay).

The detention response of a configuration is expected to be affected by the characteristics of the vegetation treatment in two ways:

1. Plant architecture.

Whilst the leaf area index was not quantified here, visual inspections indicated that the year-round vegetative coverage of the Sedum and Meadow Flower treatments were typically similar, but greater than the non-vegetated test beds. A greater density of foliage (and greater surface area) would be expected to both intercept a greater amount of rainfall as interception losses and introduce small delays to runoff by increasing the flow path of rainfall as it permeates the green roof build-up.

The shape, size and type of leaf can influence the vegetation's retention and detention performance. As a succulent, Sedum vegetation has the capacity to store moisture within its leaf structure (Jarrett *et al.*, 2006) whereas the broadleaf plants in Meadow Flower will be expected to intercept more rainfall on its leaves.

2. Plant physiology and root structure.

No direct observations of plant root and soil interactions were made. However, the presence of roots can change the size distribution and connectivity of pores within a substrate. Roots can grow to fill large voids and change the water retention and release characteristics of the substrate (Nagase & Dunnett, 2011). Soil matrix porosity has been observed to fall by >20% due to the presence of plant roots in both conventional soils (Bruand *et al.*, 1996) and – in a preliminary study – in green roof substrates (De-Ville *et al.*, 2015). Any reduction in porosity due to greater plant biomass is expected to reduce permeability and increase detention (Carbone *et al.*, 2015). The contrasting rooting types of the Sedum and Meadow Flower vegetation may therefore have contributed to the differences in detention performance. Meadow Flower contains species that have deeper roots (Brickell, 2008). Sedum has shallower fibrous roots (Snodgrass & Snodgrass, 2006; MacIvor & Lundholm, 2011) that may have increased the concentration of biomass and reduced the porosity of the substrate in the root zone to a greater extent.

Root die-back may lead to the development of preferential flow paths. The greater ability of hardy Sedum vegetation to survive dry weather (Cook-Patton & Bauerle,

2012; Farrell *et al.*, 2012; Rowe *et al.*, 2012) is expected to reduce root die-back, relative to the seasonal Meadow Flower. The opportunities for preferential flow paths to develop within the soil matrix of Sedum vegetated beds would be expected to be less than with Meadow Flower. In a horticultural setting, particle travel speeds have been found to be 152 times faster than the measured soil matrix conductivity values due to the presence of dead root macro pores (Schwen *et al.*, 2011).

Considering the more conventional detention metrics, the addition of vegetation improved peak attenuation for all rainfall depths. These differences largely reflect the differences observed in per-event retention (see Figure 4.39).

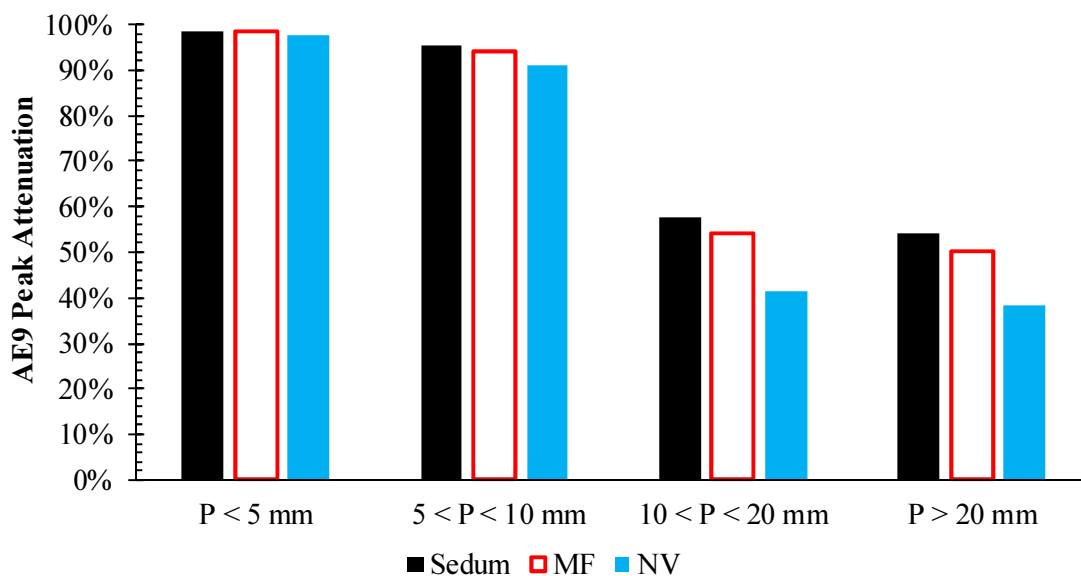


Figure 4.39: Peak attenuation for AE9 dataset, categorised by vegetation treatment

Attenuation was marginally higher for Sedum, compared to Meadow Flower, for all rainfall depths. Again, here, rainfall depth was an important influence upon the attenuation response. Differences due to vegetation increased as greater rainfall depths were considered. When  $P > 20$  mm, peak attenuation was 38.3% for non-vegetated configurations, compared to 50.2% (Meadow Flower) and 54.3% (Sedum).

Peak delays were typically short. The highest vegetation-median peak delay was associated with Sedum (80 minutes), compared with Meadow Flower (50 minutes) and non-vegetated configurations (45 minutes). The lengths of the delays observed here were consistent with the findings of Hakimdavar *et al.* (2014), who identified peak delays of

between 0.2-1.6 hours when  $P < 20$  mm, but longer delays (1.4-4.2 hours) when rainfall was greater than 20 mm but less than 40 mm. However, delays were minimal (up to 0.1 hours) when  $P > 40$  mm. This suggests that a tipping point exists in the relationship between rainfall depth and peak delay, as other influences affect the response.

Carter & Rasmussen (2006) estimated peak delays to be approximately 10 minutes. Here, delays were often greater than this, but were influenced by the rainfall characteristics. Vegetation-mean peak delays for AE9 events with runoff of 2 mm are plotted as a function of rain depth and duration in Figure 4.40.

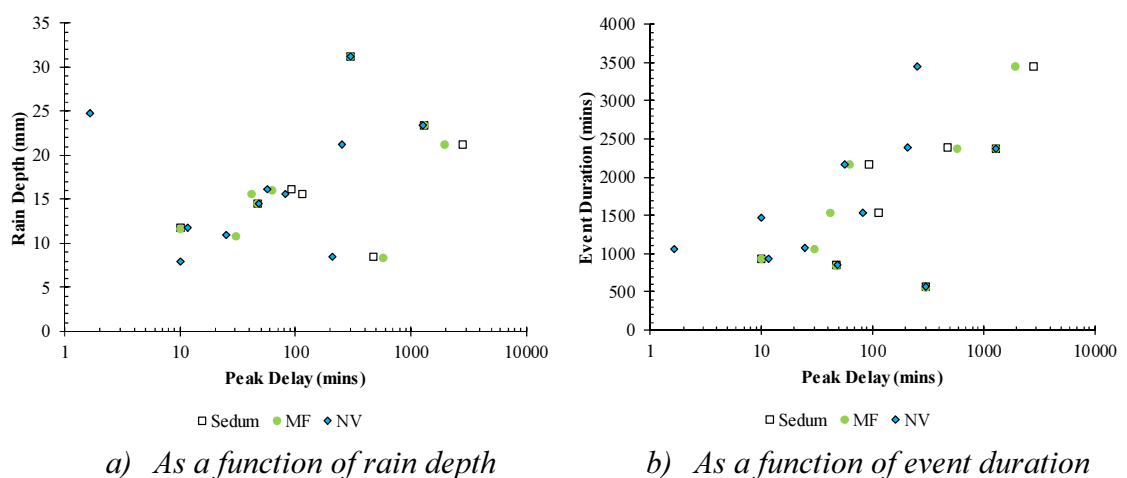


Figure 4.40: Peak delay for AE9 dataset, categorised by vegetation treatment

Here, peak delays generally increased with both the depth and duration of rainfall. Peak delays were typically less than 100 minutes for all vegetation treatments. However, peak delays ranged between 0 and 2820 minutes. The longest delays were typically associated with events where retention was high.

#### 4.5.2.2 Substrate type

The detention response of a substrate is expected to be influenced by (a) substrate depth (held constant at 80 mm in this study), and (b) substrate permeability or hydraulic conductivity. The hydraulic conductivity of a substrate is a function of the soil's structure and degree of saturation. When considering pure detention, by definition, the substrate would be at field capacity and the saturated hydraulic conductivity of the substrate should indicate detention performance. In this case,  $k$  would be expected to be lowest for HLS and highest for LECA. However, differences in substrate-median  $k$  (in  $\text{mm}^{\text{n-1}}/\text{min}$ ) were shown in Section 4.4.7 to be neither systematic nor statistically significant. The lowest  $k$

was derived for SCS-based configurations (0.0061) and the highest for LECA (0.0084). However, despite having a lower permeability, the  $k$  value for HLS (0.0069) was marginally higher than SCS.

The poor detention performance of LECA can be explained by its PSD; with 58% of particles sized between 4 and 8 mm in diameter (compared with 35% for HLS and 40% for SCS). The high proportion of large, uniformly-sized and rounded LECA particles results in a substrate that has high porosity and high permeability. Although tortuosity was not measured directly, the graded distribution of particle sizes and shapes in HLS is likely to increase the number of tortuous paths through which gravitational water must pass; reducing permeability and increasing detention times.

Predictably, the extent to which the substrate type affected attenuation was a function of rainfall depth and largely reflected retention trends. Whilst peak attenuation was lowest from LECA for rainfall events of all sizes, the differential between LECA and the commercial substrates increased as rainfall depth increased (see Figure 4.41).

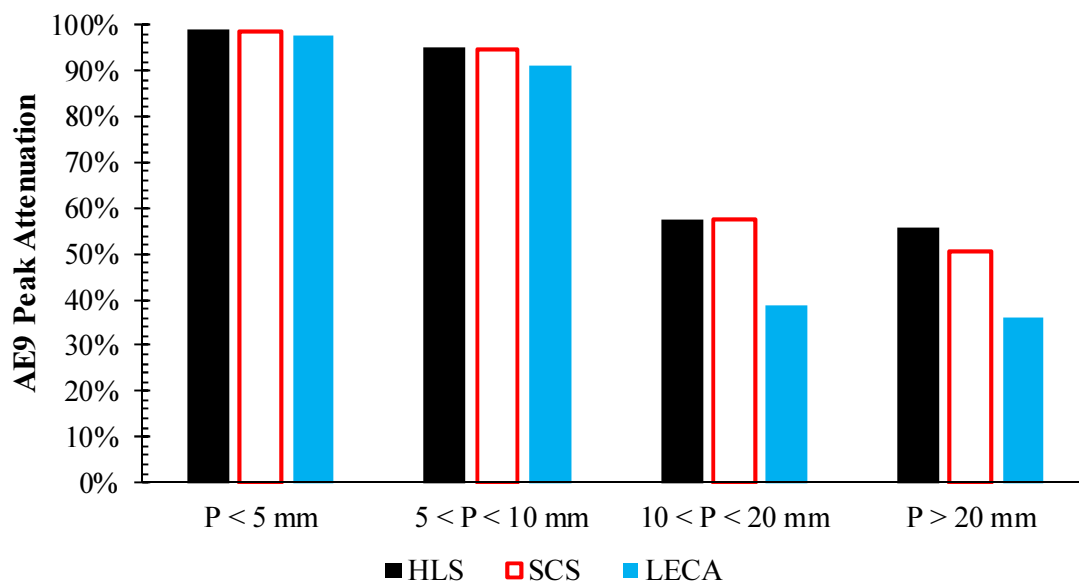


Figure 4.41: Peak attenuation for AE9 dataset, categorised by substrate type

Peak attenuation from LECA fell to 38.6% ( $10 < P < 20$  mm) and 36.2% ( $P > 20$  mm). No significant differences were observed between the responses of HLS and SCS; with the greatest difference in peak attenuation of 5.2% when  $P > 20$  mm. This would be consistent with the greater moisture storage capacity of HLS, relative to SCS, that also influenced retention. Minimum peak attenuation was 50.7% (SCS) and 55.9% (HLS).

The median peak delay was almost identical across all three substrates – 48 minutes for HLS and 50 minutes for both SCS and LECA. As such, no strong trends could be identified to describe the influence that substrate type had upon peak delays. Figure 4.42 highlights the peak delays for each substrate as a function of rainfall depth and duration.

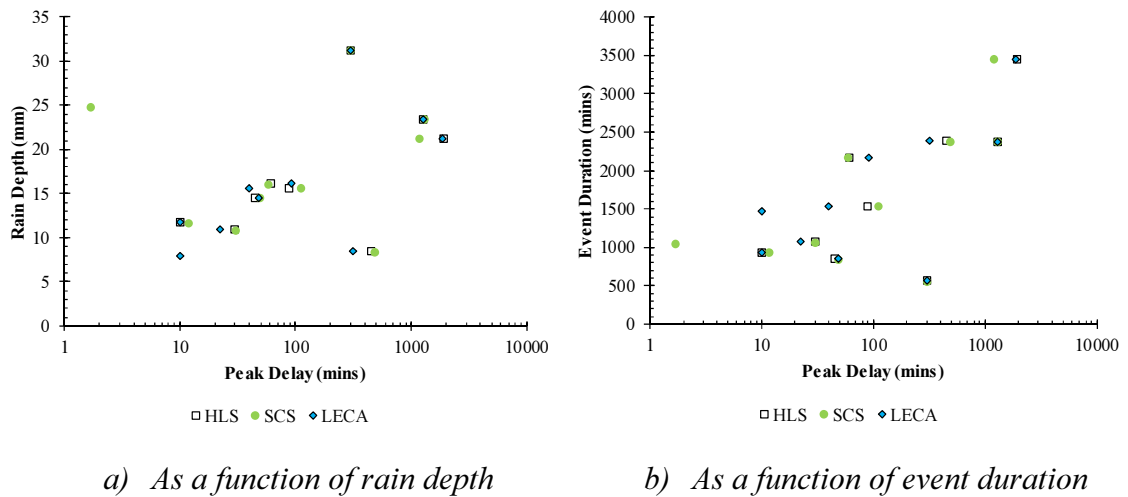


Figure 4.42: Peak delay for AE9 dataset, categorised by substrate type

As shown in Section 4.5.1.1, peak delays were generally influenced by the depth and duration of rainfall rather than by the green roof configuration.

#### 4.5.2.3 Seasonal climate

Differences in seasonal-median  $k$  (in  $\text{mm}^{n-1}/\text{min}$ ) were not statistically significant ( $p$ -value = 0.282,  $p$ -value < 0.05 significance level). The highest  $k$  value was derived in summer ( $0.0096 \text{ mm}^{1-n}/\text{min}$ ) and the lowest in winter ( $0.0056 \text{ mm}^{1-n}/\text{min}$ ). This would be consistent with the higher rainfall intensities in summer relative to winter. However, it would be contrary to the expectation that detention performance would be higher in summer than in winter, due to greater vegetation bloom.

Apparent detention, as described by peak attenuation, largely mirrored the seasonal-mean retention values observed in Section 4.5.1.3 (see Figure 4.43).

Here, seasonal-mean peak attenuation ranged between 80-93% (in spring), 85-95% (in summer), 93-98% (in autumn) and 49-66% (in winter). The range of peak attenuation values identified here was marginally greater than the range of 62-90% observed by Fassman-Beck *et al.* (2013). However, whilst peak attenuation in autumn and winter showed some reduction, relative to spring and summer, Fassman-Beck *et al.* (2013) did

not identify any significant seasonal trends. The identified seasonal differences in peak attenuation can largely be attributed to the same influences that affected retention.

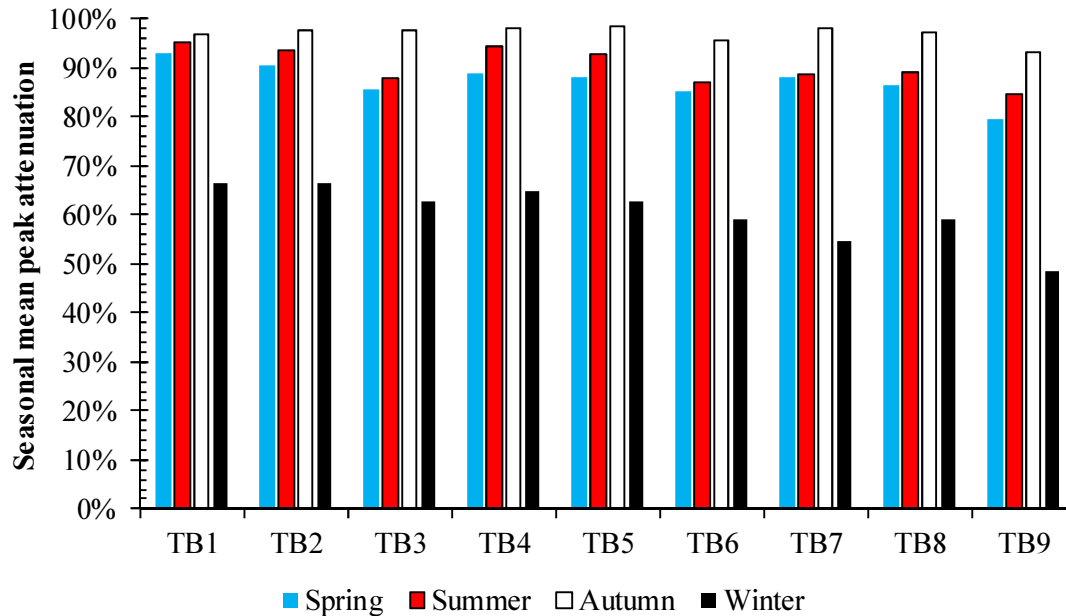


Figure 4.43: Seasonal-mean peak attenuation

#### 4.5.2.4 Summary of physical controls upon detention performance

The choice of vegetation treatment had a significant influence on detention parameter  $k$ , with detention expected to be highest with Sedum and lowest with non-vegetated beds. The density of foliage and the effect of plant roots upon substrate porosity could potentially explain this trend. The influence of substrate type and seasonal climate on  $k$  was less important. However, these variables were seen to affect apparent detention (i.e. peak attenuation and peak delay). Peak attenuation was lowest with the most permeable constructions, i.e. non-vegetated and LECA-based and highest with the most densely covered vegetation treatment (i.e. Sedum) and the substrate with the lowest permeability (i.e. HLS). As with retention, differences in peak attenuation between the configurations were greatest when rainfall depths were high. Even when rainfall exceeded 20 mm, peak attenuation from HLS and SCS was greater than 50% for all vegetation treatments. Seasonal climate influenced both peak attenuation – being highest in autumn and lowest in winter (consistent with the seasonal rainfall depths being low and high respectively) – and peak delays. The longest delays, recorded in spring and winter, were typically associated with the largest rainfall. These larger rainfall events typically had longer durations which, when combined with low peak rainfall rates, led to delays that were



often longer than the duration of smaller storms. Configuration-median peak delays were low, ranging between 28 and 75 minutes. Whilst apparent detention responses will often include the effects of retention, actual detention by extensive green roofs is expected to be limited by the shallow, highly permeable substrates and low-growing vegetation treatments.

### 4.5.3 Physical controls upon the initialisation of runoff

#### 4.5.3.1 Soil moisture deficit at first runoff

Runoff is typically only expected to occur once a substrate's field capacity has been reached (Bengtsson, 2005). However, here, runoff was observed in some instances despite there being a positive SMD (i.e. prior to field capacity). The validity of this assumption will therefore be further evaluated here. Figure 4.44 shows the depth-averaged  $\theta$  prevailing in each of the 4 TBs at the time of first runoff during AE9 events.

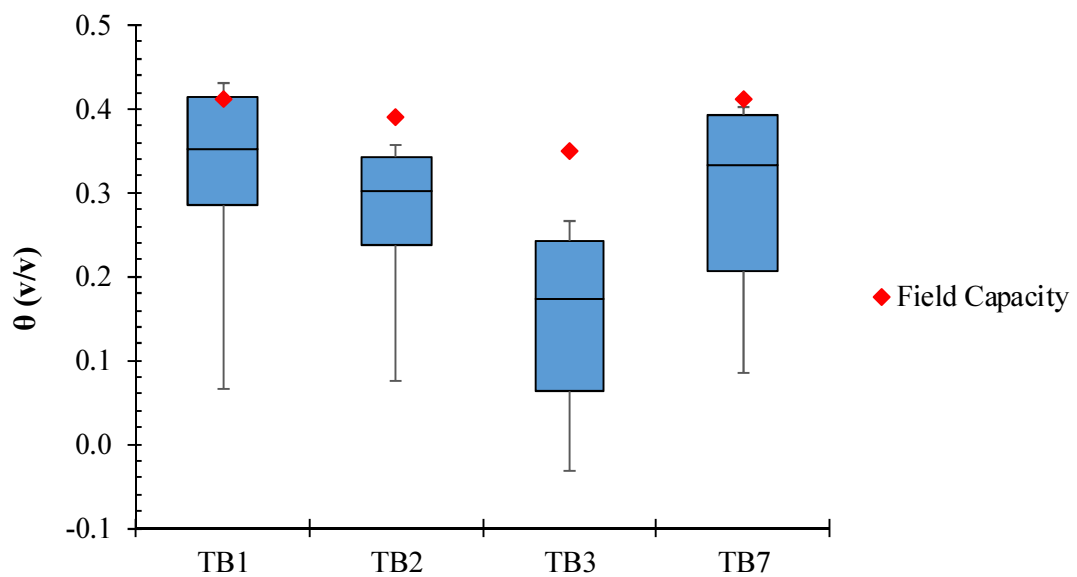


Figure 4.44: Depth-averaged  $\theta$  at first discharge

For all beds, runoff was observed prior to  $\theta_{FC}$ . Maximum values of  $\theta_t$  at the time of first runoff were similar to  $\theta_{FC}$  for all 4 tested configurations: 0.43 and 0.40 for HLS (TB1 and TB7 respectively), 0.38 for SCS and 0.30 for LECA. However, median values were below  $\theta_{FC}$  in all instances. In some cases, runoff was observed when  $\theta_t$  was less than a quarter of  $\theta_{FC}$ . The greatest difference between  $\theta_t$  at first runoff and  $\theta_{FC}$  was observed with LECA substrate. Several potential explanations can be provided to explain the earlier-than-anticipated runoff:

1. Lower practical  $\theta_{FC}$  relative to  $\theta_{FC}$  derived in the laboratory by following the FLL test methodology.
  - a. The FLL method involves saturation of the substrate via submersion. When submerged, storage capacity that is internal to the aggregate's particles may be utilised. However, during the normal wetting and drying cycles that occur in field conditions, this element of storage would not always be available.
  - b. Preferential flow paths could develop in field conditions (that would not be measured in laboratory tests on substrates) as a result of plant root activity and die-back.
2. In very dry substrates, time can be required for wetting processes to overcome hydrophobicity and enable the OM to start to re-absorb moisture. Water repellency originates from the accumulation of long-chained organic compounds (typically derived from living or decomposing plants and microorganisms) on or between soil particles and is associated with changes in soil moisture (Doerr *et al.*, 2000). These compounds can have a reduced affinity to water; leading to uneven wetting and preferential flow (Doerr *et al.*, 2000).
3. High rainfall intensities contribute faster fluxes into and through the soil matrix.
4. Vertical gradients in  $\theta$  that lead to localised exceedance of  $\theta_{FC}$ , causing downward flux prior to depth-averaged  $\theta_{FC}$  being reached.

Here, the influences of rainfall intensity and moisture distribution within the substrate will be analysed in greater detail.

#### 4.5.3.2 *Rainfall intensity*

Conceptually, more intense rainfall events would be expected to result in higher runoff rates. However, it has been demonstrated here that green roofs can attenuate peak rainfall rates, through a combination of retention and detention processes. First, the influence of rainfall intensity upon peak runoff (and delays) are analysed. Subsequently, runoff responses to EV258 are analysed to identify any practical differences arising during an event. EV258 included one of the highest peak rainfall intensities in the AE9 dataset (of 1.73 mm/5min) and generated the greatest predictive errors (see Section 4.5.1.4).

In Figure 4.45, the peak rates of runoff from each TB are categorised according to rainfall intensity. The highest rates of peak runoff were observed during events with the most intense peak rainfall. However, due to the attenuation effect, the difference in the peak rates of runoff was significantly lower than the differences in rainfall intensity. If gravitational runoff was occurring due to forcing during intense rainfall, relatively short peak delays would be expected at high rainfall intensities.

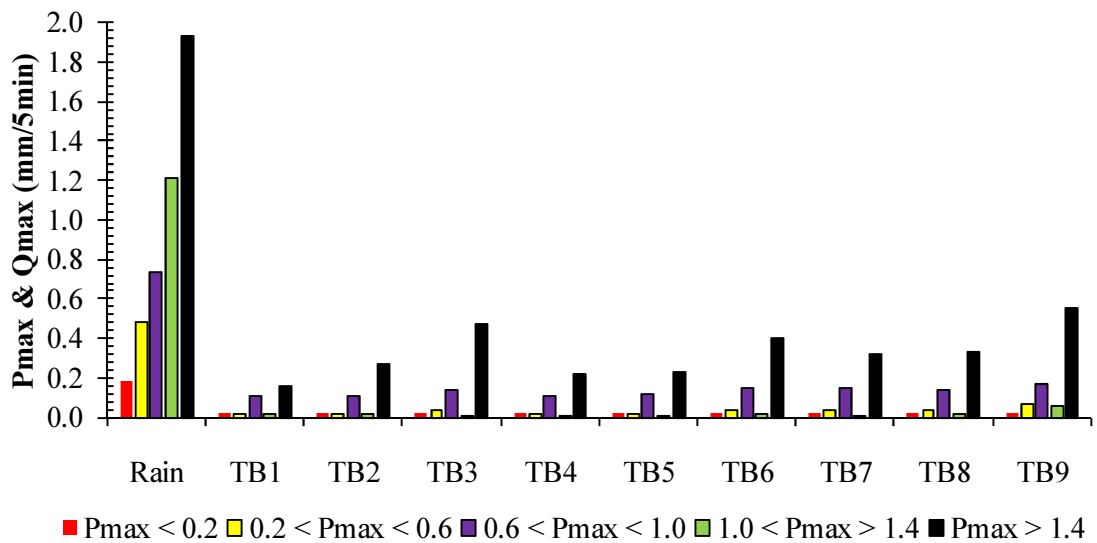


Figure 4.45: Peak rates of runoff as a function of rainfall intensity

Figure 4.46 plots peak delays for different categories of rainfall intensity.

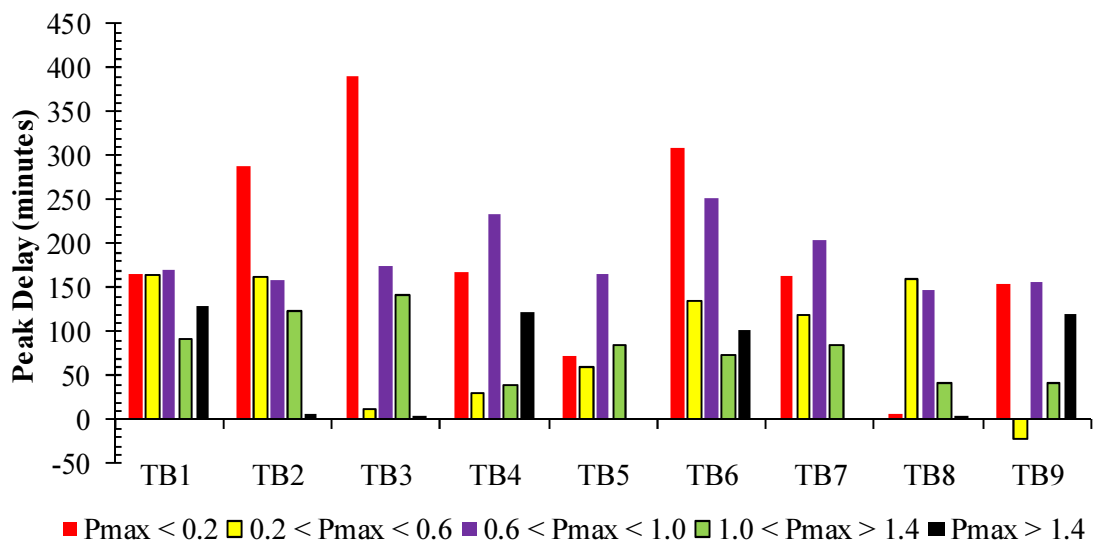


Figure 4.46: Peak delays as a function of rainfall intensity

Typically, the longest delays were associated with the lowest rainfall intensities and there was a general trend of declining delays with increasing rainfall intensity. However, this trend was not universally observed across all nine TBs. In a number of cases, peak delays approached zero once  $P_{MAX} > 1.4$  mm/5min. All things being equal, higher rainfall intensities would be expected to result in higher peak rates of runoff and shorter peak delays. However, there is no evidence here to suggest that the relationship between rainfall intensity and runoff is sufficient to induce runoff prior to field capacity. To further understand the influences leading to earlier-than-anticipated runoff, the event that resulted in the greatest predictive error - EV258 – will now be considered. Figure 4.47 highlights the range of runoff levels from each TB during EV258.

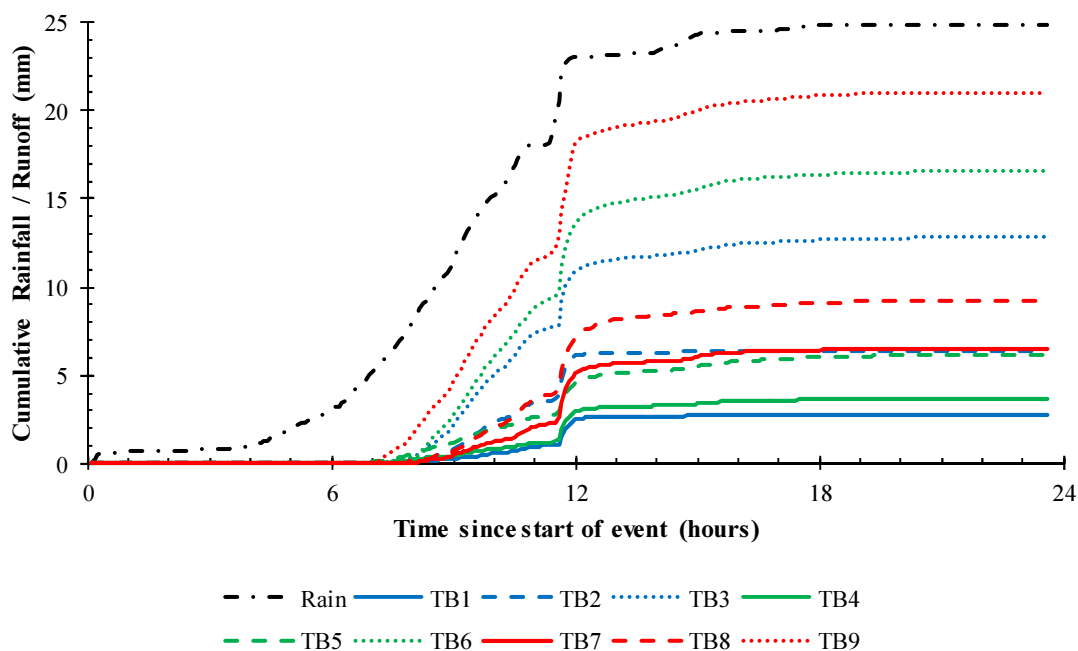


Figure 4.47: Rainfall and runoff during EV258

Runoff varied widely in response to the rainfall of 24.8 mm; ranging between 2.8 mm (TB1) and 21.0 mm (TB9). Runoff generally reflected the two periods of rainfall (i.e. the first period being the 11 hours after the initial rainfall; the second being between 11 and 12 hours). Over the initial 11 hours of EV258, 17 mm of rain fell. First runoff from all TBs occurred after 7 to 9 hours of first rainfall. However, as Figure 4.48 demonstrates, runoff was first measured from all nine TBs prior to the two most intense periods of rainfall (i.e. 0.5 mm/5min after nearly 10 hours and 1.7 mm/5min after approaching 12 hours).

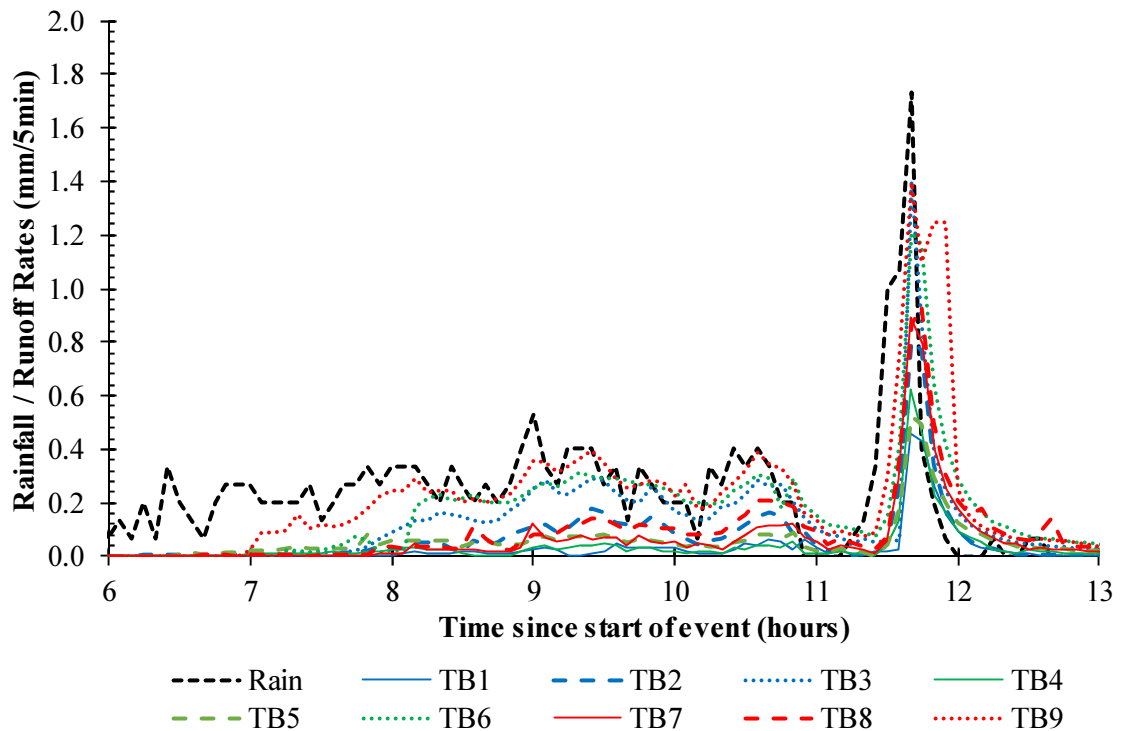


Figure 4.48: Rainfall and runoff intensities during EV258

Reflecting the broader trend observed across the AE9 dataset, the highest rates of runoff were measured when the rainfall intensity was highest. However, the initialisation of runoff prior to field capacity cannot be attributed to rainfall intensity; having already commenced prior to the peak rates of rainfall. Despite this initial runoff from all TBs, the level of attenuation observed during the period of peak rainfall was, in some instances, higher than 70%. This additional retention (and some limited detention) further supports the view that initial runoff occurred prior to field capacity.

The CS616 moisture balance data is presented for the 4 TBs during EV258 in Figure 4.49.

In all cases, runoff was measured from all 4 TBs prior to  $\theta_{FC}$ . Whilst the change in moisture content ( $\delta\theta$ ) was relatively uniform throughout the soil matrix of TB1, with the other TBs, a greater proportion of the rainfall permeated towards the lower zone. With TB3 in particular, there were signs that rainfall largely bypassed the upper zone. Whereas with TB2,  $\theta$  increased fastest in the lower zone initially, before subsequently increasing in the middle and upper zones. The lower zone of the non-vegetated TB7 was the driest zone prior to rainfall, but the wettest afterwards.

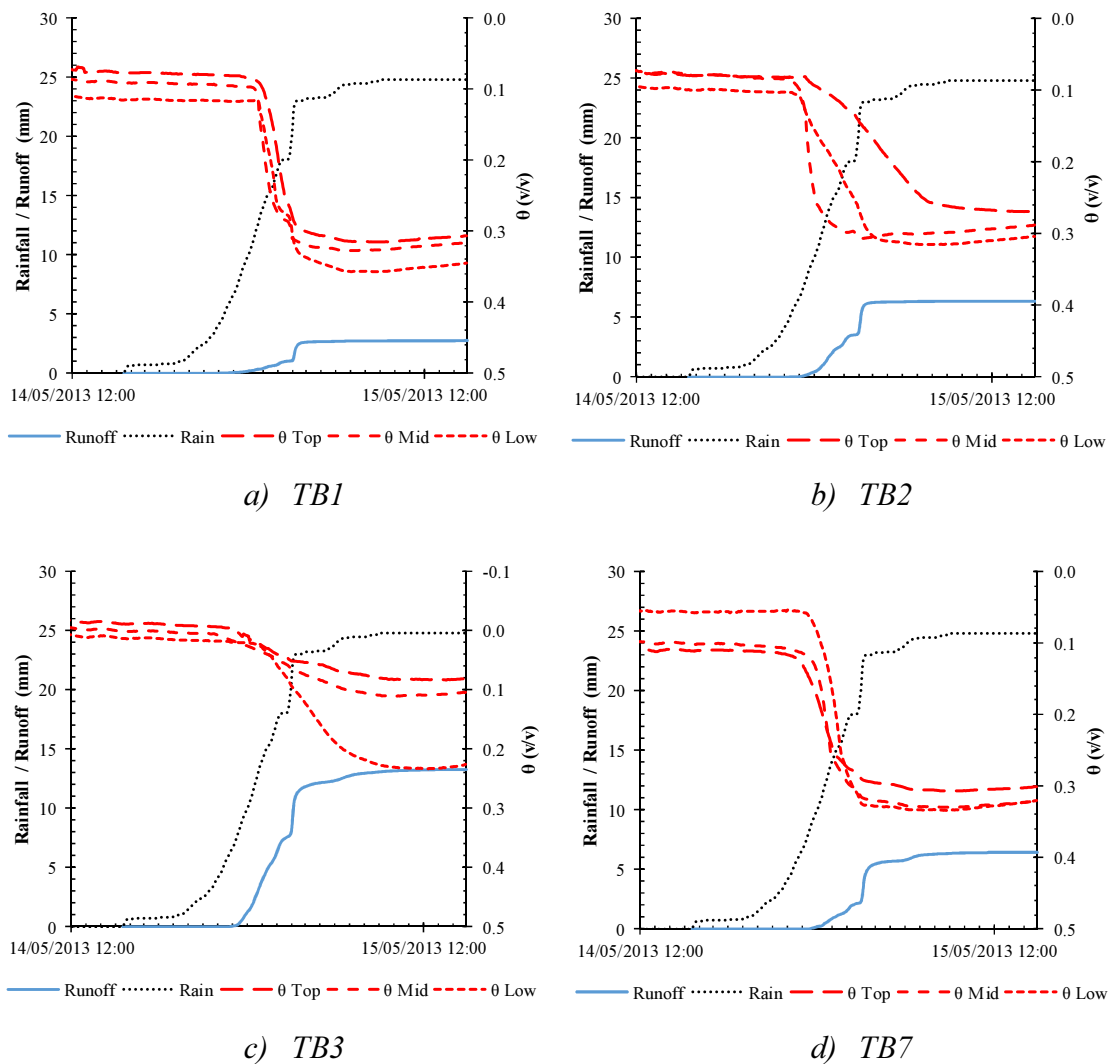


Figure 4.49: Rainfall, runoff and moisture content during EV258

In all instances, following rainfall, the upper zones were driest and the lower zones wettest. Vertical moisture gradients were therefore present in the substrate at first runoff. However, in no case did  $\theta$  reach  $\theta_{FC}$  in any of the zones. Additional influences therefore contributed to the earlier-than-expected runoff. It is expected that the dry status of the substrate in all 4 TBs prior to rainfall contributed to this runoff pattern. Dry substrates can develop preferential paths. Equally, time can be required for the wetting processes to overcome hydrophobicity and enable the organic matter to re-absorb moisture.

### 4.5.3.3 Vertical moisture distribution during wetting

Vertical moisture gradients in the substrate were observed during the wetting cycle of EV258. This could explain some observations of earlier-than-anticipated runoff. Figure 4.50 demonstrates the vertical gradients in mean  $\theta_t$  when runoff was first measured.

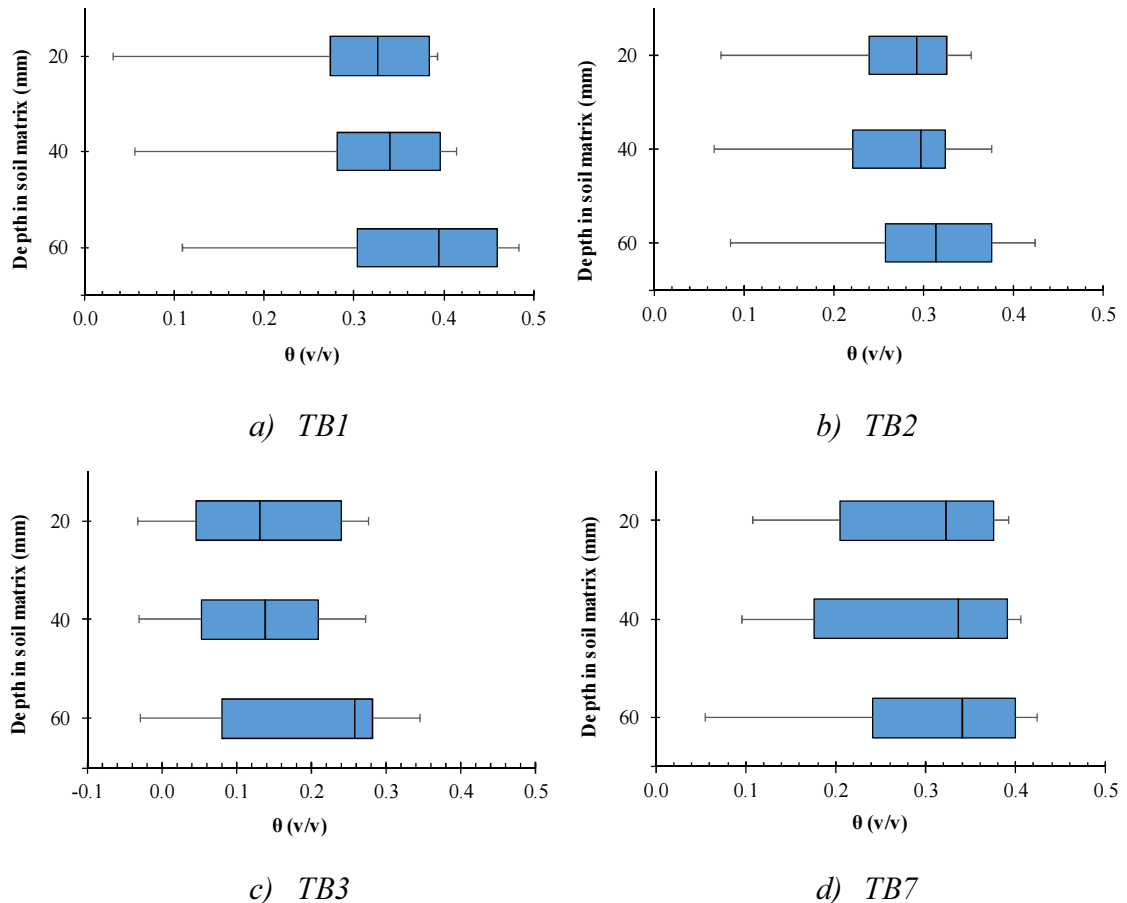


Figure 4.50: Moisture profiles at first discharge

The greatest vertical gradients were apparent in vegetated configurations and in substrates with the highest OM (i.e. HLS and LECA). Of these, the gradient was greatest with the most porous substrate (i.e. LECA). In TB1, the lowest  $\theta$  was observed in the upper zone (median: 0.33) and the highest  $\theta$  in the lower zone (median: 0.40). Runoff occurred when  $\theta$  in the upper zone was as low as 0.03. At no time did  $\theta$  in the upper zone reach  $\theta_{FC}$  (maximum: 0.39). However, in the low zone,  $\theta$  exceeded  $\theta_{FC}$ . In TB2,  $\theta$  was more evenly distributed in the upper and middle zones of the soil (median: 0.29) and only marginally greater in the lower zone (median: 0.31). However, stronger gradients were apparent with maximum values ( $\theta_{MAX}$ ).  $\theta_{MAX}$  was 0.35 in the upper zone and 0.42 in the lower zone.

Negative values were recorded with CS616 measurements in LECA. This suggests that some readings of  $\theta$  in LECA may include errors. Runoff from TB3 was observed from LECA at very low median values of  $\theta$  (0.17). Even the depth-averaged  $\theta$  (0.30) was less than  $\theta_{FC}$ . Moisture storage in the upper zone was low and almost half of that in the lower zone. In the lower zone,  $\theta$  did reach a maximum value (0.35) that was similar to  $\theta_{FC}$ . However, this threshold was not commonly reached. Maximum values in the higher zones also approached  $\theta_{FC}$  (0.28 [upper] and 0.27 [middle]). It is expected that this moisture distribution pattern is due, at least in part, to a vertical leaching/sorting of particles over time (following cyclical wetting/drying processes); such that there was an accumulation of fine particles in the lower zone (creating small pores) whilst the upper and middle zones would have been dominated by a relatively homogeneous distribution of large, round LECA particles, through which water can permeate quickly.

Whilst moisture distribution was non-uniform throughout TB7 during some events, median  $\theta$  was broadly similar throughout the soil matrix. The absence of vegetation was believed to underpin this trend. Shallow-rooted vegetation, such as Sedum, would not be expected to transpire moisture from the lower zones of an 80 mm deep substrate; instead limiting transpiration to the root zone. A variable distribution would therefore be expected to exist in vegetated configurations, with drier areas in the root zones and wetter underlying zones.

In practice (i) runoff can occur shortly before depth-averaged  $\theta_{FC}$  is reached, and (ii)  $\theta$  will often differ according to depth in the substrate, typically being less than  $\theta_{FC}$  in upper zones but with the potential to exceed  $\theta_{FC}$  in other zones (e.g. the lower zone).

#### *4.5.3.4 Summary of physical controls upon initiation of runoff*

Moisture balance is an important control upon runoff and retention. Overall, considering rainfall depth and SMD enabled accurate predictions of runoff depth. More intense rainfall typically produced higher peak rates of runoff and shorter peak delays. In some instances, runoff did occur prior to field capacity. The vertical distribution of moisture within the soil matrix contributed to this. However, it also appears that preferential wetting occurred when rain fell onto very dry substrates.



#### 4.5.4 Physical controls upon the regeneration of the SMD via ET

The presence of vertical moisture gradients in green roof substrates was demonstrated in Section 4.5.3.3. The highest moisture contents were typically measured in the lower substrate zones. Accordingly, the extent to which the SMD can be regenerated in the lower (as well as upper and middle) substrate zones via ET during the drying cycle will be an important influence on the hydrological response. Generally, ET is considered to occur in the upper soil zones of landscapes. However, extensive green roofs are shallow systems comprised of highly porous growing media. It may therefore be possible to treat an 80 mm deep substrate as a monolithic moisture store, from which moisture loss can occur on a relatively even basis from all depths of the substrate.

Here, moisture losses were analysed for four selected inter-event dry periods (one in each season). Due to the relatively short nature of many ADWPs, particularly in winter, a 24 hour period in the middle of an ADWP were assessed. By selecting a mid-point in the ADWP, the risk that losses will include the effects of detention, thus distorting ET losses, can be mitigated. Equally, this approach avoids the potentially low losses that can occur towards the end of longer ADWPs. Analysis of the responses of TB1 and TB7 allows comparison of the responses of vegetated and non-vegetated configurations. This analysis involves some very small changes in moisture content. It is acknowledged that some hourly change values fall below the accuracy thresholds of the probes and caution is therefore urged as to the use of these absolute values in other contexts. However, here, the comparative readings of the probes are of interest – establishing whether similar changes in moisture content are recorded from all three probes in the column.

In the ADWP prior to EV172, under spring conditions, there was no evidence that ET was greater in the upper and middle zones than in the lower zone (see Figure 4.51). During the hours following sunrise, higher  $\delta\theta$  would have been expected in the upper and middle (i.e. root) zones of TB1 due to plant transpiration. Yet,  $\delta\theta$  was greatest (i.e. most negative) in the lower zone. It is hypothesised that the resistance to  $\delta\theta$  would be lower in the lower zone, due to the higher  $\theta$  and lower matric pressures. This hypothesis is further substantiated as  $\theta$  was lowest in the low zone of TB7 and losses were marginally lower from here.  $\delta\theta$  (i.e. loss during the day and gain after sunset) was greatest from TB7 in the upper and middle zones.

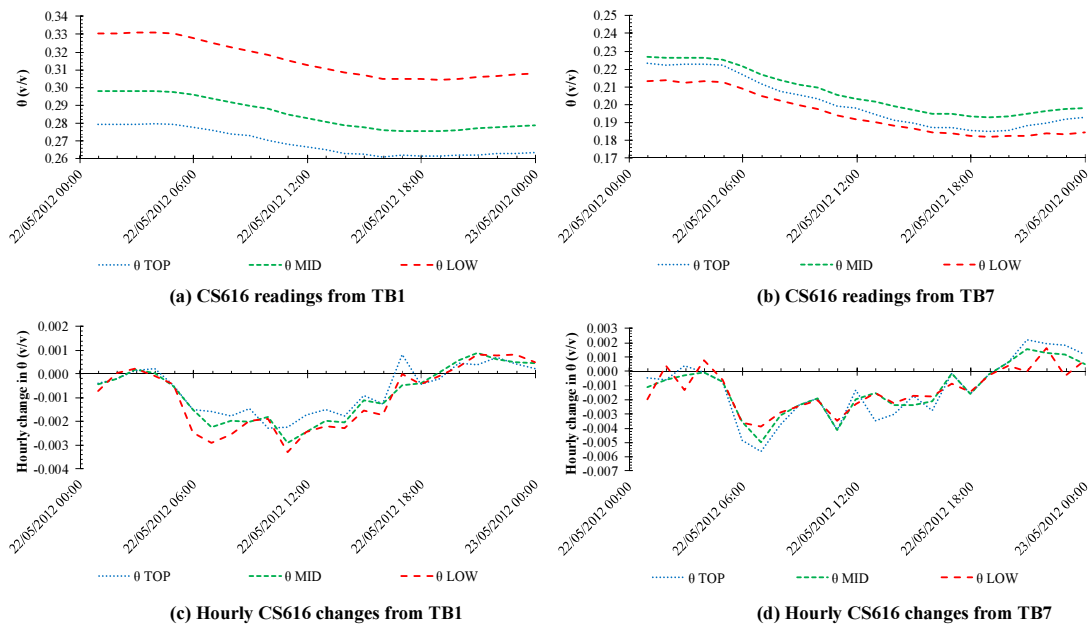


Figure 4.51: Moisture balance during a spring day – 22/05/2012 (EV172)

Considering the drying cycle during summer conditions (25<sup>th</sup> June 2013) prior to EV269,  $\delta\theta$  was consistently observed throughout the soil matrix of TB7. However, with TB1, losses were mostly observed from the upper and middle zones (see Figure 4.52).

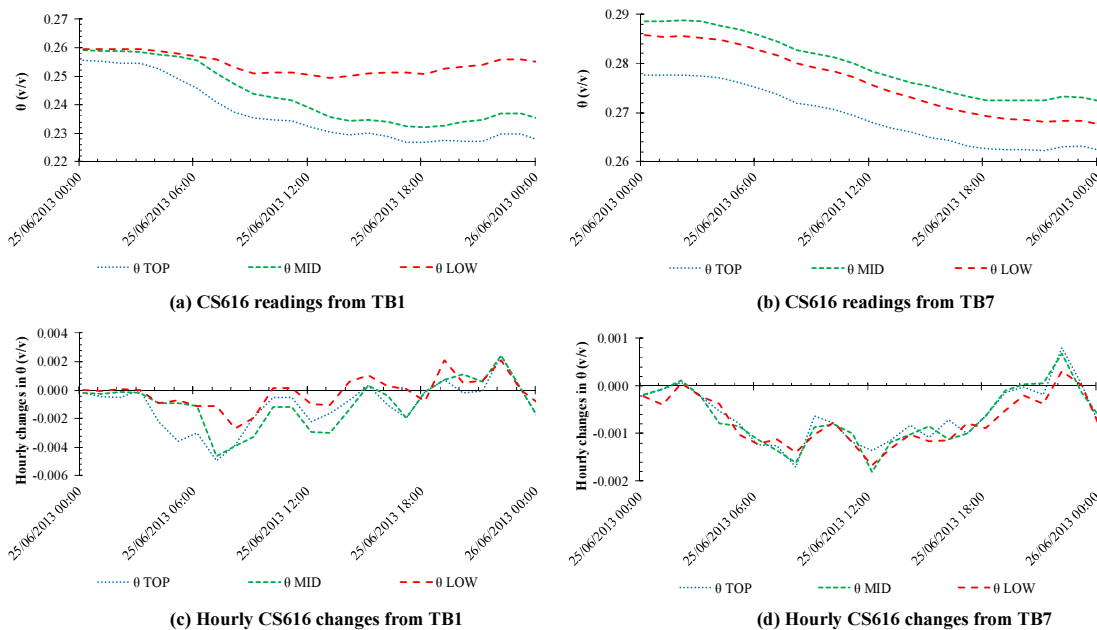


Figure 4.52: Moisture balance during a summer day – 25/06/2013 (EV269)

Evaporative losses were uniformly distributed throughout the soil matrix of TB7. The greater solar radiation during summer would typically lead to high potential evaporation; initially drying the surface layer and then causing moisture to rise from deeper within the

substrate via capillary action. The uniform losses from the bare substrate would indicate that the entire 80 mm depth acted as a monolithic unit. However, with the introduction of vegetation, in TB1, ET losses were differentially distributed; occurring mostly from the upper and middle zones (with small gains in the lower zone). This is consistent with plant transpiration taking place in the root (upper and middle) zone only.

Any moisture gains during dry periods would result from internal processes (i.e. transfer of moisture within the substrate) or from external factors (i.e. dew). Dew would typically manifest itself by increasing  $\theta$  in the upper zone first, before increasing moisture content in all zones. Gains consistent with dew were measured towards the end of the day. Whilst there appeared to be some downward movement of moisture towards the lower zone earlier in the afternoon, the later gains were relatively uniformly distributed within the substrate column.

Considering an autumn day (3<sup>rd</sup> September 2012) during the ADWP prior to EV207, similar trends were observed to those witnessed in spring conditions (see Figure 4.53).

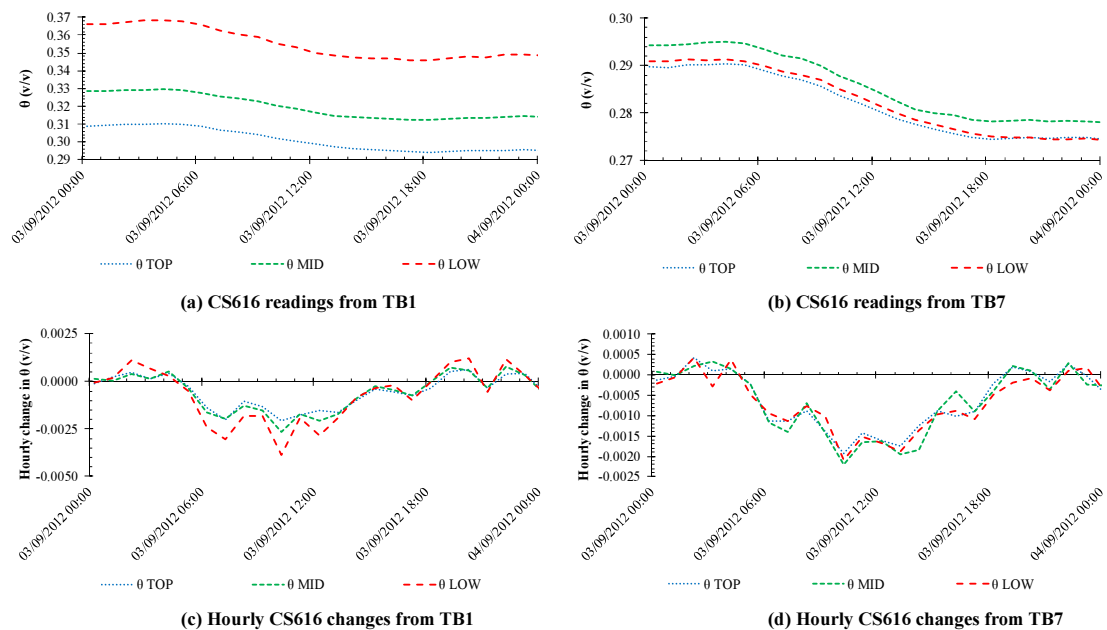


Figure 4.53: Moisture balance during an autumn day – 03/09/2012 (EV207)

In both cases, moisture was uniformly lost from within the soil column. With TB1,  $\theta$  was highest outside of the root zone, i.e. in the lower zone. Losses were still marginally greater from the lower zone of TB1. However, the vertical moisture gradients were even smaller with TB7. Here,  $\theta$  and  $\delta\theta$  were generally consistent throughout the depth of the substrate.

In the winter conditions (3<sup>rd</sup> December 2013) ahead of EV297,  $\theta$  was predictably high (approaching  $\theta_{FC}$  in the lower zone) and  $\delta\theta$  was minimal (see Figure 4.54).

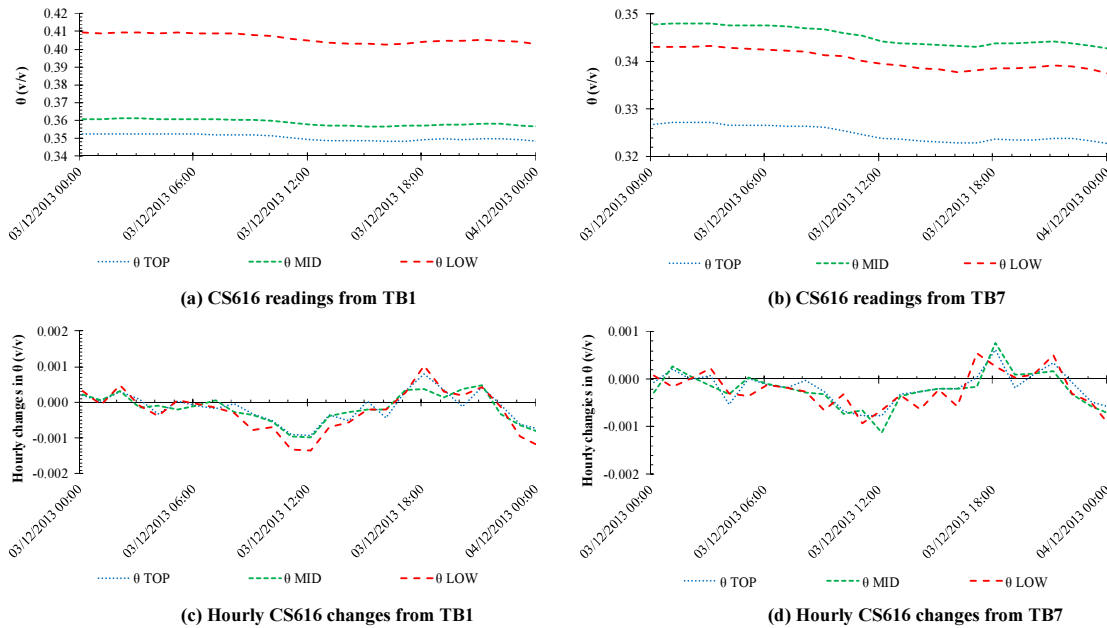


Figure 4.54: Moisture balance during a winter day – 03/12/2013 (EV297)

With both TB1 and TB7, losses recorded from all zones were minimal. Marginally higher  $\delta\theta$  occurred in the lower zone of TB1, where  $\theta$  was 0.05 higher than the middle zone. The differential in  $\theta$  between the zones of TB7 was less than half of that with TB1. As a result, and without any vegetation,  $\delta\theta$  was relatively uniform throughout the soil matrix.

#### 4.5.4.1 Summary of physical controls upon the regeneration of the SMD via ET

Moisture was removed from all depths in the 80 mm deep substrate and was generally extracted from the low zone at no lesser rate than from the overlying zones. Some differences were observed in  $\theta$  and  $\delta\theta$  as a function of depth. In the vegetated TB1 configuration, there was a tendency for  $\theta$  to be greater below the root zone. However, unexpectedly,  $\delta\theta$  was also marginally higher here in all seasons except for summer. This would be consistent with the relationship between  $\theta$  and  $\psi$ , as moisture would typically move towards drier parts of the soil where plant transpiration has reduced  $\theta$  such that  $\psi$  is more negative. The drying action in the root zone therefore caused capillary action to extract moisture from below the root zone. With the non-vegetated TB7, evaporative losses were uniformly distributed within the soil column. As a result, it would be reasonable to treat the 80 mm substrate as a monolithic unit during the drying cycle.

## 4.6 Conclusions

Large variations in the hydrological performance of green roofs have been identified here. Per-event retention and peak attenuation ranged between 7-100% and 9-100% respectively. Peak delays were as long as 47 hours.

The inverse relationship between retention and rainfall depth was evident in this study. The lowest per-event retention performance was typically associated with low probability rainfall events. For the AE9 dataset, configuration median per-event retention ranged between 98 and 100%. However, where rainfall depth exceeded 10 mm, per-event retention was between 14 and 70%.

The differential between rainfall depth and the available moisture capacity provided a highly credible indication of runoff volume. In some instances, runoff was observed prior to field capacity. This earlier-than-anticipated runoff was consistent with the observed vertical moisture gradients. However, the hydrophobicity of very dry substrates and the creation of preferential flow paths may also have contributed to a lower practical field capacity. Higher rainfall intensities can cause saturated flow conditions to develop near to the surface, creating localised gravitational forces that can temporarily exceed matric pressures in unsaturated conditions. However, there was little evidence of this here.

Systematic (but not statistically-significant) differences were observed in retention performance due to configuration. Retention performance was greatest with vegetated configurations. Interception losses of up to 8 mm were estimated from Sedum vegetation. However, faster regeneration of available capacity was typically observed from non-vegetated configurations. Minor differences were observed in the responses of Sedum and Meadow Flower, as a result of the different coverage and rooting types. Open-textured and highly permeable substrates, such as LECA, performed less well than the well-graded, less permeable substrates with higher maximum moisture storage capacity (e.g. HLS).

Seasonal climate influenced the retention responses as a result of seasonal differences in (i) the incidence of rainfall, and (ii) the inter-event regeneration of available moisture capacity. Low retention in winter (32-38%) was associated with the highest mean rainfall and the lowest pre-event moisture deficits. However, excepting winter, seasonal

differences in configuration median per-event retention percentages were minor due to low mean rainfall. Pre-event SMD and interception losses were both highest in summer. However, mean rainfall was lower than mean pre-event SMD. In summer, potential retention was therefore greater than actual retention. Differences in ET across all configurations were greatest when climatic conditions facilitated high ET losses (e.g. warm weather).

From a drying cycle perspective, the 80 mm deep substrate can be considered as a monolithic moisture store without introducing any significant predictive errors. Vertical moisture gradients were identified within the substrates. However, reductions in moisture content, consistent with capillary rise during ET, occurred in all zones of the 80 mm deep soil column.

Measurable detention effects, such as peak attenuation and peak delay are not necessarily independent from the effects of retention. Many of the influences affecting retention (i.e. rainfall, seasonal climates and configuration) therefore impacted these conventional detention metrics. Peak attenuation was inversely related to rainfall depth. When rainfall exceeded 10 mm, configuration median peak attenuation ranged between 28% and 64%. When  $P \geq 20$  mm, peak attenuation fell but still exceeded 50% for all SCS- and HLS-based configurations.

A detention parameter ( $k$ ) was used to describe each system's detention characteristics. The highest values of  $k$ , implying the most rapid runoff response, were associated with the most permeable configurations (i.e. non-vegetated and LECA beds) and the lowest were associated with HLS and Sedum vegetation. Differences in  $k$  due to vegetation treatment were statistically-significant. The lower  $k$  associated with Sedum vegetation reflected the treatment's dense year-round coverage and the effect that its shallow fibrous rooting system had upon porosity and permeability.

## 5 Regeneration of retention capacity via Evapotranspiration

### 5.1 Chapter overview

This chapter presents results and analyses of tests that were carried out to identify the inter-event regeneration of available moisture capacity in nine green roof configurations. Tests were conducted in climate-controlled laboratories, where conditions were programmed to replicate typical UK spring and summer climates. Configurations, initially at field capacity, were exposed to continuous dry weather periods of up to 28 days, during which time the weight of each microcosm was monitored to derive moisture loss (i.e. Evapotranspiration, ET). No irrigation water was applied during this time. Results are analysed to identify the influences of vegetation, substrate, climate and moisture availability on ET from green roofs. The need to model ET on a daily or hourly interval is also considered.

This work was the basis of one journal paper and one conference paper:

Poë, S., Stovin, V.R. and Berretta, C. (2015). Parameters influencing the regeneration of a green roof's retention capacity via evapotranspiration, *Journal of Hydrology*, 523, 356-367.

Poë, S. and Stovin, V. (2012). Advocating a physically-based hydrological model for green roofs: Evapotranspiration during the drying cycle, Proceedings of the World Green Roof Congress, 18-21 September 2012, Copenhagen, Denmark.

### 5.2 Motivation

As an integral component of the broader research objective of modelling the hydrological response of green roofs to storm events, the key objectives to be fulfilled here are:

- 1) To generate a robust empirical data set for ET losses via an experimental study, under laboratory-controlled conditions, aimed at identifying the drying cycle behaviour of nine different green roof configurations (with combinations of three characterised substrates and three typical planting options) when subjected to diurnal cycles representative of UK spring and summer conditions for up to 28 days without irrigation. The use of a climate chamber allowed responses to be monitored to longer ADWPs than would have been possible in field conditions.

- 2) To analyse the data set:
  - a) To identify the influence of a configuration's vegetation treatment and substrate type upon ET.
  - b) To establish the different patterns of ET losses occurring due to the differences in climatic conditions that occur both diurnally and seasonally.
  - c) To evaluate the importance of moisture balance as a parameter in the modelling of ET loss patterns.
- 3) To facilitate the development of a physically-based prediction of antecedent moisture conditions that accounts for the green roof configuration, ADWP and season when predicting ET losses during the drying cycle.

### 5.3 Materials and methods

An experimental set-up was established to continuously monitor mass balance changes (inferred as changes in moisture, i.e. ET) from microcosms of nine different green roof configurations, comprising combinations of three substrates (to a settled depth of 80 mm) and three vegetation treatments (see Figure 5.1). Each microcosm was saturated, drained to  $\theta_{FC}$  and placed onto a load cell in a climate-controlled chamber.

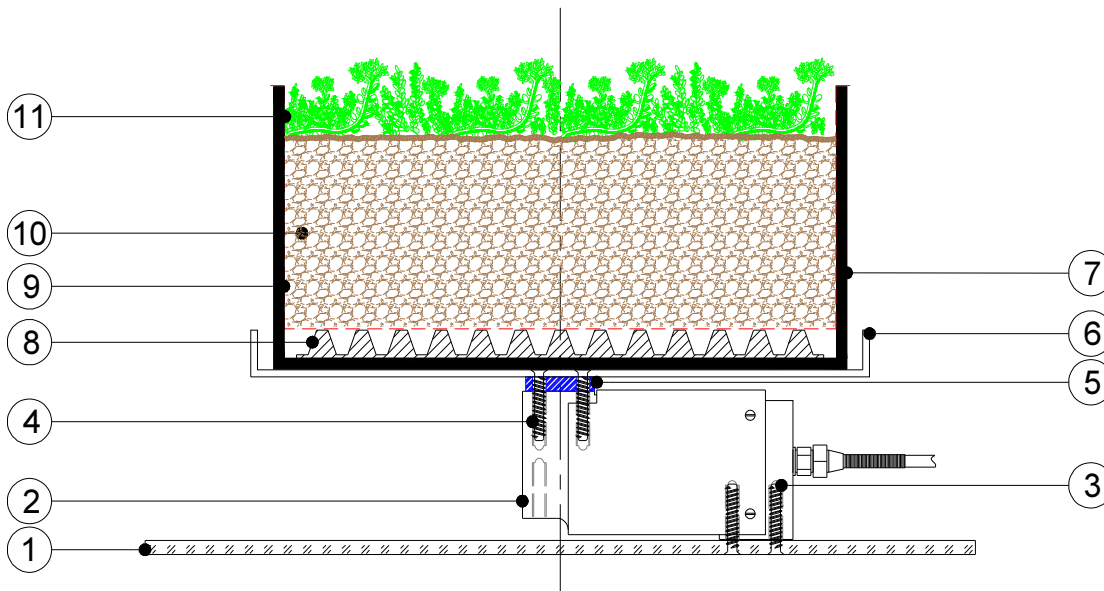


Figure 5.1: Configuration of Test Set-up



## Key:

1. Support plates; 12 mm thick Perspex;
2. Single point compression load cell (RLS010 by RDP Electronics) – 10 kg capacity;
3. M6 x 30 mm (approx.) countersunk fixings (2 number);
4. M6 x 30 mm (approx.) countersunk fixings (2 number);
5. Aluminium bar – 25 x 6 mm. 30 mm length pre-punched with 2 x 6 mm Ø holes;
6. Platform; 3 mm thick aluminium – 270 x 270 x 20 mm (external) with 2 x 6 mm Ø holes;
7. Tray from 4.5 mm thick polypropylene – 237 x 237 x 120 mm (internal dimensions) with 25 x 6 mm Ø holes pre-drilled in base;
8. ZinCo DBV12 drainage layer – 230 x 230 x 12 mm;
9. ZinCo SF filter sheet - 530 x 530 mm – trimmed to suit, in situ;
10. Growing medium – 80 mm settled depth of chosen substrate;
11. Vegetation treatment – Sedum carpet, Meadow Flower or non-vegetated.

A filter sheet prevented the loss of fine particles from the substrate. The DBV12 drainage layer (with zero storage capacity) facilitated drainage to field capacity. Microcosms of each configuration were established in polypropylene trays with internal dimensions of 237 x 237 x 120 mm (a size that was compatible with the capacity of the load cell and platform). Tray bases were perforated for drainage of gravitational water prior to the trials. 25 x 6 mm Ø holes (providing a nominal drainage capacity of 0.1 l/s) were set on a 60 mm grid, with a row of holes centred 5 mm from the tray's upstand (see Figure 5.2).



(a) Perforated tray      (b) DBV12 drainage layer      (c) Tray with filter sheet

*Figure 5.2: Composition of Microcosms*

Each microcosm was placed on to load cells within a Conviron BDW40 plant growth chamber at the University of Sheffield's Department of Animal & Plant Sciences. Starting at  $\theta_{FC}$ , no irrigation was applied throughout the trials. Typical diurnal cycles were replicated for UK spring and summer conditions. The former is of interest as, in spring, vegetation exits winter dormancy and starts to transpire soil-water, whereas summer

conditions will have greater ET and drought stress due to the longer dry periods with higher temperatures. From a storm water management perspective, summer conditions are of particular interest as long dry periods may be interspersed with intense storms.

Six trials were scheduled to take place between the 7<sup>th</sup> April and the 25<sup>th</sup> August 2011. First, the spring condition was replicated three times on a sequential basis (SP1, SP2 and SP3); followed by three replications under summer conditions (SU1, SU2 and SU3). The third test under each climatic condition trialled for 28 days; the other two ran for 14 days. From a storm water management perspective, the shorter trial periods were of most relevance – most hydrological models would input ADWPs of less than 14 days. However, extended 28 day trials were intended to identify performance trends during periods of prolonged drought. A mechanical failure within the chamber during the first spring trial led to its abortion and replacement by a fourth spring trial (SP4). The three replicate summer trials followed on from the spring trials (see Figure 5.3).

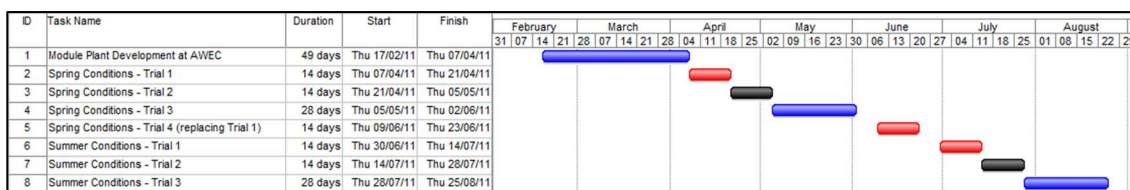


Figure 5.3: Schedule of trials

Each microcosm was established in triplicate, avoiding its employment in more than one trial per climatic condition and ensuring the health of the vegetation at the start of the trial. The decision to employ only three replicates for each test was informed by the following factors. The tests were intended to provide a preliminary assessment of the relative importance, and interactions between, several controlling variables, i.e. substrate, vegetation and climatic conditions. As only 10 load cells were available, replicate tests had to be run consecutively in the climate chamber, such that the full series of tests for each season required a minimum of 8 weeks. Although the climate chambers provided climatic control irrespective of the absolute date or season, the experimental timings also needed to be matched to the relevant external seasons to capture any effects due to the plants' seasonal growth cycle and to avoid any risk of shocking the plants by rapidly transferring them between contrasting climatic conditions.

### 5.3.1 Trial configurations

Microcosms were established to replicate each of the nine test bed (TB) configurations that were monitored and evaluated in Chapter 4. A tenth configuration, comprising a non-vegetated tray filled with a substrate that has been developed and extensively tested during an EU-funded Marie Curie IAPP collaboration at the University of Sheffield and ZinCo GmbH was also trialled. The findings of the tenth TB are not reported here.

#### 5.3.1.1 Establishment of the vegetation treatment

The vegetation layer was established under climate-controlled conditions, due to the fact that the test programme was scheduled to start in early spring, and in view of the weather conditions prevailing in the winter of 2011. On the 17<sup>th</sup> February 2011, the vegetated trays were placed in climate-controlled glasshouses – at the Arthur Willis Environmental Centre (AWEC) within The University of Sheffield’s Department of Animal & Plant Sciences (see Figure 5.4 and Figure 5.5) – so that sufficient vegetation coverage could be established prior to commencement of the trials.



Figure 5.4: AWEC Glasshouse Facility

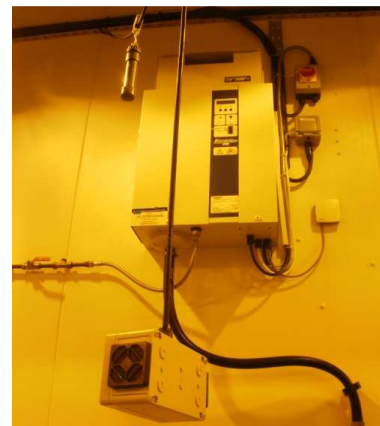


Figure 5.5: Climate Control Unit

During establishment, temperatures in the glasshouse were set to between 15 and 20 °C and each vegetated microcosm (as Figure 5.6) was regularly irrigated to establish the plant coverage (Figure 5.7).



*Figure 5.6: MF on HLS – early stage of growth*



*Figure 5.7: MF on HLS – after growth in glasshouse*

Meadow Flower did not establish well on the LECA substrate. No microcosms were therefore suitable for testing during the first completed spring trial. As such, only two data records were obtained for TB6 under spring conditions.

### **5.3.2 Data collection methods**

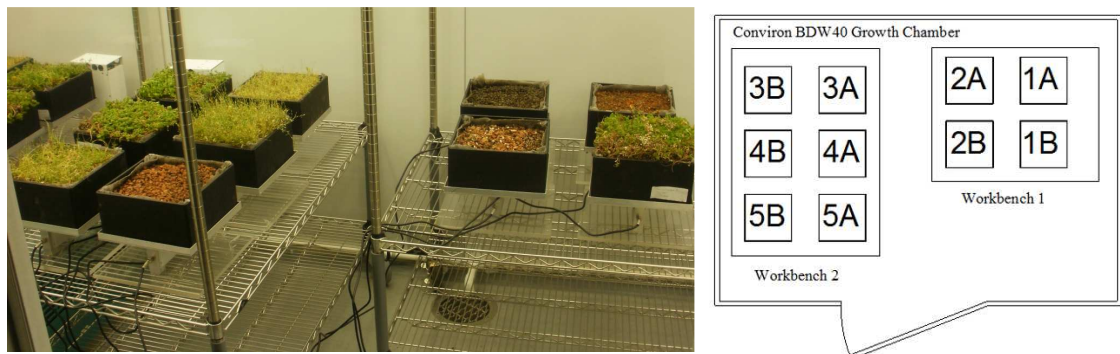
The nine microcosms were submersed in water for 2 hours and drained to  $\theta_{FC}$  by positioning the microcosms on 100 mm high, hollow circular sections to permit the free drainage of gravitational water through the perforated base – over a further period of 2 hours in accordance with the FLL guidelines (FLL, 2008).

Trays configured with LECA substrate were prone to flotation (due to the extreme lightweight composition of the substrate). The application of weight on top of the tray prevented flotation of the tray, but not the LECA substrate within the tray. Water was therefore maintained at a level just below the top of the tray and regularly re-distributed onto the top of the LECA trays; ensuring that trays were fully saturated, without loss of aggregate.

#### *5.3.2.1 Sample Arrangements*

Single point compression load cells were positioned 700 mm above the ground, on stainless steel height-adjustable work benches within the Conviron BDW40 chamber (3.7 m<sup>2</sup> area) – see Figure 5.8. This layout only deviated for the second test in spring

conditions (SP2). SP2 was conducted in an alternative chamber due to a temperature regulation failure during the aborted first spring trial.



a) Image of chamber

b) Plan of layout

Figure 5.8: Test configurations in the climate-controlled chamber

Each tray was positioned on a randomly-selected load cell within the chamber, as detailed in Table 5.1. Each load cell was connected to the Modular 600 Data logger (positioned outside of the chamber).

Table 5.1: Allocation of Trays to Load Cells

Test Condition	TB1	TB2	TB3	TB4	TB5	TB6	TB7	TB8	TB9
SP2	2A	4B	2B	4A	3B	-	1B	5B	1A
SP3	2A	2B	3A	4B	5A	1A	1B	3B	5B
SP4	1B	3A	4B	5B	3B	1A	5A	4A	2B
SU1	3A	3B	2A	5A	1B	1A	4A	4B	5B
SU2	4B	1B	3B	4A	3A	5B	2B	5A	2A
SU3	3B	1A	5A	5B	2B	4A	2A	4B	1B

### 5.3.2.2 Data Collection Equipment

The RLS010 aluminium single-point compression load cell (see Figure 5.9) is a strain gauge transducer that has a safe working capacity of 10 kg.

Prior to the experiments, each load cell was calibrated by tuning to a low of zero and a full scale value, at 10 kg, of 9.775 volts. The signal was then recorded for each cell at 2 kg intervals up to 10 kg, enabling the signal to be converted to mass (in kg) using simple linear regression equations with high accuracy ( $R^2=1$ ) for each load cell.



Figure 5.9: Load cell, platform & tray      Figure 5.10: Modular 600 Data logger

Figure 5.11 provides an example to demonstrate the strong correlation of the regression equation with the calibration tests both before and after the first test in spring.

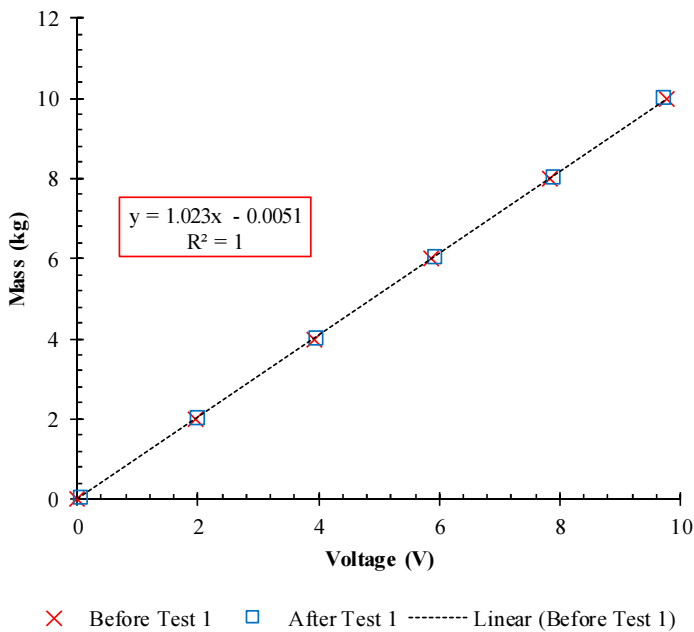


Figure 5.11: Calibration of load cell

The load cell manufacturer’s published maximum linearity error resolution (RDP Electronics Ltd, 2007) is 0.02% of the full scale value. This is equivalent to 0.032 mm of moisture loss – approximately 1% of the typical daily ET rate observed in summer by Kasmin *et al.* (2010). Linearity was checked experimentally and errors ranged between 0.05-0.21% and 0.07-0.18% in the spring and summer trials respectively. However, the

mean linearity error of every load cell was 0.00%. It is therefore expected that the higher-than-anticipated errors were attributable to manual or rounding-up errors from the visual display on the data logger during the calibration exercise. Changes in mass from each microcosm were inferred to be moisture loss/gain in mm/m<sup>2</sup>. The chamber's climatic data was captured via a separate, central logging system.

The Modular 600 Multi-Channel Signal Conditioning System (see Figure 5.10) amplified and logged the output (in mV) via the 611 Strain gauge transducer amplifier and the 650ME1 Serial interface and data logger module respectively. The 650ME1 serial interface and data logging module of the Modular 600 system was programmed using the M650 Configuration Software for Windows, supplied by RDP Electronics. Hourly iterations were programmed (337 for 14 day trials; 673 for 28 day trials). At each pass, mass readings were taken and logged to the data-logger's memory (Ref: 650ME1), from where they could be transferred into Microsoft Excel via RDP Freeware data-logging software (RDP Electronics Ltd, 2006b). As the 650ME1 has the capacity to store 65,530 readings, it was possible to collect measured data in a single set at the end of each trial. The maximum number of readings collected during any trial was 7,403.

### **5.3.3 Controlled condition settings**

ET is typically measured at hourly or daily intervals. Target climatic settings were derived from hourly temperature and relative humidity (RH) data, as recorded by a Met Office weather station in Sheffield (NGR: 4339E 3873N; Altitude of 131 m). The use of hourly data allowed diurnal cycles to be reproduced. Data from 2009 was used; this being the first year in which hourly weather station data was published (Met Office, 2009, downloaded from <http://www.metoffice.gov.uk/public/weather/climate/gcqwtdw7>).

#### *5.3.3.1 Temperature and relative humidity settings*

Spring target values were derived from data for March 2009 (mean: 7.1 °C; range: 5.0-9.8 °C), which is broadly in line with long-term average daily temperatures (1971-2000: 3.1-9.3 °C [March], 4.4-11.8 °C [April] and 7.0-15.7 °C [May]). Summer target values were derived from data for August 2009 (mean: 16.7 °C; range: 13.8-19.8 °C); generally in line with long-term average daily temperatures (1971-2000: 10.0-18.3 °C [June], 12.4-20.8 °C [July] and 12.1-20.6 °C [August]).

In spring trials, the measured diurnal temperature range was 5.1 to 9.8 °C, with a mean daily temperature of 7.1 °C and mean RH of 81.4% (ranging from 75.5% to 87.2%). For summer trials, the measured diurnal temperature range was 13.8 to 19.8 °C. Mean daily temperature was 16.7 °C and mean RH was 76.0% (ranging between 70.4 and 83.6%). Measured values replicated target values very closely in respect of temperature. However, the absence of de-humidifying technology in the chamber created a greater differential between target and actual RH. Target and measured climatic values are presented in Figure 5.12.

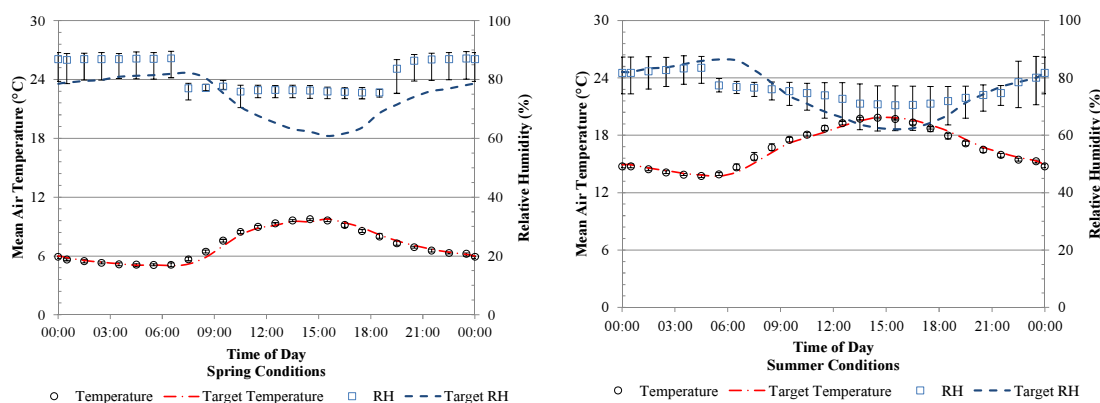


Figure 5.12: Climatic Conditions in Chamber for (a) spring and (b) summer trials

In spring, mean measured RH of 81.4% (range: 75.5-87.2%) was higher than the target mean (73.4%). Similarly, the measured range was slightly greater than the target (60.8-82.2%). These differences are not believed to be significant, when one considers that RH is more highly sensitive to small changes in absolute humidity at low temperatures. In cold air, the dew point temperature is typically closer to the actual temperature, making RH more susceptible to fluctuations than in warmer conditions. Indeed, with measured RH exceeding target RH, it is expected that measured ET was on the conservative side. In summer, the mean measured RH (76.0%) compared well to the targeted mean RH (74.8%). However, there was a greater disparity in the targeted range (62.1-86.4%) and the measured range (70.4-83.6%).

### 5.3.3.2 Solar Radiation / Daylight Hours

The daylight source was provided by metal halide and halogen incandescent lamps (16 Venture MS400W/C/HOR and 16 Philips Halogen A Pro 2yr 100W E27 230V BTT46 CL 1CT/10). A lamp loft in the Conviron BDW40 chamber mitigated heat produced by



the lighting system. Any effects of heating were accounted for by the chamber's temperature controls. The lamps provided lighting with an intensity of  $1000 \mu\text{mol}/\text{m}^2/\text{s}$  (at a distance of 1 m) and were specified with a correlated colour temperature of between 3700 K and 4200 K. Spectral aluminium lined internal walls facilitated uniformity of light within the chamber.

Daylight hours were derived from sunrise and sunset data recorded in Sheffield, via the US Naval Observatory website (accessed 2010). For spring trials, lights were switched on for 12 hours each day (between 07:00 and 19:00) replicating the average time elapsing between sunrise and sunset in March 2009. For summer trials, lighting was switched on for 17 hours per day; between 05:00 and 22:00. Target daylight hours values were based upon data from June 2009 (rather than August 2009, which was used to determine the temperature profile). August 2009 daylight hours were lower (14 hours and 36 minutes) than in June 2009 (16 hours and 50 minutes) or July 2009 (16 hours and 17 minutes). However, long-term mean sunshine (rather than daylight) hours data for these months between 1971 and 2000 (Met Office, 2009) is typically greater in August (183.2 hours) than in June (176.4 hours). With lighting effectively representing the sole means of replicating sunlight, lighting was programmed to reflect the longer (i.e. June) daylight period and was switched on for 17 hours per day; replicating the 16 hours and 50 minutes daylight time as closely as possible.

These settings reflect the historical trends of climatic data, but could also be considered to have regard for the fact that climate change is anticipated to result in warmer, drier summers.

#### 5.3.3.3 *Wind Conditions*

The capacity of the climate chamber to generate wind was limited to a vertical airflow of up to 24 l/s. Airflow was uniformly dispensed into the chamber via plenums and out via exhausts. Based upon a floor area of  $1.6 \text{ m}^2$ , this air exchange equates to  $15 \text{ l}/\text{s}/\text{m}^2$  and therefore a wind speed of 0.015 m/s. Whilst this is sufficient to maintain uniform plant canopy temperatures and disturb the boundary layer of water on the plants' leaf surface, these settings are lower than typical mean wind speeds (e.g. at an elevation of 10 metres in Sheffield [Grid reference: SK 34867 87326], estimated average wind speed is 3.7 m/s (Renew-Reuse-Recycle website, accessed 2010). As windier conditions would be

expected to induce higher ET, measurements are expected to be on the conservative side. Spatial patterns of air flow within the chamber were not monitored, although it is acknowledged that they are unlikely to have been particularly uniform. The random distribution of microcosms for each test was intended to mitigate against any bias that this may have introduced.

### **5.3.4 Data analysis and interpretation**

#### *5.3.4.1 ET values*

The term ET is employed here to encompass moisture loss from both vegetated and non-vegetated configurations. Transpiration only occurs from vegetated treatments. ET from non-vegetated configurations therefore results solely from evaporation. Several ET values are analysed and discussed here:

- 1) Configuration-mean ET: established for each of the nine configurations by taking the mean of the values derived from the 3 trial replications under each climatic regime. Given the heterogeneous nature of green roof substrates and vegetation, some variation in the individual loss rates was expected. Considering the cumulative loss over the first 14 days of the trial, the mean standard deviation over the 18 different test configurations was 7.3%, ranging from 0.5 to 19.2%. The smallest variations occurred on the non-vegetated configurations and the largest variations were generally associated with the spring tests. Figure 5.13 shows the individual loss profiles for the three replicate tests for spring and summer associated with the Sedum on HLS configuration (TB1), which had a 14-day variation of 6.9% (10.5% in spring and 3.3% in summer), and was therefore typical of the full test set. When ADWP>14 days, ET was derived from the single 28-day long replication;
- 2) Vegetation- and substrate-mean ET: a mean of the nine values covering the three configurations with the relevant vegetation treatment or substrate.
- 3) Seasonal-mean ET: mean ET from all nine configurations for each climatic condition.

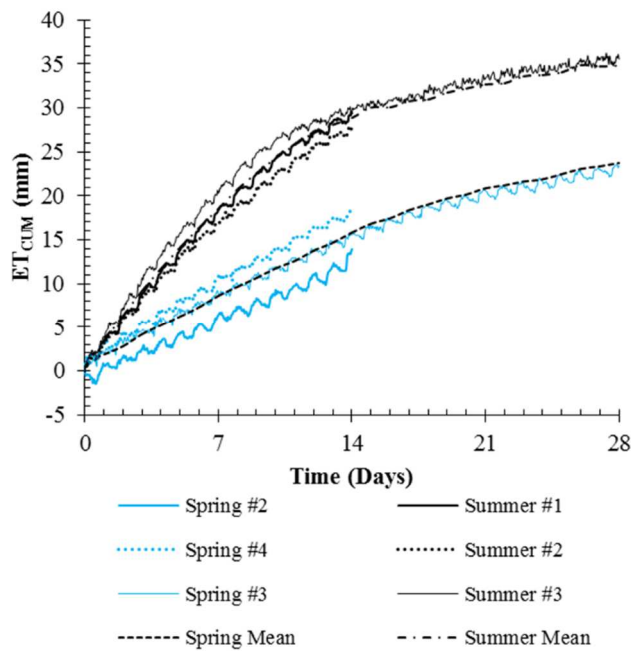


Figure 5.13:  $ET_{CUM}$  for *Sedum* on HLS (6 replications)

References will be made to daily ( $ET_D$ ) and cumulative ET ( $ET_{CUM}$ ).  $ET_D$  was calculated as the sum of hourly ET data over each 24 hour interval.  $ET_{CUM}$  was simply derived by summing  $ET_D$  measured up to the time interval in question. The statistical significance of configuration and climatic factors to  $ET_{CUM}$  was evaluated using Kruskal-Wallis and Mann-Whitney U tests at ADWPs of 3, 7, 14, 21 and 28 days. An analysis of variance (ANOVA) also identified the statistical significance of moisture available to ET rates.

#### 5.3.4.2 Moisture balance values

Residual stored moisture content,  $S_t$ , is an important influence upon ET.  $S_t$  is calculated as the maximum moisture storage capacity ( $S_{MAX}$ ) minus the soil moisture deficit at the time ( $SMD_t$ ).  $S_t$  will vary depending on ET occurring during the ADWP. There is no established protocol for determining the  $S_{MAX}$  of a vegetated configuration. It was not appropriate to start trials with an oven-dry substrate, due to the plants' requirements for water. The adopted method is predicated on an assumption that the maximum moisture storage capacity that can practicably be regenerated via ET under UK atmospheric conditions is equal to the known moisture loss (i.e.  $ET_{CUM}$ ) at Day 28 of summer trial conditions, when wilting was clearly observed. Residual moisture after this time was considered to be hygroscopic moisture ( $\theta_{<PWP}$ ).

$\theta_{<PWP}$  was measured through the post-test, destructive oven drying of the substrate only configurations. Mass readings taken before and after oven-drying indicated that residual (hygroscopic) moisture equated to  $\theta$  of 6.6% (HLS, equivalent to 5.24 mm/m<sup>2</sup>), 2.9% (SCS, or 2.23 mm/m<sup>2</sup>) and 2.1% (LECA, or 1.69 mm/m<sup>2</sup>). To validate this approach, values of  $\theta_{FC}$  for non-vegetated configurations were derived (through summation of maximum ET<sub>CUM</sub> [or  $S_{MAX}$ ] and  $\theta_{<PWP}$ ) and compared to related values obtained during substrate characterisation tests (see Table 5.2).

Table 5.2: Soil-water characteristics of the tested substrates

		HLS	SCS	LECA
$\theta_{<PWP}$	(% m <sup>3</sup> /m <sup>3</sup> )	6.6	2.9	2.1
Max. ET <sub>CUM</sub> / $S_{MAX}$	(% m <sup>3</sup> /m <sup>3</sup> )	33.7	31.5	24.2
$\theta_{FC}$	(% m <sup>3</sup> /m <sup>3</sup> )	40.3	34.3	26.3
MWHC	(% m <sup>3</sup> /m <sup>3</sup> )	41.2	39.1	35.0

The derived values of  $\theta_{FC}$  are all lower than the MWHC. Pressure plate tests established  $\theta$  for  $\psi_m$  values of 33 kPa and 1500 kPa – values that define  $\theta_{FC}$  and  $\theta_{PWP}$  (and therefore plant-available moisture) in soil science (Richards & Weaver, 1944). No meaningful results could be ascertained for LECA. For HLS and SCS, at  $\psi_m = 33$  kPa,  $\theta$  is lower than both maximum water-holding capacity (MWHC) and the derived values of  $\theta_{FC}$ . At  $\psi_m = 1500$  kPa,  $\theta$  is higher than  $\theta_{<PWP}$ . According to these test results,  $\theta$  available to plants would be 14.0 and 13.5% for HLS and SCS respectively. These values are much lower than observed in the ET trials. This conventional scientific definition of  $\theta_{FC}$  may not therefore be wholly applicable to green roof substrates. Green roofs are multi-layered structures that differ from natural soils with homogeneous textures. The highly porous and heterogeneous composition of green roof substrates is such that moisture is apparently retained at  $\psi_m$  lower than 33 kPa; being readily available between 10 and 100 kPa (Fassman & Simcock, 2011). MWHC is determined at atmospheric pressure (following FLL protocol). The differences between MWHC and  $\theta$  at  $\psi_m = 1500$  kPa of 31.2% (HLS) and 30.2% (SCS) are comparable to the respective derived  $S_{MAX}$  values. From a storm water management perspective,  $S_{MAX}$  is a more relevant moisture storage

term than the absolute values of  $\theta_{FC}$  and  $\theta_{PWP}$ ; representing the proportion of the retention capacity that can be regenerated between storm events.

Vegetation contributed additional moisture storage capacity (interception losses,  $IL$ ).  $IL$  were determined from the differences between the maximum observed  $ET_{CUM}$  from the vegetated and equivalent non-vegetated microcosms (see Table 5.3).

*Table 5.3: Moisture Balance changes with ET from planted configurations*

<b>Vegetation treatment</b>	<b>Substrate</b>	<b>S<sub>MAX</sub> (substrate only) [mm/m<sup>2</sup>]</b>	<b>S<sub>MAX</sub> (vegetated) [mm/m<sup>2</sup>]</b>	<b>Interception Losses [mm/m<sup>2</sup>]</b>
<b>Sedum</b>	<b>HLS</b>	26.97	34.75	7.78
<b>Meadow Flower</b>			34.71	7.74
<b>Sedum</b>	<b>SCS</b>	25.19	32.43	7.24
<b>Meadow Flower</b>			28.68	3.50
<b>Sedum</b>	<b>LECA</b>	19.33	28.79	9.46
<b>Meadow Flower</b>			27.05	7.72

## 5.4 Results

### 5.4.1 Configuration-mean ET

Configuration-mean ET trends are presented here and analysed (in Section 5.5) to identify the underlying physical trends. A Kruskal-Wallis test identified that seasonal differences in configuration-mean  $ET_{CUM}$  are significant (p-value: 0.05) at all ADWPs; 3 days (p-value: 0.0003), 7 days (p-value: 0.001), 14 days (p-value: 0.004), 21 days (p-value: 0.009) and 28 days (p-value: 0.024). It is therefore pertinent to consider the responses of configurations to each climatic regime separately. Figure 5.14 shows the configuration-mean  $ET_{CUM}$  for the spring and summer test series.

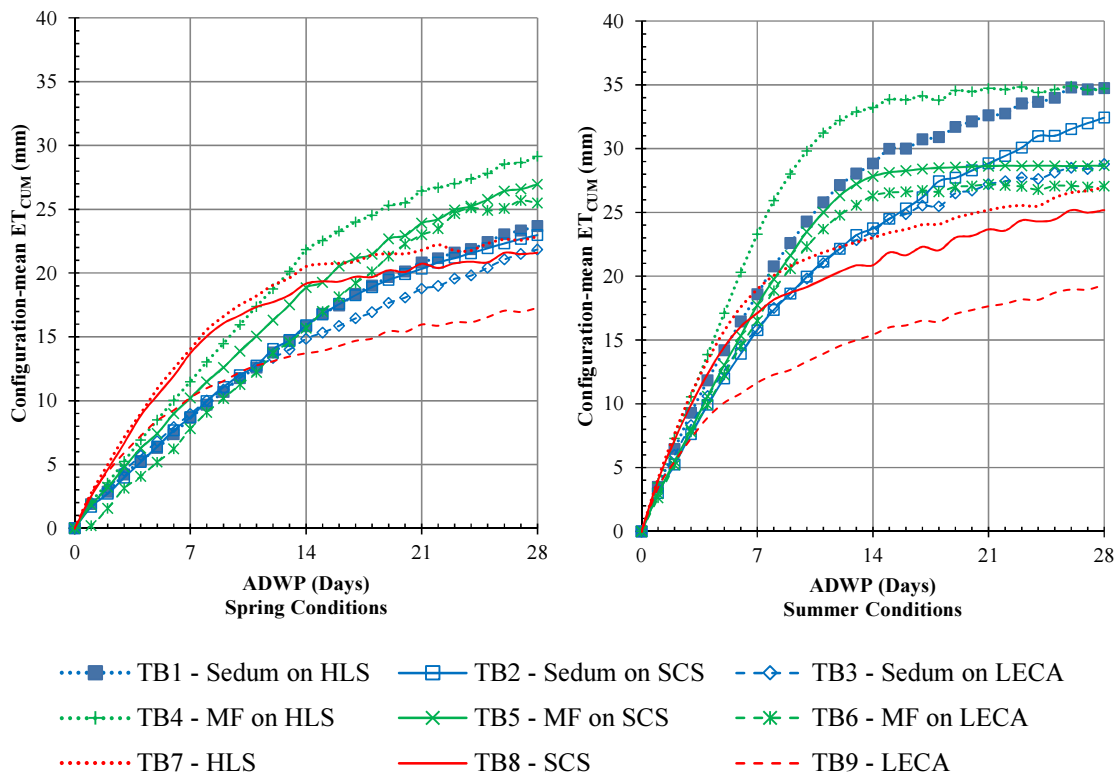


Figure 5.14: Configuration-mean  $ET_{CUM}$  for spring (left) and summer (right)

Overall, cumulative ET was greater in summer (19-35 mm) than in spring (17-29 mm). In both climatic regimes, the maximum  $ET_{CUM}$  was associated with TB4 (Meadow Flower on HLS) and the minimum was associated with TB9 (non-vegetated LECA). After 14 days in summer twice as much moisture had been removed from TB4 than TB9 (33 mm as opposed to 16 mm). In general, the 28-day  $ET_{CUM}$  was highest for configurations vegetated with Meadow Flower and lowest for non-vegetated microcosms, although initial ET rates for non-vegetated microcosms were amongst the highest observed. Although the variations with respect to vegetation treatment appeared to be more pronounced than the effects of substrate type, systematic differences due to substrate were also evident. LECA-based configurations generally exhibited the lowest ET rates and HLS-based configurations the highest. Variations due to substrate type were least evident with Sedum vegetation and most apparent with non-vegetated microcosms.

Figure 5.15 shows configuration-mean  $ET_D$  over the preceding 7 days for ADWPs of 7, 14, 21 and 28 days.

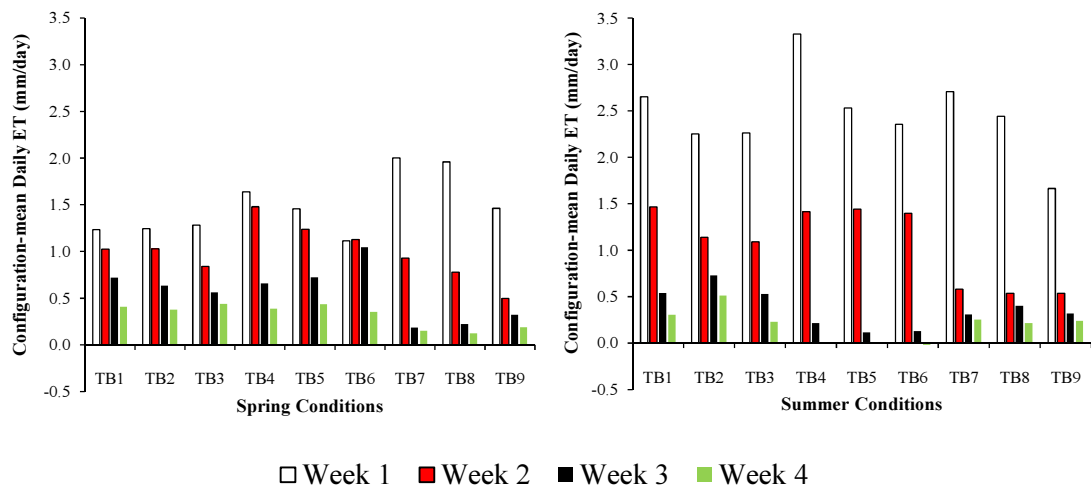


Figure 5.15: Configuration-mean  $ET_D$  for spring (left) and summer (right)

Every three groups of columns correspond to a vegetation treatment. These plots reinforce the previous observations i.e. relatively high ET was observed from non-vegetated configurations (TB7, TB8 and TB9) over week 1 but ET from vegetated systems was greater in the later stages of the trials. Within each group the consistent behaviour between the three substrate types was readily apparent; losses were consistently greatest from HLS (TBs 1, 4 and 7) and least from LECA (TBs 3, 6 and 9). It is also clear that for several of the configurations, losses in weeks 3 and 4 were zero or close to zero in summer conditions. Indeed, a net moisture gain was observed in TB6 in week 4.

In all cases there was an observable decrease in ET rate with time. This phenomenon has been widely reported elsewhere (Voyde *et al.*, 2010b; Stovin *et al.*, 2013, Berghage *et al.*, 2007). This effect was particularly pronounced in non-vegetated configurations, and also evident in the Meadow Flower configurations in summer. Initial ET rates were of the order of 1.5 mm/day in spring and 2.5 mm/day in summer. In contrast, ET rates during week 4 were below 0.5 mm/day.

Statistical analysis of the 3, 7, 14, 21 and 28 day cumulative ET values showed that differences as a result of vegetation treatment were generally only significant (p-value: 0.05) when contrasting ET from vegetated and non-vegetated configurations. No statistical differences existed between Sedum and Meadow Flower.

In view of the significant influence that moisture constraints had upon ET rates when ADWP exceeded 14 days, it is pertinent to assess mean  $ET_{CUM}$  (and standard deviation, *St. Dev*) for each configuration and season after a 14-day ADWP (see Table 5.4).

Table 5.4: Mean  $ET_{CUM}$  by vegetation and substrate after a 14 day ADWP

	Spring $ET_{CUM}$ (mm)					Summer $ET_{CUM}$ (mm)				
	Substrate			Mean	<i>St. Dev</i>	Substrate			Mean	<i>St. Dev</i>
	HLS	SCS	LECA			HLS	SCS	LECA		
<b>Vegetation:</b>										
<i>Sedum</i>	15.8	15.9	14.8		<b>0.6</b>	28.8	23.7	23.5	<b>25.4</b>	<b>3.0</b>
<i>Meadow Flower</i>	21.8	18.9	15.7	<b>18.8</b>	<b>3.1</b>	33.2	27.8	26.3	<b>29.1</b>	<b>3.6</b>
<i>Non-vegetated</i>	20.5	19.2	13.7	<b>17.8</b>	<b>3.6</b>	23.0	20.9	15.4	<b>19.8</b>	<b>3.9</b>
<b>Mean</b>	<b>19.4</b>	<b>18.0</b>	<b>14.7</b>	<b>17.4</b>	-	<b>28.4</b>	<b>24.1</b>	<b>21.7</b>	<b>24.7</b>	-
<b><i>St.Dev</i></b>	<b>3.2</b>	<b>1.8</b>	<b>1.0</b>	-	<b>2.8</b>	<b>5.1</b>	<b>3.5</b>	<b>5.7</b>	-	<b>5.1</b>

Seasonal-mean  $ET_{CUM}$  was greater in summer (24.7 mm) than in spring (17.4 mm) after a 14 day ADWP. This is consistent with the phenomenon that warmer conditions induce greater  $\psi$  (and higher ET). The higher standard deviation (*St. Dev*) in summer (5.1 mm) compared to spring (2.8 mm) was expected due to (a) the lower absolute seasonal-mean  $ET_{CUM}$  in spring and (b) the greater influence that the range of  $S_{MAX}$  had on  $ET_{CUM}$  following high antecedent ET in summer. Comparing spring and summer ET over the first 14 days, the seasonal difference in substrate-mean  $ET_{CUM}$  was greatest with HLS (9 mm), compared with SCS (6.1 mm) and LECA (7 mm). Seasonal differences were far greater in vegetated configurations (around 10 mm) compared with non-vegetated configurations (2 mm). The small *St. Dev* of 0.6 mm for *Sedum* in spring indicates a lesser reliance of *Sedum*'s transpiration on a substrate's SWCC; particularly in cooler conditions. However, in summer, as  $ET_{CUM}$  from *Sedum*-vegetated configurations exceeded ET from non-vegetated configurations, *St. Dev* also increased to 3.0 mm. Here, the differences in configuration specific  $S_{MAX}$  led to greater contrasts in  $ET_{CUM}$  between LECA and HLS. The variance in substrate-mean  $ET_{CUM}$  was greatest from HLS, where low  $ET_{CUM}$  from *Sedum* contrasted with high ET from *Meadow Flower* and non-vegetated configurations. Variance was further increased in summer, as low  $ET_{CUM}$  from non-vegetated configurations contrasted with very high  $ET_{CUM}$  from *Meadow Flower*.

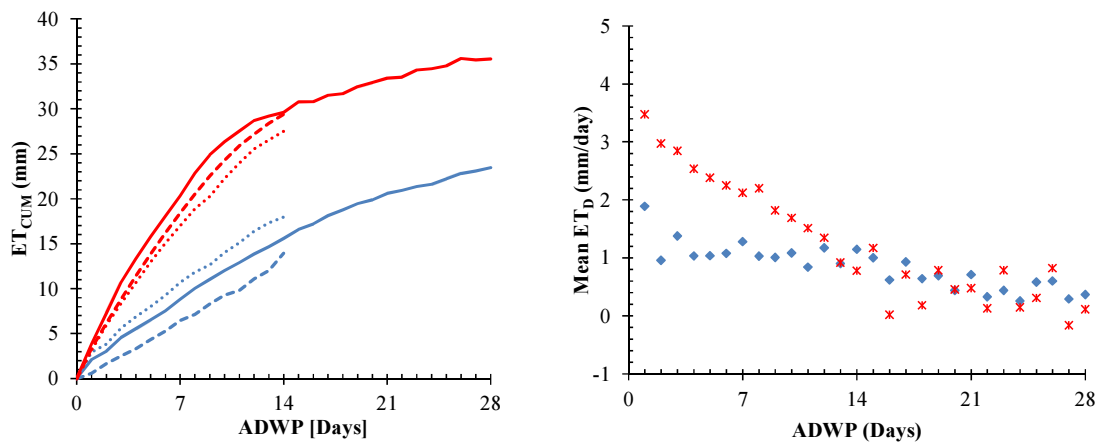


### 5.4.2 Specific ET responses of individual configurations

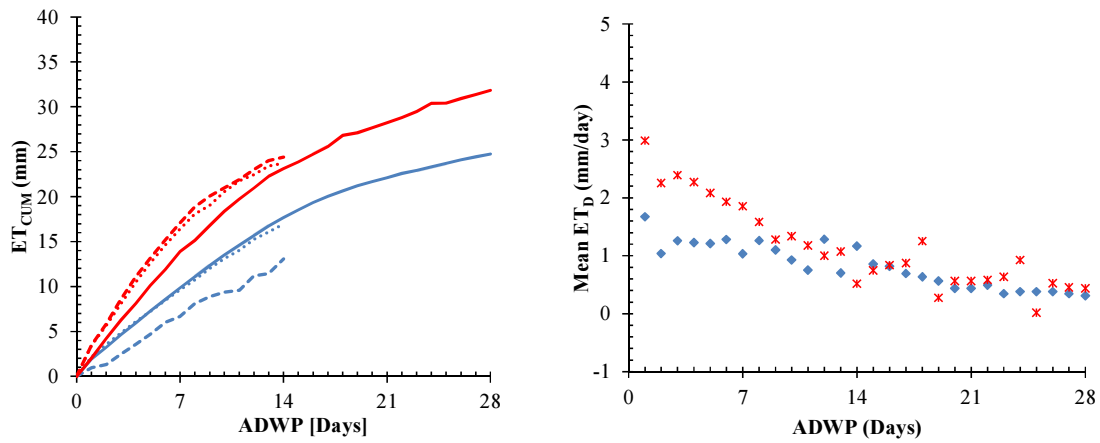
Configuration-mean ET was presented in Section 5.4.1. However, three replications were conducted for each configuration across each of the two seasons. Here, the extent to which ET varied from the mean across each 14 day trial will be analysed to identify any underlying trends of variance between responses from the same configurations. As vegetation is expected to be the main source of variance, plots are grouped by vegetation treatment. Cumulative and mean daily ET are plotted for Sedum (see Figure 5.16), Meadow Flower (see Figure 5.17) and non-vegetated beds (see Figure 5.18).

The greatest variability in responses across the three replications of each trial was observed in spring. The mean coefficient of variance (CV, i.e. standard deviation as a percentage of the mean  $ET_{CUM}$  after a 14 day ADWP) across the nine configurations in spring was 10.4%, compared to 4.2% in summer. In spring, CV was the same for the two vegetation treatments (11.9%) but lowest with non-vegetated beds (7.5%). These trends were expected to be observed. Firstly, variance in spring was expressed as a proportion of a lower mean  $ET_{CUM}$  (17.4 mm) than in summer (24.8 mm). Secondly, the sequential phasing of tests and the natural development of vegetation during spring will have contributed to the observed differences in ET. In summer, the CV was similar across all three vegetation treatments (i.e. between 4.0-4.3%). In both seasons, the CV was highest with LECA (11.5% [spring] and 6.2% [summer]) and lowest with SCS (8.9% [spring] and 1.9% [summer]).

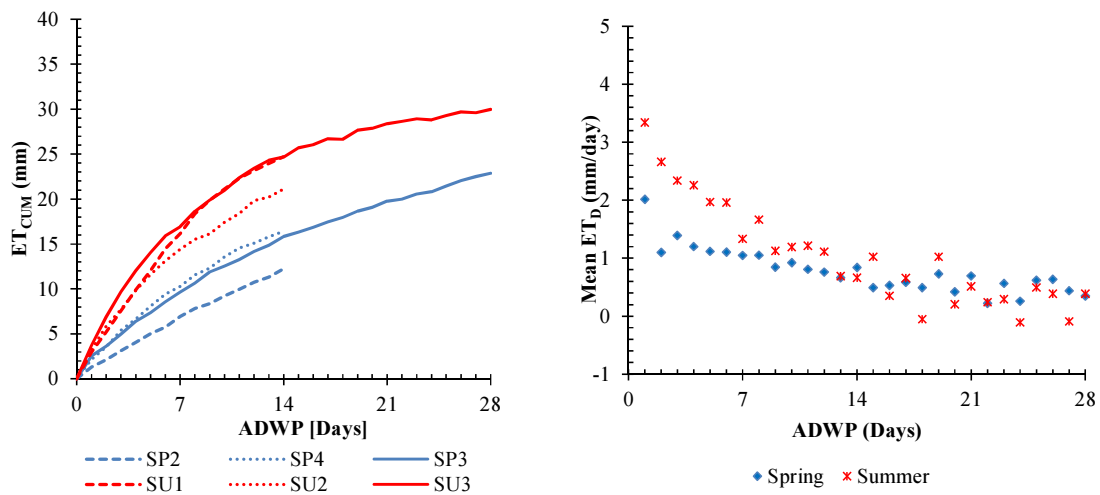
Generally, differences in cumulative ET between replications reduced over time, with relatively low variation after 14 days. It is expected that this is due to the importance of moisture balance as a control on ET (i.e. all other things being equal, ET will be lower in the microcosm with a higher SMD due to greater antecedent ET).



a) TB1 – Sedum on HLS

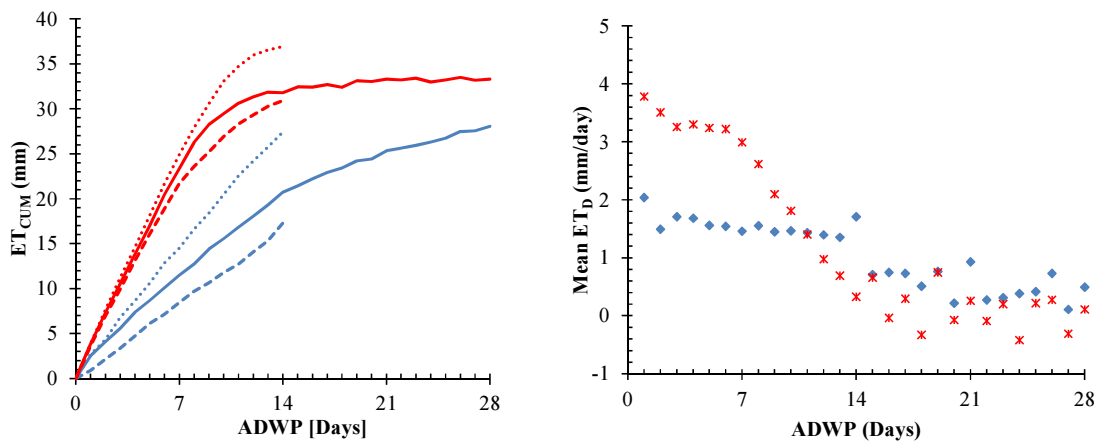


b) TB2 – Sedum on SCS

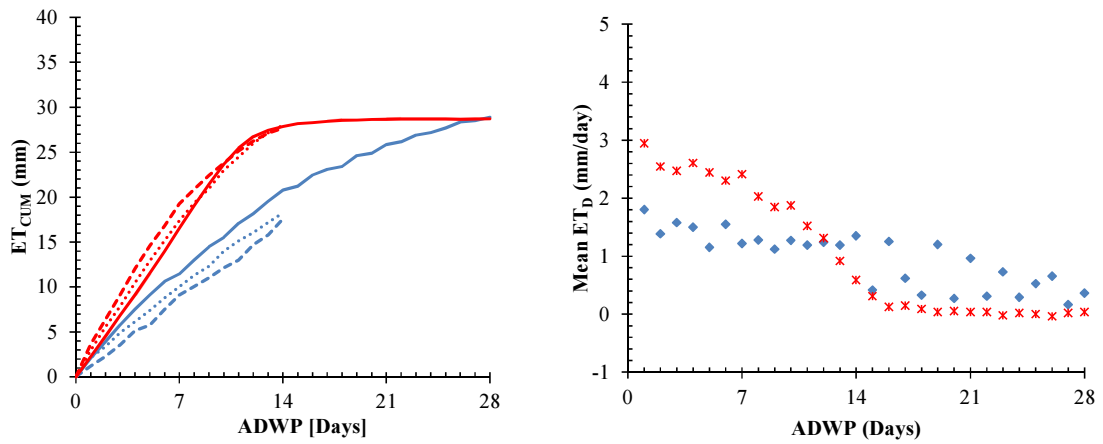


c) TB3 – Sedum on LECA

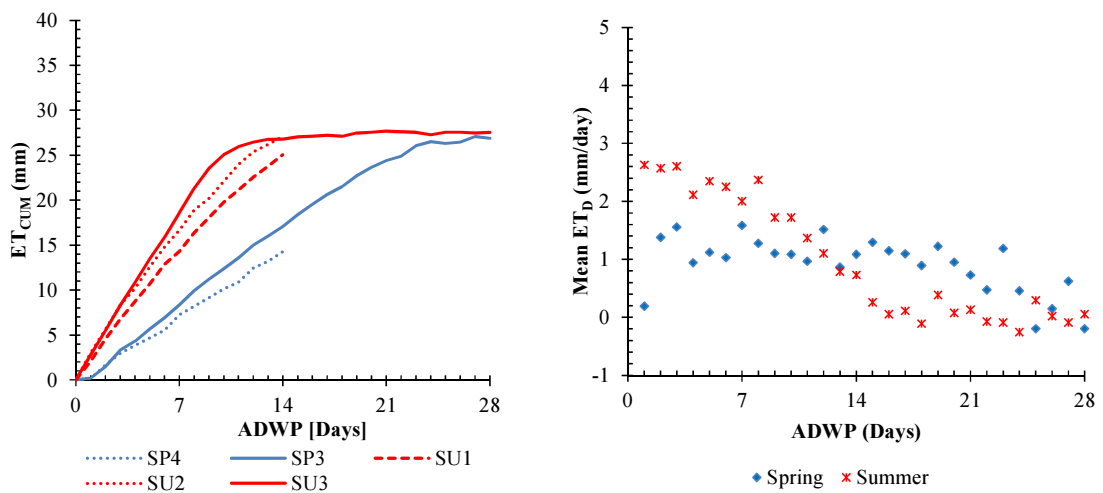
Figure 5.16: ET losses from all three Sedum-vegetated beds



a) TB4 – Meadow Flower on HLS

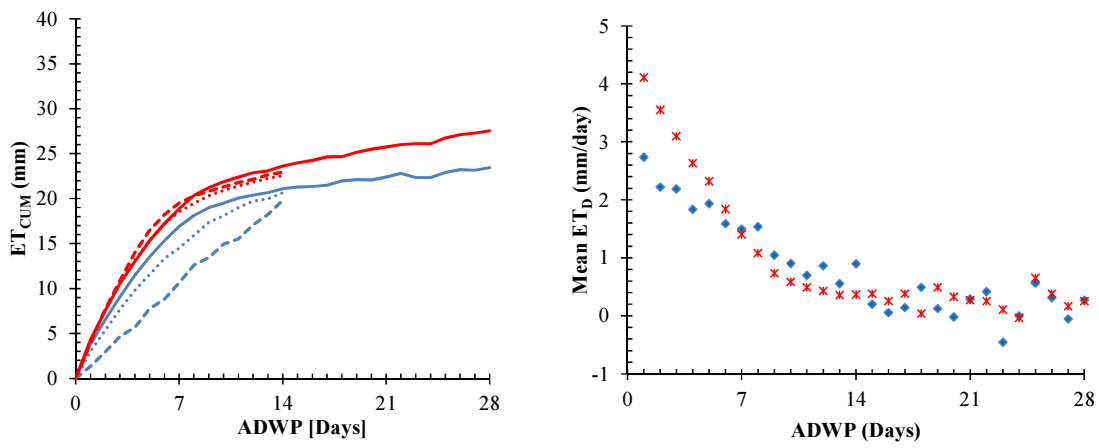


b) TB5 – Meadow Flower on SCS

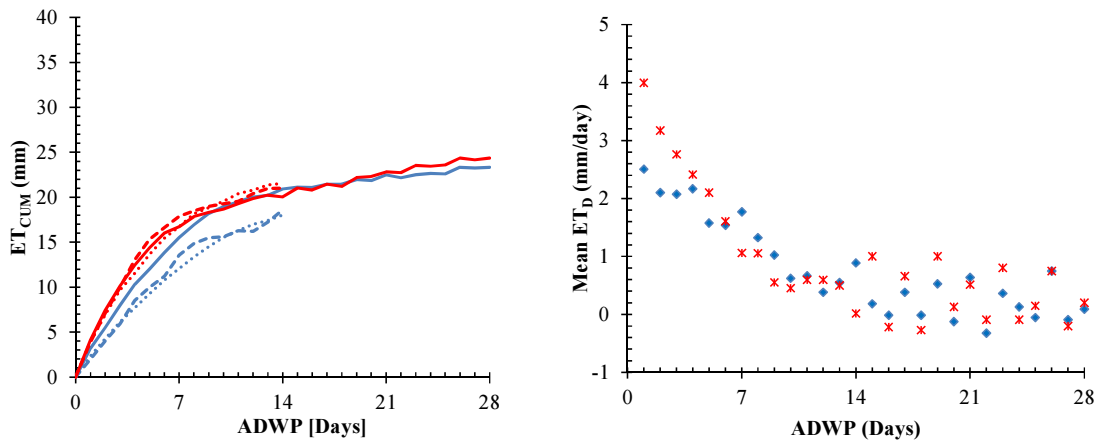


c) TB6 – Meadow Flower on LECA

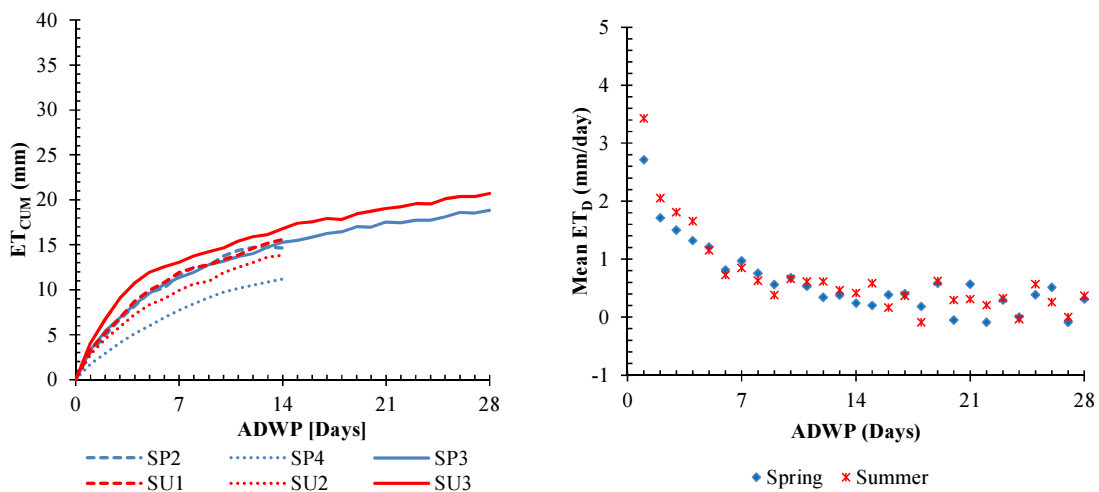
Figure 5.17: ET losses from all three Meadow Flower beds



a) TB7 – Non-vegetated HLS



b) TB8 – Non-vegetated SCS



c) TB9 – Non-vegetated LECA

Figure 5.18: ET losses from all three non-vegetated beds

### 5.4.3 Diurnal ET patterns

In view of the relatively small values associated with  $ET_D$  from extensive green roofs, the merits of considering ET at time intervals of less than a day (i.e. hourly ET,  $ET_H$ ) are questionable from a storm water management perspective. However, the diurnal distribution of ET is considered here to enhance understanding of the physical influences upon ET. The implications of simply deriving  $ET_H$  from  $ET_D/24$  will also become transparent.

The evaluation of  $ET_H$  involves small mass changes and potentially lower measurement accuracy. However, it is expected that a reasonable overview of diurnal trends can be identified by assessing mean diurnal trends over longer, weekly periods. Figure 5.19 and Figure 5.20 present the seasonal-mean diurnal ET profiles in moisture-abundant (Week 1) and moisture-constrained conditions (Week 4) respectively.

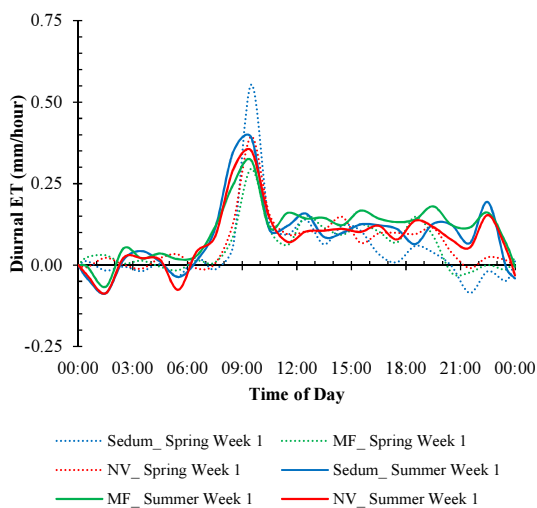


Figure 5.19: Diurnal ET (Low SMD)

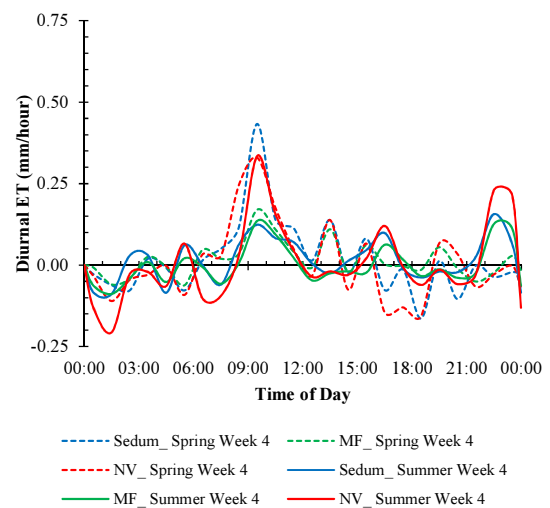


Figure 5.20: Diurnal ET (High SMD)

In all instances, peak  $ET_H$  was observed in the 2 hours following sunrise. Predictably, the highest peak  $ET_H$  – 0.55 mm/hour (spring) and 0.39 mm/hour (summer) – was observed in moisture abundant conditions. Lower peak  $ET_H$  was observed in week 4 – 0.43 mm/hour (spring) and 0.33 mm/hour (summer). ET was also measured earlier in summer (commencing at 05:30, compared with 07:30 in spring) and continuing later, until 00:00 (versus 19:30 in spring).

The cumulative diurnal ET profiles are plotted in Figure 5.21.

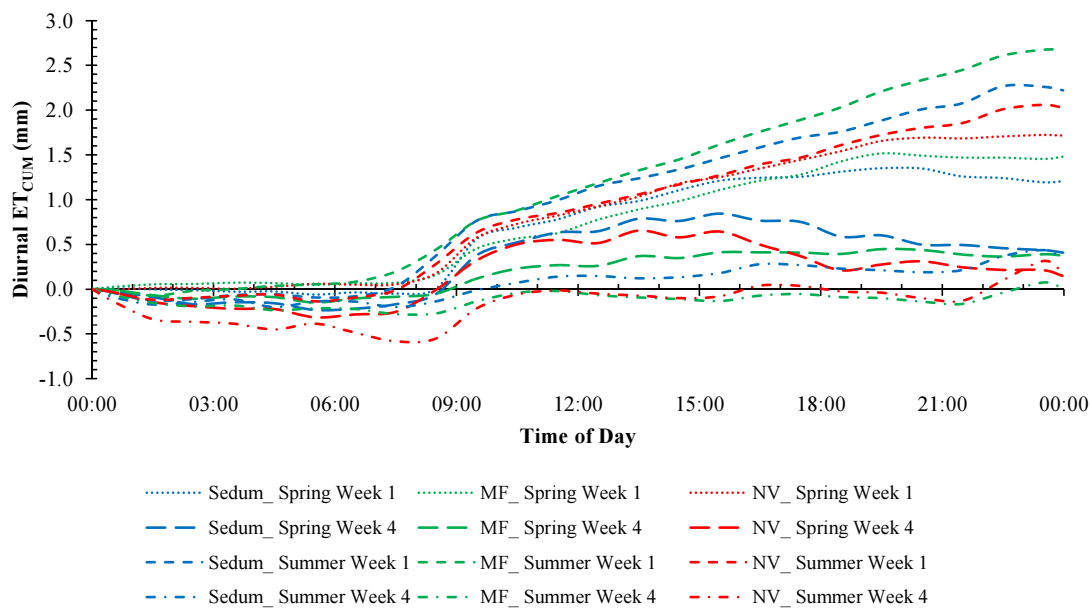


Figure 5.21: Diurnal ET loss patterns

ET was not witnessed outside the hours of daylight. This is an important observation because it is often considered that CAM plants, such as Sedum, will conserve moisture by opening stomata to metabolise in the cooler night-time conditions. There was no evidence to support this behaviour here; even during the conditions of extreme moisture deficiency (in week 4).

## 5.5 Discussion

ADWP has typically been considered a key parameter in modelling ET from green roofs. However, the range of ET values observed (in Section 5.4.1) for the same ADWP highlights the importance of factors other than time. The physical controls that influence ET – climate, moisture content and configuration (i.e. plant and substrate) – will now be considered.

### 5.5.1 The influence of climate upon ET

Conceptually, the climate can be considered a source of potential energy that acts upon the green roof to extract moisture via ET. Assuming abundant and constant  $S_i$ , summer conditions would be expected to induce higher ET than during cooler spring conditions. ET is directly related to temperature. Higher temperatures will lead to higher cumulative losses as a greater proportion of moisture that is held with higher  $\psi_m$  in small pores can be removed under increased levels of heat energy. In spring, the lower source of energy

generated in the cooler conditions is often not sufficient to break the bonds that act to retain moisture in the substrate to the same extent as observed under summer conditions.

The physical characteristics of each configuration govern its moisture retention behaviour, affecting the level of resistance to the extraction of moisture from within. However, on average, once  $S_t$  fell to approximately one quarter of  $S_{MAX}$ , moisture appeared to be held too tightly for ET to occur during spring conditions, as  $S_t$  remained relatively high, even after an ADWP of 28 days. Summer conditions were often sufficient to induce ET until  $S_t$  reached less than 10% of its  $S_{MAX}$ , emptying moisture from a higher proportion of the substrate's pores. The influences of climate and  $S_t$  are therefore intrinsically linked, as warm conditions generally induce faster initial ET; but in so doing, decrease  $S_t$  which then leads to lower subsequent ET losses.

In both seasons, ET rates fell below the maximum measured ET rate instantly (see Figure 5.22). It is hypothesised that this almost instant decline can be attributed to a combination of short-rooted vegetation and highly porous substrates.

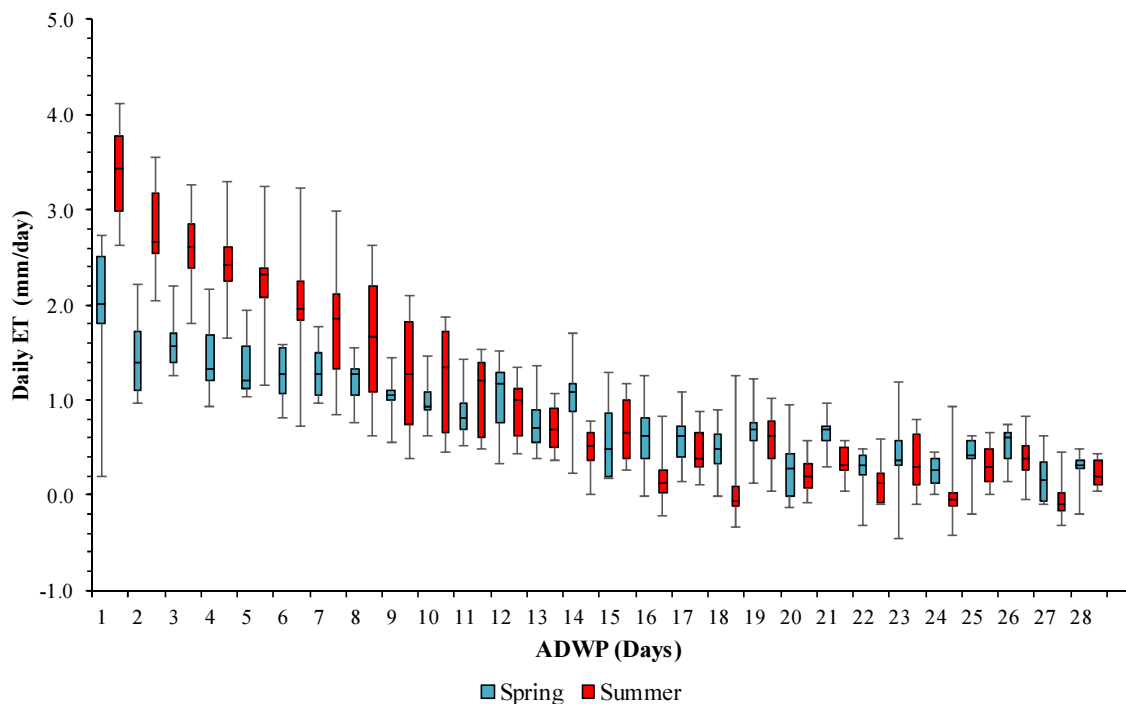


Figure 5.22: Seasonal-mean  $ET_D$

Seasonal-mean  $ET_D$  was greater in summer conditions than in spring for ADWPs of up to 12 days; such that seasonal-mean  $ET_{CUM}$  was 7.6 mm greater in summer by this time.

However, at longer ADWPs, ET appeared to have been constrained by the lower  $S_t$  that results from high antecedent rates of ET. Summer  $ET_D$  subsequently fell below spring rates (in many cases approaching zero). Lower antecedent ET in spring resulted in more sustained, consistent  $ET_D$ ; contrasting with the exponential decay in ET observed in summer trials.

The influence of season upon  $ET_D$  was most apparent when moisture availability was abundant (i.e. at short ADWPs). Median  $ET_D$  in summer fell from 3.4 mm to 1.9 mm over 7 days, then to 0.5 mm, 0.3 mm and 0.2 mm after 14, 21 and 28 days respectively. In spring, initial median  $ET_D$  of 2.0 mm was then consistently maintained at approximately 1.2 mm between day 2 and day 12, before falling to 0.7 mm after 21 days and 0.3 mm after 28 days.

Seasonal climate differences were significant to ET; most notably at shorter ADWPs, when moisture availability was not constrained by high antecedent moisture losses. However, as Figure 5.23 demonstrates,  $SMD_t$  being equal,  $ET_D$  would be expected to be higher in summer than in spring.

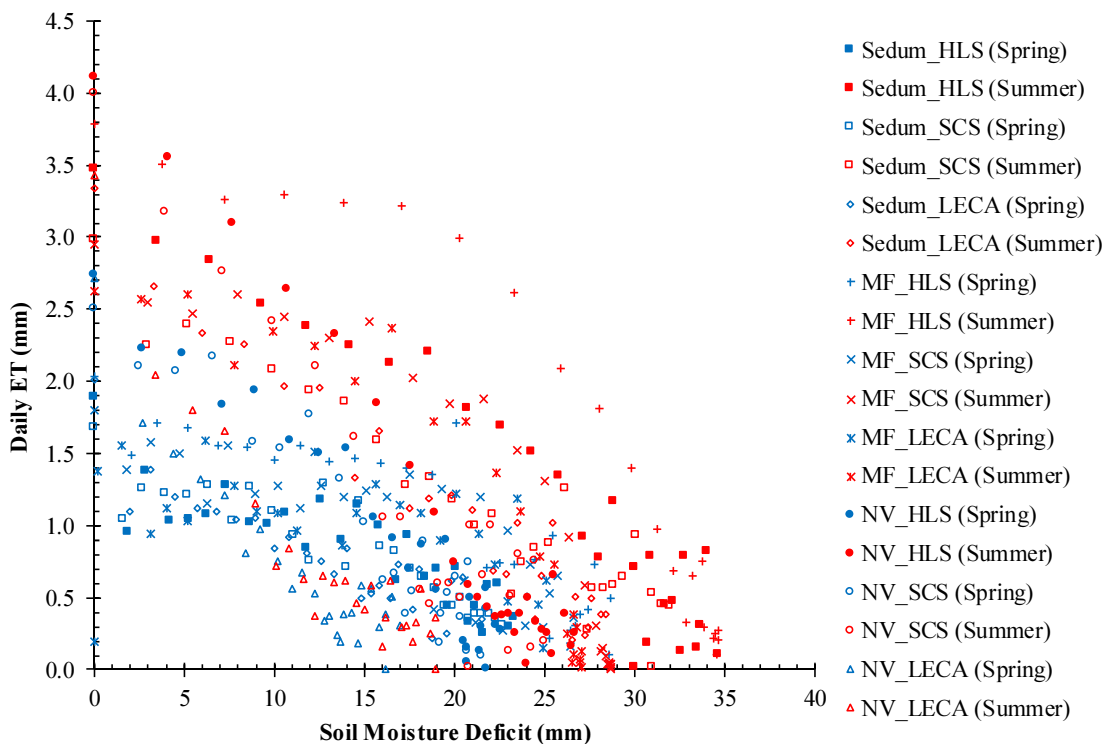


Figure 5.23: Configuration-mean daily ET as a function of moisture availability



The higher values of  $SMD_t$  observed in summer conditions indicates that a greater proportion of  $S_{MAX}$  is likely to be available to plants and the atmosphere in warm, summer conditions relative to the cooler spring climate.

### 5.5.2 The effect of moisture content upon ET

In general terms the decay of ET over time reflects the effects of reduced moisture availability.  $S_t$  had an underlying influence upon ET rates. Highest ET was recorded at the highest values of  $S_t$ ; the lowest when  $S_t$  was low. In most cases, this decline in ET occurred simultaneously with a reduction in moisture availability, as evidenced by the contrasts of rapidly declining  $ET_D$  during summer and the more consistent reduction in  $ET_D$  in spring. By considering  $ET/PET$ , and expressing moisture availability as a ratio ( $S_e$ ) of residual,  $S_t$ , to maximum storage,  $S_{MAX}$ , the constraints imposed upon ET by moisture availability can be seen (see Figure 5.24).

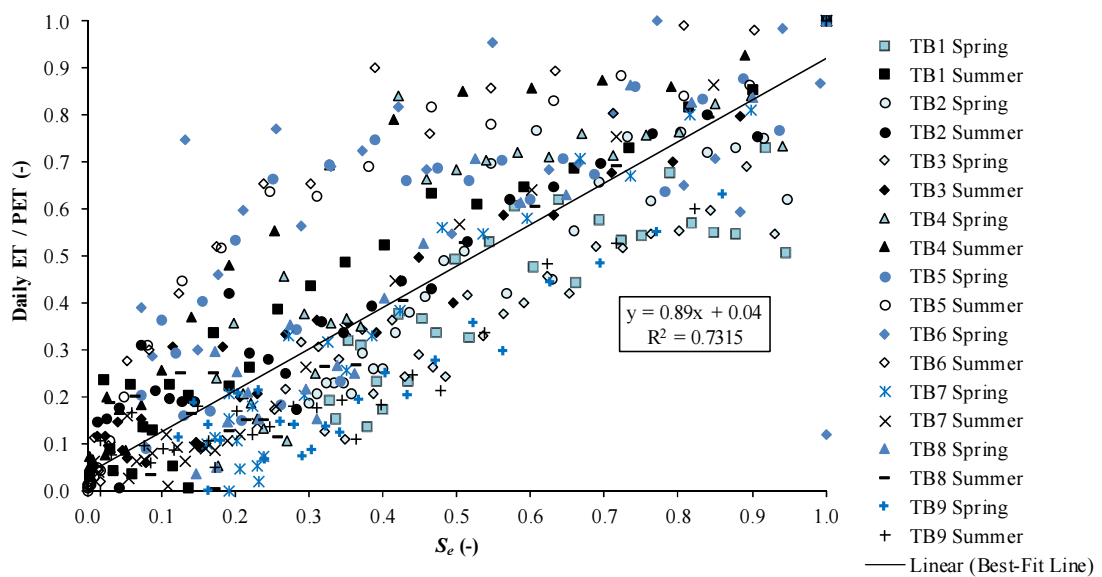


Figure 5.24 :  $ET/PET$  versus  $S_e$

In all instances, ET reduced as  $S_e$  fell. A best-fit regression line ( $R^2=0.73$ ) with a gradient of 0.89 reflects a relatively linear reduction in  $ET/PET$  as  $S_e$  fell.  $ET/PET$  in summer fell largely above the best-fit line. Certain configurations (e.g. TB1) were also seen to have nonlinear relationships between  $ET/PET$  and  $S_e$ .

An analysis of variance (ANOVA) demonstrated that the influence of  $S_e$  on  $ET/PET$  is statistically significant ( $F=0.000$ , p-value 0.05). The importance of moisture availability to ET is also apparent in Figure 5.21; comparing ET over a mean diurnal cycle when

moisture was abundant (i.e. week 1) with conditions when moisture availability was constrained (i.e. week 4).

ET was highest when moisture was abundantly available, with seasonal-mean ET of 1.5 mm/day in spring and 2.3 mm/day in summer. In moisture-constrained conditions, ET of between 0.2 and 0.3 mm/day was measured; albeit actual ET of 0.8 mm was observed during the day when moisture gains of 0.5 mm were taken into account. Moisture gain was most pronounced in the conditions where moisture was most constrained (i.e. in week 4 of summer). This is consistent with the fact that the highly negative pressures within a dry soil will create a vapour pressure gradient that would typically lead the moisture from the relatively humid air above to be drawn into the soil matrix.

The distinct change in ET as a result of reducing moisture availability highlights the importance of including moisture content as a key parameter in any modelling approach.

### **5.5.3 The effects of green roof configuration**

#### *5.5.3.1 Vegetation treatment*

The incorporation of vegetation will typically provide some level of additional moisture storage capacity (Morgan *et al.*, 2013). ET losses will be positively influenced by plant transpiration but negatively affected by reduced evaporation relative to bare soil surfaces (Nagase & Dunnett, 2012). On average, the addition of vegetation increased 28 day  $ET_{CUM}$  by 17% in spring and 23% in summer. The incremental effect of adding Sedum was greatest in summer (26%) than in spring (10%), with additional losses in summer ranging between 7.2 mm (representing 22% of  $ET_{CUM}$ ) and 9.5 mm (33%) compared to the equivalent non-vegetated configuration. The higher figure was witnessed from the LECA substrate, which has the highest permeability. It is believed that the greater incremental effect of adding Sedum into LECA can be attributed to the binding effect of the roots penetrating this highly porous substrate. The incremental effect of Sedum on HLS and SCS was lower – 7.8 mm and 7.2 mm respectively. Vegetating with Meadow Flower led to an increase in 28-day  $ET_{CUM}$  of 25% in spring and 21% in summer. The substrate type was an influence; particularly in summer when the increment ranged between 3.5 mm or 12% (SCS) and 7.7 mm or 29% (LECA). Adding Meadow Flower to HLS increased  $ET_{CUM}$  by 7.7 mm.

Any incremental effect of vegetation on ET will vary as a function of the substrate's soil-water characteristics, ADWP and climatic conditions. In all instances, ET from non-vegetated configurations initially exceeded ET from vegetated equivalents. The duration of this lag varied seasonally and by vegetation treatment. However, vegetation ultimately made a positive net contribution to  $ET_{CUM}$  (see Figure 5.25).

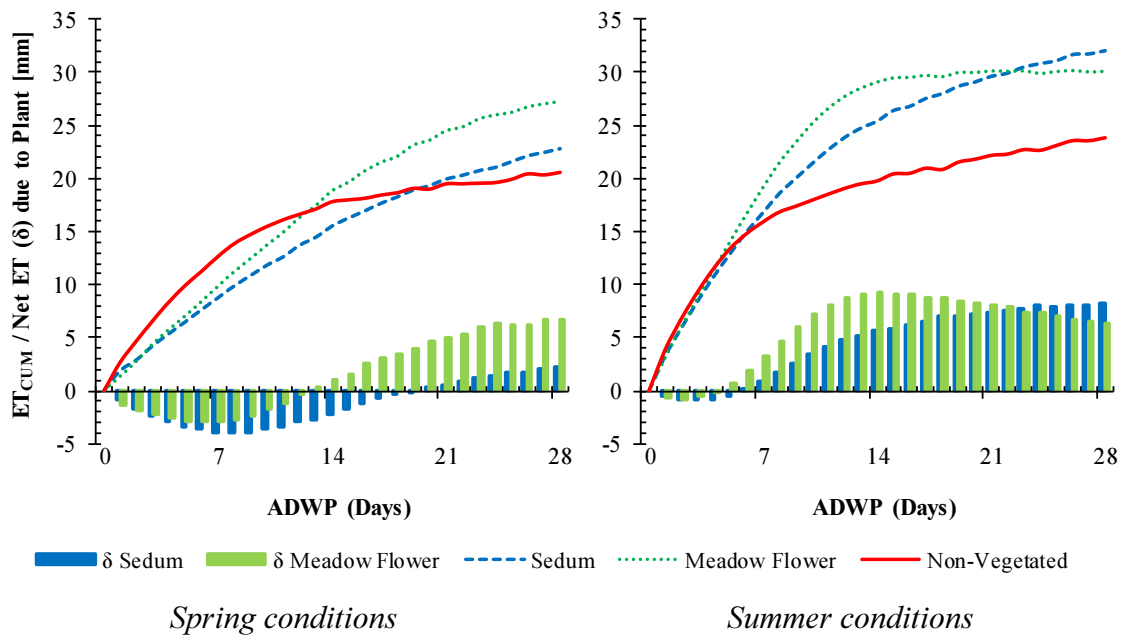


Figure 5.25:  $ET_{CUM}$  from Configurations with Different Plant Options

Initially, the addition of vegetation had a detrimental impact on ET. The duration of this lag varied seasonally and by vegetation treatment. However, vegetation ultimately made a positive net contribution to  $ET_{CUM}$ . In spring, this contribution was positive after 12 days (with Meadow Flower) or 20 days (for Sedum), ultimately increasing  $ET_{CUM}$  by 6 mm and 2 mm respectively. In summer, the net contribution to ET by vegetation was evident at an earlier stage – after 4 and 6 days for Meadow Flower and Sedum respectively – and to a much greater degree.  $ET_{CUM}$  increased by as much as 9 mm (after 14 days) through the addition of Meadow Flower (subsequently reducing below 6 mm after 28 days due to permanent wilting of the vegetation) or 9.5 mm when Sedum was added.

Sedum appeared to regulate ET to a greater extent than Meadow Flower. In spring, vegetation-mean  $ET_D$  from Sedum was lower than from Meadow Flower at virtually all stages. This was also the case for the first two weeks under summer conditions (see Figure 5.26).

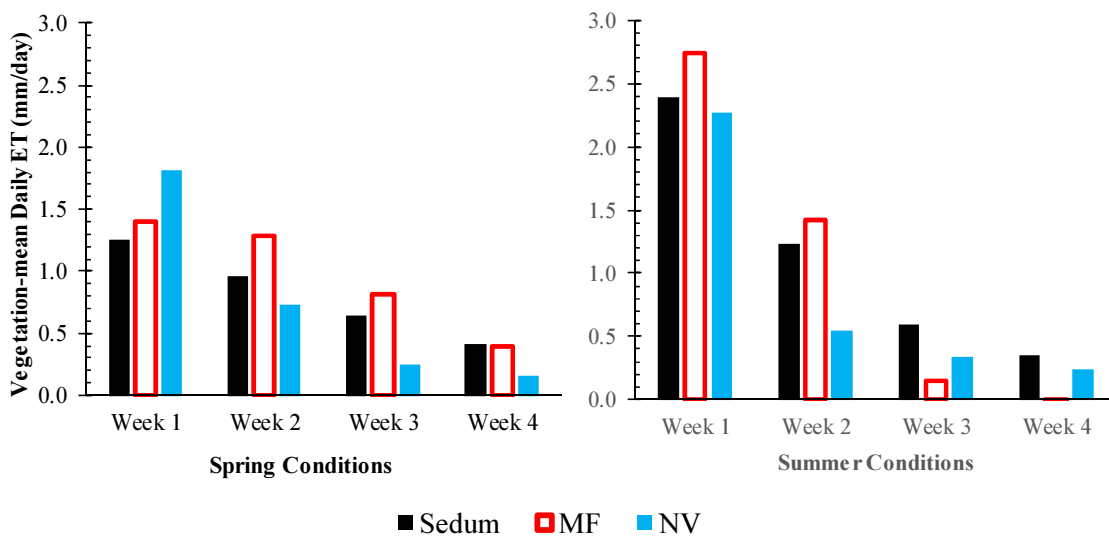


Figure 5.26: Vegetation-mean  $ET_D$  in spring & summer

This is consistent with the findings of Farrell *et al.* (2012), who identified slower ET from Sedum (compared to C3 plants) over an initial 20 day period. Sedum species typically have relatively shallow fibrous roots, whereas grasses and forbs tend to have larger root and shoot biomass that can be conducive to more effective moisture retention (Nagase & Dunnett, 2012). However, the CAM photosynthesis and leaf succulence of Sedum ensure stronger drought tolerance (MacIvor & Lundholm, 2011) compared to grasses and forbs (Lu *et al.*, 2014). The seasonal differences in  $ET_{CUM}$  for Sedum were the greatest of the vegetation treatments; as low, regulated ET in spring contrasts with faster ET and subsequent exponential decay in summer. Unlike other vegetation treatments, ET losses were observed from Sedum for more prolonged periods, even after long summer ADWPs. Yet there were no observations of higher transpiration from Sedum during night conditions; a trait that is often associated with CAM plants. Differences in ET rates attributable to substrate were marginal when Sedum was the chosen vegetation treatment.

The different transpiration rates of Meadow Flower, compared with Sedum, were most apparent in summer. Generally high ET was measured for an initial 7 day period, as vegetation-mean  $ET_D$  from Meadow Flower exceeded  $ET_D$  from Sedum in both spring (1.4 versus 1.25 mm/day) and summer (2.7 versus 2.4 mm/day). However, an almost linear decline in vegetation-mean  $ET_D$  from Meadow Flower towards zero by Day 14 (with virtually no subsequent ET thereafter) supports a hypothesis that the fast initial transpiration of Meadow Flower leads to  $ET_D$  that is constrained by a configuration's

$S_{MAX}$  at longer ADWPs. The highest  $ET_{CUM}$  (of 34.7 mm) was measured from the substrate with the greatest  $\theta_{FC}$  (i.e. HLS). Yet all plant-available moisture appeared to have been consumed; as confirmed by observations of permanent wilting.

Three key trends distinguish patterns of ET for non-vegetated configurations from their vegetated equivalents:

- a) Faster initial rates of ET, as  $ET_{CUM}$  exceeded  $ET_{CUM}$  from Sedum and Meadow Flower configurations for 12, 15 and 10 days (for HLS, SCS and LECA respectively) in spring and for 3, 6 and 1 day in summer;
- b) Lower  $ET_{CUM}$  after 28 days; and
- c) Smaller seasonal ET differentials.

In spring, vegetation-mean  $ET_D$  from non-vegetated configurations was as high as 2.8 mm/day. Vegetation-mean  $ET_D$  over the first week was 1.8 mm/day and continued to fall in the second week (to a mean of 0.7 mm/day), averaging just 0.15 mm/day in the fourth week. As a result,  $ET_{CUM}$  was limited to between 17.3 and 22.9 mm after 28 days. In summer, higher ET rates of up to 4.2 mm/day were observed, but declined instantly towards zero by Day 14. Generally, the faster decay in ET from non-vegetated configurations (relative to vegetated configurations) can be attributed to a lower albedo (i.e. the absence of a plant cover that would otherwise serve to moderate evaporation from a highly porous, dark, bare substrate surface) and to the lower  $S_{MAX}$ . The smaller seasonal increase in  $ET_{CUM}$  from non-vegetated configurations reflects (a) the constraints imposed on ET by low  $S_{MAX}$ , and (b) the greater plant transpiration in warm conditions.

The vegetation treatments trialled here were relatively young. Further root development as the vegetation ages would be expected to change the organic content and porosity of the substrate (Berndtsson, 2010). A more developed root distribution, filling a higher proportion of large voids in the substrate, would act to increase moisture retention capacity (Nagase & Dunnett, 2012).

### 5.5.3.2 *Substrate*

ET varied as a function of a substrate's soil-water characteristics; both in vegetated and non-vegetated configurations. Figure 5.27 presents substrate-mean  $ET_D$  over each of the 4 weeks.

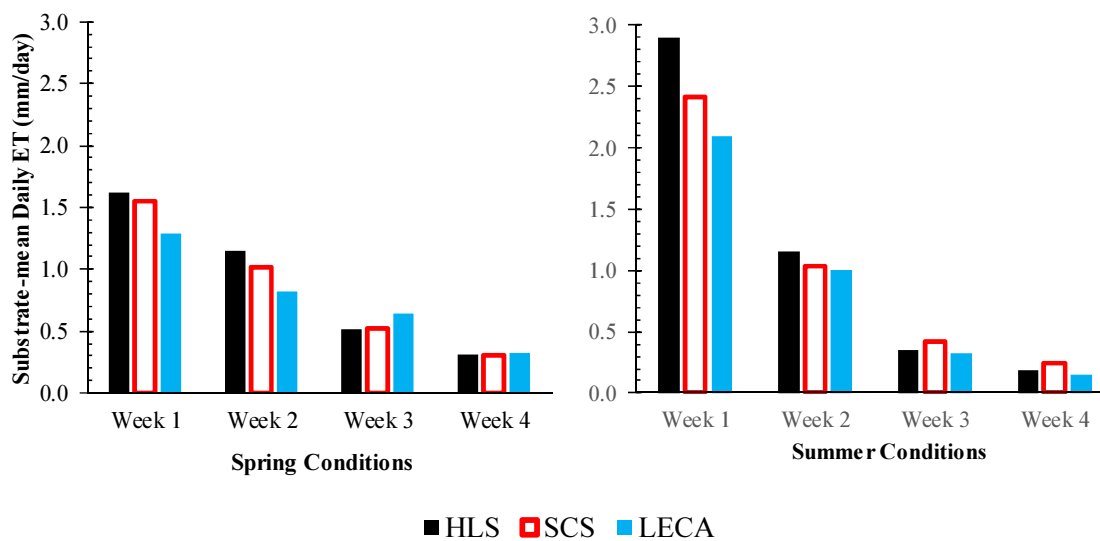


Figure 5.27: Substrate-mean  $ET_D$  in spring & summer

Substrate type appeared to influence ET less than vegetation treatment. However, in both climatic regimes and at all ADWPs, substrate-mean  $ET_D$  generally reflected the substrate's  $\theta_{FC}$  with substrate-mean  $ET_D$  greatest from HLS configurations and least from LECA. The extent to which a substrate's  $\theta_{FC}$  affected  $ET_{CUM}$  varied according to the climate. In spring, the range of substrate-mean  $ET_{CUM}$  was lower (22–25 mm) than in summer (25–33 mm). The seasonal increase in substrate-mean  $ET_{CUM}$  was greater from HLS (8 mm) than SCS (4 mm) after 28 days. This indicates that, in warm conditions, higher  $\theta_{FC}$  will generally facilitate higher  $ET_{CUM}$ . A greater proportion of the moisture that is held with higher  $\psi_m$  in the small pores of HLS can be removed via ET with the greater heat energy that is generated in warmer climatic conditions. Yet, in cooler conditions, a substrate's  $S_{MAX}$  is unlikely to be fully depleted via ET and other characteristics, such as permeability, will influence the rate of ET.

HLS is the substrate with the greatest  $\theta_{FC}$ , yet also the highest proportion of fines (and lowest permeability). SCS has a lower  $\theta_{FC}$ . Yet, substrate-mean  $ET_{CUM}$  was virtually identical (24 mm) from both substrates after 28 days in spring. This is consistent with a hypothesis that the lower heat energy in spring can induce slower moisture balance changes (particularly in the substrate's smaller pores, where moisture is retained with greater tenacity). In cooler climates, no discernible increase in ET is therefore likely to result from substrates with high  $\theta_{FC}$  and low permeability (e.g. HLS) compared to substrates with lower  $\theta_{FC}$  and higher permeability (e.g. SCS). Indeed, despite the low  $\theta_{FC}$

and very high permeability of LECA, substrate-mean  $ET_{CUM}$  was only marginally lower than from SCS in spring. However, in warm conditions, when PET was high, a lower  $S_{MAX}$  would be expected to constrain ET, as was evident from the small seasonal difference in substrate-mean  $ET_{CUM}$  of 3 mm measured with LECA after 28 days.

#### **5.5.4 Summary of key influences**

Overall, moisture content is a very important influence upon ET. ET will be greatest when moisture availability is high, but will almost instantly fall below PET when available moisture is less than  $S_{MAX}$ . A configuration's  $S_{MAX}$  varies according to vegetation treatment and substrate type. The rate at which the retention capacity is generated will be affected, significantly, by the climate (with warmer temperatures inducing greater initial rates of ET) and by the response of the vegetation treatment to the ambient conditions.

### **5.6 Conclusions**

- Seasonal differences in ET were statistically significant. ET was higher in warmer summer conditions than in lower spring temperatures. After a 14 day ADWP, vegetation-mean  $ET_{CUM}$  in spring and summer respectively was 15.5 mm and 25.4 mm (Sedum), 18.8 mm and 29.1 mm (Meadow Flower) and 17.8 mm and 19.8 mm (non-vegetated). As ADWP increased, statistical significance fell.
- Seasonal mean ET rates were 1.95 mm (spring) and 3.4 mm (summer) over a 1 day ADWP. However, in all instances, the instant decay in ET reflected reduced moisture availability
- Moisture content is a critical influence upon ET rates and retention capacity. Highest ET was observed when moisture availability was high. A factor must be applied to PET to reflect a decay in ET with falling moisture availability.
- Significant differences in ET existed between vegetated and non-vegetated configurations. ET was higher from non-vegetated configurations than from vegetated configurations for ADWPs of between 12 (Meadow Flower) and 20 days (Sedum) in spring and between 4 (Meadow Flower) and 6 days (Sedum) in summer.
- Interception losses of up to 7.8 mm (Sedum) and 7.7 mm (Meadow Flower) were observed on brick-based substrates.

- No significant differences in ET were identified between systems vegetated with Sedum and Meadow Flower. However, practical differences were observed. When  $S_e$  was high, ET from Meadow Flower was higher than from Sedum. However, the exponential decay in ET/PET with falling  $S_e$  from Meadow Flower led to permanent wilting after an ADWP of 14 days in summer.
- Substrates with high  $\theta_{FC}$  led to the greatest  $ET_{CUM}$  in most circumstances. Differences in a substrate's soil-water characteristics can have a significant influence upon ET (e.g. LECA vs HLS). However, where soil-water characteristics are relatively similar (e.g. HLS vs SCS), differences were not significant.



## 6 Model development and refinement

### 6.1 Chapter overview

In this chapter, the hydrological model is presented, refined and validated with the benefit of the empirical datasets that were generated during this research programme. The retention response of all nine configurations has been seen to clearly respond to two critical driving forces: the PET rate and the available soil moisture. Here, the importance of different PET calculation methods is reviewed. The use of crop factors to account for the influence of vegetation treatment upon ET is reviewed prior to considering the extent of any errors when PET is calculated at daily, rather than hourly intervals. Consideration is also given to existing and new moisture functions that factor down PET in line with moisture availability to estimate actual ET. The PET method and the moisture functions are selected based upon comparisons with the empirical ET data (as detailed in Chapter 5) and validated using field data from the Hadfield site. Any developed model will need to temporally distribute net rainfall to predict the runoff response. Here, detention is characterised by a reservoir-routing model that includes a generic mechanism for predicting the runoff response to a time-series or design rainfall event.

Aspects of these analyses have been published in three journal papers:

Stovin, V., Poë, S. and Berretta, C. (2013). A modelling study of long term green roof retention performance, *Journal of Environmental Management*, 131, 206-215.

Poë, S., Stovin, V. and Berretta, C. (2015). Parameters influencing the regeneration of a green roof's retention capacity via evapotranspiration, *Journal of Hydrology*, 523, 356-367.

Stovin, V., Poë, S., De-Ville, S. and Berretta, C. (2015a). The influence of substrate and vegetation configuration on green roof hydrological performance, *Ecological Engineering*, 85, 159–172.

In Stovin *et al.* (2013) and Poë *et al.* (2015), a simple linear moisture balance function was used to derive ET from PET. In this chapter, additional functions are considered.

## 6.2 Motivation

The objective of this chapter is to develop a generic approach to modelling the hydrological response of extensive green roofs whilst accounting for the influences of climate and configuration. It is intended that the model will serve as a tool for SuDS practitioners to make objective decisions when considering the inclusion of extensive green roofs within storm water management strategies. Long-term simulations can inform green roof designers about (a) annual retention performance, (b) per-event retention (possibly including high return period events), and (c) the viability of different configurations; with the identification of any drought risk underpinning the selection of the vegetation treatment and any irrigation requirement. By modelling the response of a green roof to specific design rainfall events, per-event statistics for retention, peak reduction and peak delay can be predicted; facilitating analyses of complementary and/or substitutable SuDS measures.

## 6.3 Materials and methods

### 6.3.1 Conceptual hydrological model

The retention model is essentially a moisture storage/flux model that simultaneously accounts for important interdependent moisture balance parameters – available storage capacity, inputs (e.g. precipitation) and outputs (e.g. ET, runoff). The moisture balance model predicts runoff ( $Q_{PRED}$ ) on the basis of rainfall depth ( $P$ ) and the green roof's available moisture retention capacity (or SMD); the latter being dependent upon the configuration's maximum storage capacity ( $S_{MAX}$ ) and the extent to which residual moisture ( $S_t$ ) has been depleted through ET during the ADWP. ET is predicted ( $ET_{PRED}$ ) using (i) a PET calculation that accounts for the climatic influences that drive ET, and (ii) a function that factors down ET from PET in line with moisture availability. Here,  $S_{MAX}$  does not include hygroscopic moisture but does include the maximum storage capacity of any vegetation treatment ( $S_{VEG}$ ).  $S_{VEG}$  was derived here using the maximum interception losses (see Table 5.3). Figure 6.1 depicts this conceptual hydrological model.

When precipitation exceeds the SMD, runoff will occur. Here, the surplus precipitation is considered to become transient storage ( $TS$ ).  $TS$  will commence at the point at which SMD reaches zero (i.e.  $S_t = S_{MAX}$  or  $S_e = 1$ ). Here, SMD includes any available moisture storage capacity in the vegetation.

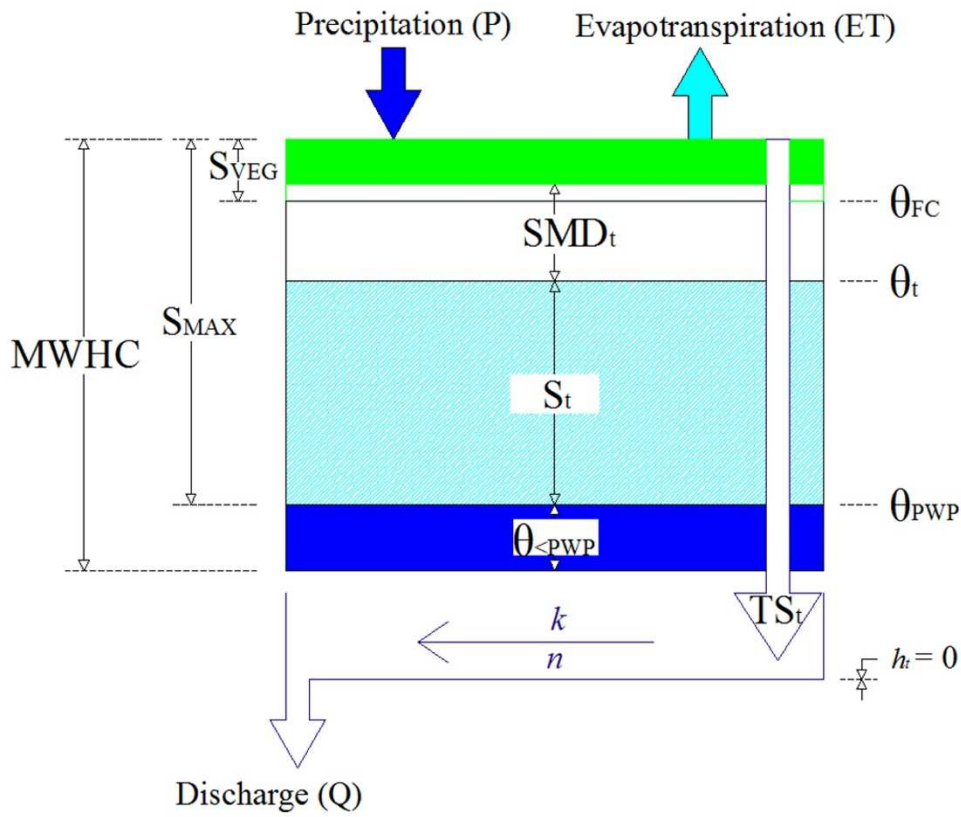


Figure 6.1: Conceptual green roof hydrological model

The delay between  $TS$  occurring and runoff taking place is calculated using the kinematic wave approximation (Lighthill & Whitham, 1955), or reservoir routing, that is applied to the residual sum of  $TS$  ( $h_t$ ) that has not yet discharged from the system as runoff ( $Q$ ).

Detention parameters,  $k$  and  $n$ , are applied to the residual sum of transient storage ( $h_t$ ) to account for delays incurred as moisture is transported through the vegetation, substrate and drainage layer towards the outlet. The proposed modelling concept therefore includes functions for both retention and detention.

### 6.3.2 Model implementation

The model first requires the continuous calculation of the moisture balance using the following retention equations:

$$S_t = \begin{cases} S_{t-1} + P_t - ET_t, & S_{t-1} + P_t - TS_t - ET_t \leq S_{MAX} \\ S_{MAX}, & S_{t-1} + P_t - TS_t - ET_t > S_{MAX} \end{cases} \quad \text{Equation 6.1}$$

Where  $P_t$  is rainfall or precipitation (in mm) at time  $t$ ;  $ET_t$  is evapotranspiration (in mm) at time  $t$ ; and  $TS_t$  is the quantity of moisture (in mm) entering transient storage at time  $t$ , calculated as:

$$TS_t = \begin{cases} 0, & S_{t-1} + P_t - ET_t \leq S_{MAX} \\ P_t - SMD_{t-1} - ET_t, & S_{t-1} + P_t - ET_t > S_{MAX} \end{cases} \quad \text{Equation 6.2}$$

Where:

$$SMD_t = S_{MAX} - S_t \quad \text{Equation 6.3}$$

and

$$ET_t = PET \cdot S_e \quad \text{Equation 6.4}$$

Where  $S_e$  equals  $S_t / S_{MAX}$ .  $S_e$  accounts for the effect that soil moisture has on the actual ET rate. Alternative methods for the calculation of PET can be included in this modelling approach. The modelling of moisture availability relies upon either an existing or a new soil moisture extraction function (SMEF).

Once  $TS$  exceeds zero, runoff ( $Q_t$ , in mm) at time,  $t$  is calculated by applying detention coefficients to the residual cumulative depth of transient storage ( $h_t$ ) using Equation 6.5:

$$Q_t = kh_{t-1}^n \quad \text{Equation 6.5}$$

Where  $k$  &  $n$  are routing coefficients that account for the time and nature of flow respectively. For  $h_t$  in mm and  $Q_t$  in mm/min,  $k$  has the units  $\text{mm}^{(1-n)}/\text{min}$ , whilst  $n$  is dimensionless.  $h_t$  is calculated with Equation 6.6:

$$h_t = h_{t-1} + TS_t - Q_t \quad \text{Equation 6.6}$$

### 6.3.3 Model validation methods

The model was validated against the empirical datasets generated during the field research programme (AE9 events). This research has sought to identify differences due to configuration. However, from a modelling perspective, it was decided that only the most typical UK extensive green roof configurations would be considered. The LECA-based configurations (i.e. TB3, TB6 and TB9) were not considered for modelling here. The use of this substrate is expected to be limited by the difficulties in characterising its

performance and its unpredictable responses during both wetting and drying cycles. The predictive accuracy of the model outputs was compared against measured values using one or more of three methods.

#### 6.3.3.1 A simple correlation - R Squared

A commonly applied statistical measure of the proportion of explained variance in observed and modelled values, the  $R^2$  statistic is the complement of the sum of squares of residuals as a proportion of the total sum of squares (see Equation 6.7).

$$R^2 = \left[ \frac{\sum(Q_o - \overline{Q_o})(Q_m - \overline{Q_m})}{\sqrt{\sum(Q_o - \overline{Q_o})^2 \sum(Q_m - \overline{Q_m})^2}} \right]^2 \quad \text{Equation 6.7}$$

An  $R^2$  statistic of 1 would indicate that the model fits observed values perfectly; whereas a value of 0 highlights that the model is not able to explain any of the variance.

#### 6.3.3.2 Nash-Sutcliffe Model Efficiency

The Nash-Sutcliffe Model Efficiency (NSME) is a means of testing goodness of fit of hydrological models, comparing modelled performance with observations, in accordance with Equation 6.8.

$$NSME = \frac{\sum_{t=1}^T (Q_o^t - Q_M^t)^2}{\sum_{t=1}^T (Q_o^t - \overline{Q_o})^2} \quad \text{Equation 6.8}$$

Where  $Q_o$  and  $Q_M$  are the observed and modelled values respectively. A NSME index of one would signal a perfect match between observed and modelled values. A value of zero would indicate that predictions would be equally accurate if the mean value of observed data were used in the model. Values below zero would mean that residual variance is greater than the data variance (i.e. that the observed mean value is a better predictor of the outcome than the model). Predictive accuracy is ‘good’ when the NSME index is between 0.65 and 0.75 and ‘very good’ when the NSME index is greater than 0.75 (Nash & Sutcliffe, 1970 in Moriasi *et al.*, 2007).

#### 6.3.3.3 Percent Bias

The Percent Bias (PBIAS) approach measures the average tendency of modelled values to be larger or smaller than observed values:

$$PBIAS = 100 \times \left[ \frac{\text{sum}(Q_M - Q_O)}{\text{sum}(Q_O)} \right] \quad \text{Equation 6.9}$$

The optimum value of PBIAS is zero. Positive values reflect an over-prediction in the modelled figure and negative values are calculated where the model under-predicts measured values. A PBIAS of less than or equal to +/-15% is considered to have ‘good’ accuracy and a PBIAS of less than or equal to +/-10% would signal a ‘very good’ predictive accuracy (Gupta *et al.*, 1999 in Moriasi *et al.*, 2007).

## 6.4 Model refinement

### 6.4.1 PET calculation

#### 6.4.1.1 Differences in PET due to calculation method

Five PET calculation methodologies were considered here: the FAO56 Penman-Monteith method ( $PET_{FAO56}$ ), Hargreaves ( $PET_{HG}$ ), Priestley-Taylor ( $PET_{PT}$ ), Thornthwaite ( $PET_{TH}$ ) and Blaney-Cridde ( $PET_{BC}$ ). Each method was introduced in Chapter 2 and represents a different trade-off between the complexity and physical basis of the calculation. The importance of the choice of method to the PET estimate was assessed against three calendar years of the Hadfield weather station data (i.e. 2011-2013). The differences in monthly mean PET during the 3 year period are highlighted in Figure 6.2.

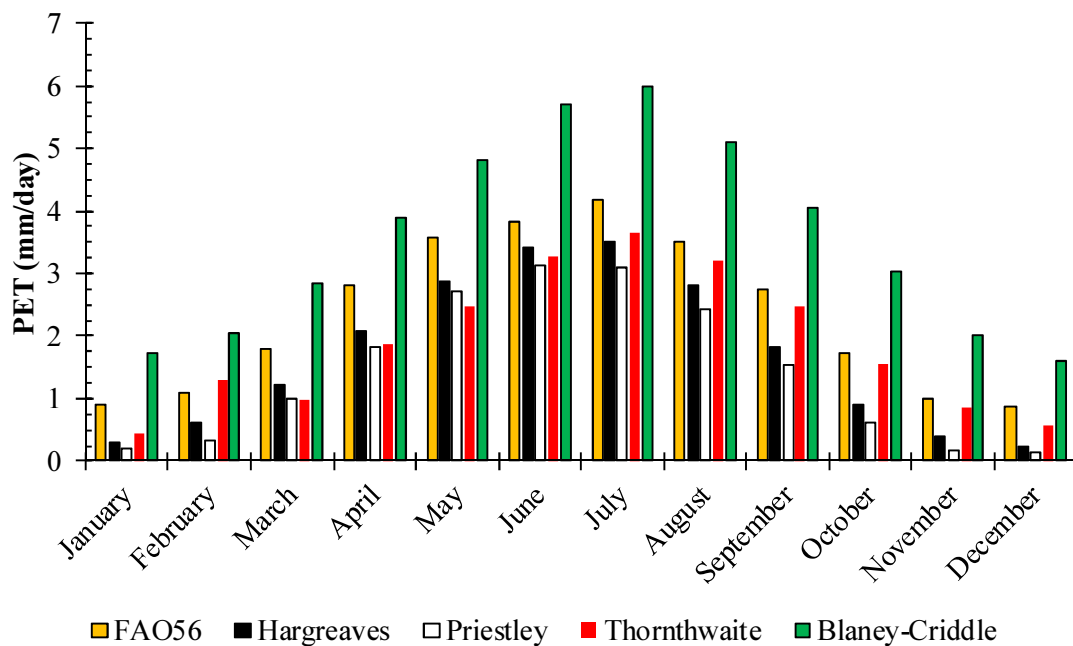


Figure 6.2: PET values for the Hadfield research site between 2011 and 2013

The choice of calculation method was an important influence on the predicted daily PET rate. This is consistent with the findings of Voyde (2011), who also identified large differences in calculated PET when applying different methods (including  $PET_{FAO56}$ ,  $PET_{HG}$  and  $PET_{BC}$ ) across a 40 day period in New Zealand. Voyde (2011) identified a mean absolute daily error between measured and modelled PET of 0.76 mm/day but with a range of between 0.14 and 2.13 mm/day depending upon the model chosen. Rezaei (2005) also concluded that the most accurate PET method varied seasonally and as a function of vegetation treatment.

Here,  $PET_{BC}$  produced the highest monthly mean PET estimate in each of the twelve months and  $PET_{PT}$  the lowest (with the exception of March and May, when  $PET_{TH}$  was lower). Standard deviations from monthly and seasonal mean daily PET were high; reflecting the importance of the calculation method to estimated PET. When expressed relative to the mean, standard deviation was highest in winter – when PET ranged between 0.22 mm/day ( $PET_{PT}$ ) and 1.79 mm/day ( $PET_{BC}$ ). However, the largest absolute standard deviation was in summer (>1 mm/day) as PET ranged between 2.88 mm/day ( $PET_{PT}$ ) and 5.60 mm/day ( $PET_{BC}$ ).

In comparing each method:

- $PET_{FAO56}$  produced seasonal mean values that were most closely matched to mean values across the five different approaches. In all seasons, seasonal mean  $PET_{FAO56}$  was greater than  $PET_{PT}$ ,  $PET_{TH}$  and  $PET_{HG}$ .
- $PET_{PT}$  produced the lowest seasonal mean PET estimate in three of the four seasons. This can be explained by the simplifying use of a proportionality constant between the radiant energy and aerodynamic terms in the calculation, which can lead to low PET estimates (de Jong & Tugwood, 1987).
- $PET_{BC}$  produced the highest PET at all times. Annual mean  $PET_{BC}$  of 3.6 mm/day was at least 1.2 mm/day greater than any other approach. Seasonal mean  $PET_{BC}$  exceeded seasonal mean PET by between 0.9 mm/day (in winter) and 1.8 mm/day (in summer).

- The two temperature-based approaches (i.e.  $PET_{TH}$  and  $PET_{HG}$ ) estimated similar PET in spring and summer conditions. However, in both autumn and winter,  $PET_{HG}$  was lower than  $PET_{TH}$  (being approximately 50% of  $PET_{TH}$  in winter).

The  $PET_{BC}$  approach was developed for use in the USA and, in view of the tendency for it to predict extremely high PET, it would not appear to be suitable for use in the UK. Similarly, the reliance of  $PET_{PT}$  upon a constant aerodynamic term contributed to a consistently low PET. Neither  $PET_{BC}$  nor  $PET_{PT}$  were therefore considered further for use in the model. Three methods ( $PET_{FAO56}$ ,  $PET_{HG}$  and  $PET_{TH}$ ) were further evaluated for suitability of use through a comparison against the laboratory-derived ET data.

#### 6.4.1.2 Comparison of calculated PET with maximum measured ET

To aid the selection of the most appropriate PET method, PET was calculated for the programmed climatic settings for the ET trials and compared against the corresponding maximum ET rates when moisture was abundantly available. Key assumptions inherent in the calculations were:

1.  $PET_{FAO56}$  was calculated for a reference crop (green grass) of uniform height (0.12 m), surface resistance (70 s/m) and albedo (0.23).
2.  $PET_{TH}$  was derived by generating monthly and annual heat index values from Met Office data for average monthly temperatures measured in Sheffield during 2009 (i.e. the same data set that was used to determine the climate chamber settings). Monthly heat index values for the months of March and August were established as 1.697 and 6.208 respectively; with the annual heat index being 34.636.
3.  $PET_{HG}$  values were derived using mean, maximum and minimum temperature data from the chambers, plus the calculated extra-terrestrial radiation ( $R_a$ ) as employed in the FAO56 calculation (i.e. 25.7 and 39.8 MJ/m<sup>2</sup>/day for spring and summer respectively).

A further important assumption was that the maximum ET measured from each initially-saturated configuration during the ET laboratory trials corresponded to the measured PET. Calculated PET was contrasted against maximum measured ET rates (see Figure 6.3).



PET<sub>FAO56</sub> provided the most accurate estimate of PET for vegetated configurations in spring. However, in summer, PET was overestimated by approximately 0.7 mm/day. PET<sub>TH</sub> and PET<sub>HG</sub> most closely reflected measured maximum ET from vegetated configurations in summer conditions. However, in spring, both of these approaches under-predicted the measured maximum ET.

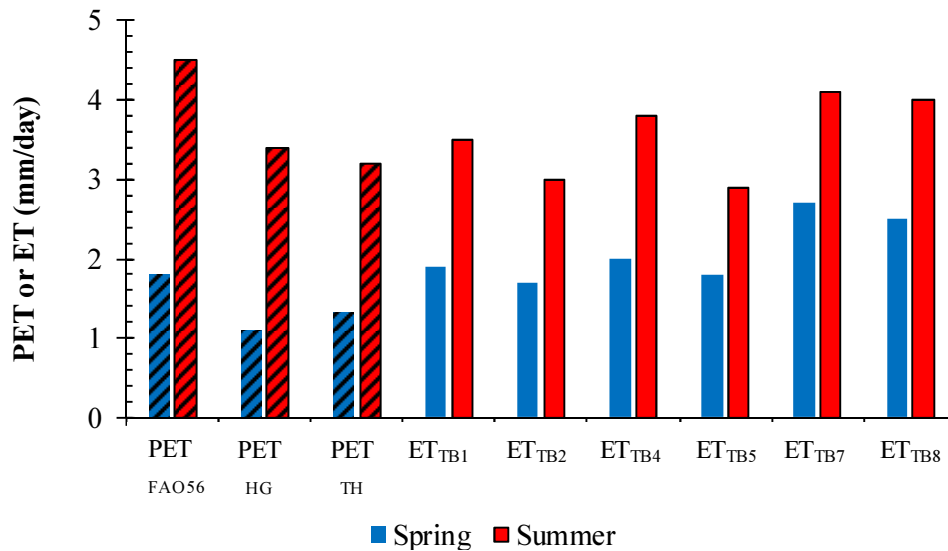


Figure 6.3: Calculated PET versus maximum measured ET

#### 6.4.1.3 Conclusions regarding the selection of the PET methodology

It has been demonstrated here that the choice of PET calculation methodology can affect the accuracy of ET predictions. Three methods were seen to produce reasonable estimates of the maximum measured ET. The Thornthwaite and Hargreaves approaches both have the benefit of simplicity, as they require only a limited number of typically-available data inputs. Either approach would therefore appear to be suitable for use in modelling ET from green roofs, particularly when simulating long-term hydrological response or when limited data availability prohibits the use of more complex calculations. However, the FAO56 approach is widely acknowledged (Cain, 1998; Beven, 2001; Liu & Todini, 2002) to be the most physically-based approach to estimating PET and is routinely adopted in many hydrological models. This approach has accepted methods to account for physical differences in vegetation treatments. The use of a crop factor and/or adjustments to the surface albedo parameter have the potential to further improve the accuracy of PET estimates for green roofs. The FAO56 approach was therefore adopted in the developed model. These further potential refinements will now be considered.

#### 6.4.1.4 Potential refinement to the FAO56 PET calculation – crop factor

The basic form of the FAO56 equation does not account for specific crop or soil characteristics (Allen *et al.*, 1998). However, there is an accepted method to account for any differences in the moisture consumption characteristics of the specific vegetation treatment. A crop coefficient,  $k_c$ , can be applied to convert PET for the reference crop of green grass to a PET estimate for the specific vegetation treatment as follows:

$$ET = PET_{FAO56} \cdot k_c \quad \text{Equation 6.10}$$

Therefore, where ET has been measured,  $k_c$  can be derived simply as:

$$k_c = ET \div PET_{FAO56} \quad \text{Equation 6.11}$$

Using measured values of seasonal mean ET for each of the three vegetation treatments and the calculated  $PET_{FAO56}$ , it was possible to calculate the values of  $k_c$  (see Table 6.1).

Table 6.1: Crop factor ( $k_c$ ) values

Vegetation	$k_c$ - Spring	$k_c$ - Summer
<b>Sedum</b>	1.06	0.78
<b>Meadow Flower</b>	1.11	0.85
<b>Non-vegetated</b>	1.50	0.91

No single value for  $k_c$  could be derived across both seasons for any of the vegetation treatments, with calculated values in summer always exceeding those in spring. Systematic differences were observed, as a result of both vegetation treatment and season. In both seasons,  $k_c$  was highest for non-vegetated treatments and lowest with Sedum vegetation; reflecting the high and low initial moisture consumption of each treatment respectively. In spring,  $k_c$  values were greater than 1, reflecting an under-estimation of PET. Yet, in summer,  $k_c$  values reflected a universal over-prediction of PET.

Clearly, the accuracy of ET predictions from a green roof can be improved by incorporating seasonally-adjusted empirical crop factors into the PET calculation. In this case, further work would be required to develop  $k_c$  values for autumn and winter seasons. In the developed model, the value of  $k_c$  was set equal to one, but with the capability of being changed to suit any specific crop.

It is acknowledged that the inclusion of further empirical factors to account for the physical influences of plant and season would negate one of the key drivers for the use of the FAO56 approach (i.e. the physical basis) and it is therefore pertinent to further consider the potential physical influences affecting these seasonal responses.

#### *6.4.1.5 Potential refinement to the FAO56 PET calculation – surface albedo*

It is hypothesised that the seasonal differences in crop factors can be explained, at least in part, by the different characteristics of an extensive green roof configuration when compared to natural growing environment in agricultural settings (i.e. environments for which PET formulae were originally developed):

- The hydraulic characteristics of green roof substrates differ to those of typical agricultural soils in several aspects, including depth (and overall storage capacity), porosity, permeability and organic/inorganic content. It is therefore reasonable to expect that important hydrological processes (e.g. capillary rise of moisture towards the surface) will be different. For example, a shallow construction (with lower  $S_{MAX}$ ) could immediately constrain ET relative to a ground level landscape that has a greater moisture capacity. Equally, this differential would be exacerbated in high PET (e.g. warm summer) conditions.
- The characteristics of green roof vegetation treatments are expected to be different to agricultural crops, in terms of both physiology (e.g. leaf succulence, root structures, age) and architecture (e.g. ground cover).

Surface albedo,  $\alpha$ , is understood to be influenced by the vegetation treatment, soil texture, climatic conditions, moisture content and solar declination; the latter leading to diurnal and seasonal changes in  $\alpha$  (Dobos, 2003). The FAO56 approach assumes that  $\alpha$  for a short-cropped grass reference crop is constant at 0.23. Measurements of albedo are not common. However,  $\alpha$  should be expected to vary with:

1. Configuration: Wark (2011) reported albedo values for Sedum of between 0.15 and 0.22. The Meadow Flower mix of wildflowers, grasses and Sedum would be expected to have a similar albedo to the short-cropped grass reference crop. Yet, dark bare soils typically absorb a greater amount of incoming radiation and Dobos (2003) estimated that such soils will have an albedo of between 0.1 and 0.2.

- Climate: Wark (2011) suggested that the reflectivity (and therefore  $\alpha$ ) of plants varied seasonally. A greater amount of radiation is typically reflected in summer than during periods of dormancy or cooler conditions, when more radiant heat tends to be absorbed.  $\alpha$  would therefore be expected to be higher in warm summer conditions.

It is therefore perhaps overly simplistic to assume that  $\alpha$  remains constant at 0.23 for all configurations and in different climatic conditions. Indeed, according to Ahuja *et al.* (2000),  $\alpha$  should be expected to vary between 0.05 and 0.45. Figure 6.4 demonstrates the sensitivity of  $PET_{FAO56}$  estimates to changes in  $\alpha$ .

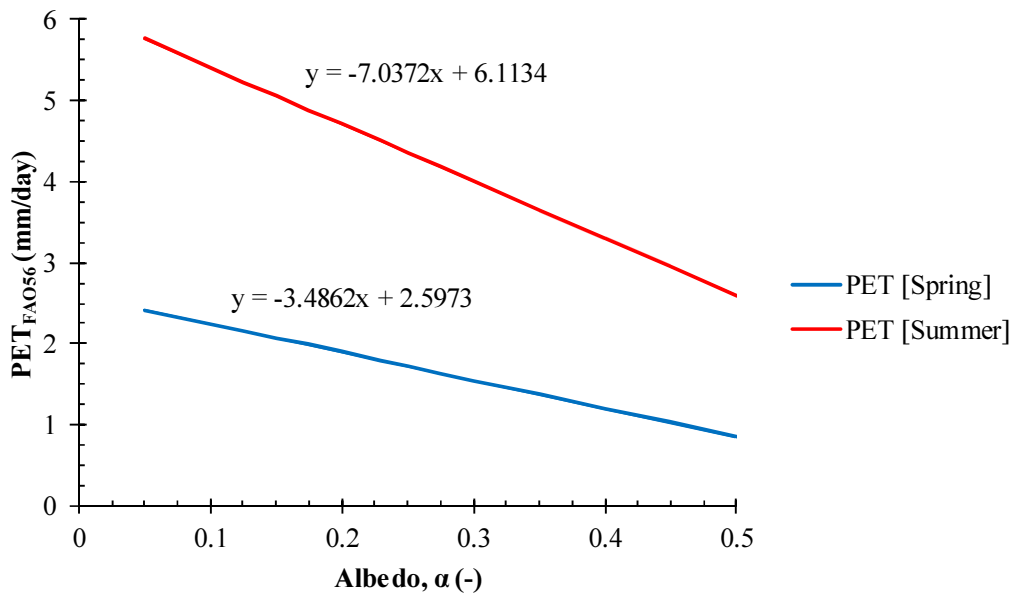


Figure 6.4: Sensitivity of  $PET_{FAO56}$  to albedo,  $\alpha$

$PET_{FAO56}$  is negatively correlated with  $\alpha$  and is approximately twice as sensitive to a change in  $\alpha$  in summer as it is in spring. A change in  $\alpha$  of 0.07 would affect PET by approximately 0.5 mm/day in summer or 0.25 mm/day in spring. Using the developed regression equations, it was possible to calculate the values of  $\alpha$  that would be necessary for  $PET_{FAO56}$  to equal maximum measured ET (see Table 6.2).

Table 6.2:  $PET_{FAO56}$  with calibrated plant- & season specific albedo coefficients

	<b>ET (spring) [mm/day]</b>	<b>ET (summer) [mm/day]</b>	<b>Calibrated <math>\alpha</math> (spring)</b>	<b>Calibrated <math>\alpha</math> (summer)</b>
Sedum_HLS	1.9	3.5	0.20	0.37
Sedum_SCS	1.7	3.0	0.26	0.44
MF_HLS	2.0	3.8	0.16	0.33
MF_SCS	1.8	2.9	0.23	0.45
HLS	2.7	4.1	-0.04	0.28
SCS	2.5	4.0	0.03	0.30
<b>Sedum mean</b>	<b>1.8</b>	<b>3.25</b>	<b>0.23</b>	<b>0.405</b>
<b>Meadow Flower mean</b>	<b>1.9</b>	<b>3.35</b>	<b>0.195</b>	<b>0.39</b>
<b>Non-vegetated mean</b>	<b>2.6</b>	<b>4.05</b>	<b>-0.005</b>	<b>0.29</b>

In spring, calibrated  $\alpha$  for vegetated configurations was similar to the reference crop albedo. However, for non-vegetated configurations, calibrated  $\alpha$  was much lower. Indeed, a negative  $\alpha$  would be necessary to reproduce the mean PET of 2.6 mm/day. Negative values of albedo are not possible. However, with  $\alpha$  set equal to 0.05 – a value that can be associated with dark bare soils (Ahuja *et al.*, 2000) –  $PET_{FAO56}$  would be within 0.2 mm of measured maximum ET of 2.43 mm/day. In summer, calibrated  $\alpha$  was higher.  $\alpha$  was in the region of 0.40 for vegetated configurations and 0.29 for non-vegetated configurations. This is consistent with the previous findings by Wark (2011). Calibrated  $\alpha$  values also differed according to substrate. This is consistent with the conclusions of Dobos (2003). Differences due to substrate were generally small in comparison to the influences of vegetation and season. However, HLS had a consistently lower calibrated  $\alpha$  than SCS.

The scope of this research programme did not extend to include measurements of  $\alpha$ . However, the empirical findings here suggest that the assumptions in FAO56 regarding  $\alpha$  could explain, at least in part, the differences between maximum measured ET and the reference PET value. As such, it is recommended that further studies are carried out in this research area. The FAO56 calculation methodology is widely acknowledged to be the most physically-based PET calculation methodology. Whilst an empirical crop factor can be used, a physical parameter, such as the surface albedo, would improve the physical basis of the modelling approach.

#### 6.4.1.6 Conclusions regarding PET method

The FAO56 method was included in the model because it has a strong physical basis, accounting for the combined influences of heat energy and vapour transfer. Further accepted refinements, such as empirical crop factors, are available to tailor the reference PET value to suit the specific configuration. Yet, there appears to be scope to further refine this approach by challenging at least one simplifying assumption – questioning the physical basis of a constant albedo coefficient instead of an albedo that varies with vegetation type and climatic influences.

### 6.4.2 Soil moisture extraction functions (SMEFs)

#### 6.4.2.1 Evaluation of the suitability of existing SMEFs in the modelling of ET

Many ET prediction tools assume PET (i.e. plentiful supply). However, it has been shown here that ET is not always equal to PET. Any ET model that fails to factor PET to account for moisture availability will typically overestimate ET losses; particularly when longer ADWPs are considered. Models that account for moisture availability are expected to increase the accuracy of ET (and runoff) predictions. Here, soil moisture extraction functions (SMEFs) were used in the calculation of ET. Initially, the suitability of existing SMEFs was reviewed. Subsequently, new potential SMEFs were proposed and evaluated.

Five of the SMEFs that were considered by Zhao *et al.* (2013) – as introduced in Equation 2.28 through to Equation 2.32 – provide a good representation of the different decay functions that model daily ET ( $ET_D$ ) as a proportion of PET with falling  $S_e$ . Figure 6.5 compares each of the five SMEFs with the experimental seasonal mean data from the ET laboratory trials.

Seasonal mean  $ET/PET$  decayed almost linearly with  $S_e$  in both spring and summer. A strong correlation was evident between the  $S_e$  Linear SMEF and seasonal mean  $ET/PET$  across both seasons ( $R^2 = 0.944$ ). As such, it was expected that the  $S_e$  Linear SMEF would predict seasonal mean ET with good accuracy.

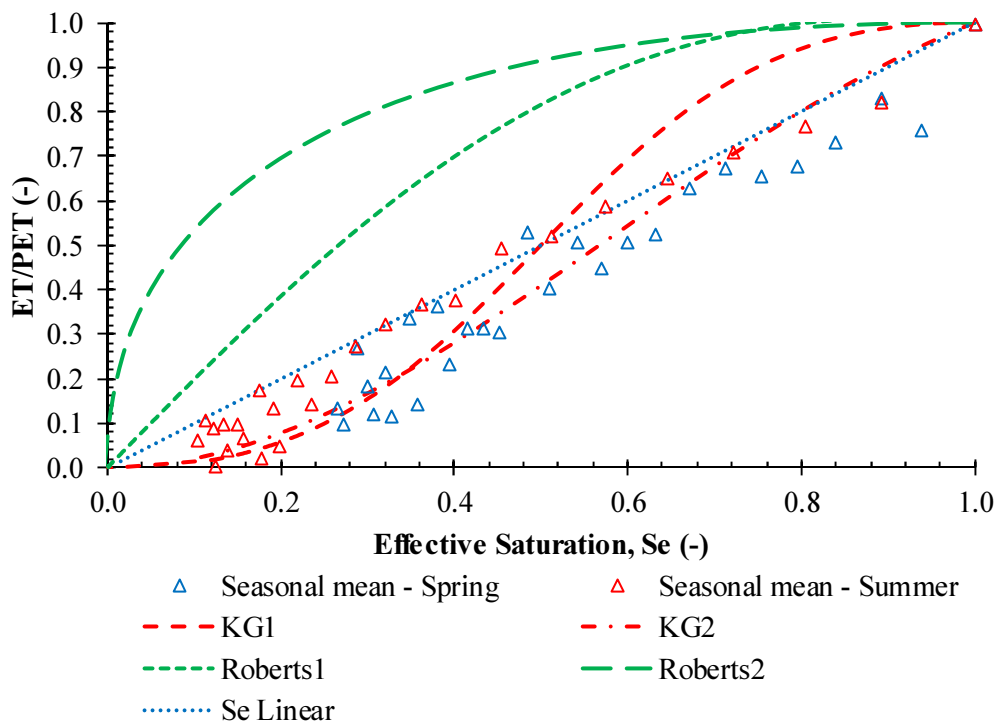


Figure 6.5: Existing Soil Moisture Extraction Functions with seasonal mean data

However, the relationship between  $ET/PET$  and  $S_e$  varied due to both configuration and seasonal climate (see Figure 6.6).

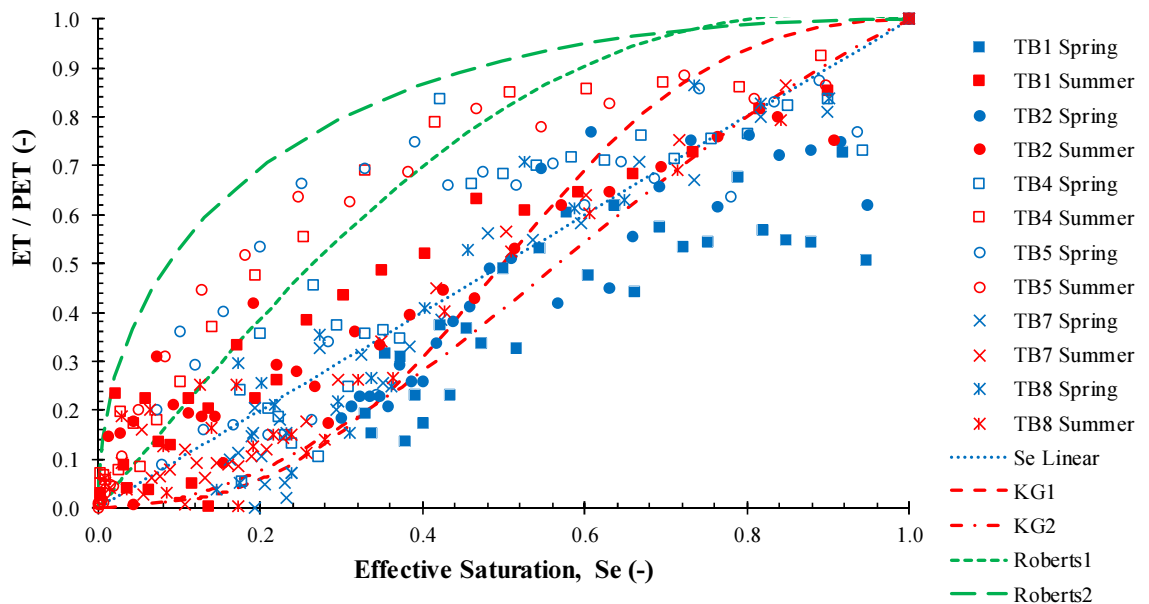


Figure 6.6: Existing SMEFs with configuration mean data

A broadly linear decay in  $ET/PET$  was observed with both Sedum vegetation and non-vegetated configurations. Meadow Flower configurations typically had high rates of ET

until, at relatively low levels of available moisture, ET quickly converged towards zero. A nonlinear SMEF would therefore be most suitable to this vegetation type.

In many cases, the initial depletion in moisture content (i.e. when ET equalled  $PET$ ) led to an instant reduction in ET relative to  $PET$ , despite  $S_e$  remaining very high (i.e.  $> 0.9$ ). ET was only equal to  $PET$  for the initial 24 hours following saturation. This was particularly evident from Sedum-vegetated configurations in spring. None of the considered existing SMEFs captured this behaviour. However, ET from Sedum and non-vegetated configurations was best represented by the  $S_e$  Linear and Koitzsch & Golf ( $KG$ ) SMEFs. The decay in ET from Meadow Flower configurations was best represented by the two Roberts SMEFs, particularly in summer. The use of each of these five SMEFs to predict ET for each configuration was therefore considered further.  $ET_{PRED}$  was compared against  $ET_{CUM}$  (as measured during the ET trials) and cumulative PET ( $PET_{CUM}$ ) after a range of ADWPs (i.e. 7, 14 and 28 days).

Figure 6.7 compares actual, potential and predicted ET from Sedum-vegetated configurations. Here, even for an ADWP of 7 days, an assumption that ET was equal to  $PET$  led to cumulative ET being overestimated by between 3.0-4.6 mm in spring and 5.1-5.7 mm in summer. These differences increased further when longer ADWPs were considered. The  $S_e$  Linear SMEF produced the most accurate predictions of ET from Sedum-vegetated configurations when applied across both seasons. However, in spring alone, ET was most accurately predicted by the  $KG2$  SMEF. In spring, none of the SMEFs fully captured the conservative ET from TB1 at ADWPs of up to 7 days. The  $KG1$  SMEF was most accurate here. However, a higher-than-observed decay was then predicted at longer ADWPs. Over a 28 day ADWP, predictive errors were lowest (0.3-1.1 mm) with the  $KG2$  SMEF, compared to 2.1-3.8 mm ( $S_e$  Linear), 2.5-3.6 mm ( $KG1$ ) and 6.8-11.1 mm (either of the Roberts SMEFs). In summer, the  $S_e$  Linear SMEF best reproduced observed ET. After 7 days, errors were between just 0.2-0.4 mm, increasing to 0.3-2.0 mm after 14 days. Errors with other methods were much higher at this time (i.e. 8.0 mm [ $KG1$ ], 4.5 mm [ $KG2$ ], 5.3 mm [ $Roberts1$ ] and 8.7 mm [ $Roberts2$ ]).



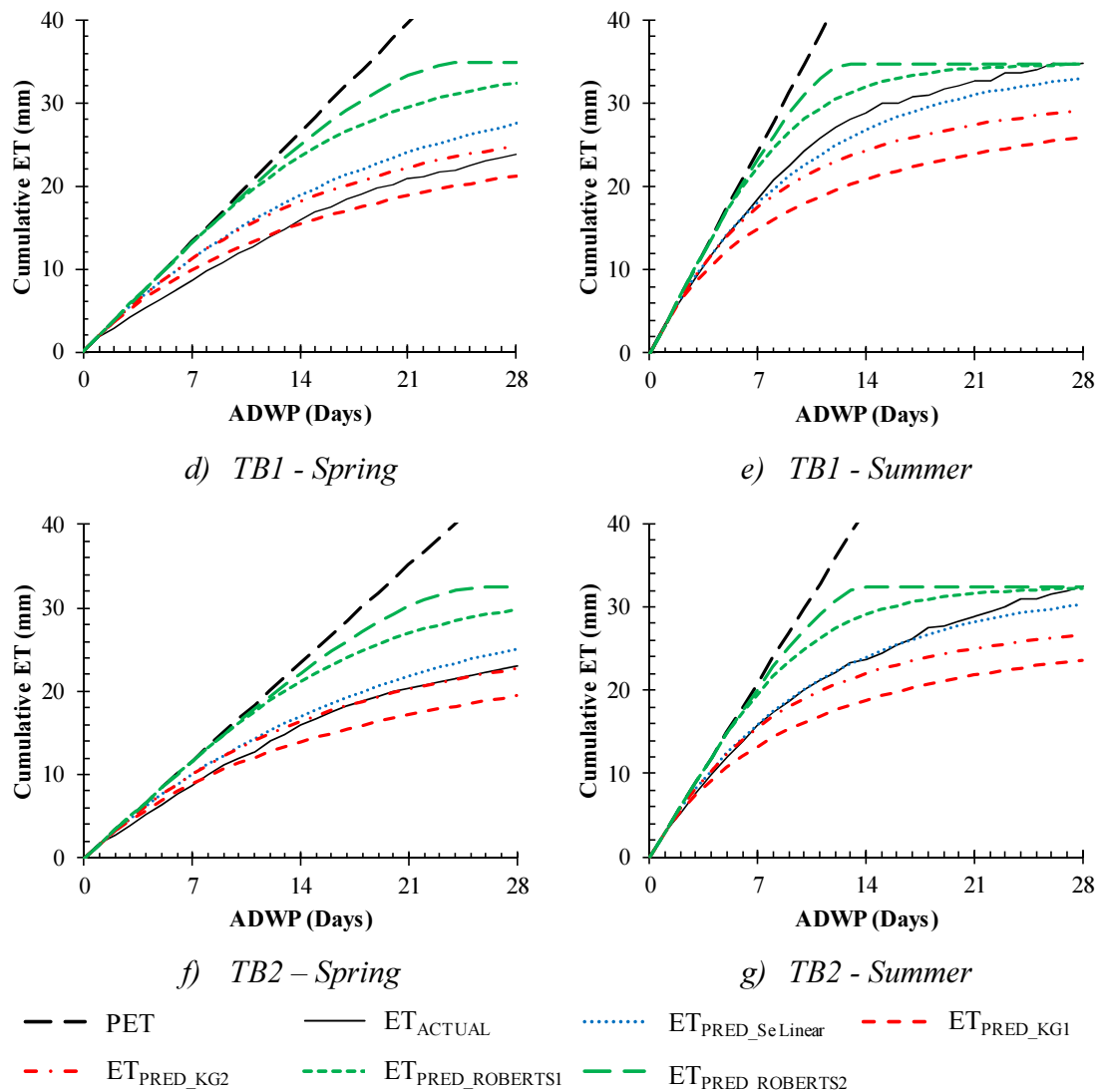


Figure 6.7:  $ET$  vs  $ET_{PRED}$  for *Sedum*-vegetated configurations using existing SMEFs

For Meadow Flower configurations, no single SMEF was able to accurately predict ET across both seasons (see Figure 6.8). In spring, accuracy was highest with the *Se Linear* approach (PBIAS < 10% throughout the 28 day ADWP). Maximum predictive errors were 2.0 mm after 14 days and 2.9 mm after 28 days. However, in summer, the *Se Linear* approach did not mimic the very high initial ET rates; such that ET was under-predicted by 5.4 mm after 14 days. Here, the most accurate predictions were generated using the *Roberts1 SMEF* (PBIAS < 10%). After 14 days, predictive errors using this SMEF were between 0.6-1.3 mm. Both *Roberts SMEFs* instantly overestimated ET from Meadow Flower in spring, with errors reaching up to 4.7 mm after 7 days (when PBIAS was 19.5%). To predict ET from thirsty vegetation treatments, such as Meadow Flower, in

both high (e.g. summer) and low (e.g. spring) PET conditions, either a seasonally-adjusted or two separate functions would appear to be required.

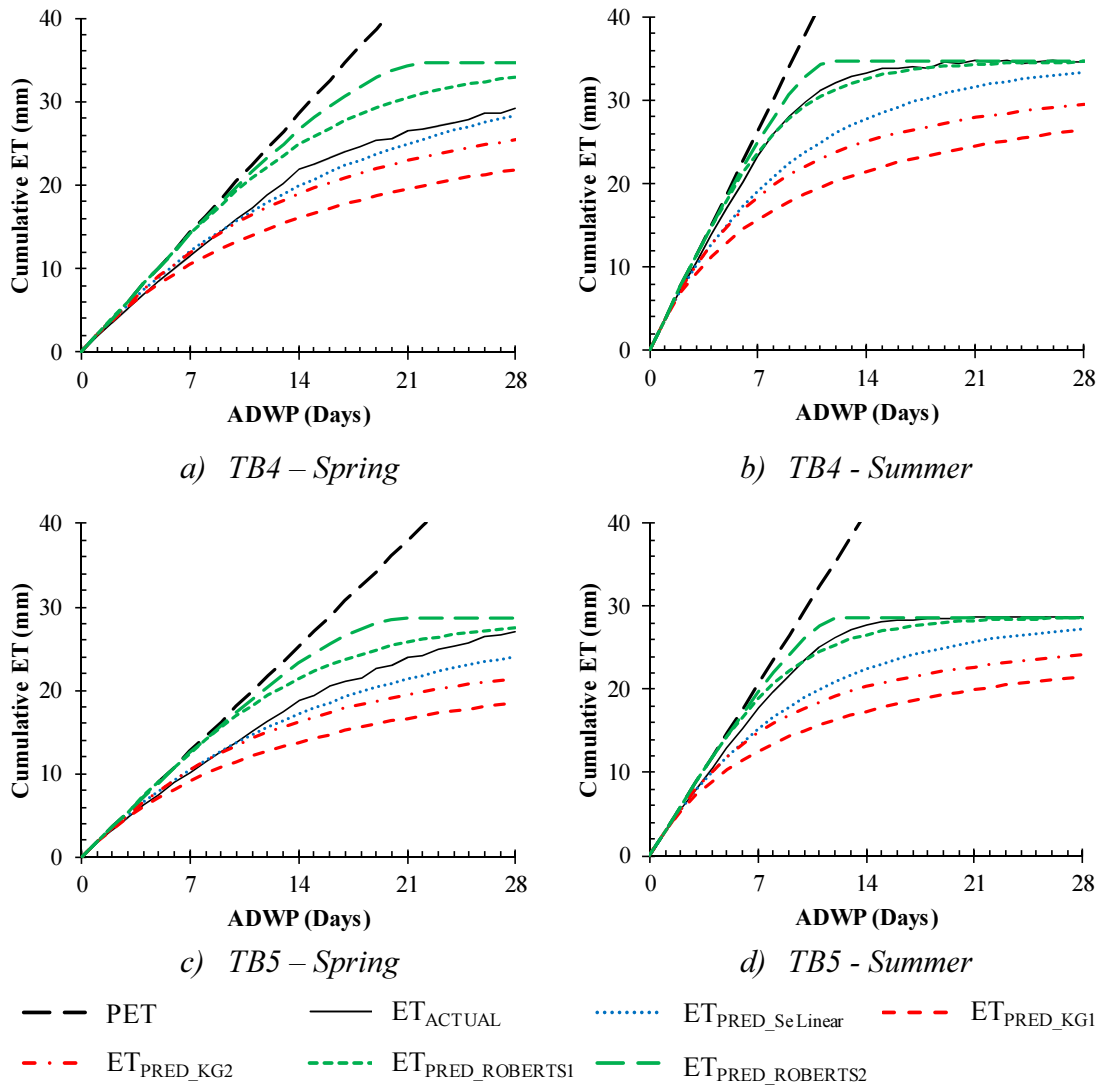


Figure 6.8:  $ET$  vs  $ET_{PRED}$  for Meadow Flower configurations using existing SMEFs

$ET$  was predicted with good accuracy for non-vegetated TBs across both seasons using *KG2* and *S<sub>e</sub> Linear* SMEFs (see Figure 6.9). Accuracy was very good over the initial 7 days. Thereafter, the *S<sub>e</sub> Linear* SMEF tended to marginally overestimate  $ET$  with errors, after 14 days, of up to 0.4 mm (in spring) and 2.1 mm (in summer). Conversely, the *KG2* SMEF generally under-predicted  $ET$  (by up to 1.6 mm after 14 days in spring and 1.5 mm in summer). At longer ADWPs, the *KG2* SMEF predicted  $ET$  in spring with better accuracy than the *S<sub>e</sub> Linear* SMEF. The reverse was true in summer. Either of these two SMEFs could feasibly be used to predict  $ET$  from non-vegetated configurations.

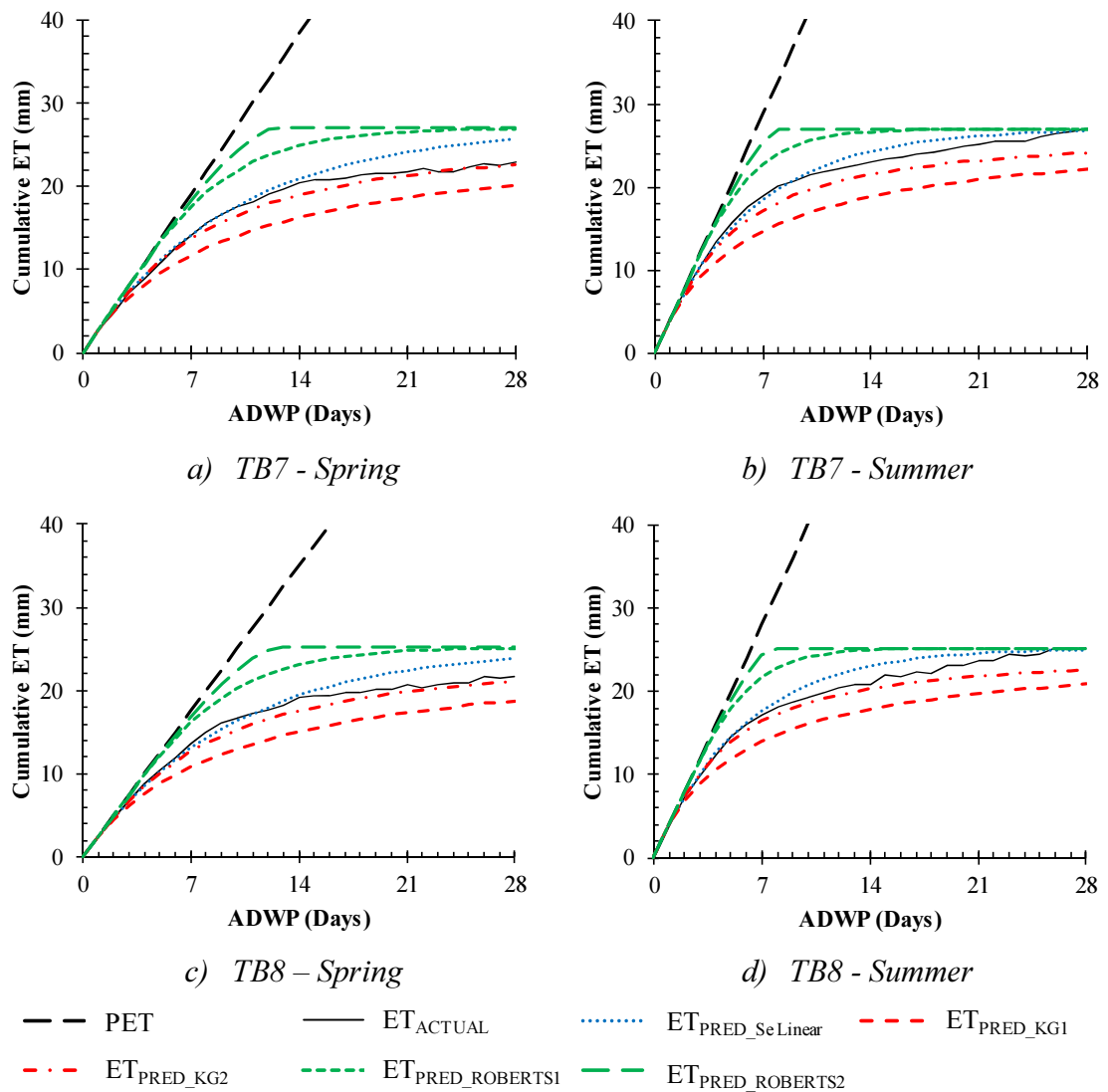


Figure 6.9:  $ET$  vs  $ET_{PRED}$  for non-vegetated configurations using existing SMEFs

#### 6.4.2.2 Conclusions regarding use of existing SMEFs

Overall, the  $S_e$  Linear SMEF provided the most accurate predictions of ET across the full range of ADWPs, seasons and configurations considered here. ET was, however, underestimated when this approach was applied to the highest PET conditions (e.g. Meadow Flower in summer). ET was over-predicted by the Roberts2 SMEF in all instances and by the Roberts1 SMEF for all scenarios except Meadow Flower configurations in summer. The KG1 SMEF underestimated ET in all instances. The KG2 SMEF consistently produced more accurate predictions than the KG1 or either of the Roberts SMEFs. However, accuracy was typically lower than with the  $S_e$  Linear SMEF.

The use of the  $S_e$  Linear SMEF is justifiable on the basis that (a) it underpins the most consistently accurate predictions of ET across all configurations and seasons, and (b) it is similar to the best-fit line for the  $ET/PET$  and  $S_e$  relationship ( $y = 0.927x + 0.029$ ). This best-fit line reflects a strong and relatively linear correlation ( $R^2 = 0.796$ ) between  $ET/PET$  and  $S_e$ . For most extensive green roof configurations, the  $S_e$  Linear SMEF will predict ET with a good (or very good) level of accuracy. Stovin *et al.* (2013) used the  $S_e$  Linear SMEF justifying its choice against international data (Berghage *et al.*, 2007; Voyde *et al.*, 2010b). It must therefore be acknowledged that the practical value of further refinements to this simple approach may be limited to certain configurations and/or extreme climate conditions. The additional modelling complexity would therefore need to be considered against the marginal benefit to predictive accuracy.

#### 6.4.2.3 New SMEF proposals

In Chapter 5, it was demonstrated that the relationship between  $ET/PET$  and  $S_e$  was (a) affected by configuration (i.e. vegetation and substrate) and climate, and (b) highly nonlinear for certain configurations. In this section, new SMEFs that capture configuration-specific behaviour were developed and evaluated. Whilst it is acknowledged that any benefits to predictive accuracy may be marginal, the capacity for a model to distinguish between the hydrological responses of different configurations would be beneficial. Three new SMEFs were proposed and contrasted against each other and against the  $S_e$  Linear SMEF. Three SMEFs were developed to account for one of two important influences upon a green roof's hydrological response. Two of the SMEFs are underpinned by the substrate's hydraulic characteristics (SWCC). The third SMEF accounts for the seasonal moisture consumption of specific vegetation treatments.

#### 6.4.2.4 SWCC-based SMEFs

Soil matric potential ( $\psi$ ) varies as a function of  $\theta$ . Conceptually, a model that is derived from the SWCC would be expected to improve the accuracy of modelling moisture balance. The developed SMEFs link the decay in ET to a resistance to moisture balance change ( $\psi$ ).  $\psi$  was calculated by converting measurements of  $\theta$  using the SWCC equations (Equation 3.1 for HLS-based configurations and Equation 3.2 for SCS-based equations). There is a negative correlation between  $ET/PET$  and  $\psi$  (see Figure 6.10).

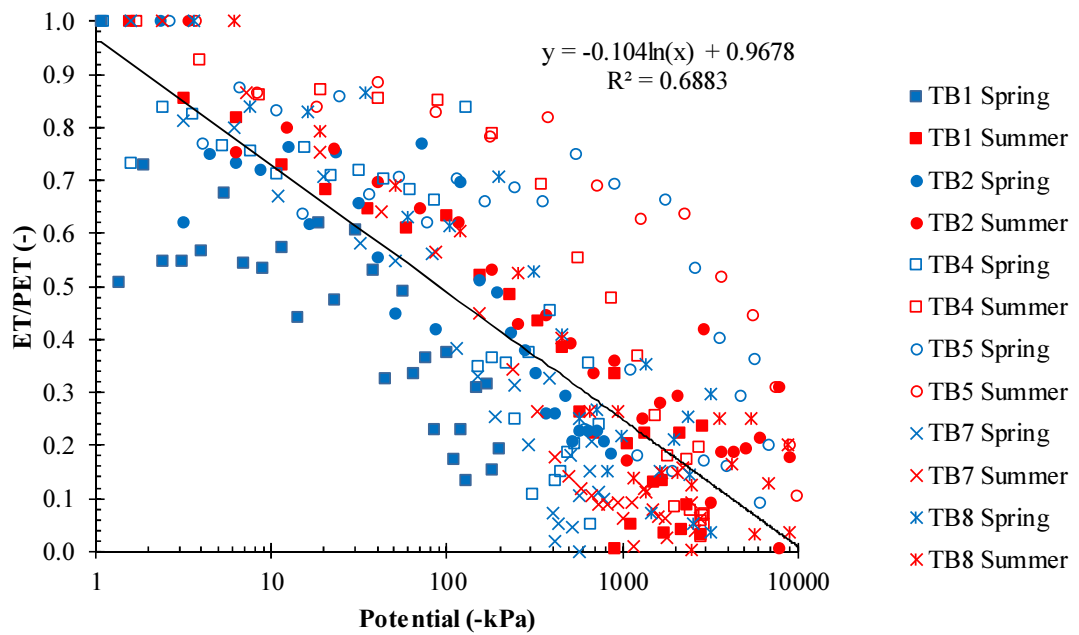


Figure 6.10: *ET/PET – Potential Relationship*

The correlation between  $ET/PET$  and  $\psi$  ( $R^2 = 0.688$ ) was weaker than the correlation between  $ET/PET$  and  $S_e$  ( $R^2 = 0.796$ ). There was no evidence that the use of  $\psi$  as a modelling parameter instead of  $\theta$  would increase accuracy. Indeed, the findings of this research indicate that seasonal climate and vegetation treatment are typically more important influences on ET than a soil's hydraulic characteristics (except when contrasting very different substrate types, e.g. LECA versus HLS or SCS). However,  $\psi$  is the driving force for moisture balance changes in the soil matrix and it is still relevant to test one of the initial hypotheses of this research, i.e. accounting for  $\psi$  in the model would increase its physical basis and accuracy.

Diffusivity is the hydraulic characteristic that is most closely associated with ET. Diffusivity represents the rate at which moisture can move in an upward direction through the soil matrix as a result of capillarity. The van Genuchten (1980) hydraulic functions for soil-water retention, hydraulic conductivity and diffusivity are widely used in hydrological modelling. These functions all include empirical shape factors that are related to a soil's hydraulic characteristics, as derived from the SWCC. Here, the SWCC data for HLS and SCS substrates was inputted into the Hydrus-1D software (Simunek *et al.*, 2008a; Simunek *et al.*, 2008b) to establish values for shape factors that could be used to calculate diffusivity (see Table 6.3).  $K_s$  values were inputted as per characteristic tests (see Chapter 3).  $\ell$  was set to 0.5, as described in Chapter 2.

Table 6.3: van Genuchten-Mualem parameter values for HLS and SCS

	$\tau$	$m$	$\beta$	$\ell$	$K_s$
HLS	0.0626	0.3299	1.4924	0.5	15
SCS	0.1422	0.2974	1.4233	0.5	35

Before calculating diffusivity using the van Genuchten-Mualem parameters, the accuracy with which these parameters reproduced the SWCC was first checked and it was seen to closely resemble the SWCCs presented in Chapter 3 (see Figure 6.11).

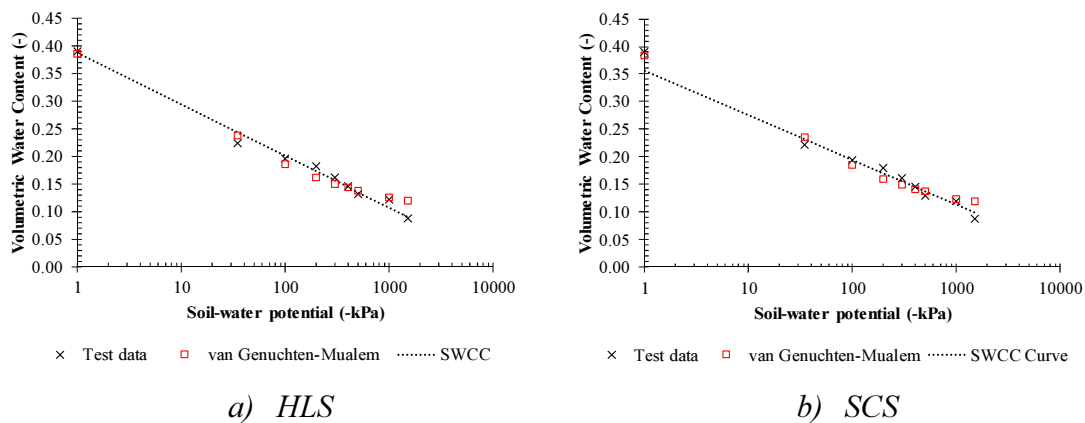


Figure 6.11: SWCC reproduced using the van Genuchten-Mualem approach

Equation 2.15 was used to calculate diffusivity for the range between  $\theta_{FC}$  and  $\theta_{<PWP}$  (at intervals of 0.01 of  $\theta$ ). Then diffusivity was expressed relative to the rate of diffusivity at  $\theta_{FC}$  as Equation 6.12:

$$D_r = \frac{D(\theta)}{D(\theta_{FC})} \tag{Equation 6.12}$$

Where  $D_r$  is the relative diffusivity and  $D(\theta)$  and  $D(\theta_{FC})$  are the rate of diffusivity at the residual moisture content and field capacity respectively.

As Figure 6.12 demonstrates, the  $D_r - S_e$  relationship is similar for HLS and SCS substrates. The relationship between  $D_r$  and  $S_e$  is almost identical for HLS and SCS when  $S_e$  is greater than 0.5. At lower values of  $S_e$ ,  $D_r$  is marginally lower for SCS than HLS. It is therefore expected that a single diffusivity-based function could be applied for both substrates without important losses in accuracy.

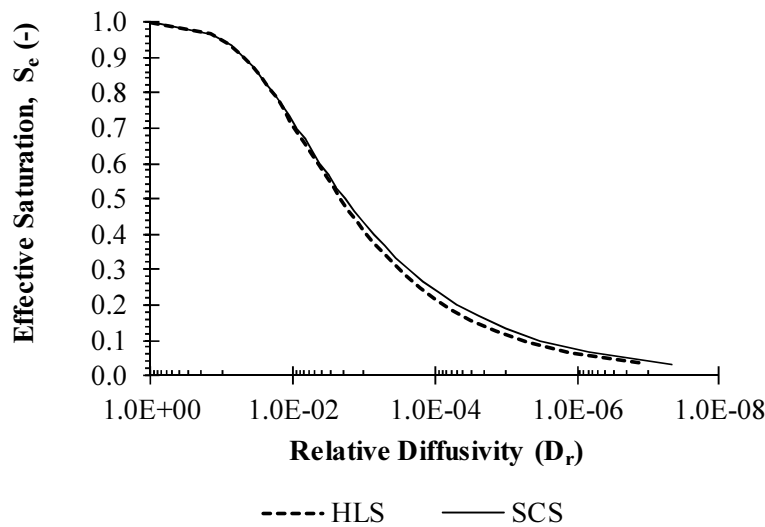


Figure 6.12: Relative diffusivity using van Genuchten-Mualem approach

Plotting  $ET/PET$  against  $D_r$  using their common relationship with  $S_e$ , Figure 6.13 presents the correlation of two potential diffusivity-based SMEFs (a logarithmic and a nonlinear function) to  $ET$  measured from both substrates.

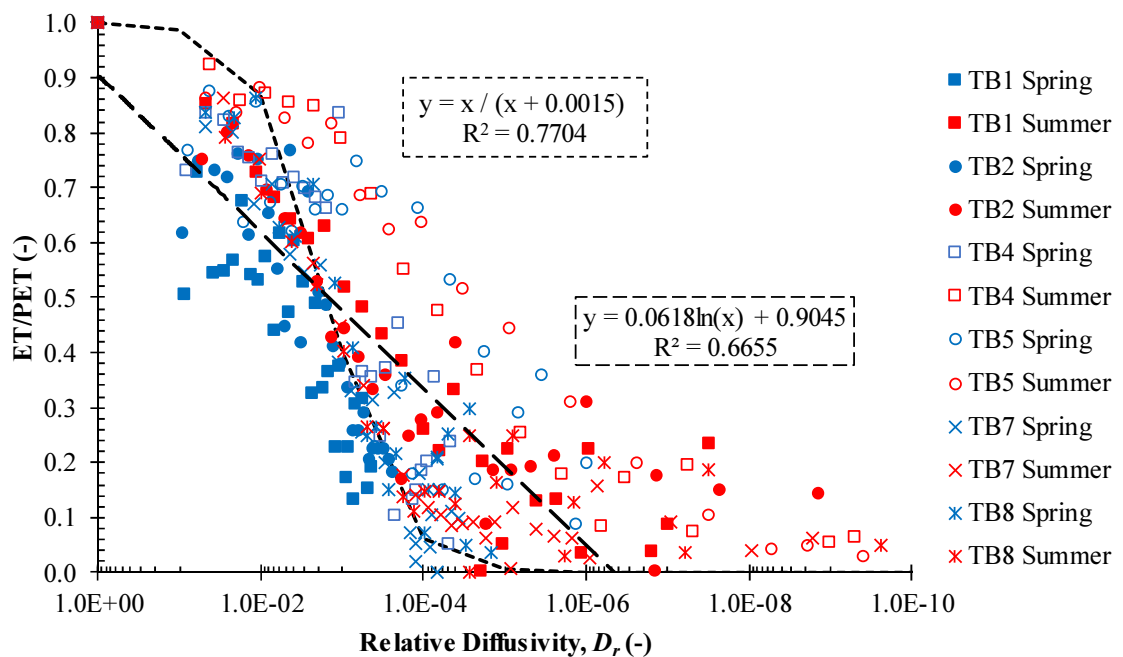


Figure 6.13: Correlation of Relative Diffusivity to  $ET/PET$

The decay in  $ET/PET$  as a function of  $S_e$  has been shown to vary due to vegetation. With Meadow Flower (particularly in summer), this decay was nonlinear. With Sedum and non-vegetated configurations, this decay was approximately linear. In view of the nature of the relationship between  $ET/PET$  and  $D_r$ , two types of function were considered here.

Firstly, a logarithmic function (*DLogFit*):

$$ET_{PRED} = PET \cdot 0.0618 \cdot \ln D_r + 0.9045 \quad \text{Equation 6.13}$$

Here, the best logarithmic function (*DLogFit*, as Equation 6.13) was more weakly correlated with observed  $ET/PET$  ( $R^2 = 0.665$ ) than the  $ET/PET-\psi$  and  $ET/PET-S_e$  relationships. *DLogFit* was most strongly correlated with measured values in spring. This equation produces negative values of  $ET/PET$  for values of  $D_r < 1 \times 10^{-6}$ . In these cases,  $ET/PET$  was assumed to be zero.

The second function was a nonlinear equation (*DNonlinFit*):

$$ET_{PRED} = PET \cdot \left( \frac{D_r}{D_r + 0.0015} \right) \quad \text{Equation 6.14}$$

Here, a stronger correlation ( $R^2 = 0.770$ ) was observed. This function predicted higher  $ET/PET$  than the *DLogFit SMEF* until  $S_e$  was equal to 0.4. Both approaches underestimated ET in summer; particularly with vegetated configurations. Correlation was strongest with non-vegetated configurations.

The practical implications of using these two diffusivity-based functions will be considered later in this section, alongside a third function.

#### 6.4.2.5 A seasonally-adjusted and vegetation-specific $S_e$ SMEF

A third SMEF was developed to capture the specific seasonal moisture consumption patterns of different vegetation treatments. This function is based upon the  $S_e$  *Linear* approach, but with an empirical power coefficient applied to  $S_e$ . This exponential form of equation ( $S_e$  *Power*) – as Equation 6.15 – is consistent with the patterns of decay identified in Chapter 5.

$$ET_{PRED} = PET \cdot S_e^{1/\varepsilon} \quad \text{Equation 6.15}$$

Where  $\varepsilon$  is a coefficient that is adjusted to suit a vegetation's seasonal response. A value for  $\varepsilon$  of less than one represents a faster reduction in  $ET/PET$  relative to  $S_e$ . A higher value of  $\varepsilon$  reflects a lower dependence of the configuration upon moisture availability, such that  $ET/PET$  is higher than  $S_e$  at virtually all stages. A nonlinear least squares approach, using



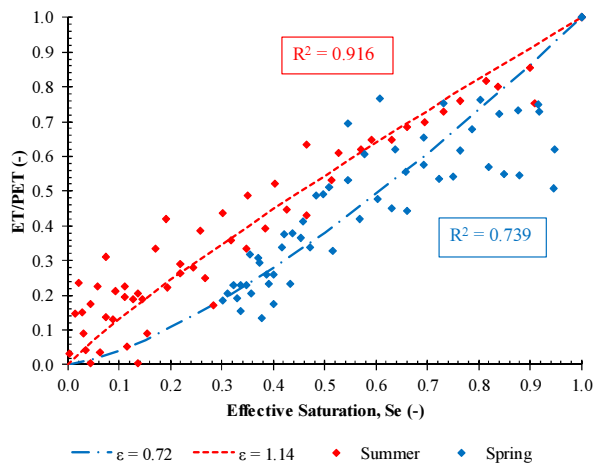
the *curvefit* toolbox in MATLAB (2007) determined best-fit coefficients for each configuration and season (see Table 6.4).

Table 6.4: Modelling decay parameters

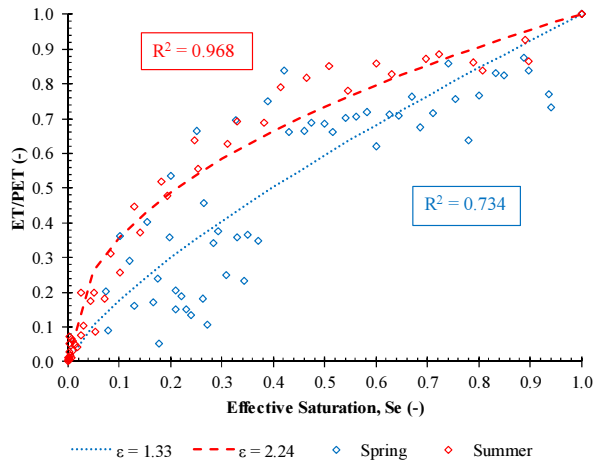
Vegetation Treatment	Test Bed	Spring		Summer	
		$\varepsilon$	$R^2$	$\varepsilon$	$R^2$
Sedum	TB1	0.72	0.589	1.14	0.895
	TB2				
Meadow Flower	TB4	1.33	0.712	2.24	0.946
	TB5				
Non-vegetated	TB7	0.82	0.817	0.87	0.889
	TB8				

$R^2$  values generally reflected a good correlation of the model outputs with observations. The weakest correlation was evident with Sedum in spring ( $R^2 = 0.589$ ). This is indicative of the scatter in the ET data for TB1 in spring (an even lower correlation,  $R^2 = 0.374$ , was recorded for the  $S_e$  Linear approach). Overall, the correlation between actual and modelled  $ET/PET$  was higher when the  $S_e$  Power SMEF was used ( $R^2 = 0.880$ ) compared to the  $S_e$  Linear SMEF ( $R^2 = 0.796$ ). This trend of stronger correlation by using the  $S_e$  Power SMEF was observed across all vegetation treatments and seasons.

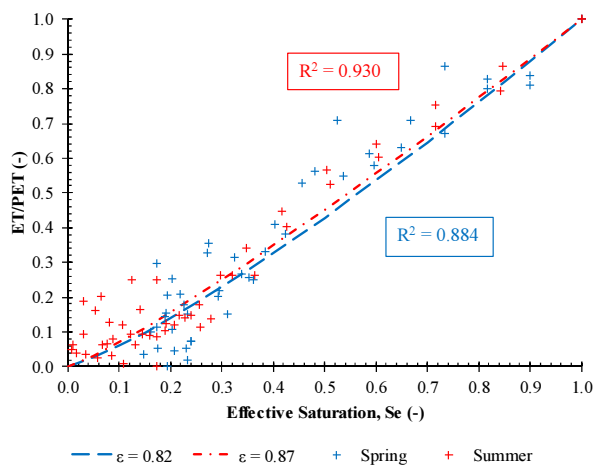
Figure 6.14 demonstrates how well-correlated the outputs of the  $S_e$  Power SMEF are with observations of  $ET/PET$  for each vegetation treatment.



a) *Sedum-vegetated configurations*



b) *Meadow Flower configurations*



c) *Non-vegetated configurations*

The greatest improvement in predictive accuracy obtained through the employment of the  $S_e$  *Power SMEF* (rather than the  $S_e$  *Linear SMEF*) was with Meadow Flower configurations in summer conditions. Here,  $R^2$  was 0.968 compared to 0.868 with the  $S_e$  *Linear SMEF*.

The main deficiency of the  $S_e$  *Linear SMEF* was the predictive accuracy of ET from Meadow Flower in summer. The  $S_e$  *Power SMEF* addresses this issue; providing improved accuracy of predictions here. For all other configurations and climatic scenarios, the accuracy of the  $S_e$  *Power* and  $S_e$  *Linear* approaches was similar. The  $S_e$  *Power SMEF* would therefore be expected to improve predictive accuracy for thirsty vegetation treatments in high PET conditions (and therefore correct the deficiency of the  $S_e$  *Linear* approach) whilst equally predicting ET from other configurations with similar, if not better accuracy.

Figure 6.14: *ET/PET vs  $S_e$  using the  $S_e$  Power SMEF*

Further research into plant moisture consumption patterns (e.g. the relationship between plant albedo and moisture) could, in future, provide a physical basis for the empirical

shape factors presented here. The feasibility of using these newly-developed SMEFs to improve the accuracy of ET predictions will now be assessed by establishing their capacity to reproduce the ET trends that were measured and presented in Chapter 5.

#### 6.4.2.6 Appraisal of the newly-developed SMEFs

The predictions generated by the three new SMEFs and the  $S_e$  Linear SMEF were compared against measured ( $ET_{CUM}$ ) and potential ( $PET_{CUM}$ ) for Sedum configurations (see Figure 6.15).

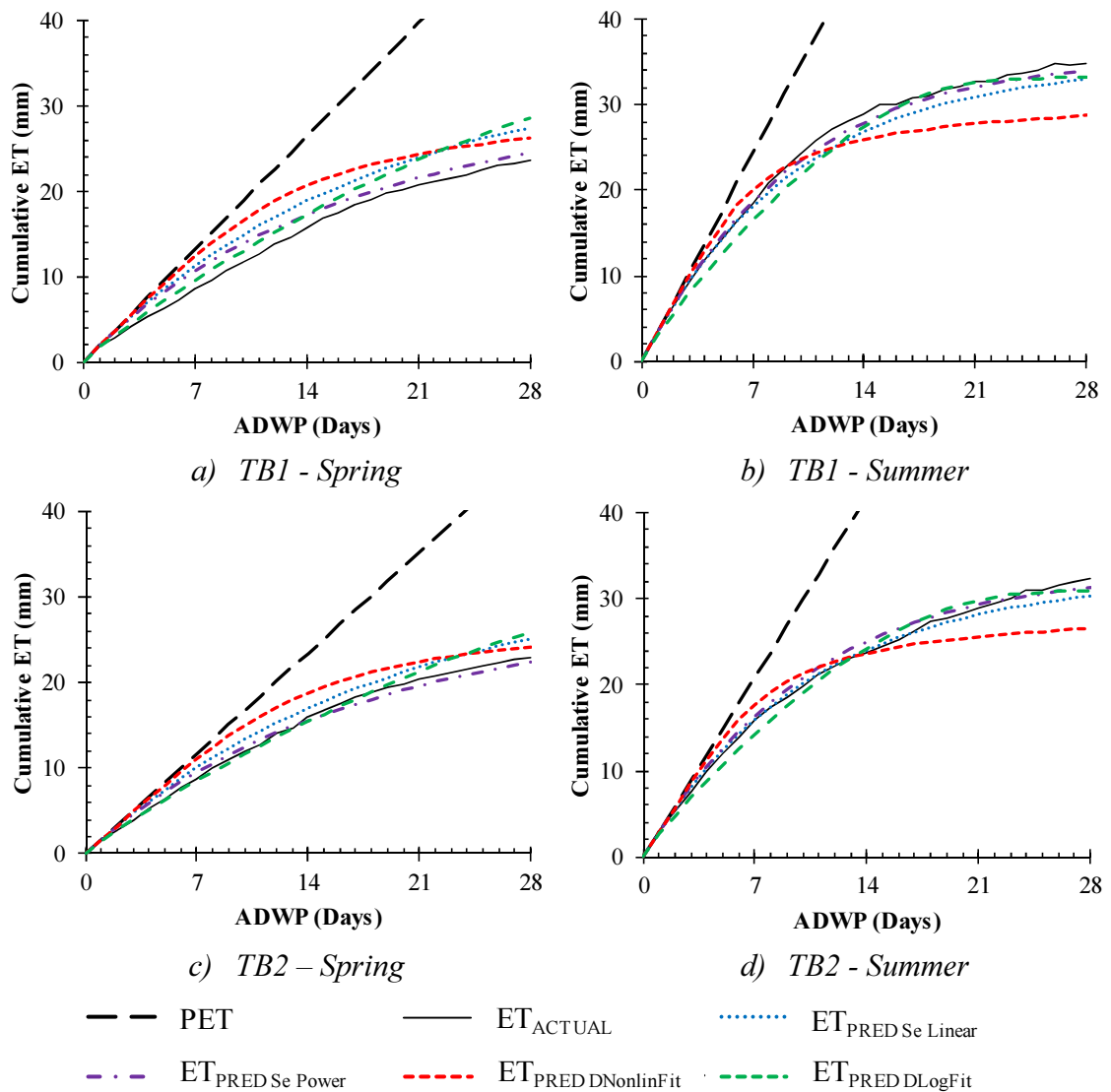


Figure 6.15:  $ET$  vs  $ET_{PRED}$  for Sedum-vegetated configurations using new SMEFs

Across both seasons, the  $S_e$  Power SMEF predicted ET from Sedum-vegetated configurations with the greatest accuracy. ET was overestimated from TB1 at short ADWPs (e.g. by 2 mm after 7 days). Generally, predictive accuracy was either good or

very good (with a minimum NSME of 0.73). The *DLogFit SMEF* also improved predictive accuracy in spring (relative to the *Se Linear SMEF*). However, in summer, the *DLogFit* approach underestimated ET at short ADWPs (e.g. 7 days) to a greater extent than the *Se Linear SMEF*. The *DNonlinFit SMEF* typically overestimated ET at shorter ADWPs and underestimated ET after longer ADWPs.

Figure 6.16 compares measured and predicted ET from Meadow Flower configurations.

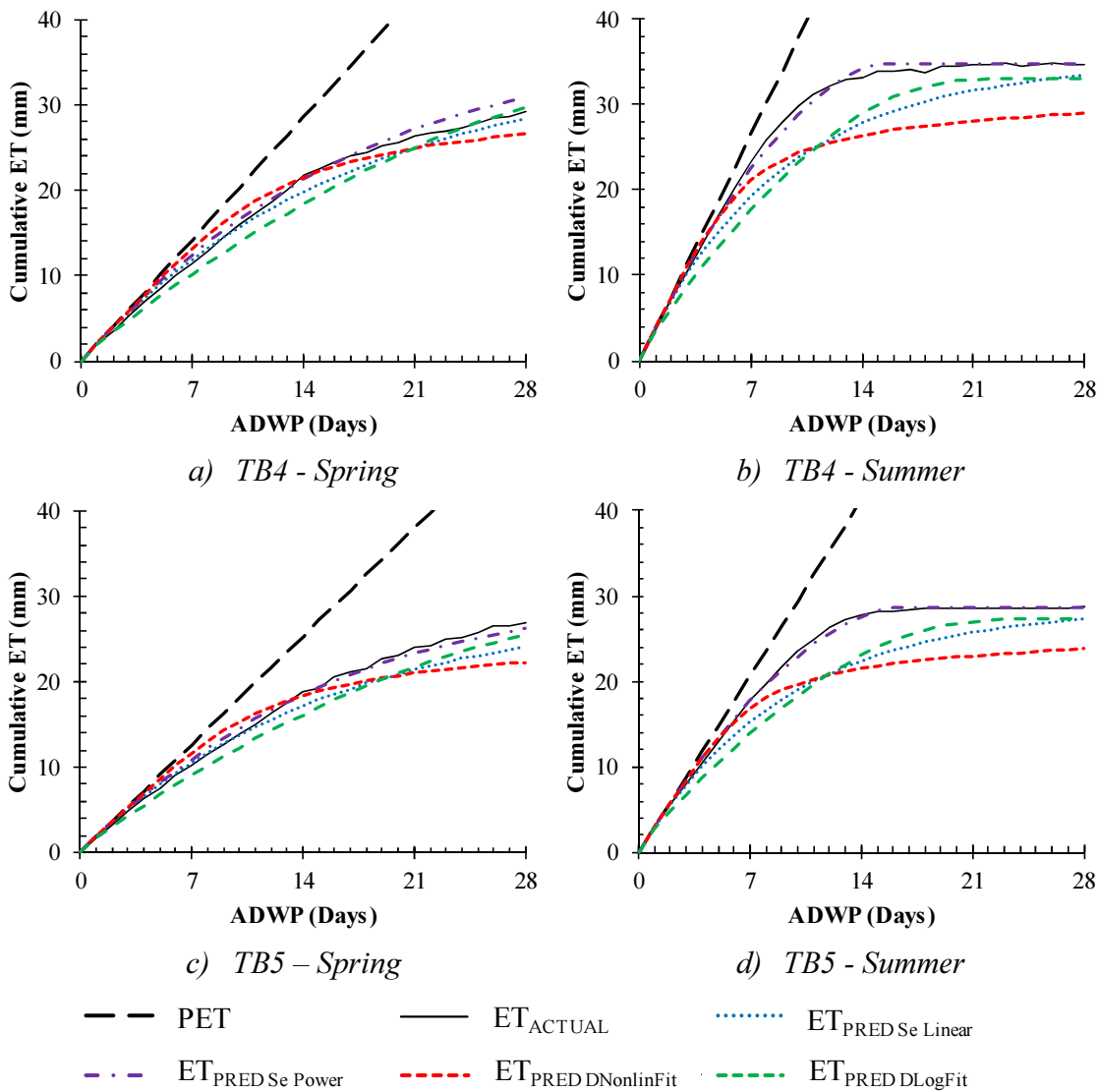


Figure 6.16: ET vs ET<sub>PRED</sub> for Meadow Flower configurations using new SMEFs

After ADWPs of 7 and 14 days, ET<sub>PRED</sub> using the *Se Power SMEF* accurately reflected observations, with good or very good accuracy (i.e. *PBIAS* < 10%) in all instances. In both seasons, ET<sub>PRED</sub> was within  $\pm 1.0$  mm of ET<sub>CUM</sub>. None of the other SMEFs was able to reproduce the response of Meadow Flower in summer conditions. After 14 days,

$ET_{PRED}$  was under-predicted by 5.4 mm ( $S_e$  Linear), 4.8 mm ( $DLogFit$ ) and 6.8 mm ( $DNonlinFit$ ).

Figure 6.17 shows the accuracy with which the newly-developed SMEFs predicted ET measured from non-vegetated configurations.

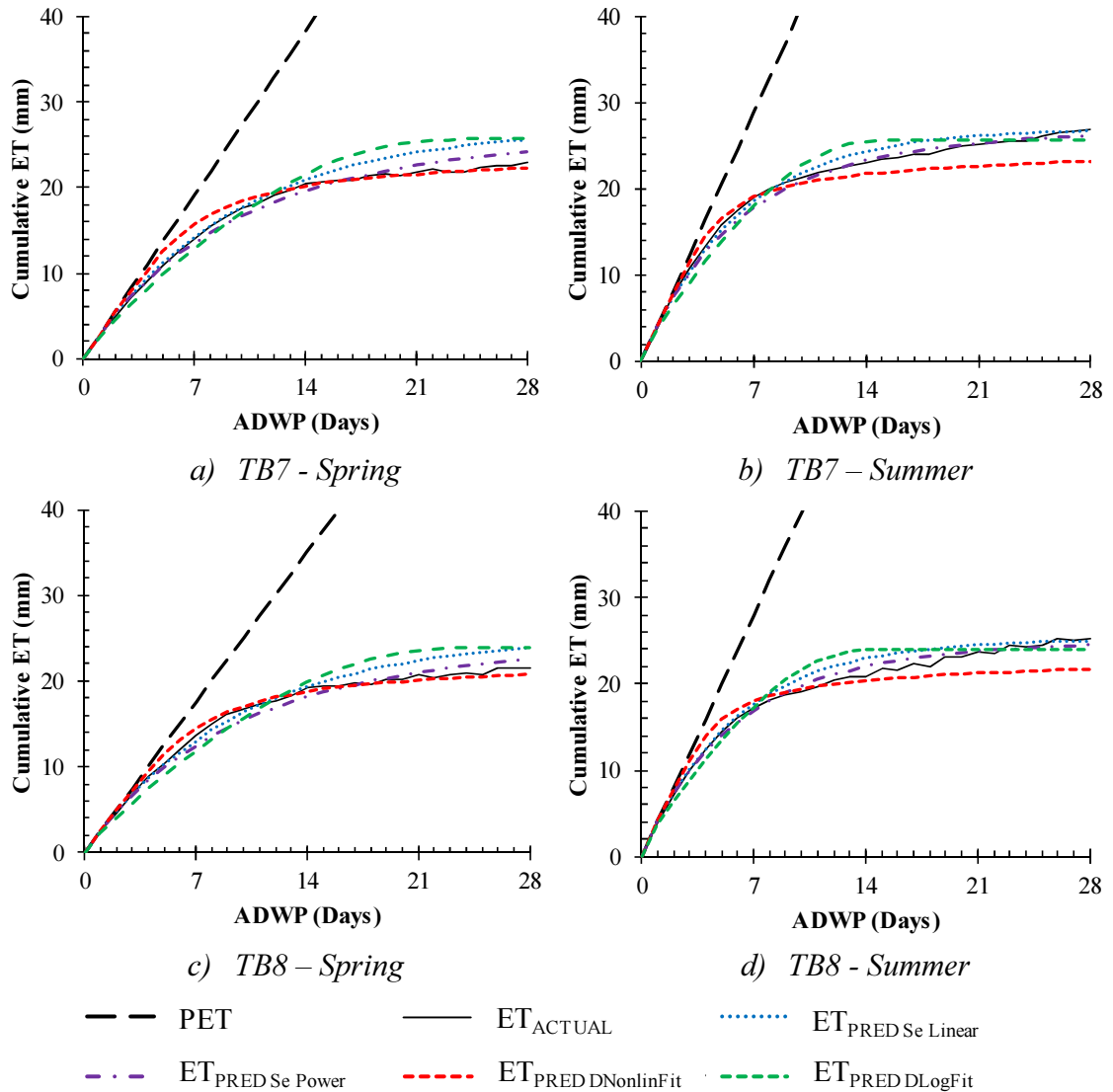


Figure 6.17:  $ET$  vs  $ET_{PRED}$  for non-vegetated configurations using new SMEFs

Generally, all SMEFs produced accurate predictions of ET from non-vegetated configurations. Both of the  $S_e$  Power and  $S_e$  Linear SMEFs produced very accurate predictions of ET for each season (with a minimum  $NSME$  of 0.94). At shorter ADWPs (i.e. 7 days), the  $S_e$  Linear SMEF produced marginally more accurate predictions than the  $S_e$  Power approach. Predictive errors ranged between 0.2-0.6 mm ( $S_e$  Linear) compared with 0.0-1.1 mm ( $S_e$  Power). The  $S_e$  Linear SMEF typically overestimated ET when

ADWPs were in excess of 12 days. However, after 14 days, the maximum error was 2.1 mm (TB8 in summer) compared to 1.1 mm with the *S<sub>e</sub> Power SMEF*. Initially, ET was overestimated when using the *DNonlinFit SMEF* and underestimated when using the *DLogFit SMEF*.

#### 6.4.2.7 Conclusions regarding newly-developed SMEFs

Comparing the two diffusivity-based approaches, the *DNonlinFit SMEF* was most accurate in summer whereas the *DLogFit SMEF* was more accurate in spring. However, overall, neither approach was able to consistently improve upon the accuracy of the *S<sub>e</sub> Linear SMEF* or address the main deficiency of the *S<sub>e</sub> Linear SMEF* (i.e. predictions of ET from Meadow Flower in summer). Indeed, for an ADWP of 14 days, predictive errors were higher (6.8 mm) with *DNonlinFit* and only marginally reduced (4.8 mm) with *DLogFit*. Seasonal mean predictive accuracy statistics demonstrate that both approaches had a lower accuracy than the *S<sub>e</sub> Linear SMEF* at ADWPs of 7, 14 and 28 days. The *DLogFit SMEF* resulted in the highest configuration mean errors for ADWPs up to 7 days (1.5 mm) and the *DNonlinFit SMEF* produced the highest mean errors across the 28 day ADWP (3.5 mm).

All predictions using the *S<sub>e</sub> Power SMEF* achieved a very good accuracy with the exception of the predictions in spring for TB1 during an initial 14 days and TB2 during an initial 7 days. After a 7 day ADWP, the mean error was just 0.8 mm; with very good accuracy in the prediction of seasonal mean ET in both spring (mean error of 1.1 mm) and summer (0.5 mm). The maximum error in the prediction of ET<sub>CUM</sub> from any individual configuration at any time throughout the 28 day ADWP was 2.0 mm (measured for TB1 after 7 days of spring). Predictive accuracy was high throughout the 28 day ADWP, with the mean predictive error against ET<sub>CUM</sub> being 0.9 mm after 14 and 0.8 mm after 28 days. The largest errors were typically associated with spring conditions, when the mean of the predictive errors after 28 days was 1.1 mm (i.e. less than 0.04 mm/day).

#### 6.4.2.8 *SMEF selection*

The *S<sub>e</sub> Power SMEF* generally modelled ET with the highest level of accuracy across the full range of vegetation treatments. This SMEF changes the shape of the response curve through the inclusion of empirical coefficients for the crop and the season. The *S<sub>e</sub> Power SMEF* has therefore been incorporated into the developed model. However, equally, the model also allows the user to select the *S<sub>e</sub> Linear SMEF* in the prediction of ET without any requirement for seasonal and/or configuration-specific calibration.

It is recognised that the coefficients adopted in the *S<sub>e</sub> Power* approach are specific to the two seasons considered here and it is possible that predictive errors would increase when considering ET in autumn and winter. However, the exponential decay in *ET/PET* was only observed in summer and is expected to be a consequence of high PET. In the cooler conditions of autumn and winter, the decay pattern would be expected to be similar to the linear relationship observed during spring. From a modelling perspective, it would be reasonable to assume that the same coefficient could be applied for both spring and autumn conditions without introducing any significant predictive errors. Differences in seasonal plant growth would be reflected in the underlying calculation of PET. In winter, the relatively low PET would also be expected to reduce the importance of the SMEF in the accurate prediction of ET. Further research would be required to support any reduction of the coefficient in winter below the spring value. When validating the *S<sub>e</sub> Power SMEF* against the Hadfield AE9 data, the  $\epsilon$  coefficient derived for spring will also be applied to autumn and winter PET values.

#### 6.4.3 **ET calculation**

Actual ET is calculated by applying a SMEF to the PET rate. However, when calculating ET, it is necessary to consider the sensitivity of the estimate to the model time step. ET calculations for green roofs have tended to be performed at daily time intervals (Berghage *et al.*, 2007; Voyde *et al.*, 2010; Marasco *et al.*, 2014). The use of the FAO56 approach with 24 hourly data is considered to produce accurate estimates unless the wind speed, dew point or cloudiness is expected to change substantially over short time periods (Allen *et al.*, 1998). In such cases, when modelling necessitates a more frequent (e.g. hourly) ET input, the daily estimate would typically be evenly disaggregated. However, it was demonstrated in Section 5.4.3 that ET varies on a diurnal basis. By evenly disaggregating

daily ET to derive hourly ET, a loss of accuracy would be expected at certain times of the day. Using configuration-mean hourly ET data from the laboratory trials for an ADWP of 10 days, Figure 6.18 demonstrates the extent to which cumulative ET varied diurnally compared to an evenly disaggregated daily ET.

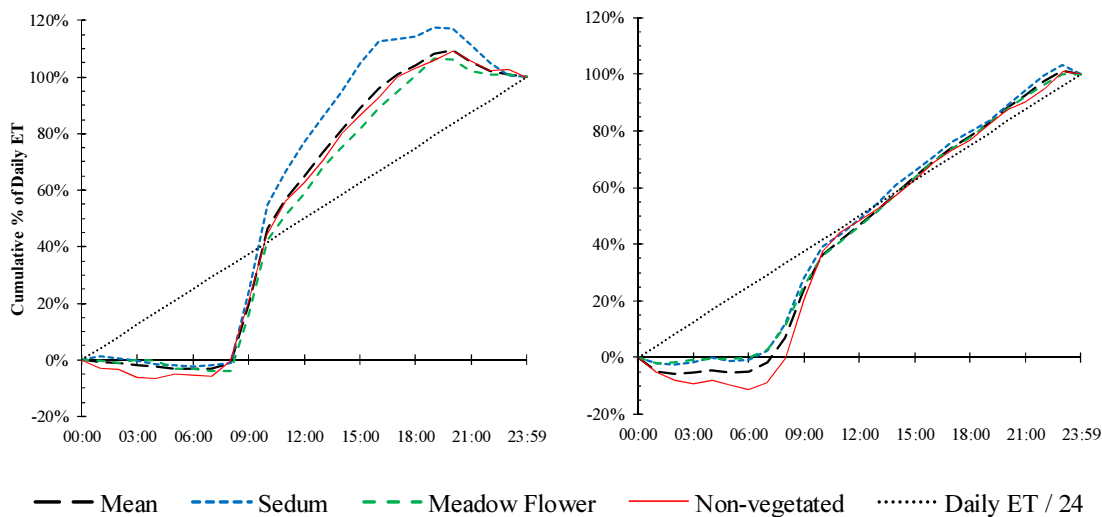


Figure 6.18: Diurnal distribution of ET in spring (left) and summer (right)

In spring, between 08:00 and 10:00, 56% of daily ET was measured from Sedum-vegetated configurations, 46% from Meadow Flower and 45% from non-vegetated configurations. Before 07:00 and after 20:00, ET was typically either zero or negative. In summer, ET started earlier. 14% of daily ET was measured from Sedum between 06:00 and 08:00 and a further 27% occurred between 08:00 and 10:00. The corresponding values for Meadow Flower were 11% and 25% and for non-vegetated configurations were 11% and 38%. ET was generally observed until 23:00 in summer.

The even disaggregation of daily ET to calculate hourly ET led to errors of up to 42% of spring ET (approximately 0.8 mm) and 32% of summer ET (approximately 1.5 mm). In summer, these errors were largely eradicated by 10:00. Yet, in spring, ET was under- or over-predicted throughout the diurnal cycle. From the perspective of modelling extreme rainfall events, maximum errors due to a simple disaggregation – 0.8 mm (spring) and 1.5 mm (summer) – would not typically justify the additional complexity of modelling the diurnal cycle. In more extreme climates, it may be justifiable to use hourly FAO56 values. Here, the developed model will calculate PET at daily intervals. When ADWPs include fractions of a day, daily PET will be proportionately disaggregated.



#### 6.4.4 Detention modelling parameters

It is important that a green roof hydrological model can represent both the retention and detention (delay) processes independently. Green roof detention processes have been modelled using several different methods, including finite element analysis (Hilten *et al.*, 2008; Palla *et al.*, 2012), unit hydrograph-based approaches (Villarreal & Bengtsson, 2005) and reservoir routing (Kasmin *et al.*, 2010; Yio *et al.*, 2013). Here, the developed model adopts the reservoir routing approach, using the  $k$  parameter, to characterise the detention performance of the system.

In section 4.4.7, configuration-specific values of  $k$  were presented. Differences in  $k$  due to substrate were not statistically significant. However,  $k$  derived for LECA configurations was higher (0.0083 [ $\text{mm}^{1-n}/\text{min}$ ]) than for HLS and SCS (0.0069 and 0.0061 respectively). Here, the performance of LECA configurations was not included in the estimation of the model parameter values (i.e. SMEF coefficients or  $k$  parameter).  $k$  values were only considered for the HLS- and SCS-based configurations (see Table 6.5).

Table 6.5: Configuration- and vegetation-specific  $k$  values

	<b>k (<math>\text{mm}^{1-n}/\text{min}</math>)</b>	<b>k (<math>\text{mm}^{1-n}/5\text{min}</math>)</b>
TB1	0.0054	0.027
TB2	0.0048	0.024
<b>Vegetation-specific (Sedum)</b>	<b>0.0049</b>	<b>0.0245</b>
TB4	0.0056	0.028
TB5	0.006	0.03
<b>Vegetation-specific (Meadow Flower)</b>	<b>0.0058</b>	<b>0.029</b>
TB7	0.0094	0.047
TB8	0.0074	0.037
<b>Vegetation-specific (Non-vegetated)</b>	<b>0.0083</b>	<b>0.0415</b>
<i>AE Median</i>	<i>0.0064</i>	<i>0.032</i>

The AE median  $k$  value across these six configurations was 0.0064  $\text{mm}^{1-n}/\text{min}$  (rather than 0.007 had the three LECA-based test beds been included). As the choice of vegetation treatment was statistically significant to the value of detention parameter  $k$ , the refined model included vegetation-median  $k$  values. The  $k$  values inputted into the model were therefore 0.0049  $\text{mm}^{1-n}/\text{min}$  (Sedum), 0.0058  $\text{mm}^{1-n}/\text{min}$  (Meadow Flower) and 0.0083  $\text{mm}^{1-n}/\text{min}$  (non-vegetated). These values were all marginally lower than the AE values presented in Section 4.4.7 that included LECA substrates.

In proposing a deviation away from configuration-specific to vegetation-median  $k$  values, it is first necessary to consider the sensitivity of runoff predictions to changes in  $k$ . Secondly, as values were derived using rainfall and runoff data at 1-minute intervals, the implications of applying  $k$  at 5-minute intervals will also be considered.

#### 6.4.4.1 Sensitivity of runoff profiles to changes in $k$

Differences between  $k$  across the test beds were large relative to the scale of  $k$  (i.e.  $k$  for TB7 was almost double that of TB2). The practical implications of these differences are expected to be small due to their very low value. To determine whether such differences would contribute to a loss in predictive accuracy if a vegetation-median value were used, Figure 6.19 demonstrates the sensitivity of runoff predictions for TB2 during EV45 as a consequence of changes in  $k$ . Here, rainfall was initially retained (red bars), leaving net rainfall (blue bars) to be distributed temporally using  $k$ .

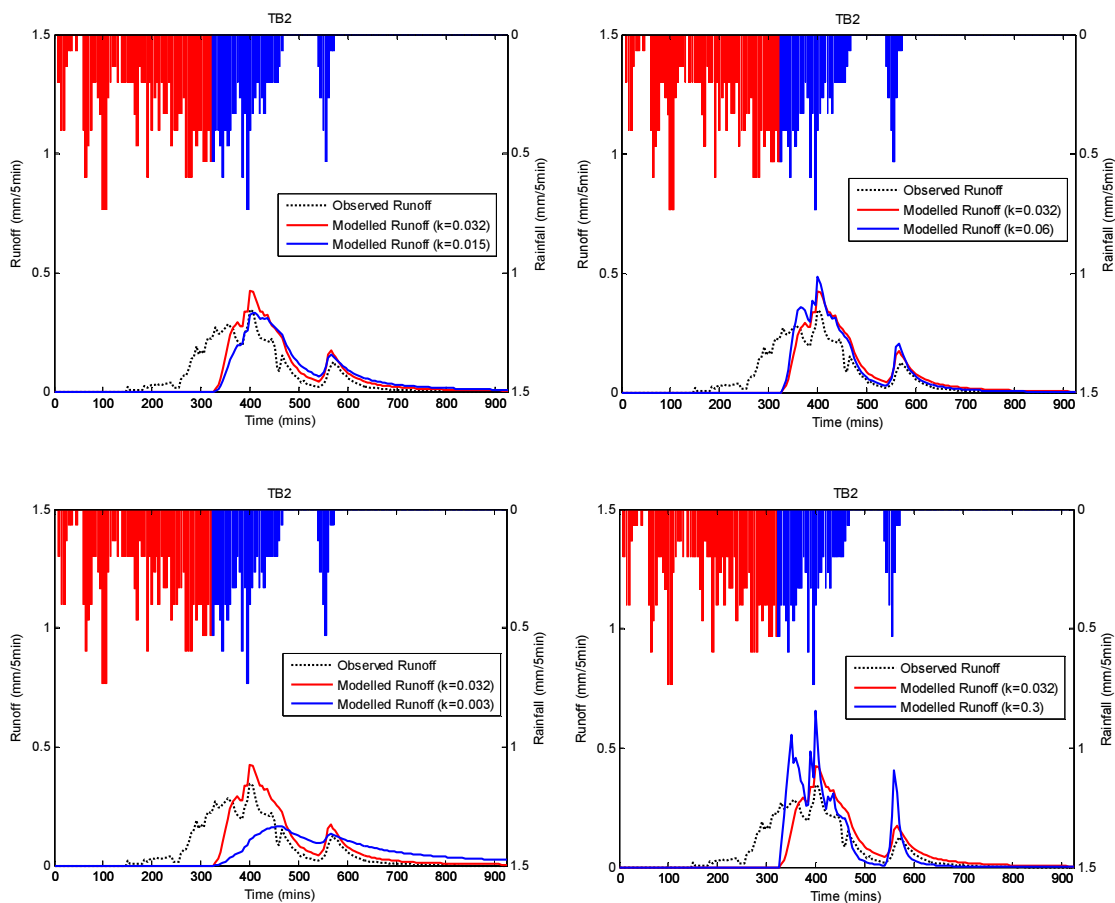


Figure 6.19: Sensitivity of runoff predictions to changes in  $k$

There were limited differences in the predicted hydrographs even when halving (top left plot) or doubling (top right) median  $k$ . NSME for runoff from TB2 was only marginally affected; changing from 0.604 (median  $k$ ) to 0.616 ( $k = 0.06$ ) and to 0.556 ( $k = 0.015$ ). Predicted centroid lag varied by approximately  $\pm 20$  minutes (positively when  $k = 0.015$  and negatively when  $k = 0.06$ ). Peak runoff predictions varied by up to  $\pm 0.08$  mm/5min against measured peak rates of 0.34 mm/5min (runoff) and 0.73 mm/5min (rainfall). Only very large changes to  $k$  made important differences to the hydrographs and predictive accuracy. By reducing median  $k$  by one order, to  $k = 0.003$  (bottom left hydrograph), peak runoff was under-predicted by almost half (0.16 mm/5min) and NSME fell to 0.318. Similarly, by increasing median  $k$  by one order, to  $k = 0.3$  (bottom right hydrograph), peak runoff was over-predicted by nearly 100% (0.65 mm/5min) and NSME fell to 0.480.

#### 6.4.4.2 Sensitivity of runoff response statistics to the rainfall/runoff time interval

It is important to highlight the sensitivity of runoff statistics, and therefore the model outputs, to the time intervals used in the calculation of runoff. The detention performance reported in Section 4.5.2 considered rainfall and runoff at 1-minute time intervals (i.e. the measurement interval). From a modelling perspective, rainfall and runoff can often be calculated at anywhere between a 1-minute and a 1-hour intensity. 5-minute time intervals are widely used in rainfall-runoff models. However, when considering rainfall and runoff at a 1-minute interval, peak attenuation would typically be higher than when a 5-minute interval is used.

During EV228, peak rainfall intensity was either 0.2 mm/min or 0.6 mm/5min. As a result:

- Peak attenuation for EV228 ranged between 36.9% (TB7) and 56.2% (TB5) when a 5-minute interval was used, compared with a range of 55.0% (TB7) up to 71.1% (TB4) for a 1-minute interval.
- The accuracy of runoff predictions varied depending upon the choice of time interval. NSME statistics reflected a higher level of accuracy when a longer, 5-minute interval was used compared with a 1-minute interval. When modelling runoff for EV228 (using the AE median  $k$ ), NSME ranged between 0.667 (TB8) and 0.949 (TB1) when a 5-minute interval was used, compared with 0.547 (TB8) and 0.872 (TB1) for a 1-minute interval.

It is therefore clear that the choice of time interval will affect the reported detention performance. For detention performance metrics to be meaningful, values must be qualified by the calculation time step (Stovin *et al.*, 2015b).

#### 6.4.4.3 Conclusions regarding the $k$ parameter value

Systematic variations in  $k$  have been identified as a result of configuration. However, these differences were relatively minor. It has been demonstrated that the model has low sensitivity to relatively large changes (e.g. doubling or halving) in  $k$ . Model outputs were sensitive to the time-step at which rainfall and runoff was modelled. The model has the capacity to model runoff by using the AE median  $k$  identified here –  $0.032 \text{ mm}^{1-n}/5\text{min}$  (or  $0.0064 \text{ mm}^{1-n}/\text{min}$ ). However, the vegetation-specific  $k$  will be the default  $k$  value; automatically being read as a result of the inputted vegetation treatment. When referencing the predicted detention response, it will be important to qualify the response with the time-step employed in the calculation.

## 6.5 Model Validation

### 6.5.1 Validation of retention model using AE9 data

The developed retention model, refined with the benefit of the ET laboratory trial data, was tested against the AE9 data from the Hadfield field research site. The initial moisture condition was set equal to each TB's measured moisture content at the start of the ADWP. ET was then modelled during the drying cycle, taking into account the  $S_{MAX}$  of each configuration. Three TBs were validated, representing typical Sedum (TB2), Meadow Flower (TB4) and non-vegetated (TB7) configurations. The model was tested for accuracy in predicting two outputs: (i) SMD at the start of the rain event and (ii) runoff depth. The accuracy of SMD predictions is considered to be an important indicator of the model's capacity to predict the drying cycle response independently from the characteristics of the subsequent rainfall event. As TB4 was not fitted with CS616 water content reflectometers, it was not possible to compare measured and predicted SMD for this TB. SMD predictions were therefore only compared with values measured from TB2 and TB7. To formulate runoff predictions, the initial moisture content of TB4 was estimated by taking mean  $S_e$  for TB2 and TB7 and multiplying it by the  $S_{MAX}$  of TB4.

Figure 6.20 compares both measured versus predicted SMD and measured versus predicted runoff using three SMEF options –  $S_e$  Linear,  $S_e$  Power or no SMEF.

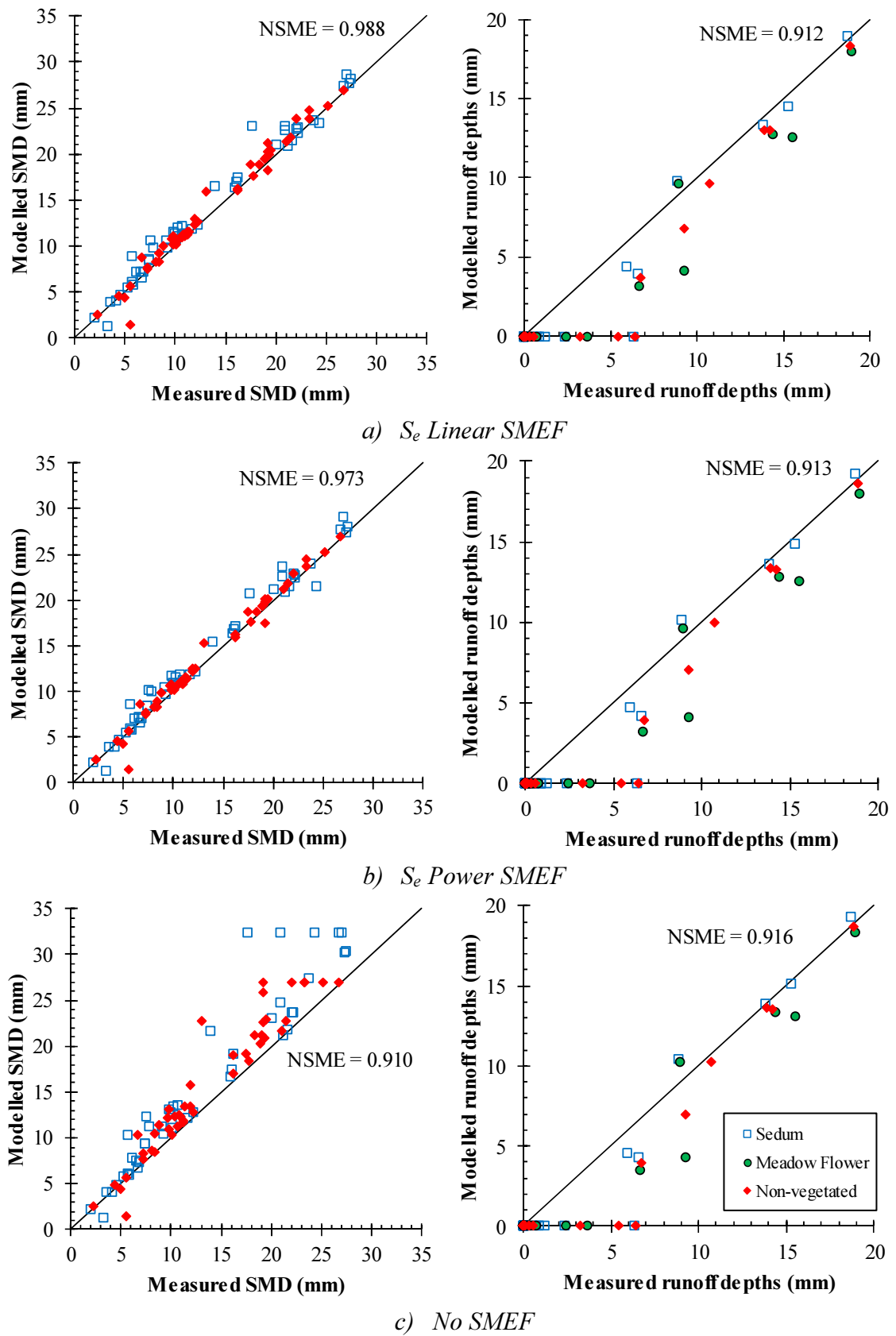


Figure 6.20: Measured vs Predicted SMD and runoff values

For the model to reproduce the observed retention responses to AE9 rainfall events, the choice of SMEF was not important to the accuracy of runoff predictions. The statistical accuracy of runoff predictions was highest when no SMEF was used ( $NSME = 0.916$ ), compared to the  $S_e$  Linear SMEF (0.912) and  $S_e$  Power SMEF (0.913). However, this trend will have been influenced by two factors:

- (i) The high proportion of small AE9 events that produced little or no runoff. Median per-event rainfall depth was 3.7 mm (mean: 6.5 mm). Comparing SMD predictions allowed differences due to SMEF choice to be assessed independently from rainfall characteristics. Considering the accuracy of SMD predictions without a SMEF, SMD was over-predicted by as much as 14.8 mm (EV207). There was a consistent over-prediction of SMD which was particularly evident when SMD exceeded 15 mm. This compares to maximum errors of 5.4 mm (EV207) and 4.1 mm (EV228) using the  $S_e$  Linear and  $S_e$  Power approaches respectively. The mean of the errors was lowest with the  $S_e$  Power SMEF; 0.98 mm and 0.61 mm for Sedum and non-vegetated TBs respectively. Errors were only marginally higher with  $S_e$  Linear (1.06 mm and 0.74 mm) and higher again with no SMEF (2.69 mm and 2.15 mm). However, statistically, the accuracy of the SMD prediction was marginally higher when using the  $S_e$  Linear SMEF ( $NSME = 0.988$ ) than with  $S_e$  Power ( $NSME = 0.973$ ). It was expected that the accuracy of predictions would have been higher for  $S_e$  Power if the SMD of Meadow Flower configurations could have been considered here. The correlation between ET and  $ET_{\text{PRED}}$  from Meadow Flower was highest using the  $S_e$  Power SMEF.
- (ii) The high number of short and cool ADWPs. Mean ADWP across the 48 AE9 events was just 1.8 days. If the AE9 dataset had included a higher number of events with greater rain depths and/or longer ADWPs, it is likely that the choice of SMEF would have had a more important influence on the accuracy of runoff predictions. The importance of ADWP to differences in predictions by each SMEF was demonstrated by modelling responses of the three configurations (all initially at field capacity) to a summer ADWP with high PET of 4.5 mm/day. With an ADWP of 1.8 days, the difference in  $ET_{\text{PRED}}$

using any of the three SMEF choices would be less than 1 mm. The differences in predictions between the  $S_e$  Power and  $S_e$  Linear SMEFs were a maximum of 0.3 mm. However, these differences would increase with longer ADWPs. For an ADWP of 5 days, differences would be up to 6.4 mm across the three approaches and 2.4 mm between the two SMEFs. These differences would increase over time (e.g. after 7 days, the difference between the two SMEFs was 4.0 mm for Meadow Flower). The choice of SMEF will therefore be expected to have a more important influence on retention predictions in warmer, drier climatic conditions.

Differences were still observed in  $ET_{\text{PRED}}$  (as derived using the three different SMEFs) for the AE9 rainfall events. Using the  $S_e$  Power SMEF, mean per-event cumulative  $ET_{\text{PRED}}/PET$  was 0.53, 0.64 and 0.44 (for Sedum, Meadow Flower and non-vegetated configurations respectively) compared to 0.57, 0.53 and 0.48 ( $S_e$  Linear SMEF) and 0.97, 0.97 and 0.92 (no SMEF). The  $ET_{\text{PRED}}/PET$  predictions produced by the  $S_e$  Power SMEF appeared to be consistent with the findings of Chapter 5 in that (a) the highest  $ET_{\text{PRED}}$  was from Meadow Flower configurations and the lowest was from non-vegetated configurations and, (b) there was an almost immediate reduction in ET from PET.

It is clear that the SMD will be overestimated if no SMEF is employed. However, it has been demonstrated here that the use of either the  $S_e$  Linear SMEF or the  $S_e$  Power SMEF improved the accuracy of predictions of SMD. The extent to which this benefits the accuracy of runoff predictions will depend partly upon rainfall characteristics.

### 6.5.2 Validation of detention model

The importance of using the reservoir routing method to model detention performance can be observed from a hydrograph that compares measured runoff from TB2 during EV228 against runoff predicted with (a) vegetation-specific  $k$  ( $0.027 \text{ mm}^{1-n}/5\text{min}$ ), (b) the AE median  $k$  ( $0.032 \text{ mm}^{1-n}/5\text{min}$ ), (c) an event-specific  $k$  ( $0.01 \text{ mm}^{1-n}/5\text{min}$ ) and (d) no routing at all (see Figure 6.21).

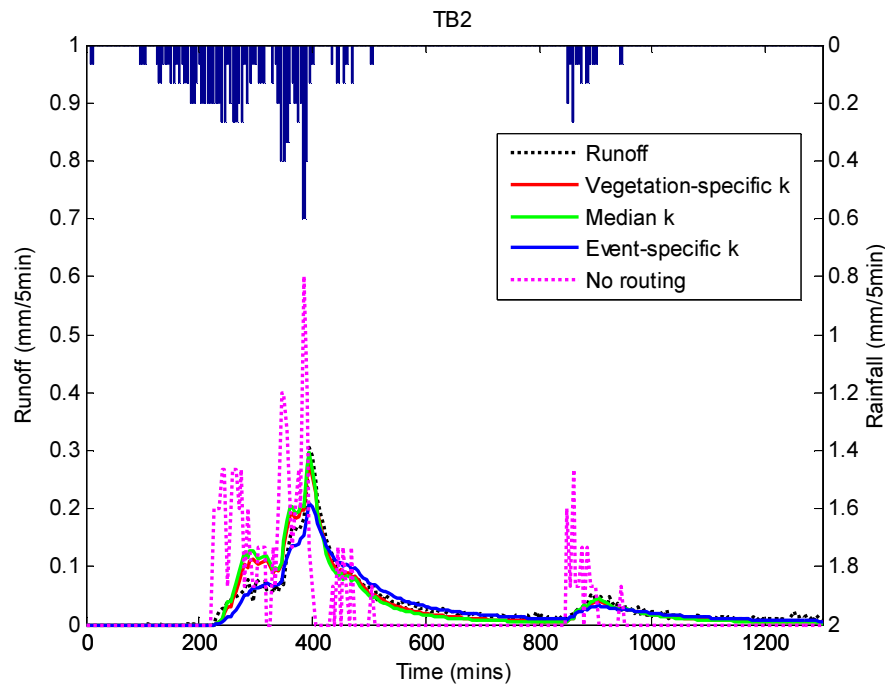


Figure 6.21: Predicted runoff response of TB1 to EV228 with and without routing

Here, the predicted peak rate of runoff was approximately double the measured peak rate when no routing was applied. However, by using the reservoir routing approach, much more accurate predictions of runoff were possible.

To validate the use in the model of detention parameter  $k$  as a vegetation-specific or single median value, predicted runoff will be compared against actual runoff measured from selected AE9 events. Rainfall and runoff exceeded 2 mm from all TBs during eight AE9 events. Here, events with a range of depths, intensities and seasons will be considered. In all cases, rainfall and runoff were considered at 5-minute intervals.

#### 6.5.2.1 Optimal $k$ values for AE9 events compared with AE values

Here, event- and configuration-specific optimised  $k$  values for the AE9 sub-set of event data are contrasted against the AE median values (see Table 6.6).

The median of the configuration-specific  $k$  values across the eight AE9 events were generally within 0.01 of the equivalent values derived using the AE dataset. As such, the AE9 median value of  $0.022 \text{ mm}^{1-n}/5\text{min}$  for all configurations combined was closely approximated to the AE median  $k$  of  $0.032 \text{ mm}^{1-n}/5\text{min}$ . Differences in  $k$  were observed both as a result of the event and of the configuration; ranging between 0.003 and 3.146.



Table 6.6: Event- and configuration-  $k$  values using least-squares fitting

Event	TB1	TB2	TB4	TB5	TB7	TB8	Median
<b>EV45</b>	0.012	0.009	0.000	0.021	0.031	0.033	<b>0.016</b>
<b>EV227</b>	0.004	0.004	0.004	0.003	0.007	0.005	<b>0.004</b>
<b>EV228</b>	0.018	0.015	0.011	0.009	0.009	0.007	<b>0.010</b>
<b>EV245</b>	0.015	0.011	0.016	0.016	0.015	0.018	<b>0.015</b>
<b>EV246</b>	0.052	0.026	0.021	0.034	0.056	0.043	<b>0.038</b>
<b>EV250</b>	0.057	0.024	0.023	0.029	0.094	0.062	<b>0.043</b>
<b>EV258</b>	0.150	0.002	0.047	0.716	3.146	0.523	<b>0.336</b>
<b>EV264</b>	0.427	0.081	0.055	0.038	0.110	0.059	<b>0.070</b>
<b>AE9 Median</b>	<b>0.035</b>	<b>0.013</b>	<b>0.019</b>	<b>0.025</b>	<b>0.043</b>	<b>0.038</b>	<b>0.022</b>
<b>AE Median</b>	<b>0.027</b>	<b>0.024</b>	<b>0.028</b>	<b>0.030</b>	<b>0.047</b>	<b>0.037</b>	<b>0.032</b>

For many routine, real (i.e. irregular in profile) rainfall events, the variations in detention performance across the configurations were relatively minor. The largest differences in optimal  $k$  were identified with event-specific  $k$ . For example, median  $k$  for EV227 and EV258 varied by nearly two orders of magnitude. It is therefore relevant to consider the accuracy of using a single median  $k$  compared against the use of an event-specific  $k$ .

#### 6.5.2.2 Application of AE $k$ values to predict responses to specific AE9 events

Runoff (in mm/5min) measured during the eight AE9 events was compared against runoff predicted using (i) event-specific  $k$ , (ii) AE median  $k$  (0.032) and (iii) vegetation-specific  $k$ . The use of median  $k$  led to good predictions of runoff for all events, except EV227 and EV258. However, the NSME statistics indicate that neither of these events were predicted with good accuracy when using event-specific  $k$  either.

Comparing the configuration-specific median NSME values for predictions using the event-specific and median values of  $k$ , only small losses of accuracy occurred when using the median  $k$ . It was expected that the use of event-specific  $k$  values would lead to the most accurate runoff predictions. However, this was not always the case. For many events, there was a large range of configuration-specific  $k$  values across the same event. Predictions were more accurate when using the AE median value of  $k$  (rather than the event-specific  $k$ ) for six of the eight events. Predicted runoff was not particularly sensitive to  $k$ . Even relatively large differences in  $k$  often made little difference to the statistical

accuracy of runoff predictions. From an optimisation perspective, deriving the optimal values of  $k$  could be considered an ill-defined problem.

Therefore, first, potential explanations were explored for the inaccurate predictions of EV227 and EV258. Secondly, hydrographs were reviewed for the two events with the lowest predictive accuracy (excluding EV227 and EV258, i.e. EV45 and EV228) and for the two events with the highest predictive accuracy (i.e. EV246 and EV264). These four events provide a good representation of different seasons and rainfall characteristics.

During EV227 (a winter event), measured peak rates of runoff were low (between 0.03 and 0.08 mm/5min) in response to peak rainfall of 0.4 mm/5min (see Figure 6.22).

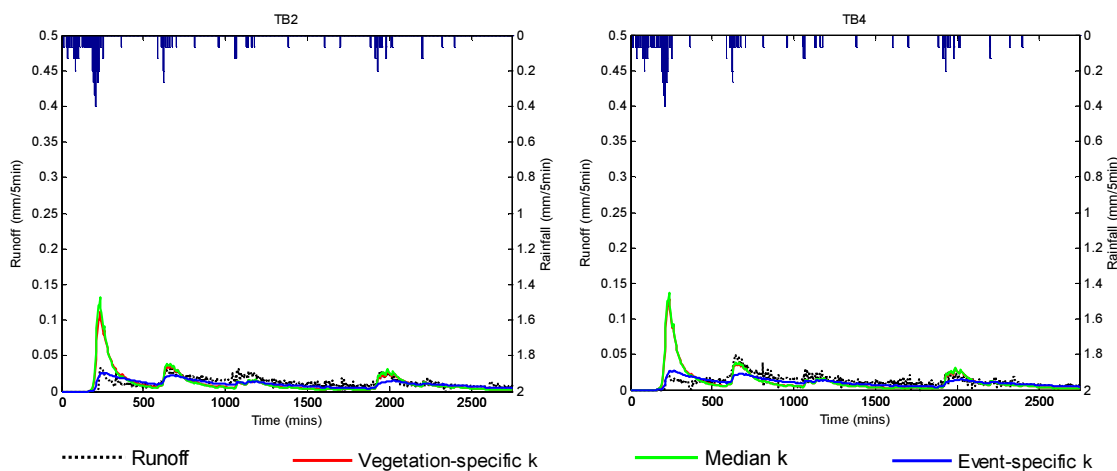


Figure 6.22: Runoff hydrographs for TB2 and TB4 during EV227 (01/12/2012)

It is hypothesised that the low measured runoff rate was due to the fact that the precipitation may have fallen as sleet, rather than rainfall. The mean temperature during the 86 hour event (40 hour ADWP, 40 hour rainfall and 6 hour dry period post-rainfall) was 3.36 °C, ranging between 0.1 and 7.2 °C. Sleet and light snow was known to have fallen in the Sheffield area around this time. As a result, there was more than one order of difference between the event-specific and median values of  $k$  (0.004 and 0.032 respectively). Predictions of peak runoff were therefore overestimated when using the median  $k$  (between 0.12 and 0.15 mm/5min).

Considering predictive errors for EV258 (a spring event), a number of the configurations (e.g. TB1 and TB7) were known to have sufficient SMD to wholly retain the 24.8 mm of rain. Yet, not only did runoff appear to start prior to reaching  $\theta_{FC}$ , but further retention

was observed after runoff had first been recorded. As a result of these retention errors, runoff was measured for several hours prior to the start of predicted runoff. The correlation between modelled and measured runoff was poor for both the event-specific and median  $k$  (see Figure 6.23).

Shortly after the peak rainfall of 1.7 mm/5min, the event-specific  $k$  forecasted peak rates of runoff that were much higher than measured and, indeed, greater than the peak rainfall rate. It is therefore apparent that the errors observed across EV227 and EV258 were attributable to the form of precipitation and retention errors (see Section 4.5.3) respectively. The event-specific, median and vegetation-specific values of  $k$  will now be tested against four of the AE9 events.

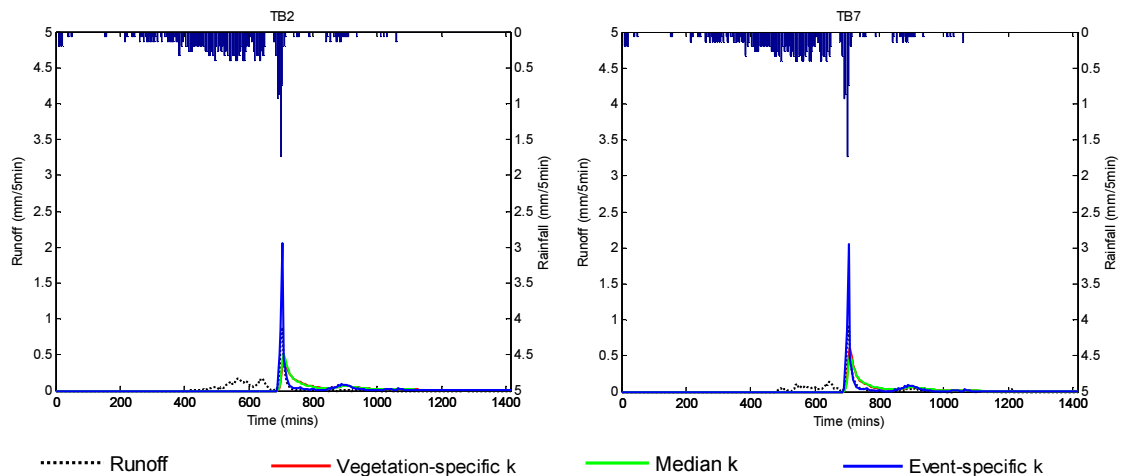


Figure 6.23: Runoff hydrographs for TB2 and TB7 during EV258 (13/05/2013)

EV45 was a summer rainfall event (August 2010) in which 31.2 mm of rain fell, with a peak rate of 0.73 mm/5min. As the hydrographs for the 6 test beds demonstrate, the accuracy of runoff predictions was adversely impacted by retention errors; most notably with TB4 (see Figure 6.24). Predictions using the median  $k$  and vegetation-specific  $k$  had a similar accuracy. The median of the NSMEs across all 6 TBs was 0.766 and 0.761 respectively. As a result of these retention errors, predictions of the centroid lag were poor. Observed centroid lag ranged between 77 minutes (TB4) and 158 minutes (TB8). Using any of the three  $k$  values, the model over-predicted lag by more than 60 minutes on average. Peak rates of runoff were predicted with good accuracy using the vegetation-specific  $k$ ; with maximum errors of 0.062 mm/5min (i.e. 18% of actual peak runoff). Use of the median  $k$  only marginally reduced accuracy, with a maximum error of

0.08 mm/5min (i.e. 23% of actual peak runoff). NSME statistics for predictions using the event-specific  $k$  indicate that this method had the highest accuracy. However, this approach also resulted in the highest errors in peak runoff predictions (0.11 mm/5min or 32% of actual peak runoff). Peak delays were predicted to be within 50 minutes of actual delays (300 minutes) using any of the three  $k$  values.

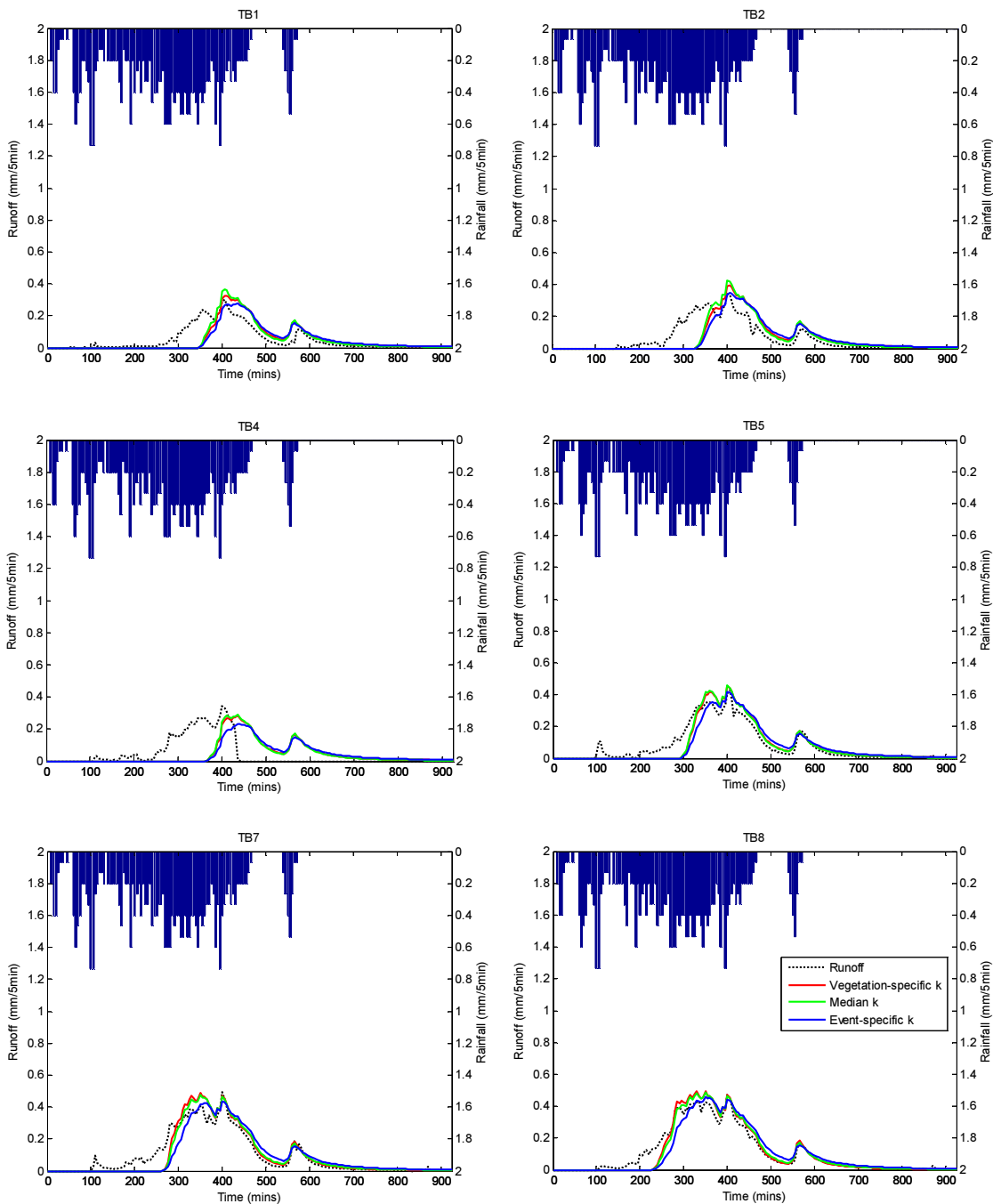


Figure 6.24: Runoff hydrographs for EV45 (30/08/2010)

EV228 was a winter event (December 2012) with rainfall of 11.7 mm and peak rainfall of 0.73 mm/5min. NSME was highest with the event-specific  $k$  (range: 0.644 [TB8] to 0.940 [TB2]; median: 0.898). Peak runoff was under-predicted by 18-39% with event-specific  $k$ ; predicting peak runoff rates of 0.21-0.23 mm/5min (see Figure 6.25).

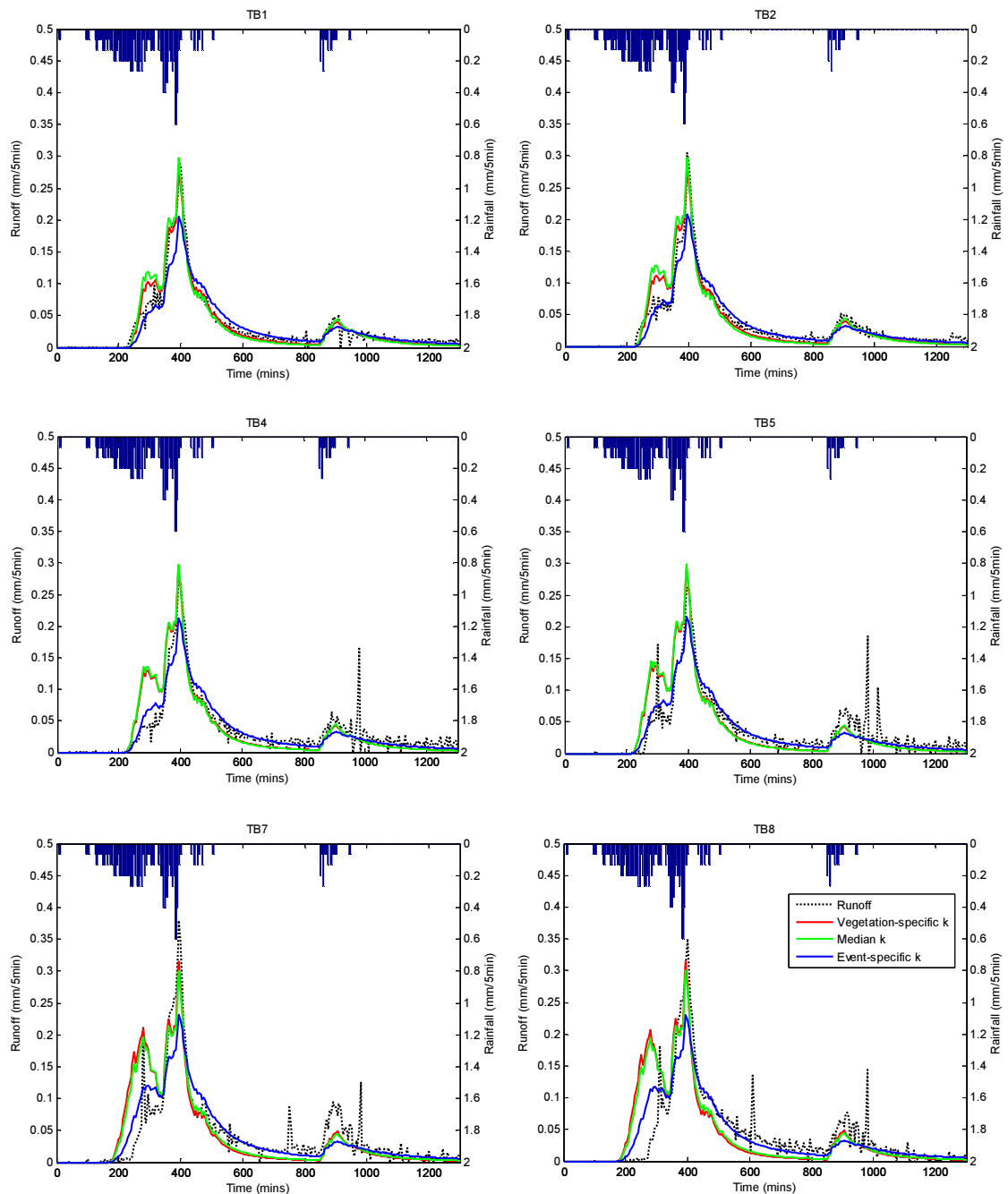


Figure 6.25: Runoff hydrographs for EV228 (05/12/2012)

The centroid lag of between 188 and 240 minutes was most accurately predicted using this approach (predicted lags were between 119 and 172 minutes). All approaches predicted peak delays of 10 minutes; closely replicating observed delays of between 10 and 15 minutes. The NSME statistics for predictions using median  $k$  were lower (between 0.644 and 0.938, with median of 0.769) than for predictions using either the event- or vegetation-specific  $k$ ; the latter having NSME of between 0.581 and 0.962 (median of 0.790). However, in practical terms, differences between median and vegetation-specific  $k$  were minor, with the accuracy of peak runoff predictions both improving as a result of using median and vegetation-specific  $k$ , rather than event-specific  $k$ .

With median  $k$ , predicted peak runoff was 0.30 mm/5min versus an observed range of 0.26-0.38 mm/5min. Errors ranged between +14% and -21% of actual peak runoff. Use of vegetation-specific  $k$  produced peak runoff predictions of 0.28-0.32 mm/5min such that errors were between +11% and -17% of actual peak runoff. Predictions of centroid lag were similar across both approaches, with averages of 125 minutes (median  $k$ ) and 127 minutes (vegetation-specific  $k$ ) versus actual mean lag of 213 minutes.

EV246 was a winter event (February 2013) where 16.1 mm of rain fell with a peak intensity of just 0.2 mm/5min. Peak runoff was 0.16 mm/5min from vegetated beds and between 0.17 and 0.21 mm/5min from non-vegetated beds. Detention performance was predicted with very good accuracy using any of the tested values of  $k$  (see Figure 6.26).

Median NSME was 0.898 (event-specific  $k$ ), 0.905 (median  $k$ ) and 0.907 (vegetation-specific  $k$ ). In response to peak rainfall of 0.2 mm/5min, actual peak runoff ranged between 0.157 (TB5) and 0.215 mm/5min (TB8), the mean of the six beds was 0.17 mm/5min. All approaches under-predicted peak runoff by similar amounts. Event-specific  $k$  predicted peak runoff of 0.147 mm/5min, compared to 0.143 mm/5min (median  $k$ ) and a range of 0.136 (Sedum-vegetated TB1 and TB2) to 0.149 mm/5min (non-vegetated TB7 and TB8). With the exception of TB8, actual peak delays were 410 minutes and these delays were reproduced by all tested  $k$  values. Centroid lags were marginally over-predicted using all tested  $k$  values, but with very minor differences (5 minutes) between all three.

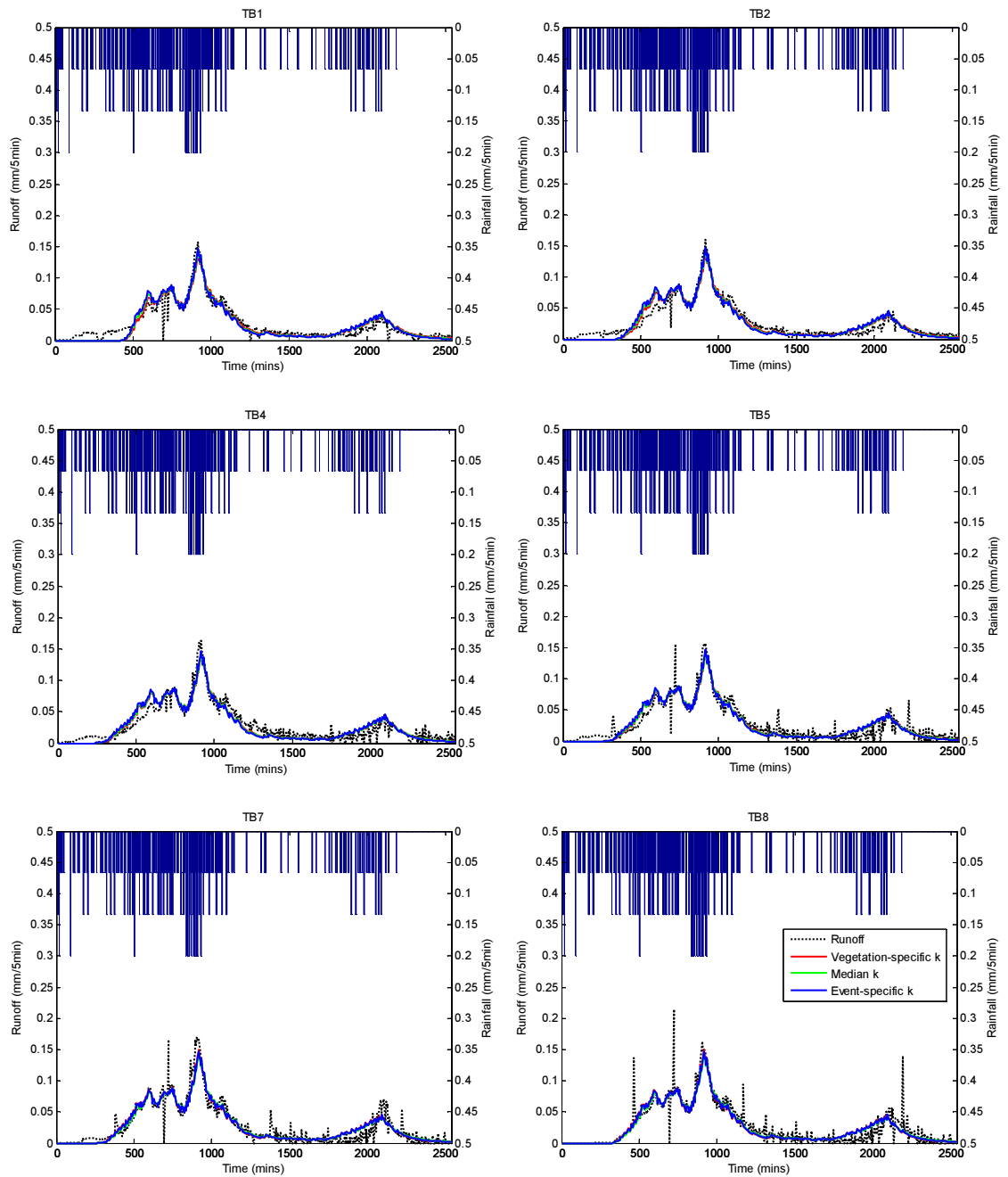


Figure 6.26: Runoff hydrographs for EV246 (09/02/2013)

EV264 was a spring event (May 2013) in which 15.6 mm of rain fell with a peak intensity of 0.6 mm/5min. Peak rates of runoff were well predicted across all TBs (see Figure 6.27).

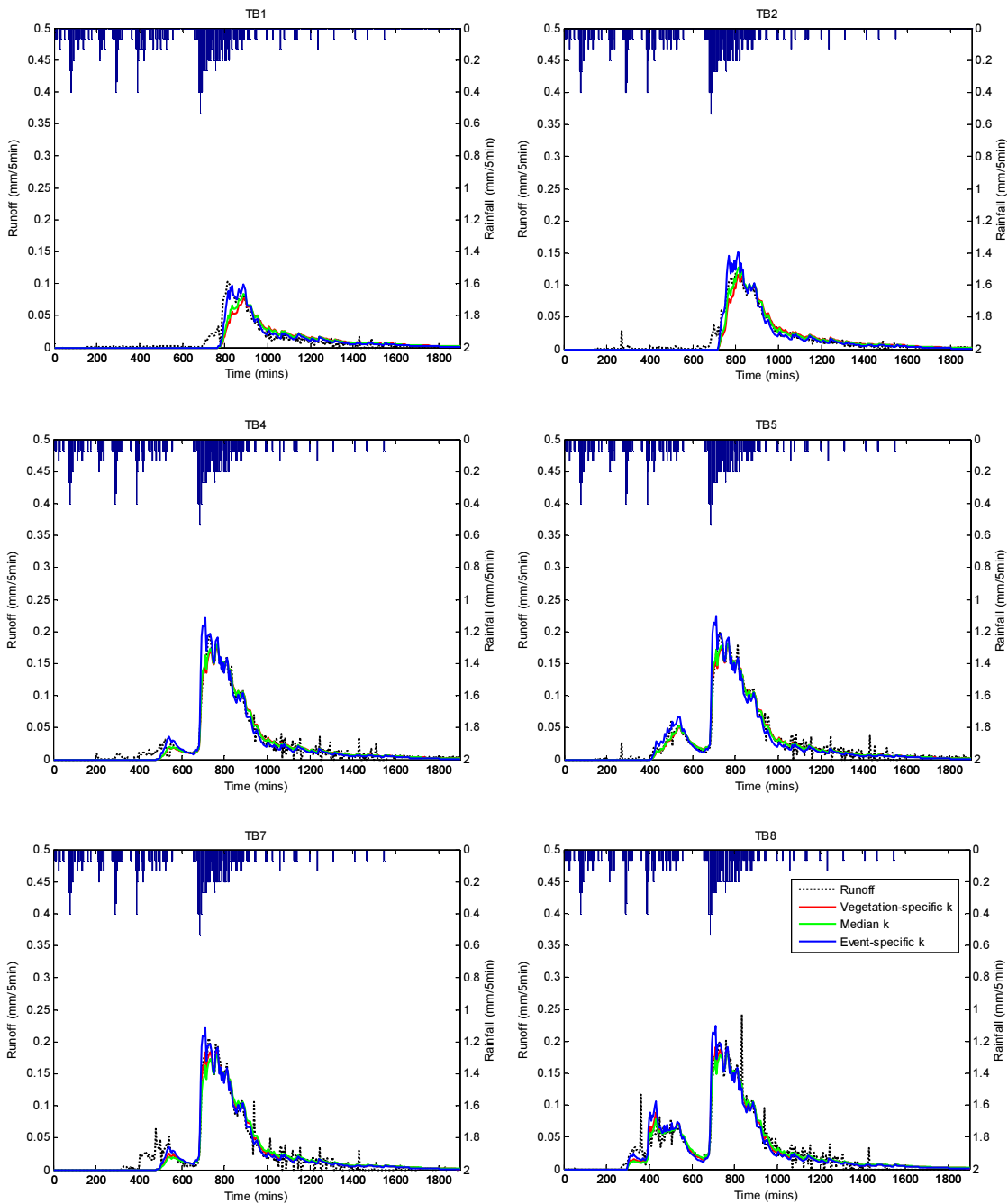


Figure 6.27: Runoff hydrographs for EV264 (28/05/2013)

NSME was highest with vegetation-specific  $k$  (Median: 0.940; range: 0.709 [TB1] to 0.976 [TB5]). However, median NSME was also similar using either median  $k$  (0.944) or event-specific  $k$  (0.932). Actual peak runoff ranged between 0.10 (TB1) and 0.24 mm/5min (TB8). Use of the event-specific  $k$  typically over-predicted these peaks, but only by a maximum of 0.03 mm/5min. Use of median and vegetation-specific  $k$  led to small under-predictions of peak runoff. Except for TB8 (actual peak runoff was



0.24 mm/5min and predicted peak runoff was 0.18mm/5min [median  $k$ ] or 0.19 mm/5min [vegetation-specific  $k$ ], predicted peak runoff was within 0.03 mm/5min (median  $k$ ) and 0.02 mm/5min (vegetation-specific  $k$ ) of observed peak runoff rates. All approaches predicted average peak delays (of 90 minutes) to within +/- 20 minutes and centroid lag (of 291 minutes) to within 26 minutes (event-specific  $k$ ), 49 minutes (median  $k$ ) or 52 minutes (vegetation-specific  $k$ ).

### 6.5.2.3 Summary of detention model validation

The use of  $k$  as a detention parameter has been shown to have the capability to predict detention performance (including peak rates of runoff and centroid lags) with good accuracy. An important modelling objective is to reduce reliance on empirical data for a specific event and/or configuration. Systematic differences in  $k$  were identified between configurations. However, the only statistically significant differences in optimised  $k$  values were due to vegetation treatment. The proposed modelling approach incorporates vegetation-specific  $k$  values for the three vegetation treatments evaluated here. However, in a context where relatively large changes in  $k$  values can be made without significant detriment to predictive accuracy, the use of a single median value of  $k$  can equally be advocated.

All values of  $k$  generally predicted detention performance with a high degree of accuracy across the AE9 events considered here. Whilst there were some exceptions, generally poor predictions of runoff were not purely associated with detention, but included errors due to retention. The model will retain the capacity to input any value desired. However, the model will include four default  $k$  values when modelling runoff at 1-minute intervals: (i) 0.0049 mm<sup>1-n</sup>/min (Sedum vegetation), (ii) 0.0058 mm<sup>1-n</sup>/min (Meadow Flower), (iii) 0.0083 mm<sup>1-n</sup>/min (non-vegetated), and (iv) 0.0064 mm<sup>1-n</sup>/min (median). Where rainfall and runoff is modelled at 5 minute intervals, these  $k$  values should be multiplied by 5.

## 6.6 Discussion

The developed model reflects widely-accepted hydrological principles by quantifying each element of the hydrological budget for the climate and the specific configuration. Commonly-applied PET methodologies are employed to account for the influence of climate upon ET. Then the model accounts for both the maximum storage capacity ( $S_{MAX}$ ) of the specific configuration and for the complex changes in moisture balance during the inter-event period. Here, the  $S_e$  Power SMEF can link the specific seasonal moisture consumption patterns of the vegetation treatment to a decay in ET with falling moisture availability. As a result, the SMD at the onset of rainfall is calculated to provide a good indication of antecedent conditions and available moisture retention capacity, as advocated by Versini *et al.* (2015). Through analysis of the AE9 data for rainfall, moisture content and weather station variables, it was possible to establish mean seasonal trends for  $S_e$  at the start of the ADWP. The use of these values would represent a typical expected response. However, simulating the worst case scenario (i.e. when the initial moisture content was equal to  $S_{MAX}$ ) is a typical modelling assumption.

Hydrological processes are known to be highly variable. Yet, the objective is to capture these processes without introducing unnecessary complexity (Elliott & Trowsdale, 2007). Here, opportunities to achieve marginal improvements in predictive accuracy have been identified. The use of crop factors, variable albedo coefficients, different SMEFs and diurnally-distributed ET all have the potential to improve the predictive accuracy of retention responses. However, these refinements would introduce additional complexity; requiring some specific calibration and/or further work to develop robust values.

The ability to model a green roof's response to a design storm event will facilitate greater transparency regarding the SuDS contribution of a green roof and enable designers to understand the extent to which complementary measures are required to fulfil the design criteria.

## 6.7 Conclusions

- A hydrological model has been developed to predict both volumetric retention and storm event runoff responses of different extensive green roof configurations;
- This continuous moisture flux model has a hydrological budget at its core with inputs (i.e. precipitation) and outputs (i.e. ET, runoff) modelled. A detention model temporally distributes any runoff, allowing peak runoff rates to be modelled for specific events;
- The FAO56 method of PET calculations provides a consistently better prediction of PET compared with four other commonly-applied models (Blaney-Criddle, Hargreaves, Priestley-Taylor and Thornthwaite) because it accounts for the important physical influences that affect ET (i.e. radiation, albedo and vapour transfer);
- However, the choice of PET model may be less critical than the influence of a configuration's moisture content. As a consequence, the retention model must include a SMEF;
- Alternatives to the  $S_e$  Linear SMEF, as originally proposed and applied in Stovin *et al.* (2013), were not found to offer significantly improved predictive performance, even where the models were more closely based on soil physics;
- Relatively small, but systematic differences in detention parameter  $k$  existed between configurations. The highest values of  $k$ , implying the most rapid rate of runoff, were associated with non-vegetated highly permeable configurations;
- The use of a single median value of  $k$  (0.0064 at 1-minute or 0.032 at 5-minute intervals) for all configurations has been justified. However, differences between vegetation treatments are statistically significant and accuracy can be marginally improved by using vegetation-specific  $k$  values;
- Many commonly-used detention metrics (e.g. peak attenuation) often include some effects of retention. Absolute values (e.g. peak runoff rates) may be more meaningful indicators of detention performance but any quoted values should be qualified by stating the time interval.

## 7 Model application

### 7.1 Chapter overview

The developed and refined model is applied to predict the hydrological performance of three typical UK extensive green roof configurations. The model is applied in two ways. Firstly, hydrological responses are simulated for a 30-year continuous time series of synthetic rainfall, temperature and PET. Secondly, responses to design storm events, calculated using the Depth-Duration-Frequency (DDF) rainfall distribution method, are modelled for a number of scenarios. The application of the model underpins a comparative assessment of different green roof configurations, based upon both their maximum moisture capacity and their moisture consumption characteristics (using a SMEF). Model outputs are further analysed to highlight the sensitivity of the model to changes in parameter values for important input assumptions (e.g. climatic conditions and initial moisture content).

Parts of this chapter have been published in a journal paper:

Stovin, V., Poë, S. and Berretta, C. (2013). A modelling study of long term green roof retention performance, *Journal of Environmental Management*, 131, 206-215.

However, the long-term simulation reported in Stovin *et al.* (2013) considered the response of a single green roof configuration in four climatically different zones of the UK. Here, a similar analysis considers the response of three different configurations in a single location (Sheffield). The simulated rainfall data was also different here. A new climatic simulation was generated to allow PET to be modelled using the FAO56 PET method. This was not possible with the data generated for and presented in Stovin *et al.* (2013). This previous model estimated PET using the Thornthwaite approach.

### 7.2 Motivation

The objectives of this chapter are (i) to demonstrate the practical value of the model to designers, (ii) to highlight the model's capacity to account for the physical influences that affect the hydrological response and (iii) to indicate the quantitative effect of configuration, length of ADWP, seasonal climate, rainfall and moisture content on the green roof's response. Hydrological simulations of retention performance and drought stress risk over a 30 year period demonstrate their potential application as a preliminary

feasibility assessment of green roof configurations and irrigation requirements. The application of the model to specific rainfall events is intended to demonstrate that designers can provide evidence of the system's response to design storm events and, in so doing comply with UK SuDS standards (CIRIA, 2015).

### **7.3 Materials and methods**

The model was applied to simulate hydrological responses to (i) a continuous 30 year period, and (ii) design rainfall events of different frequencies and distributions. In both instances, the model predicted the responses of three configurations: TB2 (Sedum mat on SCS) – a configuration that is typical of a Sedum roof in the UK; TB4 (Meadow Flower on HLS) – a good representation of a planted biodiverse roof in the UK; and TB7 (non-vegetated HLS) – a configuration that resembles a brown or unplanted biodiverse roof.

#### **7.3.1 30 year simulation**

A 30 year synthetic time series of weather variables was generated to model the long-term retention performance and drought tolerance of three green roof configurations. The UK Climate Projections (UKCP09) Weather Generator tool (<http://ukclimateprojections-ui.metoffice.gov.uk/> accessed on 23 March 2016) was used to simulate climatic conditions for a 25 km grid covering Sheffield (WXGen25km grid reference: 1275). Detailed guidance on this tool is provided by Jones *et al.* (2010).

The Weather Generator is based around a stochastic model (using probability distribution functions) that simulates future rainfall sequences and derives other weather variables from these rainfall states. This approach is criticised for its lack of physical basis:

- In real conditions, the weather is not completely random. Some weather variables are interdependent;
- The model assumes that observed relationships between weather variables will remain the same in future;
- The stochastic nature of the model means that outputs are generated for a single grid. With no correlation between adjacent grids, the model cannot be used for larger areas; and

- Extreme events are difficult to generate using the tool because the data is fitted using a 30 year historical record.

However, this tool generates statistically credible representations of future climate based on observed weather and climate signals for the UK. Data for rainfall, temperature, relative humidity and sunshine duration is generated at hourly intervals. The model therefore serves as a useful preliminary feasibility assessment tool for a green roof.

Model variants were randomly sampled, based on a ‘medium’ emissions scenario (replicating story A1B according to the IPCC Special Report on Emissions Scenarios, 2000). In view of the stochastic nature of weather predictions, the Weather Generator produces – and recommends the use of – a minimum of 100 30-year time series for each scenario. However, the objective here was to source credible climate data with which to illustrate the influence of representative climatic scenarios on the long-term retention performance of green roofs. Consequently, only the first iteration was considered here.

Synthetic hourly time series of rainfall and temperature were created for a 30 year period between 2010 and 2039. A daily time series of  $PET_{FAO56}$  was also generated for the same timescale. Monthly mean data for rainfall and PET across the 30 year simulation are shown in Figure 7.1.

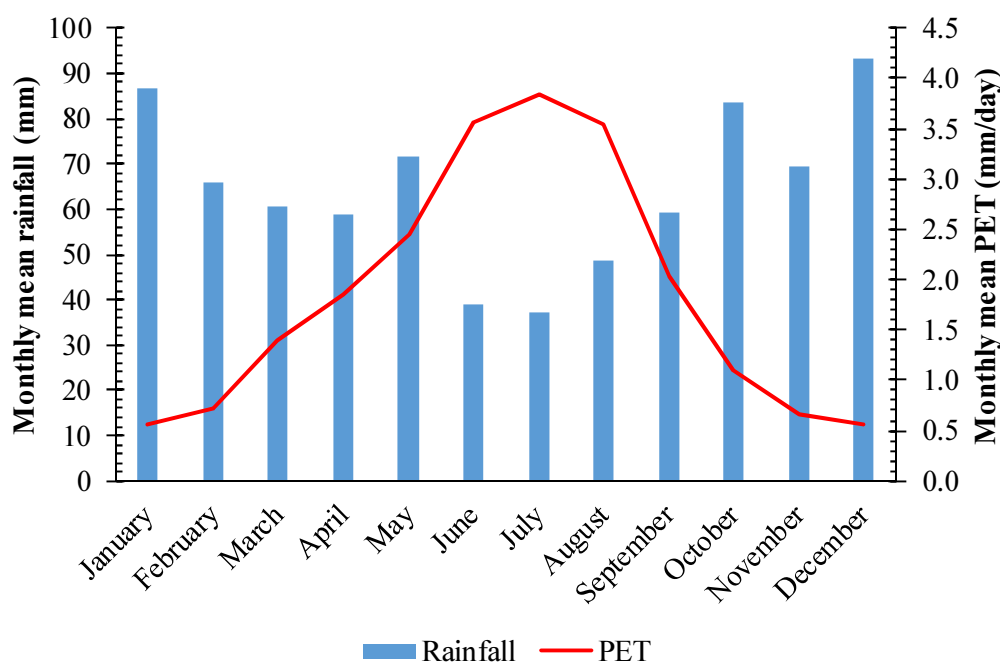


Figure 7.1: Monthly mean rainfall and PET during a 30 year simulation

The data set generated here was different to the data presented in Stovin *et al.* (2013). By running a new scenario, it was possible to simulate drying cycle behaviour using  $PET_{FAO56}$  rather than  $PET_{TH}$ . However, as a result, and in view of the random nature of the Weather Generator, a lower rainfall depth was simulated (774 mm compared with 838 mm in Stovin *et al.*, 2013). The simulated rainfall depth of 774 mm was lower than the 30-year historical average of 834.6 mm (1981-2010) for Sheffield (Grid Ref. 53.383, -1.483, see <http://www.metoffice.gov.uk/public/weather/climate/gcqzwwq04e> as accessed on 23rd June 2016). All analyses presented here relate to the later simulation. All data was generated at 1-hour intervals, with the exception of  $PET_{FAO56}$ , which was calculated in mm/day and evenly disaggregated to generate a dataset with hourly intervals. PET is known to vary diurnally. However, a simplifying assumption was made here, such that hourly PET was equal to daily PET divided by 24.

Boundary conditions for moisture storage were applied by using the specific  $S_{MAX}$  for each configuration. The model was applied with three SMEF choices for each of the modelled configurations. No crop factor was applied to  $PET_{FAO56}$  estimates and constant albedo of 0.23 was assumed. Variations in ET therefore resulted from differences in each configuration's  $S_{MAX}$  and, in the case of the  $S_e$  Power SMEF, the value of  $\epsilon$ . Model outputs included mean annual retention and mean per-event retention; the latter also being categorised to show the responses to significant rainfall events. Significant events were defined as having a return period of greater than 1 year (i.e.  $T = 1.1$  year event from a Gumbel distribution fitted to the annual maximum rainfall depths). This approach – consistent with Stovin *et al.* (2012) – focuses on the most relevant events for designers and not the ‘routine’ events for which all conventional drainage systems are designed and for which retention by green roofs will also be high. An important consideration for the long-term hydrological performance of green roofs is the frequency and length of any drought. Here, an estimate of drought stress risk was made by counting the number and duration of periods for which residual moisture,  $S_t$ , was less than 1.0 mm.

### 7.3.2 Design storm events

The model was applied to predict the response of green roofs to design storm events with different probabilities of occurrence (or return periods). Model parameters were varied to

identify the influence of configuration, seasonal climate, initial moisture content, length of ADWP and rainfall depth upon the response.

Responses from each of the three configurations were modelled across all four seasons. The model has the capacity to calculate  $PET_{FAO56}$  provided that all relevant input data is available. However, here, the drying cycle was modelled using the mean monthly PET values that were generated in the 30 year simulation. PET data was used for January (to replicate winter), April (spring), July (summer) and October (autumn).

### 7.3.2.1 Modelling assumptions affecting the drying cycle

The initial moisture condition (i.e.  $S_e$ ) at the beginning of the ADWP is explicitly calculated in a continuous simulation, but needs to be assumed for a design storm. Conceptually,  $S_e$  would be expected to be highest in winter and lowest in summer. However, most designers would assume the worst case scenario (i.e.  $S_e = 1$  or  $SMD = 0$ ). As such, this scenario was adopted as the default initial moisture content assumption. A further iteration was also considered, whereby the seasonal mean  $S_e$  was inputted as the initial moisture condition. It could be argued that this iteration represents a more typical response. Here, seasonal mean  $S_e$  was determined using the CS616 data across the 46 number AE9 events when CS616 probes were in place (see Table 7.1). As such, it was only possible to establish values for this parameter with TB1, TB2 and TB7. However, as  $S_e$  is expressed as a proportion (on a scale of 0 to 1) of  $S_{MAX}$ , the seasonal mean  $S_e$  was also applied to TB4 to estimate the response of a typical Meadow Flower configuration.

Table 7.1: Mean values of  $S_e$  at the beginning of the ADWP (AE9 events)

	Spring	Summer	Autumn	Winter
TB1	0.51	0.32	0.52	0.79
TB2	0.57	0.42	0.62	0.82
TB7	0.56	0.47	0.52	0.91
<b>Mean <math>S_e</math></b>	<b>0.55</b>	<b>0.41</b>	<b>0.55</b>	<b>0.84</b>

As expected, mean  $S_e$  at the beginning of the ADWP was highest in winter (0.84) and lowest in summer (0.41). Taking the mean  $S_{MAX}$  for TB1, TB2 and TB7 (31.4 mm), this equated to  $S_i$  of 26.4 mm in winter and 12.9 mm in summer. Mean  $S_e$  was the same (0.55 or  $S_i = 17.3$  mm) in spring and autumn. Some systematic differences were observed. With TB1,  $S_e$  was always lower than the mean of the three TBs. However, available moisture capacity was still typically greater for TB1 than with TB7 due to its higher  $S_{MAX}$ .



An important modelling parameter is the assumed length of ADWP. Here, a 7-day ADWP was simulated. However, alternative scenarios were also modelled to highlight the impact upon the runoff hydrograph of a 1, 2 and 10 day ADWP (representing a low, the mean and the maximum length of ADWP for the AE9 events, see Section 4.4.1.2).

### 7.3.2.2 Modelling assumptions affecting the wetting cycle

Synthetic rainfall data was generated using the Depth-Duration-Frequency (DDF) rainfall distribution method (as detailed in the Institute of Hydrology's Flood Estimation Handbook, FEH, 1999) for a location in Sheffield (Grid Reference SK 36000 87000). The FEH method calculates rainfall depth based on the return period, duration and climate change factor. The DDF model imposes a functional form on the relationship between rainfall and return period, as defined by 6 parameters. Coefficient values for  $c$ ,  $d_1$ ,  $d_2$ ,  $d_3$ ,  $e$  and  $f$  were taken from the FEH CD-ROM for a square kilometre grid. Depending upon the storm duration ( $SD$ ), the design rainfall depth is calculated according to a choice of Equation 7.1, Equation 7.2 or Equation 7.3.

$$\text{If } SD \leq 12 \text{ hours: } \ln P = (c \cdot y + d_1) \ln SD + e \cdot y + f \quad \text{Equation 7.1}$$

$$\text{If } 12 < SD \leq 48 \text{ hours: } \ln P = \ln P_{12} + (c \cdot y + d_2) (\ln SD - \ln 12) \quad \text{Equation 7.2}$$

$$\text{If } SD \geq 48 \text{ hours: } \ln P = \ln P_{48} + (c \cdot y + d_3) (\ln SD - \ln 48) \quad \text{Equation 7.3}$$

The developed model has the capacity to accommodate any duration. However, the responses to events with a single rainfall duration of 6 hours were considered here. CIRIA (2015) states that this duration can be used to model response unless the use of alternative durations can be justified. The three return periods considered here (i.e. 1, 30 and 100 years) are consistent with the SuDS calculation requirements in Section 3 of the SuDS standards, C753 (CIRIA, 2015). In accordance with guidelines published in the UK National Planning Policy Framework (Department for Communities & Local Government, 2012) for the design of residential properties with a design life through to the period 2085-2115, the calculated rain depth was uplifted by 30% to account for the effects of future climate change.

For design storms, rainfall and runoff responses were modelled at 1-minute intervals. One of two profiles were used to distribute the rainfall depth temporally. These profiles reflect different rainfall intensity patterns, as defined in the Flood Studies Report (NERC, 1975):

1. 50% summer profile – typically adopted for urban catchments, the profile is more peaked than 50% of summer profiles; or
2. 75% winter profile – typically used for rural catchments, this profile is more peaked than 75% of winter profiles.

Alternative profiles can be used to distribute the rainfall. However, here, rainfall was distributed according to the Winter 75 profile for winter and autumn events and the Summer 50 profile for spring and summer events. Again, the model has the capacity to distribute rainfall according to additional profiles if required.

The developed model is intended to inform design engineers about the hydrological response of green roofs to specific design rainfall events. As such, the model generates per-event statistics such as retention, peak attenuation and peak delay.

## 7.4 Results

### 7.4.1 30 year simulation

The 30 year simulation was run with a view to identifying the long-term retention performance of three typical green roof configurations; including differences in annual and per-event retention and in the incidence of drought stress. Detention was not considered here. Before analysing responses, it is necessary to place this performance into context through consideration of rainfall depths.

#### 7.4.1.1 Rainfall characteristics

Over a 30 year period, as simulated using the UKCP09 Weather Generator tool, the mean annual rainfall depth was 774 mm. On average, this depth was spread across 149 events per annum, such that the mean per-event rainfall depth was 5.2 mm. As shown in Table 7.2, the mean rainfall depth during ‘significant events’ was higher, at 41.2 mm.

*Table 7.2: Rainfall statistics from the 30 year simulation*

Total Rainfall	23221	mm
Average Annual Rainfall	774	mm
No. of Events	4472	No
Mean per event rainfall depth	5.2	mm
No. of Significant Events	83	No
Mean significant per event rainfall depth	41.2	mm

It was expected that, by definition, there would be 30 significant events over the 30 year simulation period. It is possible that a more accurate definition of ‘significant’ events could be achieved by applying a distribution other than Gumbel to the annual maximum rainfall series. Despite this, the smallest ‘significant event’ in the synthetic rainfall data was 29.9 mm, which is similar to a design storm with a 1-in-2 year return period.

#### 7.4.1.2 Simulated hydrological responses

As rainfall data was at hourly intervals, analysis of detention was not possible. However, the value of this hourly continuous simulation is in its predictions of retention performance. To simulate the responses of the three configurations during the drying cycle,  $PET_{FAO56}$  was factored down by using three SMEFs. Each configuration’s response accounted for its specific  $S_{MAX}$  (and in the case of the  $S_e$  Power SMEF, the configuration- and season-specific  $\epsilon$ ). Figure 7.2 illustrates the relatively small differences in runoff between the three configurations (when using the  $S_e$  Power SMEF) over the first year of the simulation.

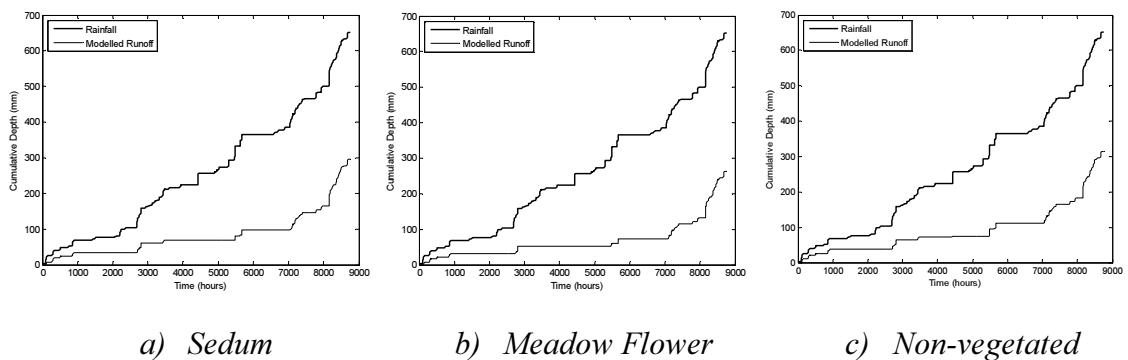


Figure 7.2: Rainfall and runoff for year 1 of a 30-year time series ( $S_e$  Power SMEF)

Here, runoff was predicted to be highest from the non-vegetated configuration and lowest from Meadow Flower. However, differences due to configuration were minor. The hydrological responses of each configuration over the entire 30 year period are summarised in Table 7.3.

Table 7.3: Summary of the hydrological responses to the 30 year simulation

Vegetation Treatment	SMEF	Mean annual retention	Mean per-event retention	Mean per significant event retention	Mean no. of drought occurrences / year
<b>Sedum</b>	None	55.6%	75.4%	26.2%	14.5
	<i>S<sub>e</sub> Linear</i>	49.4%	72.5%	19.3%	0.3
	<i>S<sub>e</sub> Power</i>	48.1%	71.8%	18.5%	0.7
<b>Meadow Flower</b>	None	56.0%	75.7%	27.1%	14.3
	<i>S<sub>e</sub> Linear</i>	49.9%	72.8%	19.9%	0.1
	<i>S<sub>e</sub> Power</i>	51.4%	73.4%	22.0%	5.5
<b>Non-vegetated</b>	None	54.3%	74.9%	23.5%	15.8
	<i>S<sub>e</sub> Linear</i>	48.0%	71.9%	17.6%	0.6
	<i>S<sub>e</sub> Power</i>	47.2%	71.5%	17.0%	0.2

Over a 30 year period, when a SMEF was not employed, simulated mean annual retention and per-event retention were higher than simulations that used a SMEF. Predictions of mean annual retention without a SMEF were higher than predictions using the *S<sub>e</sub> Power SMEF* by between 4.6% (Meadow Flower) and 7.5% (Sedum). Mean retention of significant events was higher by between 5.1% (Meadow Flower) and 7.7% (Sedum). Predictably, modelling ET as equal to PET (i.e. with no SMEF) also resulted in the largest number of droughts. The predicted frequency of drought stress was 2.6 times higher with Meadow Flower, 20 times higher for Sedum and 79 times higher for the non-vegetated configuration (relative to predictions using the *S<sub>e</sub> Power SMEF*). It has already been demonstrated that ET is not consistently equal to PET and therefore predictions generated without a SMEF must be expected to overestimate retention and understate runoff. In reporting on the results of the simulation, further comments will be limited to the simulations that employed a SMEF.

Differences in retention performance were much smaller when comparing predictions based on the *S<sub>e</sub> Linear* and *S<sub>e</sub> Power SMEFs*. Here, the choice between these two SMEFs affected mean annual retention for any configuration by a maximum of 2%. Mean per-event and per significant event retention varied by no more than 1%. Mean annual retention across all three configurations (using either SMEF) was between 47% and 52%. Retention here was higher than reported in Stovin *et al.* (2013), when retention was 39.7%. However, rainfall was higher in the simulation presented in Stovin *et al.* (2013), at 838 mm. In all cases, median per-event retention was 100%. This can largely be

explained by the small median rainfall depth (2.1 mm). Mean per-event retention of between 71% and 73% was lower than measured for AE9 events (85.1%). However, this can be explained by differences in the incidence of rainfall across the 4472 rainfall events. Here, a higher proportion of significant events were included; for which mean per-event retention was between 17% (non-vegetated) and 22% (Meadow Flower).

#### 7.4.1.3 Drought stress risk

The simulated number of droughts varied according to the configuration and SMEF type. Use of the  $S_e$  Linear SMEF correctly predicted marginally greater retention by Meadow Flower compared with Sedum. However, a greater frequency of drought was simulated with Sedum vegetation than with Meadow Flower. This would not be consistent with the previous findings of this research and only reflects the lower  $S_{MAX}$  of the Sedum-vegetated configuration. However, use of the  $S_e$  Power SMEF, which most accurately mimics the decay patterns for each vegetation treatment (most importantly with Meadow Flower) predicted responses that were consistent with observations in Chapters 4 and 5, i.e. higher retention (and higher drought stress risk) with Meadow Flower relative to Sedum.

The results of the simulation using the  $S_e$  Power SMEF were consistent with previous observations regarding the risk of drought for each vegetation treatment (see Table 7.4).

Table 7.4: Drought stress indicators

<b>Vegetation treatment:</b>	<b>No. drought stress events</b> (-)	<b>Mean duration</b> (hours)	<b>Median duration</b> (hours)	<b>Max duration</b> (hours)	<b>Min duration</b> (hours)	<b>Prop. time affected</b> (-)
<b>Sedum</b>	20	107	117	312	2	0.0082
<b>Meadow Flower</b>	166	118	84	566	1	0.0745
<b>Non-vegetated</b>	5	37	19	124	1	0.0007

The risk of drought was highest for Meadow Flower and lowest with non-vegetated configurations. Meadow Flower was at risk of drought during 7.5% of the 30 year period (equivalent to more than 25 days per year), including one continuous period in excess of 24 days. It is therefore reasonable to expect that over its life cycle routine irrigation would be required to avoid the permanent wilting of the Meadow Flower treatment. As such, a

further iteration of the simulation was run where 30 mm of irrigation water was applied when  $S_t$  reached 1 mm. In this scenario, mean annual retention fell by 1.4% to 50.0%, mean per-event retention fell by 0.4% to 73.0% and mean per significant event retention fell by 2.6% to 19.4%. Even with irrigation, in Sheffield, the performance of Meadow Flower still exceeded that of Sedum on all comparators due to the greater ET and faster regeneration of the SMD during inter-event dry periods.

Sedum vegetation was approximately eight times less likely than Meadow Flower to be at risk of drought; suffering drought stress for an equivalent of 3 days per year. It must therefore be expected that some sporadic irrigation may be required, particularly during prolonged periods of dry weather, such as the 13 day drought period seen here.

#### *7.4.1.4 Summary of long-term simulated responses*

Differences in the retention responses predicted using the  $S_e$  Linear SMEF and  $S_e$  Power SMEF were minor. The maximum difference was 2.2% in mean per significant event retention. However, the use of the  $S_e$  Power SMEF within a continuous 30-year simulation allowed previously-observed differences in retention and drought stress across each configuration to be modelled. Differences in the hydrological performance of the three configurations were minor but systematic – retention was highest with Meadow Flower and lowest from the non-vegetated configuration. Mean annual retention of the 774 mm of rainfall was between 47.2-51.4%. Mean per-event retention of significant events (mean rainfall of 41.2 mm) ranged between 17-22%. The better retention performance of Meadow Flower was associated with a greater risk of drought stress. Irrigation to mitigate this risk reduced mean annual retention by 1.4% and per significant retention by 2.6%. However, retention performance was still higher for Meadow Flower with irrigation than for Sedum without it. Through long-term simulations, designers can evaluate the performance of alternative green roof configurations and/or refine a configuration (e.g. to include irrigation or to increase soil depth). As such, a long-term simulation represents a valuable preliminary feasibility assessment tool for SuDS design practitioners.

#### **7.4.2 Design storm events**

Whilst mean annual retention and per-event retention statistics over a 30 year simulation provide a good indication of a green roof's SuDS long-term potential, response of green roofs to design rainfall events are also important to design engineers. Responses to design

rainfall events were simulated for three representative configurations (i.e. TB2, TB4 and TB7). Here, timing of runoff was considered as well as quantity. Models will typically predict a response on the basis of certain assumptions. Here, a number of assumptions (i.e. configuration, season, initial moisture content, length of ADWP and rainfall characteristics) were varied to identify the effect on the predicted outcome. The  $S_e$  Power *SMEF* was used for all simulations. As synthetic (rather than real, irregular) rainfall data was used in the model, rainfall and runoff were modelled at 1-minute intervals. Small differences (of approximately 0.4 mm) existed between net rainfall (i.e. rainfall minus SMD) and runoff. This was largely due to the definition of the rainfall event finishing 6 hours after the last rainfall. When combined with the low  $k$  value, very small amounts of runoff were still being predicted after this cut-off point. The values of  $k$  inputted into the model reflected the vegetation-median values for Sedum, Meadow Flower and non-vegetated beds excluding LECA (i.e. 0.0049, 0.0058 and 0.0083  $\text{mm}^{1-n}/\text{min}$  respectively).

#### 7.4.2.1 *Influence of configuration upon predicted hydrological response*

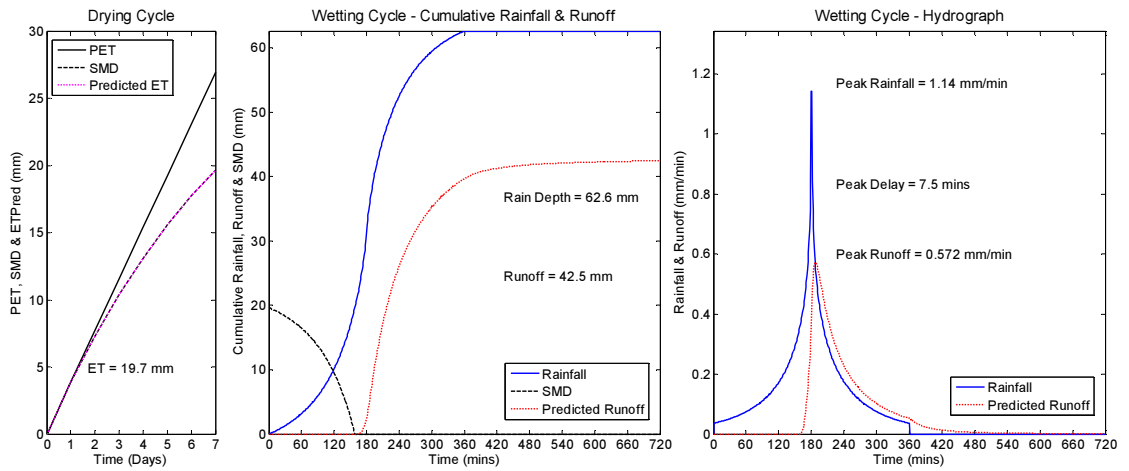
To demonstrate the outputs of the model, and the differences in the response according to configuration, Figure 7.3 highlights the responses of a Sedum (TB2), Meadow Flower (TB4) and non-vegetated (TB7) configuration to a six hour duration design rainfall event with a return period of 1 in 30 years. Modelling assumptions include (i) an ADWP of 7 days, (ii) summer seasonal conditions in the month of July (when  $\text{PET} = 3.85 \text{ mm/day}$ ), and (iii) an initial moisture condition where SMD was zero (i.e. at field capacity) at the start of the ADWP.

The calculated rainfall depth was 62.6 mm and the peak rainfall intensity was 1.14 mm/min. Predictably, runoff was highest from the non-vegetated test bed (45.2 mm, with per-event retention of 27.8%) and lowest from Meadow Flower (39.5 mm and per-event retention of 36.9%). These differences in retention are, as expected, consistent with differences in  $\text{ET}_{\text{CUM}}$  during the event's ADWP; ranging between 17.1 mm (TB7) and 22.7 mm (TB4) over the 7 day period. The influence of configuration upon runoff was also mirrored in the predictions of peak runoff. Runoff from Meadow Flower was lowest, at 0.53 mm/min (i.e. peak attenuation of 53.4%) and highest from the non-vegetated bed, 0.72 mm/min (i.e. 36.8% peak attenuation). Peak delay was not strongly affected by configuration; ranging between 3.5 and 8.5 minutes.

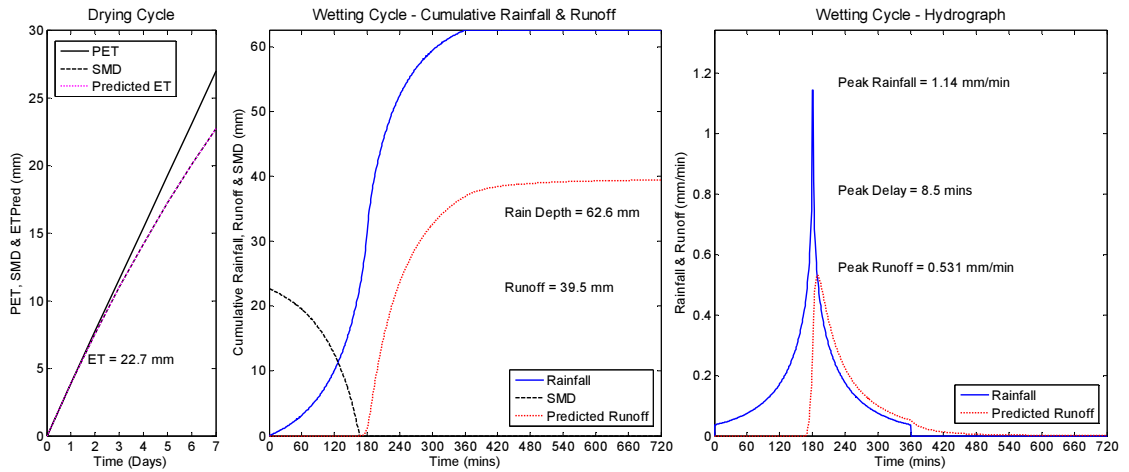
#### 7.4.2.2 *Importance of seasonal climate*

The influence of the seasonal climate upon the hydrological response was considered by simulating the response of TB2 to the same conditions considered in Section 7.4.2.1 with one exception – the season. Spring, autumn and winter conditions were modelled (see Figure 7.4) and contrasted against the previously-considered summer scenario. The choice of season affected the modelled response in two ways. Firstly, ET rates during the ADWP varied seasonally and secondly the temporal distribution of runoff was different in autumn and winter (with peak rainfall of 0.46 mm/min) compared to spring and summer (1.14 mm/min). As expected, after a 7 day ADWP, retention was predicted to be highest in summer (32.1%) and lowest in winter (6.5%). Retention in spring (17.4%) was predicted to be higher than retention in autumn (11.5%). Predicted peak attenuation was also typically highest in summer (49.8%) and lowest in both winter and autumn (5.4%), when the peak runoff rate was 0.44 mm/min. In summer, the peak rate of runoff was reduced to 0.57 mm/min compared to 0.68 mm/min in spring (when peak attenuation was 40.2%). Again here, differences in peak delay were negligible across all seasons (ranging between 4.5 and 9.5 minutes).

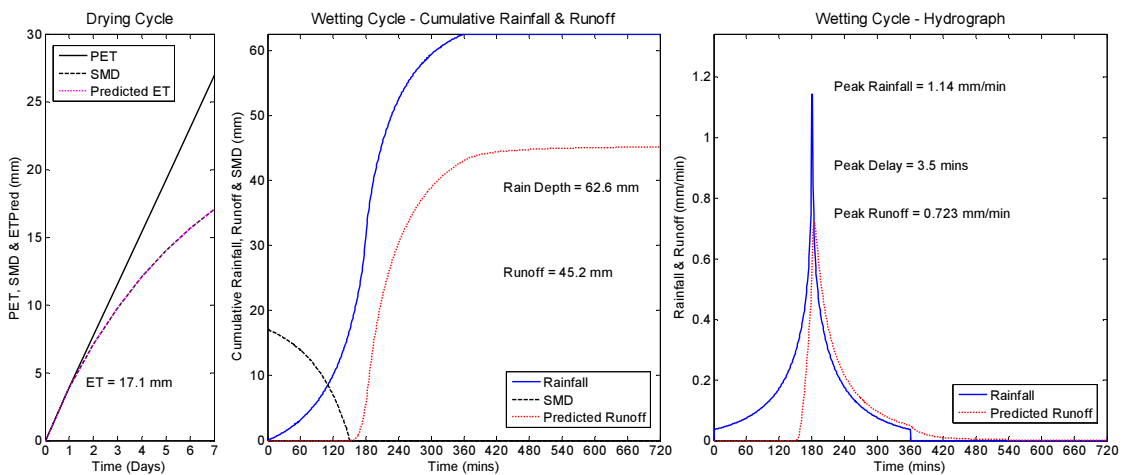




a) TB2 - Sedum

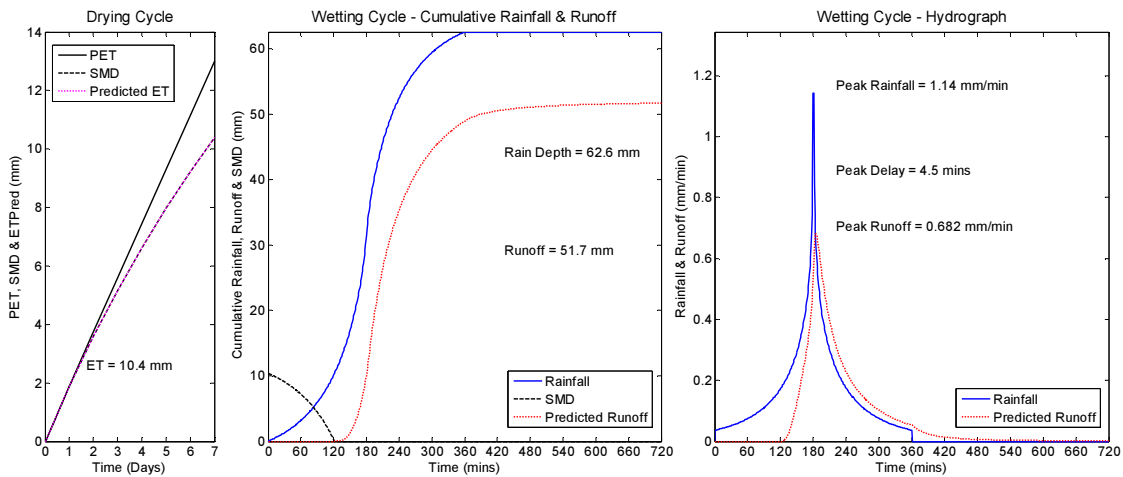


b) TB4 - Meadow Flower

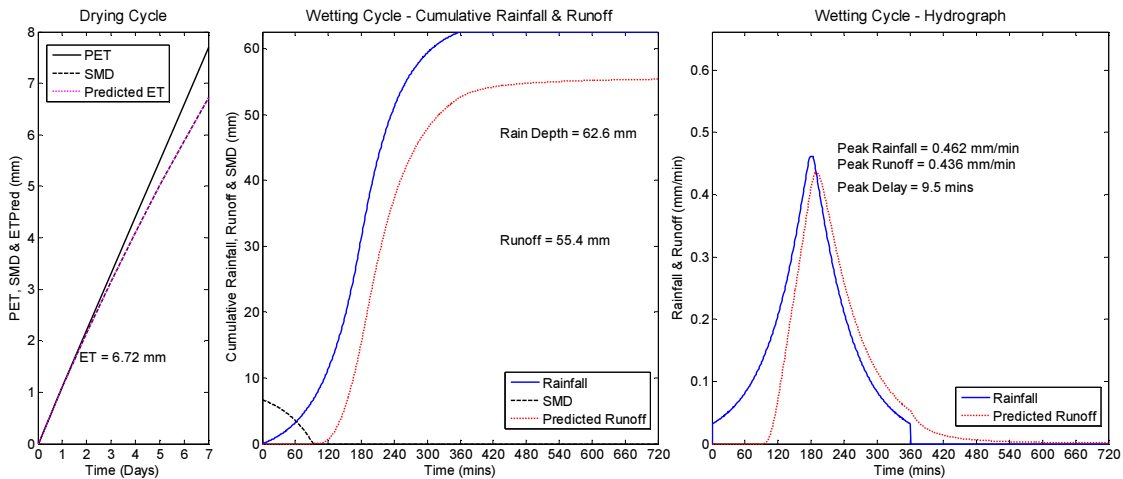


c) TB7 - Non-vegetated

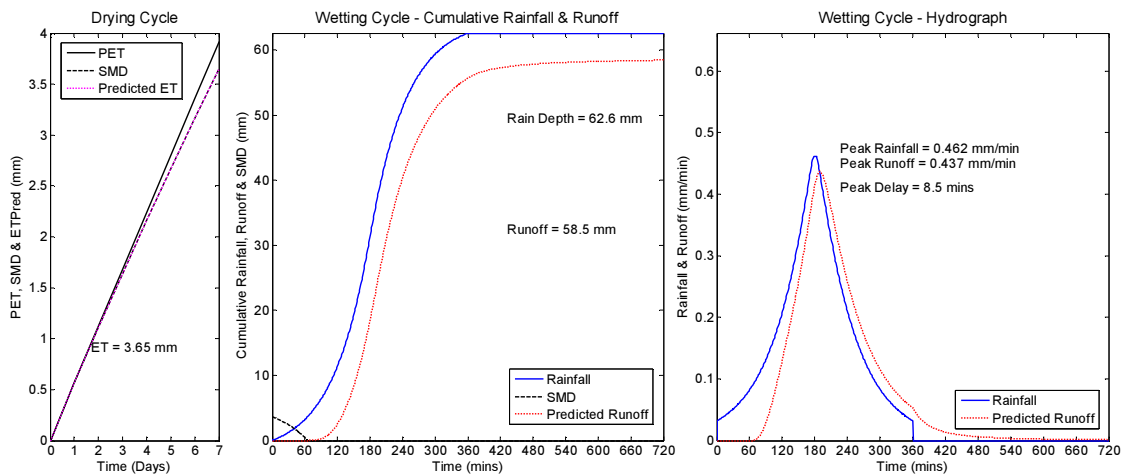
Figure 7.3: Responses of TB2, TB4 & TB7 to 6 hour, 1 in 30 year event in summer



a) Spring



b) Autumn



c) Winter

Figure 7.4: Influence of season on response of TB2 to 1 in 30 year event

### 7.4.2.3 Importance of initial moisture condition

Hydrological calculations for SuDS measures typically assume that SMD is zero at the beginning of the ADWP. However, often, this will not be the case. Not all rainfall events will saturate the green roof. Here, seasonal mean  $S_e$  at the beginning of the ADWP (as summarised in Table 7.1) was used to calculate the initial SMD for TB2: 19.1 mm in summer (i.e.  $[1-0.41] \times S_{MAX}$ ) and 14.6 mm in spring (i.e.  $[1-0.55] \times S_{MAX}$ ). Figure 7.5 demonstrates the outcomes in summer and spring respectively.

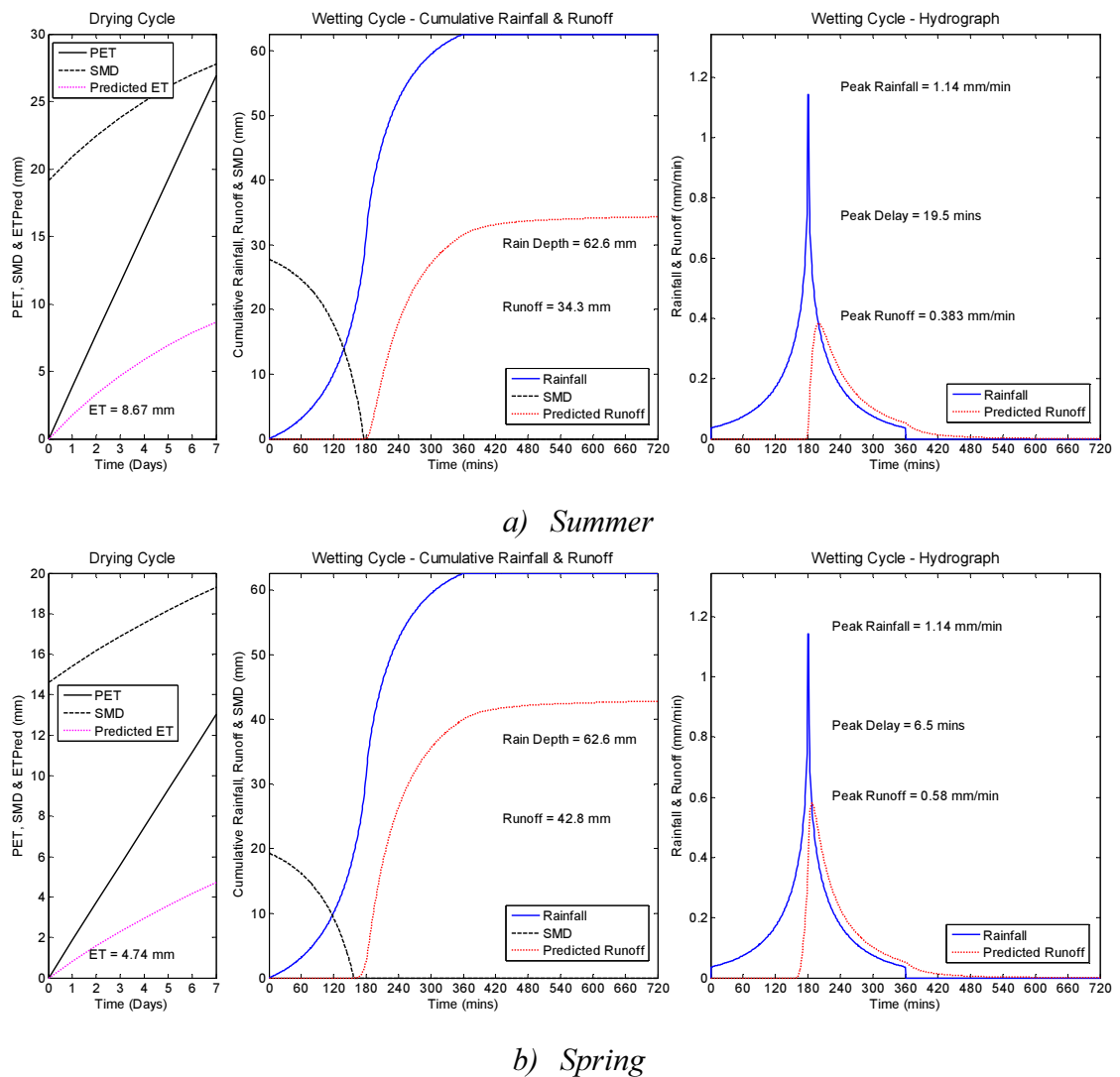


Figure 7.5: Influence of SMD on response of TB2 to 1 in 30 year event

In summer, ET was constrained by lower moisture availability; totalling 8.7 mm compared to 19.7 mm when initial SMD was zero. However, by the end of the ADWP, SMD was 8.1 mm higher than the worst case scenario. As a result, predicted runoff was

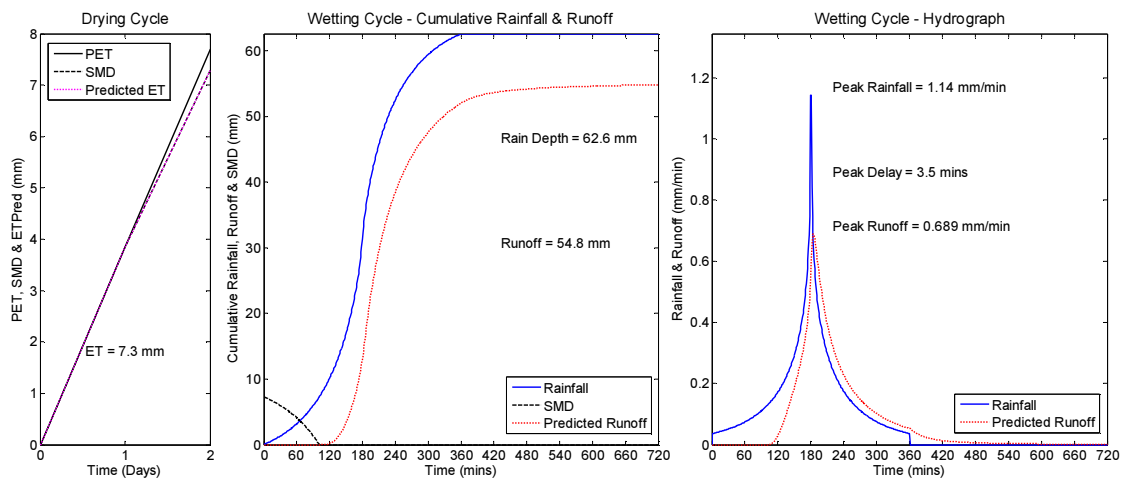
34.3 mm (versus 42.5 mm in the worst case scenario), peak runoff was 0.38 mm/min (versus 0.57 mm/min) and peak delay was 19.5 minutes (versus 7.5 minutes). Similar trends were observed in spring as, when assuming seasonal mean  $S_e$ , ET was also constrained (4.7 mm versus 10.4 mm), total runoff was lower (42.8 mm versus 51.7 mm), peak runoff was lower (0.58 mm/min versus 0.68 mm/min) and peak delay was longer (6.5 minutes versus 4.5 minutes).

The initial moisture assumption had an important effect on runoff predictions. However, using a SMEF, ET predictions based on a seasonal mean  $S_e$  initial condition were lowered in line with the reduced moisture availability; partially offsetting the assumption regarding initial SMD. The extent to which this initial assumption is offset by reduced ET will vary with the length of ADWP. Shorter ADWPs will lead to a lower offset.

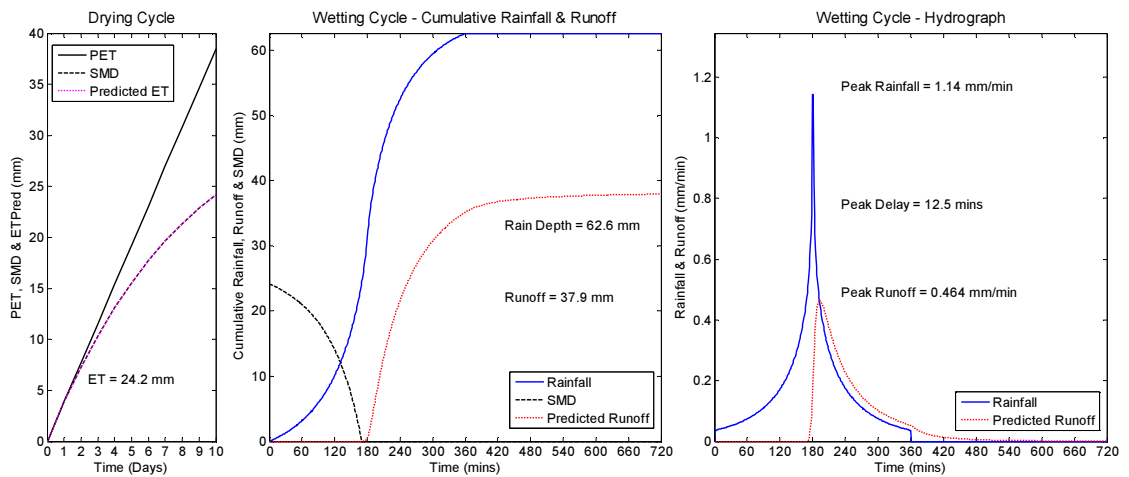
#### 7.4.2.4 Importance of ADWP

The length of ADWP is recognised as an important influence upon the hydrological performance of green roofs (Stovin *et al.*, 2012), representing the time during which the green roof has the opportunity to regenerate its available moisture capacity ahead of the next rainfall event. Here, two alternative ADWP lengths were considered and contrasted against the base scenario of a 7 day ADWP: a 2 day ADWP – being representative of the mean length of ADWP during the AE9 events, as summarised in Section 4.4.1.2 – and a 10 day ADWP – the maximum observed ADWP during the AE9 events (see Figure 7.6).

Retention was predictably lowest (12.5%) following the shortest ADWP (i.e. 2 days) and highest (39.5%) following the longest ADWP (i.e. 10 days). The 16.9 mm difference in runoff was consistent with differences in  $ET_{CUM}$  during the drying cycle. The decay in ET with respect to time (and more directly moisture availability) was evident here. Highest mean daily ET was predicted during the shortest ADWPs. ET was highest over the 2 day ADWP (3.65 mm/day), compared with 2.81 mm/day (between 2-7 days) and 1.5 mm/day (7-10 days). The higher runoff following the 2 day ADWP contributed to a 0.1 mm/min increase in the peak rate of runoff (compared to 0.57 mm/min in an event following a 7 day ADWP). Similarly, by extending the ADWP from 7 to 10 days, peak runoff fell by 0.1 mm/min to 0.46 mm/min. It was notable that, even after a 2 day ADWP, peak rates of runoff during a 1 in 30 year event were reduced by 37.5% in both spring and summer (albeit much lower attenuation occurred in autumn and winter).



a) ADWP of 2 days



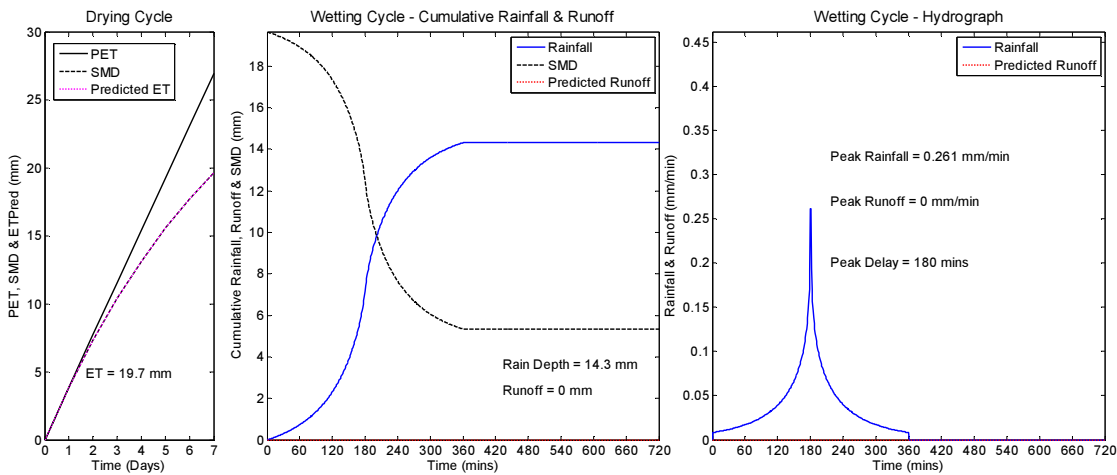
b) ADWP of 10 days

Figure 7.6: Influence of ADWP on response of TB2 to 1 in 30-year event in summer

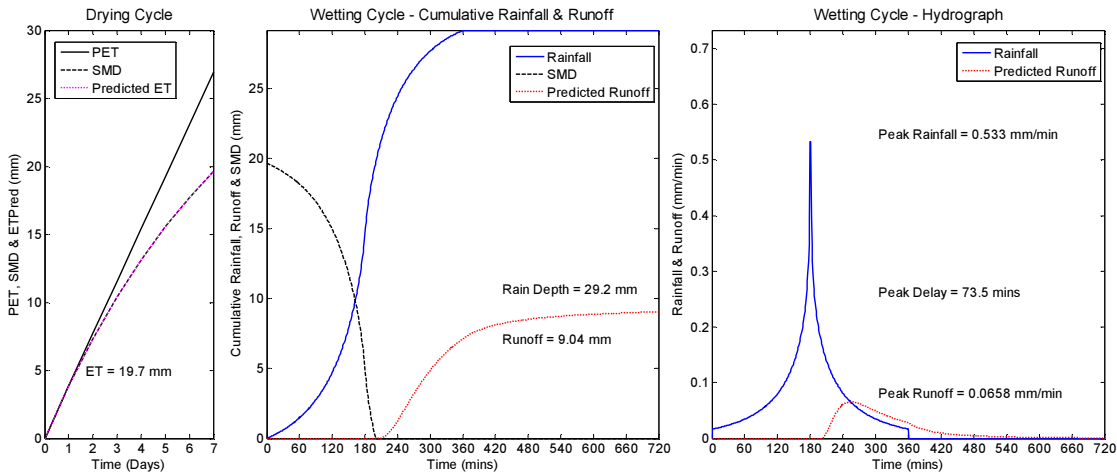
The length of ADWP is clearly an important modelling parameter. All other things being equal, the longer the ADWP, the higher the anticipated ET and retention. Here, summer conditions were calculated. Similar trends would be expected across all seasons. However, the extent to which retention is affected by ADWP depends on seasonal climate and moisture availability. For example, in spring, a reduction in the ADWP from 7 to 2 days led to a lower reduction in retention (10.9%) than in summer (19.8%).

#### 7.4.2.5 Importance of return period

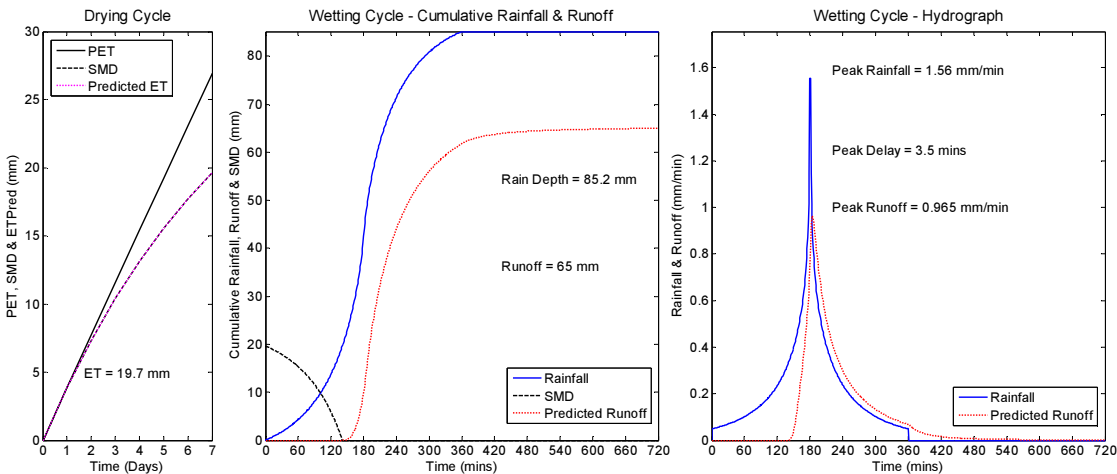
The hydrological performance of any drainage device will be strongly influenced by the depth (and intensity) of rainfall. The response of TB2 to design rainfall events with return periods of 1, 2 and 100 years will now be considered (see Figure 7.7).



a) Return period of 1 year



b) Return period of 2 years



c) Return period of 100 years

Figure 7.7: Influence of return period on response of TB2 to a summer event

The response of TB2 to a 1 in 1 year design rainfall event of six hours duration was analysed. Rain depth was 14.3 mm. Peak rainfall was 0.26 mm/minute. Following a 7 day

ADWP in summer conditions, the SMD of 19.7 mm was sufficient to wholly retain this event. Runoff would have been predicted if the ADWP had been less than 5 days. A 1 in 2 year event was modelled to demonstrate the runoff response of green roofs to relatively frequent events (rather than the lower probability events required in SuDS design). Here, rain depth of 29.2 mm exceeded the SMD to produce runoff of 9.0 mm. Per-event retention was 69.2%. The peak rainfall intensity of 0.53 mm/min resulted in peak runoff of 0.07 mm/min (i.e. peak attenuation was 86.8%) that was delayed by 73.5 minutes.

Predictably, as higher rainfall depths were considered, the relative hydrological performance fell. For a 1 in 30 year storm event of 6 hours duration, rainfall depth was 62.6 mm and peak rainfall was 1.14 mm/minute. Retention was 32.1% as 42.5 mm of runoff occurred with a peak intensity reaching 0.57 mm/min (i.e. peak attenuation was 49.8%). The rainfall event with a 100 year return period produced a rain depth of 85.2 mm and a peak rainfall rate of 1.56 mm/minute. The greater rainfall depth predictably resulted in a lower per-event retention of 23.7% (20.2 mm). This compares against a maximum permissible retention (i.e. if SMD were equal to  $S_{MAX}$ ) of 38.1%. Peak runoff was reduced by 38.1% to 0.97 mm/min.

Generally, retention and peak attenuation were inversely related to rainfall depth. Here, the response to each event was limited by the SMD at the start of rainfall. As such, when rainfall exceeded SMD, retention was typically equal to the SMD and runoff was the difference. As larger rainfall depths were considered, so the retention percentage reduced. Peak attenuation was also inversely related to rain depth and intensity, almost halving when comparing a 1 in 2 year event (69.2%) to a 1 in 100 year event (38.1%).

#### *7.4.2.6 Summary of influences affecting predicted response of green roofs*

Here, it has been demonstrated that the developed model can account for important physical influences that have been identified to affect the hydrological response of green roofs. The configuration, initial moisture content and the length and seasonal climate during the ADWP will affect the predicted response of a green roof to a given design rainfall event. Often, a change in one of the model inputs will affect another. For example, by changing the ADWP assumptions, the influence of configuration upon the response will be affected. Here, the developed model has been shown to have the capacity to capture such inter-dependencies. Table 7.5 summarises the responses of the three

configurations to a 6-hour 1 in 30 year rainfall event for different initial moisture content assumptions (i.e. seasonal mean  $S_e$  and  $SMD = 0$ ), during all four seasons and across two lengths of ADWP (2 days and 7 days).

Table 7.5: Responses to design rainfall events with 30 year return period

		Winter (January)			Spring (April)			Summer (July)			Autumn (October)		
Peak Rainfall		0.46 mm/min			1.14 mm/min			1.14 mm/min			0.46 mm/min		
Initial Moisture Condition	ADWP (Days)	Per Event Retention (%)	Peak Runoff (mm/min)	Peak Delay (mins)	Per Event Retention (%)	Peak Runoff (mm/min)	Peak Delay (mins)	Per Event Retention (%)	Peak Runoff (mm/min)	Peak Delay (mins)	Per Event Retention (%)	Peak Runoff (mm/min)	Peak Delay (mins)
<i>Sedum</i>													
$S_t = \text{Seasonal mean}$	2	10	0.4	10	27	0.6	6	37	0.5	11	26	0.4	12
$S_t = \text{Seasonal mean}$	7	14	0.4	10	32	0.6	7	45	0.4	20	29	0.4	14
$S_t = S_{MAX}$	2	3	0.4	10	6	0.7	4	12	0.7	4	4	0.4	10
$S_t = S_{MAX}$	7	7	0.4	10	17	0.7	5	32	0.6	8	12	0.4	10
<i>Meadow Flower</i>													
$S_t = \text{Seasonal mean}$	2	11	0.4	9	29	0.6	6	41	0.5	13	28	0.4	12
$S_t = \text{Seasonal mean}$	7	15	0.4	9	37	0.5	9	54	0.3	31	33	0.4	15
$S_t = S_{MAX}$	2	2	0.4	9	6	0.7	4	13	0.7	4	4	0.4	9
$S_t = S_{MAX}$	7	7	0.4	9	19	0.7	4	37	0.5	9	12	0.4	9
<i>Non-vegetated</i>													
$S_t = \text{Seasonal mean}$	2	9	0.4	8	23	0.8	4	30	0.7	4	22	0.4	8
$S_t = \text{Seasonal mean}$	7	12	0.4	8	28	0.7	4	36	0.6	6	25	0.4	9
$S_t = S_{MAX}$	2	2	0.4	8	6	0.8	3	12	0.8	3	4	0.5	8
$S_t = S_{MAX}$	7	6	0.4	8	17	0.8	3	28	0.7	4	11	0.5	8

With the seasonal mean initial moisture condition, retention ranged between 9-15% in winter, 23-37% in spring, 30-54% in summer and 22-33% in autumn. Differences in retention due to configuration were greatest in summer (7 day ADWP), when retention by Sedum was 9% higher than the non-vegetated TB but 9% lower than Meadow Flower. The highest peak attenuation (73.7%) and longest peak delay (31 minutes) were observed in summer. When SMD at the beginning of the ADWP was zero, retention was much



lower: 2-7% in winter, 6-19% in spring, 12-37% in summer and 4-12% in autumn. The highest peak reduction was 53.5% and the longest peak delay was 10 minutes.

In summer, maximum retention was 54% (based on seasonal mean initial moisture and a 7 day ADWP). Lower retention was predicted in spring (with a maximum of 37%), autumn (33%) and winter (15%). However, for an initially saturated configuration and a 7 day ADWP, retention fell to just 7% in winter, 12% in autumn, 19% in spring and 37% in summer. Differences due to configuration were greatest in summer. Here, maximum per-event retention ranged between 30% (non-vegetated) and 54% (Meadow Flower).

## 7.5 Discussion

Differences in the predicted responses of the three configurations to design storm events were minor. This was expected in the context of large infrequent rainfall events. The difference in the  $S_{MAX}$  of Sedum (TB2) and Meadow Flower (TB4) configurations (2.3 mm) represents just 2.7% of the 1 in 100 year rainfall depth modelled here. Assumptions regarding initial moisture content affected retention by up to 28% (i.e. 17.5 mm) depending upon whether  $S_e$  was assumed to be one or equal to the seasonal mean at the beginning of the ADWP. The importance of ADWP upon the hydrological response was dependent upon seasonal factors. Per-event retention was up to 24% higher in summer when the ADWP increased from 2 to 5 days. However, in winter, the increase in retention was just 5% (or 3.1 mm). In calculating the response to design storm events, the designer must make certain assumptions in the knowledge that they are important to the predicted outcome; particularly in respect of the length of, and seasonal climate during the ADWP. Subject to these assumed parameter values, retention (in mm) can range between zero and  $S_{MAX}$ . Consideration must therefore be afforded within SuDS design guidance to ensure that the appropriate scenario (or range of scenarios) are modelled.

The use of continuous simulation, as advocated in Stovin *et al.* (2015b) overcomes the issues of ADWP assumption affecting predicted retention performance. Using a SMEF, simulated mean annual retention by all three configurations was between 47.2% (non-vegetated) and 51.4% (Meadow Flower). These values are consistent with the mean annual retention figures that were reported by Stovin *et al.* (2012) and Locatelli *et al.* (2014). In response to a mean rainfall depth of 5.2 mm, mean per-event retention was between 71.5% and 73.4%. For events with a return period greater than one year, mean

per-event retention fell to between 17% and 22% (mean rainfall was 41.2 mm). The fact that retention diminished with increasing rainfall depth reflects the widely reported inverse relationship between rainfall and retention (Rowe *et al.*, 2003; Banting *et al.*, 2004; Stovin *et al.*, 2012). Through the use of the *S<sub>e</sub> Power SMEF*, empirical observations relating to the retention performance and drought stress risk of the different vegetation treatments were reproduced. Whilst the highest retention was observed with Meadow Flower, there was a corresponding increase in drought risk. Designers would therefore need to consider any detrimental impact that any supplementary irrigation may have on the available moisture capacity and retention performance. In the specific case of Meadow Flower, irrigation reduced mean annual retention by 1.4% to 50.0%.

## 7.6 Conclusions

- Through its application, it was possible to demonstrate the model's capacity to reproduce empirical observations; capturing the complex inter-event processes that vary as a function of seasonal climate (using ADWP and PET as modelling parameters) and configuration (as governed by  $S_t$ ,  $S_{MAX}$  and the SMEF in the model) and temporally distributing any surpluses via calibrated detention parameter,  $k$ .
- Differences in predicted retention responses due to configuration were minor but systematic. Over a 30 year simulation (774 mm mean annual rainfall), mean annual retention was lowest with non-vegetated beds (47.2%) and highest with Meadow Flower (54%). For a 1 in 30 year design rainfall event (62.6 mm rainfall), configuration affected per-event retention by a maximum of 1% in winter and autumn, 2% in spring and 9% in summer.
- The influence of seasonal climate upon ET manifested itself in retention and typical detention metrics. Retention of a 1 in 30 year event (62.6 mm of rainfall) was 32.1% in summer but 6.5% in winter. Similarly, peak attenuation was just 5.4% in winter (peak rainfall of 0.46 mm/min) compared with 49.8% in summer (1.14 mm/min peak rainfall).
- Without using a SMEF to factor down PET, unrealistic predictions were made for both retention performance (improving mean annual retention by 7.5% compared

with the *S<sub>e</sub> Power SMEF*) and drought stress risk (estimating the frequency of drought to be 79 times higher than with the *S<sub>e</sub> Power SMEF*).

- Modelling responses to design rainfall events requires a number of assumptions to be made by designers. The values inputted against these assumptions can have a significant influence upon the predicted responses. Long-term continuous simulations can support such per-event calculations and simultaneously provide valuable insight into the long-term performance of different configurations, identifying any irrigation requirements.

## 8 Conclusions

### 8.1 Chapter overview

In this chapter the main conclusions of the research are summarized, the fulfilment of the initial research objectives discussed and recommendations are made for further work in related research areas.

### 8.2 Summary

New data has been collected from field test beds (rainfall, runoff and moisture content) and from microcosms (ET rates). Green roofs can provide valuable additional drainage capacity to complement traditional drainage systems and other SuDS components. The hydrological response will vary due to configuration, rainfall characteristics and antecedent moisture conditions. Green roofs have a finite retention capacity that is governed by the vegetation and substrate configuration. The extent to which this maximum capacity ( $S_{MAX}$ ) is available for retention at the onset of any individual rainfall event will depend on the removal of moisture through ET during the antecedent dry weather period (ADWP). Retention depths can range between zero and  $S_{MAX}$ . When expressed as a percentage, retention is inversely related to rainfall depth, with low probability, high volume events typically leading to low retention percentages. Predictably, the detention effect of extensive green roofs is limited by their shallow substrate depth. However, peak rates of runoff are often reduced as a result of retention and detention combined. Uncertainty surrounding expected performance has been reduced through the development of a physically-based green roof hydrological model. The developed model accounts for the specific characteristics of green roofs, has a plant- and moisture-adjusted ET rate and facilitates time-series analysis of runoff. When modelling responses to design storm events, assumptions regarding antecedent moisture conditions (i.e. length of and climate during the ADWP) can have an important influence on modelled outcomes. Seasonal climate has a significant impact on ET and retention. From a hydraulic perspective, the SuDS contribution of green roofs in winter is minimal, but is typically much greater in summer. As such, designers tasked with mitigating year-round flood risk must combine extensive green roofs with additional downstream retention and detention measures (e.g. blue roofs) to form more holistic SuDS networks.

### 8.3 Key findings

In this section, the important findings of the research are summarised. However, the three key findings were:

1. Rainfall minus soil moisture deficit (SMD) provided a highly credible indication of runoff, despite the existence of vertical moisture gradients and some observations of runoff prior to field capacity ( $\theta_{FC}$ )
2. Retention was typically highest from configurations with the highest maximum capacity ( $S_{MAX}$ ). Retention by vegetated configurations benefitted from an interception storage capacity of up to 8 mm. However, in certain instances (e.g. non-vegetated configurations), higher retention was observed despite lower  $S_{MAX}$  due to the faster regeneration of the SMD via ET.
3. In all instances, ET rates fell instantly below PET. The decay in ET reflected reduced moisture availability but varied seasonally and by vegetation treatment. Seasonal differences in ET were large with vegetated configurations (approx. 10 mm higher in summer than in spring) but small with non-vegetated configurations (2 mm).

#### 8.3.1 Influence of a configuration's physical characteristics

1. Combinations of three substrates – HLS, SCS and LECA – and three vegetation treatments – Sedum, Meadow Flower and Non-vegetated – were trialled. To ensure that the findings of this work are transferable, laboratory tests defined basic physical characteristics of the substrates and established soil-water characteristic curves (SWCC) for HLS and SCS. Qualitative assessments of the void size distribution (VSD) of the substrate and the year-round coverage of the vegetation were also performed.
2. HLS contained the highest proportion of small particles (2.3% less than 0.063 mm diameter) and the lowest median particle size ( $d_{50} = 4.2$  mm), resulting in the highest maximum water-holding capacity, MWHC (41.2%) and the lowest permeability (1-15 mm/min).

3. SCS had the lowest porosity (59.8%) but the highest median particle diameter ( $d_{50} = 5.2$  mm). SCS had a marginally lower MWHC (39.1%) than HLS. The high proportion of crushed brick and the lowest organic matter (OM) content (2.3%) creates the optimal nutrient-poor growing conditions for Sedum vegetation.
4. LECA has a very high porosity (84.8%) and poorly graded size-distribution, with a high proportion of large and similarly-sized spherical particles. LECA has the lowest MWHC (35.0%) and the highest permeability of the tested substrates.
5. Only minor differences were identified in the SWCC of the two brick-based substrates (HLS and SCS). No meaningful SWCC could be derived for LECA.
6. Differences identified between the values derived for MWHC and the conventional definition of field capacity,  $\theta_{FC}$  ( $\psi = 0.33$  kPa) were 16.1% and 17.1% (v/v) for HLS and SCS respectively. Further work is recommended to establish whether the conventional definition of  $\theta_{FC}$  applies to highly porous green roof substrates.
7. Sedum is a hardy vegetation treatment containing low growing species with succulent leaves and shallow fibrous roots. Sedum is expected to have the highest interception losses and the greatest tolerance to drought of the trialled vegetation treatments.
8. The Meadow Flower mix contained a range of grasses and wildflowers in addition to three Sedum species. ET and the risk of drought stress will typically be higher with Meadow Flower than with Sedum due to the larger leaf sizes and a greater variation in plant height, rooting depth and leaf shapes.

### **8.3.2 Hydrological responses of green roofs in field conditions**

1. The hydrological responses of nine small (3 m<sup>2</sup>) test beds, combining three substrates and three vegetation treatments, were monitored in Sheffield (UK) over a continuous 4 year period between February 2010 and February 2014. Rainfall, runoff, climate (air temperature, solar radiation, relative humidity and wind speed) and moisture content were monitored.

2. Over the four year period, 323 events were recorded with rainfall greater than 2 mm. Valid runoff responses were measured for between 164 (TB9) and 257 (TB6) events. A full record was available for all nine test beds (AE9) for a subset of 48 events.
3. Mean AE9 per-event rainfall of 6.5 mm varied seasonally with highest rainfall in winter (12.4 mm) and lowest (3.8 mm) in autumn. Mean ADWP was 1.8 days and the maximum ADWP was 10 days. Two AE9 events had a return period greater than 1 year. Nine AE9 events had rainfall greater than 10 mm; four of which exceeded 20 mm.

#### *8.3.2.1 Retention response*

1. The maximum observed retention depth from any bed was 23.2 mm (from TB4 in response to EV45, when 31.3 mm of rain fell).
2. The greatest difference in retention due to configuration was 19.2 mm, measured as the difference between the responses of TB4 and TB9 to EV45.
3. In response to a median rainfall depth of 3.7 mm, configuration-median per-event retention for AE9 events was between 98% (TB8) and 100% (TB2).
4. The lowest per-event retention percentage was 7.1% by the non-vegetated TB9 (EV246). The lowest per-event retention by a Meadow Flower configuration was 11.1% (TB4, EV246) and by a Sedum configuration was 13.9% (TB2, EV246).
5. For events with rainfall greater than 10 mm, mean per-event retention ranged between 14% (TB9) and 70% (TB1). Mean per-event retention fell further when rainfall exceeded 20 mm; ranging between 14.9% (TB9) and 54.8% (TB1).
6. The contribution of vegetation to retention response was only observed when rainfall depth exceeded 10 mm. Here, vegetation-mean per-event retention was highest with Sedum (49.0%) and lowest with non-vegetated configurations (32.6%).
7. Interception losses were as high as 8.0 mm with Sedum (TB3). Median interception losses for Sedum were 2.4 mm; in part reflecting the low median rainfall (3.7 mm).

8. Even when rainfall depth exceeded 10 mm, no significant differences were observed in substrate-mean per-event retention by HLS (49.8%) and SCS (45.5%). However, per-event retention was lower with LECA (29.1%).
9. Differences in configuration-mean per-event retention due to seasonal climate were observed, ranging between:
  - a. 74% (TB9) and 91% (TB1) in spring (mean ADWP: 1.5 days; mean rain depth: 8.1 mm);
  - b. 84% (TB9) and 97% (TB1, TB4) in summer (mean ADWP: 2.4 days; mean rain depth: 6.0 mm);
  - c. 89% (TB9) and 98% (TB7, TB8) in autumn (mean ADWP: 1.6 days; mean rain depth: 3.8 mm);
  - d. 31% (TB9) and 38% (TB1) in winter (mean ADWP: 0.9 days; mean rain depth: 12.4 mm).

#### 8.3.2.2 Detention response

1. Configuration-median peak attenuation ranged between 98% and 99% (with rainfall and runoff at 1-minute intervals). Minimum values ranged between 9% (TB9) and 26% (TB2). When rainfall depth exceeded 20 mm, configuration-median peak attenuation ranged between 25.2% (TB9) and 64.4% (TB1).
2. In spring, seasonal-mean peak rainfall of 0.50 mm/5min resulted in seasonal-mean peak runoff of between 0.06 and 0.17 mm/5min. In summer, peak rainfall of 0.67 mm/5min resulted in peak runoff of between 0.04 and 0.12 mm/5min. In autumn, peak rainfall was 0.68 mm/5min and peak runoff between 0.01 and 0.05 mm/5min. In winter, peak rainfall was 0.41 mm/5min and peak runoff ranged between 0.15 and 0.23 mm/5min.
3. For events with rainfall greater than 20 mm, peak attenuation was 38.3% (non-vegetated beds), 50.2% (Meadow Flower) and 54.3% (Sedum).
4. Peak delay was strongly influenced by the duration and intensity of rainfall. The longest observed delay was 47 hours. When rainfall depth exceeded 10 mm,



configuration-median peak delay was between 45 minutes (TB5 and TB7) and 95 minutes (TB2).

5. Many of the conventional detention parameters are distorted by the effects of retention. Only when a system is at  $\theta_{FC}$  at the onset of rainfall will these parameters reflect detention performance alone.
6. Detention parameter ( $k$ ) was used to describe the detention characteristics of each individual system. A high value of  $k$  reflects low detention performance and faster runoff response.  $k$  was optimised for each test bed and each AE event. Configuration-median  $k$  ranged between  $0.0048 \text{ mm}^{1-n}/\text{min}$  (TB2) and  $0.0128 \text{ mm}^{1-n}/\text{min}$  (TB9).
7. Systematic and statistically-significant differences in  $k$  existed due to vegetation treatment. Vegetation-median  $k$  was lowest for Sedum ( $0.0051 \text{ mm}^{1-n}/\text{min}$ ), highest for non-vegetated beds ( $0.0092 \text{ mm}^{1-n}/\text{min}$ ) and  $0.0070 \text{ mm}^{1-n}/\text{min}$  for Meadow Flower.
8. Differences in  $k$  due to substrate were not statistically-significant.  $k$  was highest for LECA ( $0.0084 \text{ mm}^{1-n}/\text{min}$ ), reflecting its high porosity and permeability.  $k$  was similar for HLS ( $0.0069 \text{ mm}^{1-n}/\text{min}$ ) and SCS ( $0.0061 \text{ mm}^{1-n}/\text{min}$ ).

#### 8.3.2.3 Initialisation of runoff

1. Runoff was observed prior to  $\theta_{FC}$ . Maximum values of  $\theta$  at the time of first runoff were 0.43 (HLS), 0.38 (SCS) and 0.30 (LECA). Median values were lower.
2. Vertical moisture gradients were observed in the substrates and were greatest in vegetated configurations. The highest  $\theta$  was typically in the low zone of the substrate. However, other factors (e.g. preferential paths or hydrophobicity in dry substrates and rainfall intensity) may also have contributed to runoff prior to  $\theta_{FC}$ .
3. High peak rates of runoff and short delays typically followed the most intense rainfall.

#### 8.3.2.4 *Regeneration of SMD via ET*

1. Pre-event configuration-mean soil moisture deficit (SMD) – an indicator of retention potential – was much higher in summer (16.2-17.7 mm [TB2]) than in spring (10.9-13.0 mm), autumn (9.3-13.6 mm) and winter (0.1-4.1 mm).
2. Except in summer, at short ADWPs, mean pre-event SMD was typically regenerated more quickly with non-vegetated TB7 than with Sedum-vegetated TB1. However, retention was typically greater with TB1 due to its greater overall storage capacity.
3. Moisture content was typically greatest in the low zone of substrates. However, changes in moisture content was measured from all zones of the substrate. It is therefore possible to consider the 80 mm deep substrate as a monolithic unit from a modelling perspective.

#### 8.3.2.5 *Summary of hydrological performance in field conditions*

Systematic differences in retention existed across the nine configurations. However, these were not always statistically-significant. SMD was typically regenerated more quickly by non-vegetated configurations. However, retention was greater with vegetated beds due to their higher overall moisture storage capacity. The regeneration of SMD was influenced by season. The highest SMD was observed in summer. However, the reported retention responses were affected by rainfall depths; with lower rainfall measured in summer than in spring or winter. Conventional measurable detention effects are not necessarily independent of the effects of retention. Peak attenuation, like retention, was inversely correlated with rainfall depth. Detention parameter  $k$  was used to describe detention performance. The highest  $k$ , implying the most rapid runoff response, was typically associated with the most permeable configurations.

#### **8.3.3 Regeneration of capacity via ET during controlled condition tests**

1. Microcosms of nine test beds were saturated, drained to  $\theta_{FC}$  and placed on load cells within a chamber that was programmed to replicate up to 28 diurnal cycles in spring and summer conditions. No irrigation water was added. Changes in mass were inferred as changes in moisture content.

2. For all test beds, there was an observable decrease in the ET rate over time. Seasonal-mean ET rates were 1.95 mm and 3.4 mm over a 1 day ADWP but fell instantly. Over a 7 day ADWP, mean ET was 1.5 mm/day (spring) and 2.5 mm/day (summer); falling to below 0.5 mm/day after 21 days.
3. The maximum moisture storage capacity ( $S_{MAX}$ ) constrained ET from all configurations. Once residual moisture content ( $S_t$ ) fell to a quarter of  $S_{MAX}$ , moisture appeared to be held too tightly for ET to occur in spring conditions. In summer, ET was still measured when  $S_t$  was less than 10% of  $S_{MAX}$ , albeit at much lower levels than PET.
4. The decay in ET rates reflected reduced moisture availability. Highest ET was observed when  $S_e$  was highest. The lowest ET was recorded when  $S_e$  was low. The decay in ET/PET with falling  $S_e$  was linear in many cases, but exponential with Meadow Flower.
5. The addition of vegetation had a statistically-significant influence on ET. However, differences between Sedum and Meadow Flower were systematic but not statistically-significant.
6. When  $S_e$  was high, ET from Meadow Flower was higher than from Sedum. However, thereafter, the lower residual moisture constrained ET from Meadow Flower to a greater degree and at an earlier stage than it did from Sedum.
7. Interception losses of between 7.2 and 7.8 mm were observed with Sedum vegetation on brick-based substrates. This compares to between 3.5 and 7.7 mm with Meadow Flower. These values are similar to the interception losses observed in field conditions.
8. ET from non-vegetated configurations exceeded ET from vegetated microcosms for ADWPs of up to 4 (Meadow Flower) and 6 days (Sedum) in summer and up to 12 (Meadow Flower) and 20 days (Sedum) in spring.
9. Seasonal climate had a statistically-significant influence on ET. Cumulative ET over a 28 day ADWP in summer ranged between 19-35 mm compared to 17-29 mm in spring. Seasonal mean daily ET was higher in summer than in spring

for ADWPs up to 12 days. By this time, seasonal-mean cumulative ET was 7.6 mm greater in summer. However, the greater residual moisture content subsequently facilitated higher daily ET rates in spring.

10. Seasonal differences were greatest from vegetated (approx. 10 mm) rather than non-vegetated (approx. 2 mm) configurations. After a 14 day ADWP, in spring vegetation-mean cumulative ET was 15.5 mm (Sedum), 18.8 mm (Meadow Flower) and 17.8 mm (non-vegetated). In summer, equivalent values were 25.4 mm (Sedum), 29.1 mm (Meadow Flower) and 19.8 mm (non-vegetated).
11. Higher initial rates of ET were observed (a) from non-vegetated and Meadow Flower configurations and (b) during summer. In both cases, the greater SMD generated by the higher antecedent ET rates constrained further ET. Over long ADWPs (e.g. 14 days), configurations with lower initial ET (e.g. Sedum) regenerated a similar SMD.

#### **8.3.4 Development of a hydrological model for extensive green roofs**

1. The developed model fulfils the three criteria called for by CIRIA (2015). The moisture balance model (i) accounts for the influences of configuration and climate, (ii) estimates ET with a plant- and seasonally-influenced soil moisture extraction function (SMEF), and (iii) models runoff with high temporal resolution by adopting a reservoir routing approach, with detention responses characterized by detention parameter  $k$ .
2. The model has been developed with the use of empirical data for responses to wetting and drying cycles and reflects the specific characteristics of the substrates and vegetation treatments.
3. The retention model element reflects that fact that the difference between rainfall depth and SMD generally provided a highly credible indication of runoff volume.
4. The choice of PET method can affect the accuracy of ET predictions. The FAO56 method and two simplistic approaches (Thornthwaite and Hargreaves) reproduced the maximum ET rates measured in the chamber with good accuracy. The FAO56 approach is acknowledged to be the most physically-based PET method.

5. No single crop factor ( $k_c$ ) could be identified across both spring and summer for each vegetation treatment. However, PET estimates were sensitive to albedo ( $\alpha$ ) values. Further research is recommended to better understand how  $\alpha$  varies for each vegetation treatment and with climate and moisture availability.
6. Predictions based on PET alone will overestimate ET. SMEFs were employed here to represent decay functions in ET/PET with falling  $S_e$ .
7. The model calculates ET at daily, rather than hourly intervals. For ADWPs of less than, or fractions of one day, even disaggregation of daily ET is assumed. This simplifying assumption could lead to maximum errors of 0.8 mm in spring or 1.5 mm in summer. Hourly intervals can be used where additional complexity can be justified.
8. To model runoff time-series, configuration-median values were established for detention parameter  $k$ . A single median  $k$  was calculated using the six beds with brick-based substrates ( $0.0064 \text{ mm}^{1-n}/\text{min}$  or  $0.032 \text{ mm}^{1-n}/5\text{min}$ ).
9. Vegetation treatment had a significant influence on  $k$ . Vegetation-median  $k$  values were therefore calculated for Sedum ( $0.0049 \text{ mm}^{1-n}/\text{min}$  or  $0.0245 \text{ mm}^{1-n}/5\text{min}$ ), Meadow Flower ( $0.0058 \text{ mm}^{1-n}/\text{min}$  or  $0.029 \text{ mm}^{1-n}/5\text{min}$ ) and non-vegetated beds ( $0.0083 \text{ mm}^{1-n}/\text{min}$  or  $0.0415 \text{ mm}^{1-n}/5\text{min}$ ).
10. The detention model component has low sensitivity to relatively large changes in  $k$ . A single median  $k$  can therefore be employed without significant loss of accuracy. However, to reflect the statistical significance of vegetation on  $k$ , the model incorporated vegetation-median  $k$  as the default values.
11. Rainfall and runoff statistics are sensitive to the time interval employed in the calculation. Peak values at 1-minute intervals will typically be greater than at 5-minute intervals. When referring to detention performance, it will be important to reference the time interval used.

### 8.3.5 Application of the developed hydrological model

1. The developed and refined model was applied to predict hydrological responses of three extensive green roof configurations – Sedum-vegetated (TB2,  $S_{MAX} = 32.43$  mm), Meadow Flower (TB4,  $S_{MAX} = 34.71$  mm) and non-vegetated (TB7,  $S_{MAX} = 26.97$  mm) – to both a continuous 30 year simulation and design storms with various probabilities (and associated rainfall depths and peak rates).
2. Long-term simulations provide valuable insight into the long-term retention performance of different green roof configurations and/or geographical climates, identifying any anticipated irrigation requirements.
3. Modelling responses to design storm events provides drainage engineers with a comparable basis against which to evaluate the feasibility of green roofs and any other SuDS components. However, a number of assumptions are required regarding antecedent moisture conditions. The model outputs are highly sensitive to these modelling assumptions.

#### 8.3.5.1 Long-term continuous simulation of retention performance

1. Application of the model with and without a SMEF indicated the importance of predicting ET by applying a SMEF to PET. When no SMEF was included in the model, the simulation demonstrated a difference in mean annual retention of up to 7.7%. The drought stress risk of Sedum was predicted to be approximately 20 times higher than when a SMEF was used.
2. For simulations employing a SMEF, the long-term continuous simulation demonstrated minor but systematic differences in retention responses. Mean annual retention was lowest from the non-vegetated bed (47.2-48.0%), highest from Meadow Flower (49.9-51.4%) and between 48.1% and 49.4% from Sedum.
3. Similar differences and rankings in mean per-event retention were observed. With a mean rainfall depth of 5.2 mm, simulated mean per-event retention ranged between 71.5% and 73.4%. For significant rainfall events (mean rainfall depth of 41.2 mm), per-event retention ranged between 17.0% and 17.6% (non-vegetated), 18.5% and 19.3% (Sedum) and 19.9% and 22.0% (Meadow Flower).

4. Differences in simulated retention due to the choice between the  $S_e$  *Linear* and  $S_e$  *Power SMEFs* were less than 2% in configuration-mean annual retention and less than 1% in per-event retention (including significant events). However, the use of the  $S_e$  *Power SMEF* most accurately mimicked observed decay patterns for each vegetation treatment. The risk of drought was modelled to be highest with Meadow Flower (7.45% or 25 days per year) and lower with Sedum (0.8% or 3 days per year).
5. The simulation tool enabled the identification of the requirement for irrigation and the impact that this would have on the hydrological response. By modelling the addition of 30 mm of irrigation water once  $S_t$  fell to 1.0 mm, mean annual retention by Meadow Flower fell by 1.4% to 50.0% whilst per-significant event retention fell by 2.6% to 19.4%.

#### 8.3.5.2 *Retention and detention responses to design storm events*

1. The model was applied to design storm events for three configurations, with a number of iterations to highlight the importance of ADWP, initial moisture content, return period, season and configuration to predicted responses.
2. In response to a 1 in 30 year rainfall event, when modelled rainfall had a depth of 62.4 mm and a peak intensity of 1.14 mm/min (50% summer), following a 7 day ADWP, predicted retention ranged between 17.4 mm or 27.8% (non-vegetated) and 23.1 mm or 36.9% (Meadow Flower). Predicted peak runoff ranged between 0.53 mm/min (Meadow Flower) and 0.72 mm/min (non-vegetated).
3. The model captured seasonal differences in predicted runoff responses. Retention by Sedum-vegetated TB2 in summer was 32.1%, compared to 17.4% in spring, 11.5% in autumn and 6.5% in winter. Modelled peak attenuation was highest in summer (49.8%, with peak runoff of 0.57 mm/min), compared to 40.2% in spring (0.68 mm/min) and 5.4% in winter and autumn (with peak runoff of 0.44 mm/min in response to a peak rainfall rate of 0.46 mm/min).
4. Typically designers assume the worst case scenario regarding moisture content (i.e. SMD = 0) at the beginning of the ADWP. However, the AE9 data highlighted that the pre-event SMD was not typically zero. Seasonal-mean pre-event SMD

was 19.1 mm in summer, 14.6 mm in spring and autumn and 5.2 mm in winter. Modelling with the seasonal-mean SMD (instead of assuming an SMD of zero) at the start of a 7 day ADWP led to lower ET during the ADWP but still increased retention.

5. The model captured the decay in ET relative to PET, particularly at longer ADWPs. With a short ADWP of 2 days, ET from TB2 was close to PET (mean ET of 3.65 mm/day). However, after a 10 day ADWP, predicted cumulative ET was 24.2 mm (i.e. a lower mean ET of 2.4 mm/day).
6. The inverse relationship between rainfall depth and retention was modelled. For a 1 year return period, retention of the 14.3 mm of rainfall was 100%. For a 2 year return period event, retention was 69.2% of 29.2 mm of rainfall. For a 100 year return period event, retention was 23.7% of the 85.2 mm of rainfall.
7. Differences in responses to low probability events due to configuration were limited by the small differences (of up to 2.3 mm) in the  $S_{MAX}$  of the configurations. The maximum difference equates to approximately 2.7% of a 1 in 100 year event.

### 8.3.6 Concluding remarks

1. There is a trade-off between high initial rates of ET from a non-vegetated bed and the greater moisture storage capacity of a vegetated bed. Here, retention was typically greater due to the climate and the high interception losses associated with vegetation.
2. Comparing Sedum with Meadow Flower, there is a similar trade-off. Meadow Flower will typically regenerate the SMD more quickly (due to high ET). However, this can exacerbate the risk of drought stress. Unless irrigation measures are included, the vegetation is at risk of permanently wilting.
3. Systematic trends have been identified here. However, their significance in the wider SuDS environment is limited by the small size of these differences in the context of the large rainfall depths in low probability events.



4. The Sedum-vegetated TB2 has a  $S_{MAX}$  of 32.43 mm. The maximum permissible retention of a 1 in 30 year event would be 48.2% and for a 1 in 100 year event would be 38.0%.
5. Green roofs can provide complementary drainage capacity within an interconnected network of SuDS devices. As a result of this work, designers have greater transparency of the physical controls that will influence the hydrological response of the selected green roof configuration.

## 8.4 Discussion

The overall aim of this project was to improve the understanding of the physical controls that affect a green roof's hydrological response, such that a model can be developed to account for the relevant physical parameters and processes. This has been met by:

1. Monitoring and evaluating hydrological responses of nine test beds comprising three substrates and three vegetation treatments over a four year period.
2. Measuring climatic conditions at the field research site to allow evaluation of factors that underpin the regeneration of retention capacity during the ADWP.
3. Measuring the moisture balance at different depths in the substrate to understand the distribution of moisture in the substrate and the extent to which ET occurred from all depths of the substrate; concluding that no significant loss of accuracy would arise by treating the 80 mm deep configuration as a monolithic unit.
4. Controlled condition tests to identify trends in the regeneration of SMD via ET for the entire range between  $\theta_{FC}$  and  $\theta_{PWP}$ . This would not normally be possible in field conditions due to the regular incidence of rainfall.
5. Evaluation, selection, refinement and validation of modelling methods to predict retention and detention responses for the specific configuration and climate.
6. Simulating the retention responses of different green roof configurations to a continuous 30-year time-series of synthetic climatic data; allowing the comparative assessment of different green roof configurations and the identification of any anticipated irrigation requirements.

7. Developing a design storm response model that can provide design engineers with SuDS performance statistics that are comparable to and compatible with other drainage measures being considered.

## 8.5 Further work

1. The ET trials conducted here investigated ET trends during the two seasons with the highest PET (i.e. spring and summer). Controlled condition tests to establish ET rates during autumn and winter would provide further substantiation of a green roof's year-round hydrological performance.
2. Here, empirical factors have been proposed as part of a vegetation- and season-specific SMEF – the *S<sub>e</sub> Power SMEF*. These coefficients are expected to reflect physical and physiological characteristics of the vegetation treatments. Further work could focus on the identification of plant traits (e.g. albedo) that may provide a physical basis for the empirical coefficients employed in the *S<sub>e</sub> Power SMEF*.
3. The focus of this work has been on the most typical form of green roof. Extensive green roofs are shallow in depth, lightweight by composition and lower cost than more intensive green roofs. The relationship between ET/PET may differ with deeper substrates (i.e. intensive roofs with 200 mm of substrate). Further work is required to identify the impact on hydrological performance of deeper substrates.
4. The field research was conducted over a 4 year period. Vegetation is expected to change seasonally and as the green roof ages. Soil porosity is expected to change as plant leaves and roots decompose. A greater understanding of these ageing effects on the hydrological performance of green roofs is therefore advocated.
5. Calculation methods to substantiate the expected performance of SuDS are relatively new and further work is required to provide designers with a consistent set of assumptions regarding antecedent conditions (e.g. ADWP length and climate) that are to be modelled.

---

## References

- Alfredo K., Montalto F. & Goldstein A. (2010). Observed and modelled performances of prototype green roof test plots subjected to simulated low- and high-intensity precipitations in a laboratory experiment. *Journal of Hydrologic Engineering*, 15(6), 444-457.
- Ahuja, L., Rojas, K.W. & Hanson, J.D. (2000). Root zone water quality model - Modelling Management Effects on Water Quality and Crop Production. *Water Resources Publications LLC*, USA.
- Allen, R., Pereira, L., Raes, D., & Smith, M. (1998). Crop evapotranspiration - Guidelines for computing crop water requirements. *FAO Irrigation & Drainage Papers* - 56. Food & Agriculture Organisation of the United Nations, Rome.
- Alumasc (2006a). Product Data Sheet: Drainage Mat DBV12. Published 27.02.2006.
- Alumasc (2006b). Product Data Sheet: Floradrain FD-25E. Published 27.02.2006.
- Argue, J. (1986). Storm drainage design in small urban catchments: a handbook for Australian practice (ARRB SR34). Melbourne, Australia: ARRB.
- Arya, L.M. & Paris, J.F. (1981). A physicoempirical model to predict the soil moisture characteristic from particle-size distribution and bulk density data. *Soil Science Society of America Journal*, 45:1023-1030.
- Baker, R., & Frydman, S. (2009). Unsaturated soil mechanics - Critical review of physical foundations. *Engineering Geology*, 106, 26-39.
- Banting, D., Doshi, H., Li, J., Missiois, P., Au, A., Currie, B., Verrati, M. (2004). Report on the Environmental Benefits and Costs of Green Roof Technology for the City of Toronto. Ryerson University for City of Toronto and Ontario Centres of Excellence – Earth and Environmental Technologies, Toronto.
- Barbu, I.A. & Ballestero, T.P. (2014). Unsaturated Flow Functions for Filter Media Used in Low-Impact Development—Stormwater Management Systems. *Journal of Irrigation & Drainage Engineering*, 2015.141.
- BBC: [www.bbc.co.uk/gardening/plants](http://www.bbc.co.uk/gardening/plants), accessed on 29 June 2016.
- Beattie, D. & Berghage, R. (2004). Green Roof Media Characteristics: The Basics. *Greening Rooftops for Sustainable Communities, Portland*.
- Bengtsson, L., Grahn, L., & Olsson, J. (2005). Hydrological function of a thin extensive green roof in southern Sweden. *Nordic Hydrology*, 36(3), 259-268.

- Benvenuti, S. (2014). Wildflower green roofs for urban landscaping, ecological sustainability and biodiversity. *Landscape & Urban Planning*, 124, 151-161.
- Berardi, U., GhaffarianHoseini A.H. & GhaffarianHoseini, A. (2014). State-of-the-art analysis of the environmental benefits of green roofs. *Applied Energy*, 115, 411–428.
- Berghage, R. D., Jarrett, A. R., Beattie, D. J., Kelley, K., Husain, S., Rezaei, F., Long, B., Negassi, A., Cameron, R. & Hunt, W. F. (2007). Quantifying Evaporation and Transpirational Water Losses from Green Roofs and Green Roof Media Capacity for Neutralizing Acid Rain. National Decentralized Water Resources Capacity Development Project. University Park, Pennsylvania: Penn State University.
- Berghage, R., Beattie, D., Jarrett, A., & O'Connor, T. (2007). Green roof run-off water quality. *Greening Rooftops for Sustainable Communities, Minneapolis*.
- Berghage, R.D., Beattie, D., Jarrett, A.R., Thuring, C., Razaeei, F., O'Connor, T., Razaci, F. & O'Connor, T.P. (2009). Green Roofs for Stormwater Runoff Control, EP A/600/R-09/026. Cincinnati, OH.
- Berndtsson, J., Emilsson, T. & Bengtsson, L. (2006). The influence of extensive vegetated roofs on run-off water quality. *Science of the Total Environment*, 355, 48-63.
- Berndtsson, J.C. (2010). Green roof performance towards management of runoff water quantity and quality: A review. *Ecological Engineering*, 36(4), 351-360.
- Berretta, C., Poë, S. & Stovin, V. (2014). Moisture content behaviour in extensive green roofs during dry periods: The influence of vegetation and substrate characteristics. *Journal of Hydrology*, 511, 374-386.
- Berretta, C., Poë, S. & Stovin, V. (2014b). The Influence of Substrate and Vegetation on Extensive Green Roof Hydrological Performance. *Proceedings of the 13th International Conference on Urban Drainage, Sarawak, Malaysia*.
- Beven, K. (2001). *Rainfall-Runoff Modelling*. Chichester: John Wiley & Sons Ltd.
- Brady, N. & Weil, R. (2008). *The Nature and Property of Soils*, 14th Edition. New Jersey: Pearson Prentice Hall.
- Brenneisen, S. (2003). The benefits of biodiversity from green roofs-key design consequences. *In: Conference proceedings Greening Rooftops for Sustainable Communities, Chicago*.
- Brickell, C.D. (2008). *RHS A-Z Encyclopedia of Garden Plants*. Royal Horticultural Society.
- Bruand, A., Cousin, I., Nicoullaud, B., Duval, O. & Begon, J.C. (1996). Backscattered electron scanning images of soil porosity for analyzing soil compaction around roots. *Soil Science Society of America Journal*, 60, 895–901.

- 
- Buccola N. & Spolek G. (2010). A pilot-scale evaluation of green roof runoff retention, detention, and quality. *Water, Air & Soil Pollution*, 216(1-4), 83-92.
- Buckingham, E. (1907). Studies on the movement of soil moisture. Bulletin 38. USDA Bureau of Soils, Washington, DC.
- Butler, C. & Orians, C.M. (2011). Sedum cools soil and can improve neighboring plant performance during water deficit on a green roof. *Ecological Engineering*, 37, 1796–1803.
- Cain, J. (1998). Modelling evaporation from plant canopies - Report No. 132. Wallingford, UK: Institute of Hydrology.
- Campbell Scientific, Inc. (2006). CS616 & CS625 Water Content Reflectometers User Guide. 2002-2003. Issued Aug 2006.
- Carbone, M., Garofalo, G., Nigro, G. & Piro, P. (2015). A conceptual model for predicting hydraulic behaviour of a green roof. *Procedia Engineering*, 70, 266 - 274.
- Carson, T.B., Marasco, D.E., Culligan, P.J. & McGillis, W.R. (2013). Hydrological performance of extensive green roofs in New York City: observations and multi-year modelling of three, full-scale systems. *Environmental Research Letters*, 8, 2, pp.24036-24048(13).
- Carter, M.R. (1993). Soil Sampling and Methods of Analysis, Lewis Publishers, CRC Press, 1993.
- Carter, T. & Jackson, C. (2007). Vegetated roofs for storm water management at multiple spatial scales. *Landscape & Urban Planning*, 80, 84-94.
- Carter, T. & Keeler, A. (2008). Life-cycle cost-benefit analysis of extensive vegetated roof systems. *Journal of Environmental Management*, 87, 350-363.
- Carter, T. & Rasmussen, T. (2006). Hydrologic behaviour of vegetated roofs. *Journal of American Water Resources Association*, 42(5), 1261-1274.
- CEH (1999). Flood Estimation Handbook. Centre for Ecology and Hydrology, Wallingford, UK.
- Chahinian, N., Moussa, R., Andrieux, P. & Voltz, M. (2005). Comparison of infiltration models to simulate flood events at the field scale. *Journal of Hydrology*, 306, 191-214.
- Chorley, R. (1969). Introduction to Physical Hydrology. Great Britain: Methuen & Co. Ltd.
- CIBSE (2007). CIBSE Knowledge Series KS11 - Green Roofs. Plymouth: CIBSE Publications.

CIRIA (2007a). *Building Greener – Guidance on the use of green roofs, green walls and complementary features on buildings*. CIRIA, London.

CIRIA (2007b). *The SuDS Manual*, CIRIA, C697. London.

CIRIA (2015). *The SuDS Manual*, CIRIA, C753. London.

Clark, C., Adriaens, P. & Talbot, F. (2008). Green Roof Valuation: A Probabilistic Economic Analysis of Environmental Benefits. *Environmental Science & Technology*, 42, 2155-2161.

Colli M., Palla, A., Lanza, L.G. & Crasso M. (2010). Hydrological performance of green-roof systems from a laboratory test-bed. *World Green Roof Congress, London*.

Cook-Patton, S.C. & Bauerle, T.L. (2012). Potential benefits of plant diversity on vegetated roofs: A literature review. *Journal of Environmental Management*, 106, 85-92.

Costanza, R., d'Arge, R., de Groot, R., Farber, S., Grasso, M., Hannon, B., Limburg, K., Naeem, S., O'Neill, R.V., Paruelo, J., Raskin, R.G., Sutton, P. & van den Belt, M. (1997). The value of the world's ecosystem services and natural capital. *Nature*. 387:253-260.

Darcy, H. (1856). *Les fontaines publiques de la ville de Dijon*. Dal-mont, Paris

DEFRA (2002). *Climate Change Scenarios for the United Kingdom - The UKCIP02 Scientific Report*, April 2002.

DEFRA (2008). *Future Water: The Government's water strategy for England*. HMSO, Norwich, UK.

DEFRA (2011). *National Standards for sustainable drainage systems: Designing, constructing, operating and maintaining drainage for surface runoff*. DEFRA, London.

Del Barrio, E.P. (1998). Analysis of the green roofs cooling potential in buildings. *Energy & Buildings*, 27, 179-193.

DeNardo, J., Jarrett, A., Manbeck, H., Beattie, D. & Berghage, R. (2005). Stormwater mitigation and surface temperature reduction by green roofs. *Transactions of ASAE*, 48(4), 1491-1496.

Department for Communities and Local Government (DCLG) (2012). *Technical Guidance to the National Planning Policy Framework*. DCLG, London.

De-Ville, S., Menon, M. & Stovin, V. (2015). Using X-Ray Microtomography to identify physical changes in green roof substrates as a result of ageing. *In: The Annual Postgraduate Research Student Conference, 15 April 2015, Sheffield, UK*.

- 
- Dexter, A., Czyz, E., Richard, G. & Reszkowska, A. (2008). A user-friendly water retention function that takes account of the textural and structural pore spaces in soil. *Geoderma*, 143, 243-253.
- Di Rado, H., Beneyto, P., Mroginski, J. & Awruch, A. (2009). Influence of the saturation-suction relationship in the formulation of non-saturated soil consolidation models. *Mathematical & Computer Modelling*, 49, 1058-1070.
- DiGiovanni, K., Gaffin, S. & Montalto, F. (2010). Green roof hydrology: Results from a small-scale lysimeter setup (Bronx, NY). *Low Impact Development 2010: Redefining Water in the City - Proceedings of the 2010 International Low Impact Development Conference*, pp 1328-1341.
- Dobos, E. (2003). Albedo. *Encyclopedia of Soil Science*. Springer International Publishing AG. DOI: 10.1081/E-ESS 120014334.
- Doerr, S.H., Shakesby, R.A. & Walsh, R.P.D. (2000). Soil water repellency: its causes, characteristics and hydro-geomorphological significance. *Earth-Science Reviews*, 51, 33-65.
- Dunnett, N. & Kingsbury, N. (2004). *Planting Green Roofs and Living Walls*, Timber Press, Cambridge, UK.
- Dunnett, N., Nagase, A. & Hallam, A. (2008b). The dynamics of planted and colonising species on a green roof over six growing seasons 2001–2006: influence of substrate depth. *Urban Ecosystems*, 11, 373–384.
- Dunnett, N., Nagase, A., Booth, R. & Grime, P. (2008a). Influence of vegetation composition on runoff in two simulated green roof experiments. *Urban Ecosystems*, 11, 385–398.
- Elliott, A.H. & Trowsdale, S.A. (2007). A review of models for low impact urban storm water drainage. *Environmental Modelling & Software*, 22 (3), 394–405.
- Ennos, A.R. (1999). The aerodynamics and hydrodynamics of plants. *The Journal of Experimental Biology*, 202, 3281–3284.
- Environment Agency (2009). *Flooding in England: A national assessment of flood risk*. Environment Agency, Bristol, UK.
- Environment Agency (2010). *Delivering benefits through evidence: the costs of the summer 2007 floods in England*. Environment Agency, Bristol, UK.
- Farrell, C., Ang, X. Q. & Rayner, J.P. (2013). Water-retention additives increase plant available water in green roof substrates. *Ecological Engineering*, 52, 112–118.

Farrell, C., Mitchell, R.E., Szota, C., Rayner, J.P. & Williams, N.S.G. (2012). Green roofs for hot and dry climates: Interacting effects of plant water use, succulence and substrate. *Ecological Engineering*, 49, 270-276.

Fassman, E. & Simcock, R. (2008). Development and Implementation of a Locally-Sourced Extensive Green Roof Substrate in New Zealand. *World Green Roof Congress, London*.

Fassman, E. & Simcock, R. (2012). Moisture Measurements as Performance Criteria for Extensive Living Roof Substrates. *Journal of Environmental Engineering*, 138 (8), 841-851.

Fassman, E.A., Simcock, R. & Voyde, E. (2010). Extensive green (living) roofs for storm water mitigation. Part 1: Design and construction. Auckland Uni Services Technical Report to Auckland Council. Auckland Council TR2010/017.

Fassman-Beck, E., Voyde, E., Simcock, R. & Hong, Y.S. (2013). 4 living roofs in 3 locations: does configuration affect runoff mitigation? *Journal of Hydrology*, 490, 11–20.

Feller, M. M. (2011). Quantifying Evapotranspiration in Green Infrastructure: A Green Roof Case Study, Villanova University.

Ferreira, T. & Rasband, W. (2011). ImageJ User Guide, IJ1.45M.

Fitter, A. H. & Peat, H. J. (1994). The Ecological Flora Database. *Journal of Ecology*, 82, 415-425.

FLL - Forschungsgesellschaft Landschaftsentwicklung Landschaftsbau (2008). Guidelines for the Planning, Construction and Maintenance of Green Roofing. Bonn, Germany: Forschungsgesellschaft Landschaftsentwicklung Landschaftsbau e.V.

Flood and Water Management Act (2010). UK Government Bill.

Friedrich, C. (2005). Principles for selecting the proper components for a green roof growing media. *Greening Rooftops for Sustainable Communities, Washington, D.C.*

Garnier, E., Navas, M-L. & Grigulis, K. (2016). Plant Functional Diversity - Organism Traits, Community Structure and Ecosystem Properties. Oxford University Press, Oxford, UK.

Gedge, D. & Frith, M. (2004). Green roof benefits and cost implications: A report for Sustainable Eastside, London. Livingroofs.org in association with Ecology consultancy.

Gedge, D. (2003). From rubble to redstarts, p. 233–241. *In Proc. of 1st North American Green Roof Conference: Greening rooftops for sustainable communities, Chicago*.



- 
- Germann, P. & Beven, K. (1985). Kinematic wave approximation to infiltration into soils with sorbing macro pores. *Water Resources Research*, 21(7), 990-996.
- Getter, K., Rowe, D. & Andresen, J. (2007). Quantifying the effect of slope of extensive green roof storm water retention. *Ecological Engineering*, 31, 225-231.
- Gobel, P., Dierkes, C. & Coldewey, W.G. (2007). Storm water run-off concentration matrix for urban areas. *Journal of Contaminant Hydrology*, 91, 26-42.
- Graceson, A., Hare, M., Monaghan, J. & Hall, N. (2013). The water retention capabilities of growing media for green roofs. *Ecological Engineering*, 61, 328-334.
- Graceson, A., Monaghan, J., Hall, N. & Hare, M. (2014). Plant growth responses to different growing media for green roofs. *Ecological Engineering*, 69, 196-200.
- Grant, G., Engelback, L., Nicholson, B., Gedge, D., Frith, M. & Harvey, P. (2003). Green Roofs: Their existing status and potential for conserving biodiversity in urban areas. English Nature.
- Greater London Authority (2008). Living Roofs and Walls, Technical Report: Supporting London Plan Policy. London: Greater London Authority.
- Green Roof Organisation [GRO] (2014). GRO Green Roof Code of Best Practice for the UK 2014. Groundwork Sheffield, Sheffield, UK.
- Green, W.H. & Ampt, G. (1911). Studies of soil physics, part I – the flow of air and water through soils. *Journal of Agricultural Science*, 4, 1-24.
- Gupta, H.V., Sorooshian, S. & Yapo, P.O. (1999). Status of automatic calibration for hydrologic models: Comparison with multilevel expert calibration. *Journal of Hydrological Engineering*, 4 (2), 135-143.
- Hakimdavar, R., Culligan, P.J., Finazzi, M., Barontini, S. & Ranzi, R. (2014). Scale dynamics of extensive green roofs: Quantifying the effect of drainage area and rainfall characteristics on observed and modelled green roof hydrologic performance. *Ecological Engineering*, 73, 494-508.
- Hargreaves, G.H. & Allen, R.G. (2002). History and evaluation of Hargreaves evapotranspiration equation. *Journal of Irrigation & Drainage Engineering*, 129, 53-63.
- Hargreaves, G.L. & Samani, Z.A. (1985). Reference crop evapotranspiration from temperature. *Applied Engineering in Agriculture*, 1~2, 96-99.
- Hickman, J., Schneider, D., Wadzuk, B.M. & Traver, R.G. (2010). Determination of evapotranspiration in SCM's using a weighing lysimeter: An experimental approach. *Proceedings of the World Environmental & Water Resources Congress*, pp 3990-3999.

Hillel D. (1971). *Soil and water: physical principles and processes*. Academic Press, London.

Hillel, D. (1998). *Environmental Soil Physics*. Academic Press, San Diego.

Hilten R.N., Lawrence T.M. & Tollner E.W. (2008). Modeling storm water runoff from green roofs with HYDRUS-1D. *Journal of Hydrology*, 358(3–4): 288-293.

Hilten, R.N. (2005). An analysis of the energetics and storm water mediation potential of greenroofs. Master of Science Thesis, University of Georgia.

Hoffman, L. (2006). *The Earth Pledge Green Roof Stormwater Modeling System. Greening Rooftops for Sustainable Communities, Boston.*

Horton, R.E. (1940). The infiltration-theory of surface-runoff. *Eos Transactions American Geophysical Union*, 21(2), 541–541.

Hutchinson, D., Abrams, P., Retzlaff, R. & Liptan, T. (2003). Stormwater monitoring two ecoroofs in Portland, Oregon, USA. *Greening Rooftops for Sustainable Communities, Chicago.*

Hwang, S.I. & Choi, S.I. (2006). Use of a lognormal distribution model for estimating soil water retention curves from particle-size distribution data. *Journal of Hydrology*, 323, 325–334.

Ines, A. & Droogers, P. (2002). Inverse modelling in estimating soil hydraulic functions: a Genetic Algorithm approach. *Hydrology & Earth System Sciences*, 6(1), 49-65.

Itenfisu, D., Elliott, R.L., Allen, R.G. & Walter, I.A. (2003). Comparison of reference evapotranspiration calculations as part of the ASCE standardization effort. *Journal of Irrigation & Drainage Engineering*, 129, 440-448.

Jarrett, A. R., Hunt, W. F., and Berghage, R. D. (2006). Annual and individual-storm green roof storm water response models. Paper No. 062310, *ASABE Annual Int. Meeting, Portland, OR.*

Jarrett, A.R. & Berghage, R.D. (2008). Annual and individual green roofs storm water response models. *6th Greening Rooftops for Sustainable Communities Conference, Baltimore, MD.*

Jayasooriya, V.M. & Ng, A.W.M. (2014). Tools for Modeling of Stormwater Management and Economics of Green Infrastructure Practices: a Review. *Water Air & Soil Pollution*, 225:2055.

Jennings, G., Hunt, B. & Moran, A. (2003). A North Caroline field study to evaluate green roof run-off quantity, run-off quality and plant growth. *ASAE Annual International Meeting, Las Vegas, Nevada.*

- 
- Jensen, M.E., Burman, R.D. & Allen, R.G. (1990). Evapotranspiration and irrigation water requirements. *ASCE Manuals and Reports on Engineering Practice No. 70*, ASCE, New York.
- Jhorar, R., van Dam, J., Bastiaanssen, W. & Feddes, R. (2004). Calibration of effective soil hydraulic parameters of heterogeneous soil profiles. *Journal of Hydrology*, 285, 233-247.
- Johnston, C., McCreaery, K. & Nelms, C. (2004). Vancouver Public Library green roof monitoring project. *Greening Rooftops for Sustainable Communities, Portland*.
- Jones, P., Harpham, C., Kilsby, C., Glenis, V. & Burton, A. (2010). UK Climate Projections science report: Projections of future daily climate for the UK from the Weather Generator. UK Climate Projections.
- Kasmin, H. (2010). Hydrological Performance of Green Roofs (PhD Thesis). University of Sheffield, Department of Civil and Structural Engineering. Sheffield, UK. 216 pp.
- Kasmin, H., Stovin, V. & Hathway, E. (2010). Towards a generic rainfall-runoff model for green roofs. *Water Science & Technology*, 62, 4, 898-905.
- Kattge, J., Bönisch, G., Günther, A., Wright, I., Zanne, A., Wirth, C., Reich, P.B. & the TRY Consortium (2012). TRY - Categorical Traits Dataset. Data from: TRY - a global database of plant traits. TRY File Archive <https://www.try-db.org/TryWeb/Data.php#3>.

Kattge, J., Diaz, S., Lavorel, S., Prentice, I. C., Leadley, P., Bönisch, G., Garnier, E., Westoby, M., Reich, P. B., Wright, I. J., Cornelissen, J. H. C., Violle, C., Harrison, S. P., Van Bodegom, P. M., Reichstein, M., Enquist, B. J., Soudzilovskaia, N. A., Ackerly, D. D., Anand, M., Atkin, O., Bahn, M., Baker, T. R., Baldocchi, D., Bekker, R., Blanco, C. C., Blonder, B., Bond, W. J., Bradstock, R., Bunker, D. E., Casanoves, F., Cavender-Bares, J., Chambers, J. Q., Chapin III, F. S., Chave, J., Coomes, D., Cornwell, W. K., Craine, J. M., Dobrin, B. H., Duarte, L., Durka, W., Elser, J., Esser, G., Estiarte, M., Fagan, W. F., Fang, J., Fernández-Méndez, F., Fidelis, A., Finegan, B., Flores, O., Ford, H., Frank, D., Freschet, G. T., Fyllas, N. M., Gallagher, R. V., Green, W. A., Gutierrez, A. G., Hickler, T., Higgins, S. I., Hodgson, J. G., Jalili, A., Jansen, S., Joly, C. A., Kerkhoff, A. J., Kirkup, D., Kitajima, K., Kleyer, M., Klotz, S., Knops, J. M. H., Kramer, K., Kühn, I., Kurokawa, H., Laughlin, D., Lee, T. D., Leishman, M., Lens, F., Lenz, T., Lewis, S. L., Lloyd, J., Llusià, J., Louault, F., Ma, S., Mahecha, M. D., Manning, P., Massad, T., Medlyn, B. E., Messier, J., Moles, A. T., Müller, S. C., Nadrowski, K., Naeem, S., Niinemets, Ü., Nöllert, S., Nueske, A., Ogaya, R., Oleksyn, J., Onipchenko, V. G., Onoda, Y., Ordonez, J., Overbeck, G., Ozinga, W. A., Patiño, S., Paula, S., Pausas, J. G., Peñuelas, J., Phillips, O. L., Pillar, V., Poorter, H., Poorter, L., Poschlod, P., Prinzing, A., Proulx, R., Rammig, A., Reinsch, S., Reu, B., Sack, L., Salgado-Negret, B., Sardans, J., Shiodera, S., Shipley, B., Siefert, A., Sosinski, E., Soussana, J.-F., Swaine, E., Swenson, N., Thompson, K., Thornton, P., Waldram, M., Weiher, E., White, M., White, S., Wright, S. J., Yguel, B., Zaehle, S., Zanne, A. E., Wirth, C. (2011). TRY - a global database of plant traits. *Global Change Biology*, 17, 2905-2935.

Kelleners, T.J., Seyfried, M.S., Blonquist, J.M., Bilskie, J. & Chandler D.G. (2005). Improved Interpretation of Water Content Reflectometer Measurements in Soils. *Soil Science Society of America Journal*, 69, 1684-1690.

Kleyer, M., Bekker, R. M., Knevel, I. C., Bakker, J. P., Thompson, K., Sonnenschein, M., Poschlod, P., van Groenendael, J.M., Klimes, L., Klimesova, J., Klotz, S., Rusch, G.M., Hermy, M., Adriaens, D., Boedeltje, G., Bossuyt, B., Dannemann, A., Endels, P., Götzenberger, L., Hodgson, J.G., Jackel, A.-K., Kühn, I., Kunzmann, D., Ozinga, W.A., Römermann, C., Stadler, M., Schlegelmilch, J., Steendam, H.J., Tackenberg, O., Wilmann, B., Cornelissen, J.H.C., Eriksson, O., Garnier, E., & Peco, B. (2008). The LEDA Traitbase: a database of life-history traits of the Northwest European flora. *Journal of Ecology*, 96, 1266-1274.

Koehler, M. & Schmidt, M. (2008). Benefits for Sustainable Water Management - Green Roof Technology. *World Green Roof Congress, London*.

Koehler, M. (2005). Urban storm water management by extensive green roofs. *World Green Roof Congress, Basel, Switzerland*, 150-156.

Koshimizu, H. (2008). A test calculation of the storm water outflow attenuation by green roofs in a high-density city area. *World Green Roof Congress, London*.

Kühn, I., Durka, W. & Klotz, S. (2004). BiolFlor - a new plant-trait database as a tool for plant invasion ecology. *Diversity & Distribution*, 10, 363-365.

- 
- LaBerge, K., Worthington, K., Mulvaney, P. & Bolliger, R. (2005). City of Chicago green roof test plot study: Stormwater and temperature results. *Greening Rooftops for Sustainable Communities, Washington D.C.*
- Lamera, C., Becciu, G., Rulli, M.C. & Rosso, R. (2014). Green roofs effects on the urban water cycle components. *Procedia Engineering*, 70, 988 – 997.
- Lazzarin, R.A., Castellotti, F. & Busato, F. (2005). Experimental measurements and numerical modelling of a green roof. *Energy Build*, 37 (12), 1260–1267.
- Li, Y. & Babcock, R.W. (2014). Green roof hydrologic performance and modelling: A review. *Water Science & Technology*, 69(4), 727-738.
- Lighthill, M. & Whitham, G. (1955). On kinematic waves. I. Flood movement in long rivers. *Royal Society London Archives*, 229, 1178, 281-316.
- Liu, K. & Minor, J. (2005). Performance evaluation of an extensive green roof. National Research Council Canada (NRCC), Toronto.
- Liu, Z. & Todini, E. (2002). Towards a comprehensive physically-based rainfall-runoff model. *Hydrology & Earth System Sciences*, 6(5), 859-881.
- Locatelli, L., Mark, O., Mikkelsen, P.S., Arnbjerg-Nielsen, K., Jensen, M.B. & Binning, P.J. (2014). Modelling of green roof hydrological performance for urban drainage applications. *Journal of Hydrology*, 519, 3237-3248.
- Lu, J., Yuan J., Yang, J., Chen, A. & Yang, Z. (2015). Effect of substrate depth on initial growth and drought tolerance of *Sedum lineare* in extensive green roof system. *Ecological Engineering*, 74, 408–414.
- Lu, J., Yuan, J., Yang, J. & Yang, Z. (2014). Responses of morphology and drought tolerance of *Sedum lineare* to watering regime in green roof system: A root perspective. *Urban Forestry & Urban Greening*, 13, 682-688.
- Lucas R. (1918). Ueber das Zeitgesetz des kapillaren Aufstiegs von Flüssigkeiten. *Kolloid Zeitschrift*, 23, pp. 15-22.
- Luce, C. & Cundy, T. (1992). Modification of the kinematic wave-Philip infiltration overland flow model. *Water Resources Research*, 28 (4), 1179-1186.
- Lundholm, J., MacIvor, J.S., MacDougall, Z. & Ranalli, M. (2010). Plant species and functional group combinations affect green roof ecosystem functions. *PLoS ONE*, 12, 5(3), e9677.
- Lundholm, J.T. (2007) Green Roofs and Facades: A Habitat Template Approach, *Urban Habitat*, 4, 1.

- Luo, H., Huang, B., Liu, X. & Zhang, K. (2011). Green Roof Assessment by GIS and Google Earth. *Procedia Environmental Sciences*, 10, 2307 – 2313.
- MacIvor, J.S. & Lundholm, J.T. (2011). Performance evaluation of native plants suited to extensive green roof conditions in a maritime environment. *Ecological Engineering*, 37, 407-417.
- MacMillan, G. (2004). York University rooftop garden storm water quantity and quality performance monitoring report. *Greening Rooftops for Sustainable Communities, Portland*.
- Madre, F., Vergnes, A., Machon, N. & Clergeau, P. (2014). Green roofs as habitats for wild plant species in urban landscapes: First insights from a large-scale sampling. *Landscape & Urban Planning*, 122, 100 – 107.
- Manning, J. (1987). *Applied Principles of Hydrology*. Merrill Publishing, Ohio.
- Marasco, D.E., Hunter, B.N., Culligan, P.J., Gaffin, S.R. & McGillis, W.R. (2014). Quantifying evapotranspiration from urban green roofs: A comparison of chamber measurements with commonly used predictive methods. *Environmental Science & Technology*, 48, 10273-10281.
- Marcelino, V., Cnudde, V., Vansteelandt, S. & Caro, F. (2007). An evaluation of 2D-image analysis techniques for measuring soil micro porosity. *European Journal of Soil Science*, 58, 133–140.
- MATLAB (2007). MATLAB version R2007b. The MathWorks Inc., Natick, Massachusetts.
- McMahon, T.A., Peel, M.C., Lowe, L., Srikanthan, R. & McVicar, T.R. (2013). Estimating actual, potential, reference crop and pan evaporation using standard meteorological data: a pragmatic synthesis. *Hydrology & Earth System Sciences*, 17, 1331–1363.
- Mentens, J., Raes, D. & Hermy, M. (2006). Green roofs as a tool for solving the rainwater run-off problem in the urbanized 21st century? *Landscape & Urban Planning*, 77, 217-226.
- Mermoud, A. & Xu, D. (2006). Comparative analysis of three methods to generate soil hydraulic functions. *Soil & Tillage Research*, 87, 89-100.
- Met Office (2009). <http://www.metoffice.gov.uk/public/weather/climate/gcqzwtw7> as accessed in October 2010.
- Met Office (2016). Data downloaded from: <http://www.metoffice.gov.uk/public/weather/climate/gcqzwwq04e> as accessed on 23rd June 2016.

- 
- Metselaar, K. (2012). Water retention and evapotranspiration of green roofs and possible natural vegetation types. *Resources Conservation & Recycling*, 64, 49-55.
- Miller, C. (2003). Moisture management in green roofs. Proc. *Greening Rooftops for Sustainable Communities*, Chicago.
- Mollerup, M., Hansen, S., Petersen, C. & Kjaersgaard, J. (2008). A MATLAB program for estimation of unsaturated hydraulic soil parameters using an infiltrometer technique. *Computers & Geosciences*, 34, 861-875.
- Monterusso, M.A., Rowe, D.B. & Rugh, C.L. (2005). Establishment and persistence of *Sedum* spp. and native taxa for green roof applications. *HortScience*, 40, 391-396.
- Monterusso, M.A., Rowe, D.B., Rugh, C.L. & Russell, D.K. (2004). Runoff water quantity and quality from green roof systems. *Acta Horticulturae*, 639, 369-376.
- Moran, A., Hunt, B. & Smith, J. (2005). Hydrologic and water quality performance from green roofs in Goldsboro and Raleigh, North Carolina. *Greening Rooftops for Sustainable Communities*, Washington D.C.
- Morgan, S., Celik, S. & Retzlaff, W. (2013). Green roof storm-water runoff quantity and quality. *Journal of Environmental Engineering – ASCE*, 139(4), 471-478.
- Moriassi, D.N., Arnold, J.G., Van Liew, M.W., Bingner, R.L., Harmel, R.D. & Veith, T.L. (2007). Model evaluation guidelines for systematic quantification of accuracy in watershed simulations. *American Society of Agricultural & Biological Engineers*, 50 (3), 885-900.
- Mualem, Y. (1976). A new model predicting the hydraulic conductivity of unsaturated porous media. *Water Resources Research*, 12(3), 513-522.
- Nagase, A. & Dunnett, N. (2008). Extensive green roofs using geophytes in the UK: Effect of substrate depth and covering plants. *World Green Roof Congress*, London.
- Nagase, A. & Dunnett, N. (2011). The relationship between percentage of organic matter in substrate and growth in extensive green roofs. *Landscape & Urban Planning*, 103, 230e236.
- Nagase, A. & Dunnett, N. (2012). Amount of water runoff from difference vegetation types on extensive green roofs: Effects of plant species, diversity and plant structure. *Landscape & Urban Planning*, 104(3-4), 356-363.
- Nagase, A. & Dunnett, N. (2010). Drought tolerance in different vegetation types for extensive green roofs: effects of watering and diversity. *Landscape & Urban Planning*, 97, 318–327.
- Nash, J.E. & Sutcliffe, J.V. (1970). River flow forecasting through conceptual models: Part 1. A discussion of principles. *Journal of Hydrology*, 10(3), 282-290.

National SUDS Working Group (2004). Interim Code of Practice for Sustainable Drainage Systems. National SUDS Working Group.

Nawaz, R., McDonald, A. & Postoyko, S. (2015). Hydrological performance of a full-scale extensive green roof located in a temperate climate. *Ecological Engineering*, 82, 66–80.

NERC (1975). Flood Studies Report. Natural Environment Research Council, London, UK.

NERC (1999). Flood Estimation Handbook (CD). Natural Environment Research Council, London, UK.

NERC (Natural Environment Research Council), 1999, Flood Estimation Handbook (FEH) CD.

Niachou, A., Papakonstantinou, K., Santamouris, M., Tsangrassoulis, A. & Mihalakakou, G. (2001) Analysis of the green roof thermal properties and investigation of its energy performance. *Energy & Buildings*, 33, 719-729.

Nikam, B.R., Kumar, P., Garg, V., Thakur, P.K. & Aggarwal, S.P. (2014). Comparative evaluation of different potential evapotranspiration estimation approaches. *International Journal of Research in Engineering & Technology*, 3, 6.

Nyambayo, V. & Potts, D. (2010). Numerical simulation of evapotranspiration using a root water uptake model. *Computers & Geotechnics*, 37, 175–186.

Oudin, L., Hervieu, F., C, Perrin C., Andréassian, V., Anctil, F. & Loumagne, C. (2005). Which potential evapotranspiration input for a lumped rainfall-runoff model? Part 2 – Towards a simple and efficient potential evapotranspiration model for rainfall-runoff modelling. *Journal of Hydrology*, 303, 290-306.

Ouldboukhitine, S. E., Belarbi, R. & Djedjig, R. (2012). Characterization of green roof components: Measurements of thermal and hydrological properties. *Building & Environment*, 56, 78–85.

Packman, J. (1990). New Hydrology model. WaPUG spring meeting 1990.  
<http://www.wapug.org.uk/>

Palla, A., Gnecco, I. & Lanza, L.G. (2009). Unsaturated 2-D Modelling of Subsurface Water Flow in the Coarse-Grained Porous Matrix of a Green Roof. *Journal of Hydrology*, 379 (1-2), 193-204.

Palla, A., Gnecco, I. & Lanza, L.G. (2010). Hydrologic restoration in the urban environment using green roofs. *Water*, 2, 140-154.

Palla, A., Gnecco, I. & Lanza, L.G. (2012). Compared performance of a conceptual and a mechanistic hydrologic models of a green roof. *Hydrological Processes*, 26(1), 73-84.



- 
- Palla, A., Lanza, L.G. & La Barbera, P. (2008). A green roof experimental site in the Mediterranean climate. *11<sup>th</sup> International Conference on Urban Drainage, Edinburgh*.
- Palla, A., Sansalone, J.J., Gnecco, I. & Lanza, L.G. (2011). Storm water infiltration in a monitored green roof for hydrologic restoration. *Water Science & Technology*, 64, 766.
- Parliamentary Office of Science and Technology [POST] (2007). Urban Flooding - Post note No. 289.
- Paula, S., Arianoutsou, M., Kazanis, D., Tavsanoğlu, Ç., Lloret, F., Buhk, C., Ojeda, F., Luna, B., Moreno, J.M., Rodrigo, A., Espelta, J.M., Palacio, S., Fernández-Santos, B., Fernandes, P.M. & Pausas, J.G. (2009). Fire-related traits for plant species of the Mediterranean Basin. *Ecology*, 90, 1420.
- Plants for a Future: [www.pfaf.org](http://www.pfaf.org), accessed on 29 June, 2016.
- Poë, S. & Stovin, V. (2012). Advocating a physically-based hydrological model for green roofs: Evapotranspiration during the drying cycle. *Proceedings of the World Green Roof Congress, Copenhagen*.
- Poë, S., Stovin, V. & Dunsiger, Z. (2011). The Impact of Green Roof Configuration on Hydrological Performance. *Proceedings of the 12th International Conference on Urban Drainage, Porto Allegre, Brazil*.
- Poë, S., Stovin, V.R. & Berretta, C. (2015). Parameters influencing the regeneration of a green roof's retention capacity via evapotranspiration. *Journal of Hydrology*, 523, 356-367.
- Priestley, C. H. B. & Taylor, R. J. (1972). On the assessment of surface heat flux and evaporation using large-scale parameters. *Monthly Weather Review*, 100(2), 81-92.
- Raats, P. (2001). Developments in soil-water physics since the mid-1960s. *Geoderma*, 100, 355-387.
- Razzaghmanesh, M. & Beecham, S. (2014). The hydrological behaviour of extensive and intensive green roofs in a dry climate. *Science of the Total Environment*, 499, 284-296.
- RDP Electronics Limited (2006a). Model RLS Single-Point Compression Load Cell. RDP Group. Wolverhampton. England.
- RDP Electronics Limited (2006b). Modular 600 Multi-Channel Signal Conditioning System. RDP Group. Wolverhampton. England.
- Renew-Reuse-Recycle website (accessed 2010):  
[www.renew-reuse-recycle.com/noabl.pl?go=Go&postcode=s1+3jd&osx=&osy=&country=gb](http://www.renew-reuse-recycle.com/noabl.pl?go=Go&postcode=s1+3jd&osx=&osy=&country=gb)
-

Rezaei, F. & Jarrett, A.R. (2006). Measure and Predict Evapotranspiration Rate from Green Roof Plant Species. Penn State College of Engineering Research Symposium, Penn State University.

Rezaei, F. (2005). Evapotranspiration rates from extensive green roof plant species. Master's Thesis. Pennsylvania State University, USA.

Richards, L.A. & Weaver, L.R. (1944). Moisture retention by some irrigated soils as related to soil-moisture tension. *Journal of Agricultural Resources*, 69, 215-235.

Richards, L.A. (1931). Capillary conduction of liquids through porous mediums. *Physics*, 1 (5), 318-333.

Rideal, E. K. (1922). On the flow of liquids under capillary pressure, *Philosophical Magazine Series*, 6, 44, 1152-1159.

Romano, N. & Palladino, M. (2002). Prediction of soil water retention using soil physical data and terrain attributes. *Journal of Hydrology*, 265, 56-75.

Rossmann, L.A. (2004). Storm water management model User's manual version 5.0. Water Supply and Water Resources Division, National Risk Management Research Laboratory, Cincinnati (USA).

Rossmann, L.A. (2010). Storm water management model - User's Manual, Version 5.0, United States Environmental Protection Agency, Cincinnati, Ohio, United States.

Rowe, D., Clayton, R., Van Woert, N., Monterusso, M. & Russell, D. (2003). Green roof slope, growing media and vegetation influence run-off: Greening rooftops for sustainable communities. *First North American Green Roofs Conference, Chicago*.

Rowe, D.B., Getter, K.L. & Durhman, A.K. (2012). Effect of green roof media depth on Crassulacean plant succession over seven years. *Landscape & Urban Planning*, 104, 310-319.

Rowell, D. (1994). *Soil Science: Methods and Applications*. Essex: Longman.

Royal Horticultural Society: [www.rhs.org.uk](http://www.rhs.org.uk), accessed 29 June 2016.

Sailor, D. (2008). A green roof model for building energy simulation programs. *Energy & Buildings*, 40, 8, 1367-1622.

Santamouris, M., Pavlou, C., Doukas, P., Mihalakakou, G., Synnefa, A., Hatzibiros, A. & Patargias, P. (2007). Investigating and analysing the energy and environmental performance of an experimental green roof system installed in a nursery school building in Athens, Greece. *Energy*, 32, 9, 1781-1788.

Sayed, O.H. (2001). Crassulacean Acid Metabolism 1975-2000, A checklist. *Photosynthetica*, 39(3), 339-352.

- 
- Schmidt, M. (2006). The Evapotranspiration of Greened Roofs and Facades. *Greening Rooftops for Sustainable Communities, Boston*.
- Schroll, E., Lambrinos, J., Righetti, T. & Sandrock, D. (2011). The role of vegetation in regulating storm water runoff from green roofs in a winter rainfall climate. *Ecological Engineering*, 37 (4), 595–600.
- Schwarz, R. (2010). Moisture content measurement in green roof substrates: Comparison of different CS616 probes. Knowledge Transfer Account. Engineering & Physical Sciences Research Council and University of Sheffield, Report Ref: 004-DHH-10.
- Schwen, A., Bodner, G., Scholl, P., Buchan, G.D. & Loiskandl, W. (2011). Temporal dynamics of soil hydraulic properties and the water-conducting porosity under different tillage. *Soil Tillage Research*, 113 (2), 89–98.
- Seyfried, M.S. & Murdock, M.D. (2001). Response of a new soil sensor to variable soil, water content, and temperature. *Soil Science Society of America Journal*, 65, 28-34.
- Simmons, M.T., Gardiner, B., Windhager, S. & Tinsley, J. (2008). Green roofs are not created equal: the hydrologic and thermal performance of six different extensive green roofs and reflective and non-reflective roofs in a sub-tropical climate. *Urban Ecosystems*, 11 (4), 339–348.
- Šimunek, J., Šejna, M., Saito, H., Sakai, M. & van Genuchten, M.T. (2008a). The Hydrus-1D Software Package for Simulating the Movement of Water, Heat, and Multiple Solutes in Variably Saturated Media, Version 4.0, HYDRUS Software Series 3. University of California Riverside, Department of Environmental Sciences. Riverside, CA. 315 pp.
- Šimunek, J., van Genuchten, M.T. & Šejna, M. (2008b). Development and applications of the HYDRUS and STANMOD software packages, and related codes. *Vadose Zone Journal*, 7 (2), 587–600.
- Šimunek, J., Vogel, T. & Van Genuchten, M.T. (1994). The SWMS\_2D code for simulating water flow and solute transport in two-dimensional variably saturated media, Version 1.21. Research Report No. 132, Riverside, California (USA).
- Simunek, J., Wendroth, O. & van Genuchten, M. (1998). Parameter estimation analysis of the evaporation method for determining soil hydraulic properties. *Soil Science Society of America Journal*, 62, 894-905.
- Singh, J., Knapp, H.V. & Demissie, M. (2004). Hydrologic modeling of the Iroquois River watershed using HSPF and SWAT. ISWS CR 2004-08. Champaign, Ill.: Illinois State Water Survey. Available at: [www.sws.uiuc.edu/pubdoc/CR/ISWSCR2004-08.pdf](http://www.sws.uiuc.edu/pubdoc/CR/ISWSCR2004-08.pdf).

- Snodgrass, E.C. & Snodgrass, L.L. (2006). *Green Roof Plants: A Resource and Planting Guide*. Timber Press, Portland, Oregon.
- Solecki, W.D., Rosenzweig, C., Parshall, L., Pope, G., Clark, M., Cox, J. & Wiencke, M. (2005) Mitigation of the heat island effect in urban New Jersey. *Environmental Hazards*, 6, 39-49.
- Sonne, J. (2006) Evaluating green roof energy performance, *ASHRAE Journal*, February 2006.
- Starry, O., Lea-Cox, J.D., Kim, J. & van Iersel, M.W. (2014). Photosynthesis and water use by two *Sedum* species in green roof substrate. *Environmental & Experimental Botany*, 107, 105–112.
- Stovin, V. (2009). The potential of green roofs to manage Urban Stormwater. *Water & Environment Journal*, 24, 3, 192-199.
- Stovin, V., Poë, S. & Berretta, C. (2013). A modelling study of long term green roof retention performance. *Journal of Environmental Management*, 131, 206-215.
- Stovin, V., Poë, S., De-Ville, S. & Berretta, C. (2015a). The influence of substrate and vegetation configuration on green roof hydrological performance. *Ecological Engineering*, 85, 159–172.
- Stovin, V., Vesuviano, G. & De-Ville, S. (2015b). Defining green roof detention performance. *Urban Water Journal*. ISSN 1573-062X
- Stovin, V., Vesuviano, G. & Kasmin, H. (2012). The hydrological performance of a green roof test bed under UK climatic conditions. *Journal of Hydrology*, 414-415, 148-161.
- Synnefa, A., Santamouris, M. & Akbari, H. (2007) Estimating the effect of using cool coatings on energy loads and thermal comfort in residential buildings in various climatic conditions. *Energy & Buildings*, 39, 1167-1174.
- Tabari, H., Grismer, M.E. & Trajkovic, S. (2011). Comparative analysis of 31 reference evapotranspiration methods under humid conditions. *Irrigation Science*, 31, 2, 107-117.
- Teemusk, A. & Mander, U. (2007) Rainwater runoff quantity and quality performance from a green roof: The effects of short-term events. *Ecological Engineering*, 30, 271-277.
- The Green Roof Guide: <http://www.greenroofguide.co.uk/what-are-green-roofs/>
- Thorntwaite, C. W. (1948). An approach toward a rational classification of climate. *The Geographical Review*, 38, 1, 55-94.

- 
- Tuller, M., Or, D. & Dudley, L.M. (1999). Adsorption and capillary condensation in porous media: Liquid retention and interfacial configurations in angular pores. *Water Resources Research*, 35, 7, 1949-1964.
- UK Climate Projections (UKCP09) Weather Generator tool, <http://ukclimateprojections-ui.metoffice.gov.uk/> accessed on 23 March 2016.
- UKWIR (2016). Development of the UKWIR Runoff Model: Main Report. Ref: 14/SW/01/6.
- United States Department of Agriculture (USDA): <http://planthardiness.ars.usda.gov>, accessed on 29 June 2016.
- [US Naval Observatory website \(accessed 2010\):](http://www.usno.navy.mil/USNO/astronomical-applications/data-services/rs-one-year-world?searchterm=sun+rise)  
<http://www.usno.navy.mil/USNO/astronomical-applications/data-services/rs-one-year-world?searchterm=sun+rise>.
- van Dam, J., Huygen, J., Wesseling, J., Feddes, R., Kabat, P., van Walsum, P., et al. (1997). Soil Water Atmosphere Plant (SWAT) Technical Document 45. Wageningen. The Netherlands: DLO Winand Staring Centre.
- van Dam, J.C. (2000). Field scale water flow and solute transport. SWAP model concepts, parameter estimation and case studies. PhD thesis, Wageningen Universiteit, 167 pp.
- van Dam, J.C., Groenendijk, P., Hendriks, R.F.A. & Kroes, J.G. (2008). Advances of modeling water flow in variably saturated soils with SWAP. *Vadose Zone Journal*, 7, 640–653.
- van den Honert, T. (1948). Water transport in plants as a catenary process. *Discussions of the Faraday Society*, 3, 146-153.
- van Genuchten, M. (1980). A Closed-Form Equation for Predicting the Hydraulic Conductivity of Unsaturated Soils. *Soil Science Society of America Journal*, 44.
- van Seters, T., Rocha, L. & MacMillan, G. (2007). Evaluation of the runoff quantity and quality performance of an extensive green roof in Toronto, Ontario. *Greening Rooftops for Sustainable Communities, Minneapolis*.
- van Seters, T., Rocha, L., Smith, D. & MacMillan, G. (2009). Evaluation of green roofs for runoff retention, runoff quality, and leachability. *Water Quality Research Journal of Canada*, 44, 33–47.
- van Woert, N., Rowe, D., Andresen, J., Rugh, C., Fernandez, R. & Xiao, L. (2005). Green roof storm water retention: Effects of roof surface, slope and media depth. *Journal of Environmental Quality*, 34, 1036-1044.

- Vanuytrecht, E., Van Mechelen, C., Van Meerbeek, K., et al. (2014). Runoff and vegetation stress of green roofs under different climate change scenarios. *Landscape & Urban Planning*, 122 (2), 68–77.
- Versini, P., Ramier, D., Berthier, E. & de Gouvello, B. (2015). Assessment of the hydrological impacts of green roof: From building scale to basin scale. *Journal of Hydrology*, 524, 562–575.
- Verstraeten, W., Veroustraete, F. & Feyen, J. (2008). Assessment of Evapotranspiration and Soil Moisture Content Across Different Scales of Observation. *Sensors*, 8, 70-117.
- Vesuviano, G. & Stovin, V. (2013). A generic hydrological model for a green roof drainage layer. *Water Science & Technology*, 68, 4, 769-775.
- Vesuviano, G. (2014). A Two-stage Runoff Detention Model for a Green Roof. Ph.D. Thesis in Civil Engineering. The University of Sheffield, UK.
- Vesuviano, G., Sonnenwald, F. & Stovin, V. (2013). A two-stage storage routing model for green roof detention. *Water Science & Technology*, 69, 6, 1191-1197.
- Vijayaraghavan, K. & Raja, F.D. (2014). Design and development of green roof substrate to improve runoff water quality: Plant growth experiments and adsorption. *Water Research*, 63, 94-101.
- Villareal, E., Semadeni-Davies, A. & Bengtsson, L. (2004). Inner city storm water control using a combination of best management practices. *Ecological Engineering*, 22(4-5), 279-298.
- Villarreal E.L. (2007). Runoff detention effect of a sedum green-roof. *Nordic Hydrology*, 38(1), 99-105.
- Villarreal, E.L. & Bengtsson, L. (2005). Response of a Sedum green-roof to individual rain events. *Ecological Engineering*, 25(1), 1-7.
- Voyde, E. (2011). Quantifying the Complete Hydrologic Budget for an Extensive Living Roof. PhD Thesis, Department of Civil & Environmental Engineering, University of Auckland.
- Voyde, E., Fassman, E. & Simcock, R. (2010a). Hydrology of an extensive living roof under sub-tropical climate conditions in Auckland, New Zealand. *Journal of Hydrology*, 394, 384-395.
- Voyde, E., Fassman, E., Simcock, R. & Wells, J. (2010b). Quantifying Evapotranspiration Rates for New Zealand Green Roofs. *Journal of Hydrologic Engineering*. 15 (6), 395-403.

- 
- van Woert, N.D, Rowe, D.B., Andresen, J.A., Rugh, C.L. & Xiao, L. (2005). Watering regime and green roof substrate design affect Sedum plant growth. *HortScience*, 40, 659–664.
- Wadzuk, B. M., Schneider, D., Feller, M. & Traver, R. G. (2013). Evapotranspiration from a Green Roof Stormwater Control Measure. *Journal of Irrigation & Drainage Engineering*, 139, 12, 995-1003.
- Wang, Y., Grove, S. & Anderson, M. (2008). A physical-chemical model for the static water retention characteristic of unsaturated porous media. *Advances in Water Resources*, 31, 701-713.
- Wark, C. (2011). Cooler Than Cool Roofs: How Heat Doesn't Move Through a Green Roof - A 7-part series on the fundamentals of energy and green roofs. Originally published at greenroofs.com (April 2010 - April 2011).
- Washburn, E.W. (1921). The dynamics of capillary flow. *Physical Review*, 17, 3, 273-283.
- Weiß, M. & Menzel, L. (2008). A global comparison of four potential evapotranspiration equations and their relevance to stream flow modelling in semi-arid environments. *Advances in Geosciences*, 18, 15–23.
- Western, A.W. & Seyfried, M.S. (2005). A calibration and temperature correction procedure for the water-content reflectometer. *Hydrological Processes*, 19, 3785-3793.
- White, R. E. (1997). Principles & Practice of Soil Science - The Soil as a Natural Resource (3rd Edition ed.). Blackwell Publishing, Victoria, Australia.
- Whittinghill, L.J., Rowe, D.B., Cregg, B.M. & Andresen, J.A. (2014). Comparison of storm water runoff from sedum, native prairie, and vegetable producing green roofs. *Urban Ecosystems*, 18, 1, 13-29.
- Wilson, E. (1990). Engineering Hydrology, Fourth Edition. Palgrave Macmillan, Basingstoke.
- Wolf, D. & Lundholm, J.T. (2008). Water uptake in green roof microcosms: effects of plant species and water availability. *Ecological Engineering*, 33, 179-186.
- Wong, N.H., Chen, Y., Ong, C.L. & Sia, A. (2003a) Investigation of thermal benefits of rooftop garden in the tropical environment. *Building & Environment*, 38, 261-270.
- Wong, N.H., Cheong, D.K.W., Yan, H., Soh, J., Ong, C.L. & Sia, A. (2003b) The effects of rooftop garden on energy consumption of a commercial building in Singapore. *Energy & Buildings*, 35, 353-364.

Wright, I. J., Reich, P. B., Westoby, M., Ackerly, D.D., Baruch, Z., Bongers, F., Cavender-Bares, J., Chapin, T., Cornelissen, J. H. C., Diemer, M., Flexas, J., Garnier, E., Groom, P.K., Gulias, J., Hikosaka, K., Lamont, B.B., Lee, T., Lee, W., Lusk, C., Midgley, J.J., Navas, M.L., Niinemets, U., Oleksyn, J., Osada, N., Poorter, H., Poot, P., Prior, L., Pyankov, V.I., Roumet, C., Thomas, S.C., Tjoelker, M.G., Veneklaas, E.J. & Villar, R. (2004). The worldwide leaf economics spectrum. *Nature*, 428, 821-827.

Yang, W-Y., Li, D., Sun, T. & Ni, G-H. (2015). Saturation-excess and infiltration-excess runoff on green roofs. *Ecological Engineering*, 74, 327–336.

Yio, M.H.N., Stovin, V., Werdin, J. & Vesuviano, G. (2013). Experimental analysis of green roof detention characteristics. *Water Science & Technology*, 68 (7), 1477-1486.

Young, P., Jakeman, A. & McMurtrie, R. (1980). An instrument variable method for model order identification. *Automatica*, 16, 281–294.

Zhao, L., Xia, J., Xu, C., Wang, Z., Sobkowiak, L. & Long, C. (2013). Evapotranspiration estimation methods in hydrological models. *Journal of Geographical Sciences*, 23(2), 359-369.

Zoppou, C. (2001). Review of urban storm water models. *Environmental Modelling & Software*, 16, 195–231.